ENGINEERING CAR-T CELLS

TO OVERCOME THE IMMUNOSUPPRESSIVE

MICROENVIRONMENT OF SOLID TUMOURS

Silvia Panetti

A thesis submitted to the University of Birmingham
for the degree of
DOCTOR OF PHILOSOPHY

Institute of Immunology and Immunotherapy
College of Medical and Dental Science
University of Birmingham
January 2023

ABSTRACT

Chimeric antigen receptor (CAR)-T cell therapies have revolutionised the treatment landscape for cancer patients. However, engineered adoptive lymphocyte-based therapies face significant resistance in solid tumour microenvironments due to amino acid and nutrient scarcity, as well as significant infiltration of suppressive myeloid cells. Here, we investigated the microenvironment of different solid tumours and assessed the detrimental effects of myeloid-derived suppressor cells (MDSCs) on the autologous and engineered anti-cancer immunity. We demonstrated a novel strategy to improve CAR-T cell efficacy and tumour clearance by depleting MDSCs with a repurposed CD33-directed immunoconjugate, Gemtuzumab Ozogamicin. In addition, we designed metabolically enhanced CAR-T cell constructs, to endow the T cells with increased L-arginine catabolic activity. We found that arginase-transduced CAR-T cells were able to recognise and lyse target cells in a comparable fashion to the anti-GD2 control. However, they presented an enhanced bioenergetic flexibility, evidenced by the increased maximal respiration achieved during the MitoStress test ($p = 0.010$), and a higher intracellular abundance of key metabolites, such as pyruvate ($p = 0.028$) and glutamine ($p = 0.003$). Ultimately, the novel CAR-T cells were shown to have a proliferative advantage upon antigen stimulation ($p = 0.015$) and induce superior tumour reduction in vivo ($p = 0.010$) compared to the standard CAR-T cells.

ACKNOWLEDGEMENTS

It does take a village.

I feel a bit overwhelmed at the thought that I might be almost done with this chapter of my life. It has been an exciting one, but it was also an emotional, physical and scientific challenge. (Without forgetting a pandemic and the birth of my first child, Vincent.)

Thank you to my supervisors, Frank and Carmen, who always kept their door open for me. Thanks for trusting me with this project and thanks for all the guidance and help you gave along the way. Thank you for investing in me.

Thank you to all the patients who donated to research. You are at the heart of what we do.

Thank you to the funders of this research, Robert and Sarah Martin, alumni of the University of Birmingham. Your support has made this happen and I am forever grateful.

Thank you to my homeland, Italy, for providing me with the best state-run education in the first 19 years of life, for teaching me the beauty and fulfilment of learning.

Thank you to Swansea University for giving me the warmest welcome to the UK and to Nick Jones, then a PhD student, for introducing me to the joys of research 8 years ago.

Thank you to my amazing colleagues. Stone, I can't think of a person I relied on more than you. You are an amazing scientist and mentor. Sarah, you have been my undiscussed pillar, who kept me sane during these years. I cannot wait for our next Diet Coke (?) together.
Vic, Ugo, Luci, Naz and Ashley, how many lunch breaks with Italo-Greek lessons? How many spillages, tears and laughs? Thanks for lighting up my days.

Thank you to my wonderful families. My hero and extension of my own soul, Matt, for taking on single-dad duties for what felt like years and encouraging me every second. The Beans for their huge help and patience. My parents and grandparents, for nourishing my curiosity since I was born and supporting me till here.

Nothing could have been achieved without you. Thank you.

TABLE OF CONTENTS

TABLE OF FIGURES

1. INTRODUCTION

1.1 The Immune System

The immune system is a finely orchestrated organisation of cells, tissues and organs providing a host defence from foreign threats, such as pathogens, otherwise able to compromise the integrity and health of the organism.

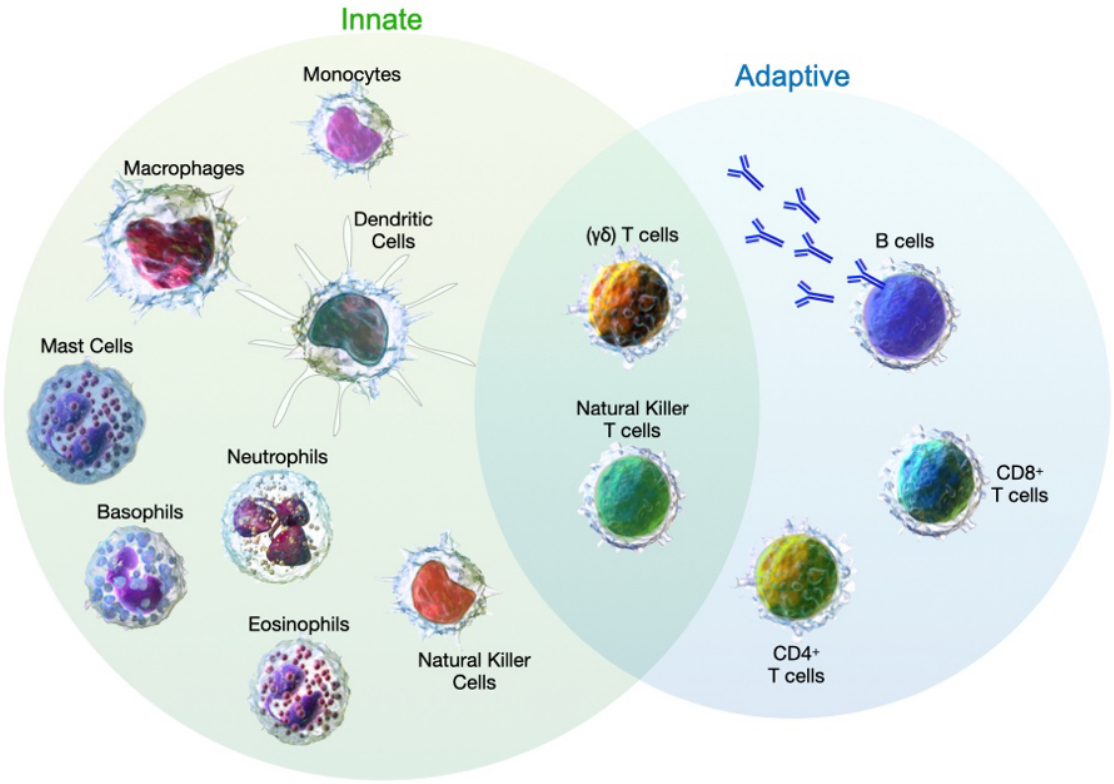

Figure 1: The immune system.

The cells of the innate and adaptive immune system.

Evolutionarily, the necessity for defence mechanisms is highly conserved and the development of an apparatus with such role stems at the very beginning of multicellular life (Beutler 2004). These defence mechanisms, fundamentally based on danger-sensing tools and danger-neutralising means, progressed to become increasingly complex and dynamic, to protect from a wide range of bacterial, viral and fungal infections.

In vertebrates, this translated into the development of two distinct, yet connected, arms of the immune system: the innate and the adaptive.

1.1.1 Innate Immunity

Beutler said: "Innate immunity is enormously broad, and it is sometimes difficult to decide where the innate immune system ends and the rest of the host begins" (Beutler 2004). This is because it comprises, not only the canonical immune cells, but also the physical barriers, i.e. the epithelium, associated with the secretion of anti-microbial peptides and mucins (Dann and Eckmann 2007) and a repertoire of commensal bacteria living in those tissues.

The innate immune cells base their function on a system of danger and pathogen sensing receptors, such as Toll-like receptors and NOD-like receptors among others, able to recognise lipopolysaccharide (LPS) from gram-negative bacteria and viral RNAs (Heil et al. 2013; Caruso et al. 2014). Upon receptor engagement, recruitment of more immune cells is mediated by chemokines and cytokines, i.e. inflammation (Liew and Kubes 2019).

Granulocytes, such as neutrophils, are characterised by the ability to release granules loaded with toxic products (e.g. defensins and reactive oxygen species (ROS)). In addition, the can engulf pathogens by phagocytosis or immobilise them by forming neutrophil extracellular traps (NETs). They represent the 50-70% of circulating leukocytes and, being short-lived, they are constantly replenished by the bone marrow under granulocyte-colony stimulating factor (G-CSF), interleukin (IL)-6 and IL-4 signals (Summers et al. 2010)

Blood-circulating monocytes, tissue-resident macrophages and dendritic cells (DC) are also proficient phagocytic cells. They can digest the target and display it in the form of peptides on their major histocompatibility complex (MHC) on their surface for the adaptive immune system to sample. For this reason, they are also referred to as antigen presenting cells (APCs). The peculiarity of DCs is the characteristic stellate shape, allowing for maximal surface exposure. They are excellent at antigen cross-presentation and stimulation and priming of cytotoxic T cell responses by producing copious amounts of IL-12. Different DC subsets differ in their transcriptional signature and molecular targets. These include cDC1 mainly specialise in the detection of viral and intracellular pathogens and produce type III interferon (i.e. IFN-λ), while cDC2 mostly respond to bacterial and fungal antigens and are proficient at recruiting a more diverse immune response (e.g. T_H2, T_H17) (Nizzoli et al. 2013).

A group of innate cells with lymphoid origin and lacking hypervariable antigen receptors, called innate lymphoid cells (ILCs), can specialise in a range of cytokine secretion signatures, such as INF-γ (group 1 ILCs), IL-5 and IL-13 (group 2 ILCs) and IL-17 and IL-22 (group 3 ILCs) (Spits et al. 2013).The most well studied, natural killer (NK) cells, are group 1 ILCs and they are key in providing detection of cellular stress during viral infection or cancer, via their danger-

associated molecular patterns (DAMPs), as well as clearing antibody-bound pathogens by induction of antibody-dependent cell-mediated cytotoxicity (ADCC) (Wilk and Blish 2018).

1.1.2 Antigen Presentation and the Major Histocompatibility Complex

MHC molecules, in humans also referred to as human leukocyte antigen (HLA), are a family of highly polymorphic cell surface proteins existing in two main subforms: class I and class II. MHC class I are present ubiquitously throughout the nucleated cells and are characterised by the ability to display short peptides, originated intracellularly by the proteasomes. They mediate T cell sampling of the cellular proteome, in order to screen for intracellular threats, such as viruses.

Conversely, MHC class II molecule expression is restricted to specific cell types, i.e. APCs. Class II molecules facilitate the presentation of pathogens or antigens acquired from the extracellular space and processed into peptides (Janeway et al. 2001).

Overall, the innate compartment of immunity represents an efficient way to address infectious agents by taking advantage of a ready-made arsenal of receptors to recognise conserved pathogenic traits. However, the sheer number of threats to our health and their creative escape mechanisms posed a challenge for the organism and induced the development of a substantially more flexible and heterogeneous system, which could tailor its response for the exact occasion.

1.1.3 Adaptive Immunity

Human adaptive immunity consists of two major populations of cells, B and T lymphocytes, produced in the bone marrow from a common lymphoid progenitor (CLP) and circulating throughout the body via the bloodstream and the lymphatic system. The lymphatic system is an essential network of vessels transporting immune cell-rich lymph and connecting key structures and organs of the immune systems. These include primary lymphatic organs, site of lymphocyte formation and maturation; secondary lymphatic organs (SLO), harbouring the mature cells and coordinating lymphocyte priming; and the more recently described tertiary lymphoid structures (TLS), impromptu SLO-resembling immune aggregates formed at sites of chronic inflammation or cancer (Giraldo and Germain 2016).

Prerogative of the adaptive immune system is the highly diverse repertoire of B cell receptors (BCRs) and T cell receptors (TCRs). This is obtained by a phenomenon of in-frame somatic recombination, also known as V(D)J recombination, elucidated in 1976 by Nobel Laureate Tonegawa and colleague (Hozumi and Tonegawa 1976).

V(D)J recombination is the somatic rearrangement of the immunoglobulin and TCR gene loci at the origin of the highly diverse repertoire of receptors of the adaptive immune system. It takes place during early B and T lymphocyte development in the primary lymphoid organs, i.e. bone marrow and thymus respectively, and it relies on the expression of the recombination-activating gene (RAG)-1 and RAG-2. Deletion of such genes in murine models results in abnormally small lymphatic organs and failure to produce mature T or B cells, leading to severe combined immunodeficiency (Mombaerts et al. 1992;Shinkai et al. 1992). The random-like rearrangement of the V(D)J regions results in an estimated repertoire of 10^{11} potential antibody affinities and 10^{8} different αβTCR clonotypes in the human body (Eren et al. 2012).

B lymphocytes are an essential player of what is defined as humoural immunity, in that they are the body's source of antibodies (Ab), i.e. immunoglobulins. Soluble Ab contribute to the immune response in several ways: they opsonise pathogenic threats to prompt phagocytic cells, they neutralise toxins, they induce complement activation and ADCC (Forthal 2015). Antibodies are Y-shaped glycoproteins characterised by a fragment antigen-binding (Fab) domain or paratope, and a fragment crystallizable region (Fc) domain. Whilst Fab domains dictates the antigens or epitopes recognised by the molecule, the Fc domains define the class of the antibody, i.e. what type of immune response it will induce. In particular, there are five classes of antibodies in humans, IgM, IgD, IgE, IgG and IgA, with IgG being the most common and effective Ig in circulation, IgE being specialised in helminth infection and mast cell activation, and IgA mainly found in mucosal tissues in its dimerised form (Figure 2).

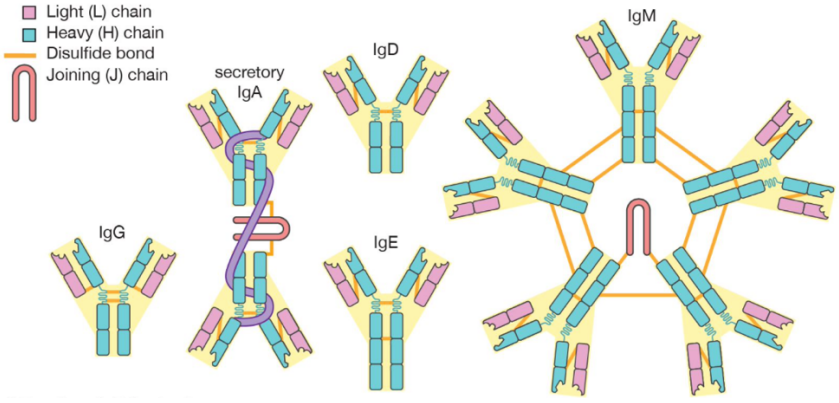

Figure 2: Immunoglobulins

The five classes of antibodies IgG, IgA, IgD, IgE and IgM, represented with their main structural features. Image taken from: Encyclopædia Britannica.

1.1.4 T Cell Development and Self-Tolerance

T cell development relies majorly on the thymus, an organ providing a specialised signalling environment for each developmental stage (e.g. Notch), where uncommitted progenitor cells from the bone marrow begin a sequential process of maturation (Rothenberg 2019). This begins in the corticomedullary junction of the thymus, where lymphoid cells, referred to as thymocytes, seed at arrival; they lack the typical surface markers of the T cell lineage, such as the main cluster of differentiation (CD) 3, as well as the subtypes CD4 or CD8, and are therefore defined as double negative (DN) cells.

V(D)J recombination of the TCR β-chain takes place during DN stage in the cortex, after which both CD4 and CD8 are upregulated to characterise double positive (DP) cells. DP cells can subsequently undergo TCR α-chain rearrangement until an efficient αβ pairing is reached. Always within the cortex, a process coordinated by MHC-expressing epithelial cells grants the positive selection of TCRs that can recognise self MHC molecules: only those TCRs will be useful to the organism and will be able to engage with antigen presentation once fully mature. In addition, based on the interactions with MHC class I and class II, positively selected early-T cells are now able to commit to a single phenotype, either $CD4^+$ or $CD8^+$ and migrate back towards the medulla (Germain 2002)(Starr, Jameson, and Hogquist 2003).

Here, a further selection round, this time aimed at the elimination of self-reactive TCRs takes, place in within the medullary thymic epithelial cells (mTECs), a unique tissue capable to mirror self-antigens from all around the body. In the specific, through a phenomenon referred to as promiscuous gene expression, mTECs manage to reproduce a broad range of peripheral self-molecules. This process is tightly regulated by the autoimmune regulator (AIRE) transcription factor, among others (Derbinski et al. 2016). Remarkably, it is estimated that the TEC

population as a whole has the capability to express over 19,000 protein-coding genes (Sansom et al. 2014).

Depending on the strength of the signal, autoreactive thymocytes will be eliminated by apoptosis or, alternatively, re-programmed to become regulatory T cells (T_{REG}), in charge of promoting self-tolerance within the organism (Venanzi, Benoist, and Mathis 2004).

Negative selection of mTEC-reactive thymocytes marks the establishment of what is defined as central tolerance: the core immunological distinction between self and non-self.

1.1.5 Naïve T Cells

Successfully selected thymocytes, as low as 2% of the initial thymocyte count, can finally egress the thymus as fully mature $CD4^+$ or $CD8^+$ naïve T cells (Haynes et al. 2000). This will enable them to travel to secondary lymphoid organs, from the spleen to peripheral lymph nodes, guided by chemotactic ligands in the lumen of high endothelial venules (HEVs), such as CCL21 and glycosylation-dependent cell adhesion molecule-1 (GLYCAM1), recognised by the homing molecules on T cells, CCR7 and L-selectin (also CD62L) respectively.

The spleen is a key site of T cell activation. Its anatomical structure allows for the compartmentalised interaction between the white pulp, rich in T cells and B cell follicles, and the blood-containing red pulp, rich in pathogens, debris and APCs (Mebius and Kraal 2005).

On a similar note, lymph nodes throughout the body also provide an organised structure to facilitate interactions between naïve T cells and APCs (Kaldjian et al. 2001).

1.1.6 T Cell Receptor and Antigen Presentation

Each naïve T cell bears on its surface up to 10^5 identical TCR molecules, unique to that particular cell, composed of the V(D)J recombined α and β chains, as well as the signalling complex named CD3, which includes γ, δ, ε and ζ chains in the configuration shown in Figure 3. The continuous recirculation of naïve T cells through the blood and the lymphatic system aims at the screening of as many peptide antigens as possible, presented on MHC class I and class II molecules. These differ in structure and pattern of expression, despite having similar immunological roles.

The MHC class I molecules, the main in humans being HLA-A, -B and -C, are heterodimers consisting of a transmembrane α-chain and a small non-polymorphic β2 microglobulin chain. The peptide-binding portion is embedded within the α-chain, accommodating for short peptides, around 8-10 amino acid long, at times up to 14 (Burrows, Rossjohn, and McCluskey 2006). They are expressed in all nucleated cells throughout the body and are used ubiquitously for the presentation of endogenous peptides upon proteasomal degradation of intracellular products (Blees et al. 2017). Crucially, MHC class I molecules solely engage with T cells expressing the CD8 co-receptor, i.e. $CD8^+$ T cells or Cytotoxic T Lymphocytes (CTLs).

On the other hand, the MHC class II molecules, of which the most common are HLA-DR, -DP and -DQ, are formed by two homogenous transmembrane peptide chains, α and β, which together shape the peptide-binding site and allow for longer peptides to be presented, generally between 15 and 24 amino acids. Their expression is restricted to professional

antigen presenting cells for the sampling of peptides of extracellular origin exclusively to T cells expressing the CD4 co-receptor, i.e. $CD4^+$ T Cells or T Helper Cells (Th).

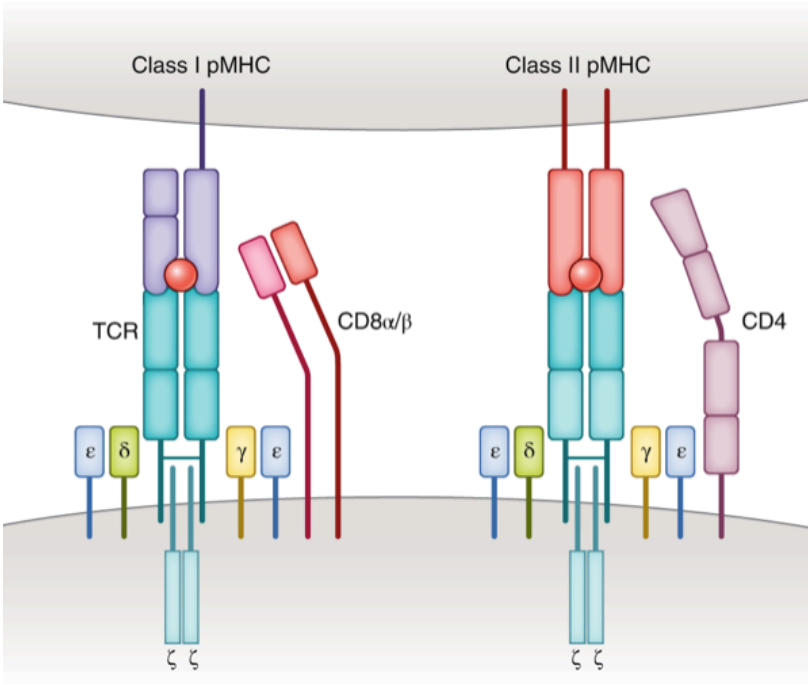

Figure 3: Classical αβ TCR interaction with MHC complex.

Structural diagram of CD8+ T cells (left) and CD4+ T cells (right) and TCRs interaction with the respective peptide-loaded MHC class I and class II molecules. Adapted from: Joglekar and Li (2021).

1.1.7 T Cell Activation

Optimal T cell activation requires the synergic work of two distinct signalling events: the engagement of the TCR with its cognate peptide:MHC complex and the presence of a co-stimulatory signal.

Firstly, upon antigen recognition by the TCR, a sequence of alterations within its cytoplasmic

tail takes place, such as the phosphorylation of the immunoreceptor tyrosine-based activation motifs (ITAMs) of the CD3ζ chains and consequent recruitment of ζ-associated protein (ZAP-70). The signal is in turn transduced downstream, eventually allowing the nuclear translocation of specific transcription factors, e.g. nuclear factor of activated T cells (NFAT), nuclear factor-κB (NF-κB) and activator protein-1 (AP-1) to induce key changes in gene expression (Figure 4).

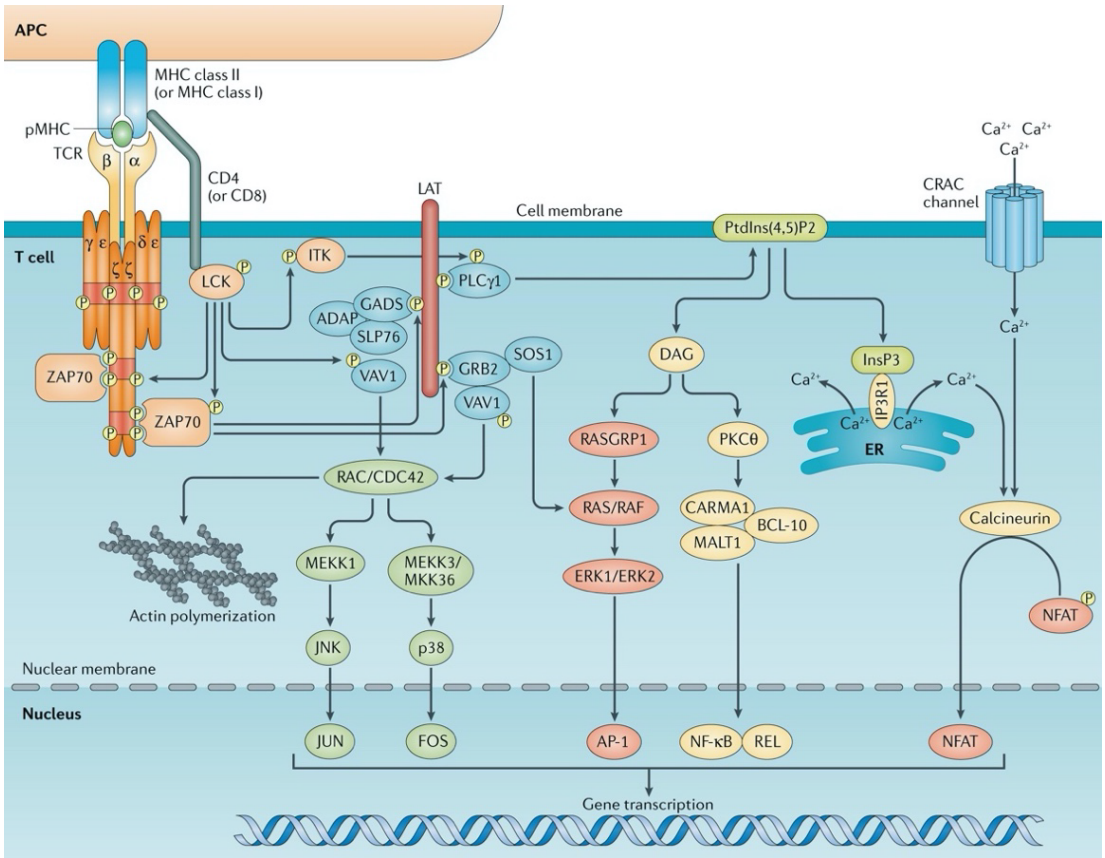

Figure 4: TCR signalling

Following peptide recognition, a signalling cascade initiate the T cell activation programme of the cell through the modulation of gene transcription. Taken from: (Gaud, Lesourne, and Love 2018)

In addition, to sustain an optimal T cell activation the triggering of a simultaneous co-stimulatory signal through a separate set of receptors is required. The quintessential T cell co-stimulatory receptor is CD28, a surface molecule constitutively expressed by naïve T cells which binds to B7-1 (or CD80) and B7-2 (or CD86) molecules on APCs. Ligation of CD28 induces phosphorylation of its cytoplasmic tail and consequent amplification of the signal transduction initiated by TCR signalling. CD28 stimulation is found not only to quantitatively amplify the signalling cascade within the cell, but also induce the expression of a second wave of co-stimulatory receptors, e.g. inducible co-stimulatory molecule (ICOS), OX40 or 4-1BB (Acuto and Michel 2003), as well as promoting key structural rearrangements of the cytoskeleton (Burkhardt, Carrizosa, and Shaffer 2008).

Activation of naïve T cells upon immunological synapse formation and co-stimulation induces a strong proliferative signal which results in the exponential clonal expansion of T cells bearing the same TCRs in order to clear the pathogenic threat. In addition, the production of pro-survival cytokines, such as IL-2, is stimulated (Vella et al. 1998).
On the contrary, T cell activation in absence of co-stimulation will result in an impaired response, marked by an anergic T cell phenotype, discussed further in 1.1.9 (Macián et al. 2004).

1.1.8 T Cell Differentiation and Memory Formation

Ultimately, T cell activation results in the gain of effector function and mounting of the immune response. Upon encounter of the cognate peptide:MHC class II complex, $CD4^+$ T cells

are mainly characterised by the ability to produce a wide range of cytokines, depending on the type of threat detected, which supports the maturation of other leukocytes and orchestrates the immune response as a whole. In fact, it has been shown that T Helper cells cover a pivotal role in the expansion and memory formation of $CD8^+$ T cells (Janssen et al. 2003) and B cell class switching via the CD40-CD40L axis (Lederman et al. 1992). The cytokine milieu during CD4 T cell priming is essential in shaping the type of immune response and determining their differentiation into the T_H1, T_H2, T_H9, T_H17, iTreg and T_{fh} subsets (Tay, Richardson, and Toh 2021). An overview on the $CD4^+$ T cell subtypes, the environment that induces their differentiation, the transcription factor and the produced cytokines characterising them is depicted in Figure 5.

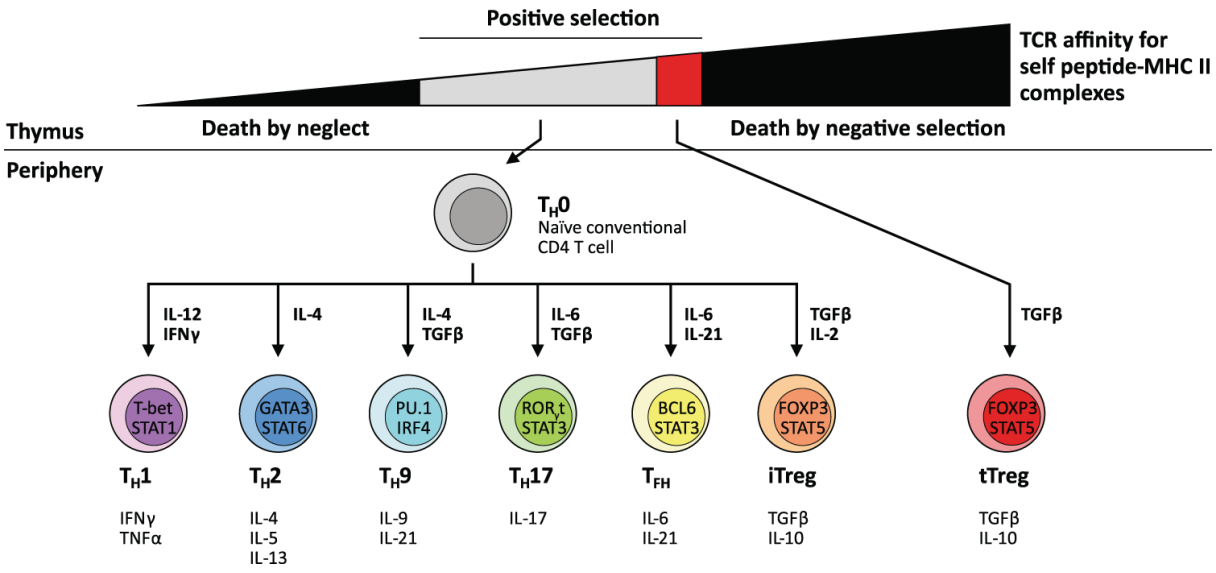

Figure 5: $CD4^+$ T cell subpopulations.

CD4+ T Helper cells can dynamically differentiate, based on the microenvironmental signals, into different subtypes with characteristic roles and cytokine repertoire. Adapted from: (Tay, Richardson, and Toh 2021)

On the other hand, $CD8^+$ T cells, activated by peptide:MHC class I complex, have conventionally been associated with a cytotoxic response characterised by pro-inflammatory INF-γ and release of cytolytic molecules, such as perforin A and granzyme B, to promptly induce death on the target cell (Thiery et al. 2011). However, recent research has shown that cytotoxic CD8 T lymphocytes might be able to shape the immune response based on the environment and, much like CD4 T Helper cells, be able to secrete a wide range of cytokines, relatively comparable to those of CD4 T cells. (Reviewed in St. Paul and Ohashi 2020).

The exponential proliferation of T cell clones persists until complete clearance of the threat, at which point only a small proportion of clones will survive and differentiate into long-lived phenotypes to constitute immunological memory for that antigen in the event of a second encounter. Central memory T cells (T_{CM}) are characterised by their expression of CCR7 and CD62L, allowing them to recirculate through the lymph nodes, as well as the long-lived isoform of CD45, i.e. CD45RO (Michie et al. 1992); re-stimulation of such cells will induce a more potent response and immediate clonal expansion of effector cells. Effector memory T cells (T_{EM}), on the other hand, lack lymph node homing receptors and are generally thought to be able to infiltrate inflamed peripheral tissues via inflammatory cytokine receptors, e.g. CCR3 (Sallusto, Mackay, and Lanzavecchia 1997) and elicit an immune response even in absence of APC co-stimulation (van Stipdonk, Lemmens, and Schoenberger 2001). For completeness, the traits of further memory T cell subsets have been hypothesised due to their expression profiles of specific markers; these are the rarer T memory stem cells (T_{SCM}) with amplified self-renewal ability (Gattinoni et al. 2011), the tissue resident and peripheral memory T cells (T_{RM} and T_{PM}) (Gerlach et al. 2016), as well as the potential existence of a

virtual memory, for which antigen-inexperienced T cells display memory traits (Marusina et al. 2017). All in all, these cells contribute to the establishment of a key aspect distinguishing the adaptive immune system, i.e. the retainment of a life-long immunological memory for previous antigens, which lies at the base of the essential medical practice of vaccination.

Interestingly, a study by Saeed et al. questions whether immunological memory is in fact a prerogative of the adaptive immune system in light of the fact that long term epigenetic reprogramming events are detectable in myeloid cells after infection, a phenomenon described as 'trained immunity' (Saeed et al. 2014) and attributed to metabolic changes (Bekkering et al. 2018).

1.1.9 Peripheral Tolerance and T cell Anergy

A fundamental duty of the immune system is to prevent damage to healthy tissues.
For this reason, peripheral mechanisms to damp the immune response are in place both, to mark the resolution of the threat and to avoid autoimmune reactivity.
Whilst the greater part of auto-reactive TCRs are eliminated during the strict selection in the thymus, some TCRs might present with cross-reactivity issues once in circulation. In order to overcome the TCRs inability to distinguish self from non-self antigens, co-stimulatory ligands in the environment are upregulated based on the level of inflammation and threat sensed, helping T cells to engage in proper activation exclusively when necessary, in a safety loop of signals. Similarly, inhibitory ligands are upregulated upon pathogen clearance to avoid unnecessary tissue damage (Medzhitov and Janeway Jr 2000).

An example of such signalling axis is represented by the co-stimulatory B7 ligands binding to CD28 on naïve T cells; however, after activation cytotoxic T lymphocyte antigen 4 (CTLA-4) is upregulated on the T cell surface and, due to a 10-fold higher affinity to the B7 ligands, it imparts an inhibitory signal to promote the resolution of the immune response (Krummel and Allison 1995) through dephosphorylation of the CD3-ζ chain (Lee et al. 1998). CTLA-4 knock-out mice are affected by lethal lymphoproliferation (Waterhouse et al. 1995) and progressive autoimmunity (Verhagen et al. 2009).

Tolerogenic signals can also be delivered by the microenvironment. When stimulated by LPS, TNFα and GM-CSF, DCs are efficient APCs with high levels of co-stimulatory ligands on their surface; however, when stimulation is suboptimal (e.g. in presence of IL-10), they can acquire tolerogenic abilities and mediate G1 cell cycle arrest and therefore T cell anergy (Kubsch et al. 2003).

Anergy, a mechanism to induce T cell hyporesponsivness, can be broadly distinguished into two main types: clonal anergy and adaptive tolerance. While the first is caused by defective T cell activation, is obtained by inhibition of Ras/MAP signalling and it can be reversed by IL-2; the latter mostly involves naïve T cells within an overall immunosuppressive microenvironment, which inhibits Ca^{2+} signalling and therefore impairs effector functions and ability to proliferate upon antigen stimulation (Schwartz 2003; Silva Morales and Mueller 2018).

1.2 Cancer

Cancer is a broad term to describe a group of more than 200 diseases associated with uncontrolled cell replication, enhanced survival of the cells and consequent tumour formation within the tissue of origin and beyond. Even though significant progress has been madein the understanding of this condition over the past 50 years, the World Health Organisation describes it as the second leading cause of death in 2018 and warns that a significant increase in cancer cases is expected in the decades to come (World Health Organization 2020). Surgical removal is the most effective treatment, when the primary tumour is accessible and localised; radiotherapy and chemotherapy still represent helpful tools in the perioperative stage and to control tumour progression (Urruticoechea et al. 2010). However, relatively recent realisations concerning the role of the immune system in tumour development and clearance led the scientific community to pursue ways to enhance and deploy such assets. Despite the progress made, further light needs to be shed in order to tackle those cancers still harbouring high mortality rates and poor treatment options.

1.2.1 Oncogenesis

Oncogenesis is the result of a multi-step genetic alteration within a cell, occurring in an age-dependent manner and requiring four to seven theoretical events (Renan 1993) including different types of transformation, from point mutation to chromosome rearrangements (Kinzler and Vogelstein 1998). Such mutations enable the malignant cell to acquire independence from mitogenic growth signals and insensitivity for growth-suppressors,

altogether promoting subsistence and endless proliferation.

Due to the overall unlikelihood of this step-wise transition from normal to oncogenic, it has been recognised that most tumours originate from chance or inherited mutations within key gatekeeping genes, such as *TP53, RB1, ATM, BRCA1*. Mutation in such compartments of the DNA repair machinery inevitably leads to further genome instability and enhanced oncogenesis (Lengauer, Kinzler, and Vogelstein 1998)(Burkhart and Sage 2008).

In addition, strategies to sustain growth are enabled, e.g. the constitutive activation of B-Raf signalling in about 40% of melanomas (Davies and Samuels 2010); K-Ras in 90% of pancreatic carcinomas (Krasinskas et al. 2013) and 35% of colorectal carcinomas (Hartman et al. 2012); as well as the angiogenic switch to overcome hypoxia and starvation of the tissues by upregulation of vascular endothelial growth factor (VEGF)(Hanahan and Folkman 1996; Ferrara 2009).

Ultimately, upon rapid and uncontrolled cell replication, malignant tumours can acquire the ability to metastasise, i.e. leave the primary site of disease via blood or lymph circulation and seed into a different tissue. This is promoted by a process called epithelial to mesenchymal transition (EMT), conferring enhanced plasticity to the cancer cell in order to efficiently invade and adapt to new microenvironments via the activation of transcription factors typical of embryogenesis, e.g. Snail, Twist, and Six1 (Micalizzi, Farabaugh, and Ford 2010).

1.2.2 Role of the Immune System in Cancer

Despite the common notion about the immune system being developed to discriminate and clear ‘foreign’ in order to preserve ‘self’, evidence supporting the existence of a natural

immune activity against 'self' malignancies has been collected for over a century.
Firstly, the observation of spontaneous tumour regression upon severe episodes of bacterial infection led Coley to purposefully induce bacterial infections in sarcoma patients, as the earliest attempt of cancer immunotherapy (Coley 1893). The hypothesis of immunological surveillance was later shaped by the works of Thomas and Burnet, which independently suggested the existence of immunological responses due to tumour-associated antigens (TAAs) (L. Thomas 1959)(Burnet 1970).
Following a few decades of controversy, studies on absent or impaired immune systems were demonstrated to correlate with more frequent and rapidly growing cancers. This was shown in the context of perforin- and IFN-γ-knockout mouse models (van den Broek et al. 1996)(Dighe et al. 1994), as well as in human studies, such as the insurgence of donor-derived tumours in post-transplant immunosuppressed patients (Strauss and Thomas 2010) and the increased risk of malignancies in acquired immunodeficiency syndrome (AIDS) patients (Boshoff and Weiss 2002).

Tumour-infiltrating lymphocytes (TILs) have been isolated from tumour tissues since the 70s (Galili et al. 1979); however the crucial role of NK and T cells in cancer immunosurveillance was subsequently sealed by evidence showing the prognostic value of lymphocyte infiltration in several types of cancers, among which melanoma (Clemente et al. 1996), lung (Villegas et al. 2002) ovarian (Nelson 2008) and colorectal cancers (Galon et al. 2006).
The lymphocyte-based anti-cancer endeavour, however, was also found to act as selective pressure towards a less immunogenic tumour populations, as shown by Shankaran (Shankaran et al. 2001). This was subsequently described as the phenomenon of

immunoediting, for which the antagonism between immune system and cancer induces the acquisition of escape mechanisms in the genetically plastic malignant cells (Dunn et al. 2002). Indeed, the ability of the tumour to avoid immunosurveillance represents one of the hallmarks of cancer and adds another dimension to the complexity of the pathology (Hanahan et al. 2011).

Overall, immune infiltrates are not seen across all cancer types with equal proportions and equal diversity. On one hand, certain tumours are characterised by low to no T cell infiltration and are labelled as 'cold'; generally, this is the case of tumours with a low mutational burden, due to the associated reduced levels of tumour-derived antigens, such as pancreatic cancer. 'Hot' tumours, on the other hand, display robust immune infiltration, inflammatory cytokines and an overall higher mutational burden, such as lung cancer or melanoma.
At times, within the same cancer type, the two phenotypes can be distinguished. For example, this is the case in colon cancer, for which *KRAS* mutation is a predictor of a 'cold' tumour, as opposed to the 'hot' microsatellite instable (MSI) microenvironment (Lal et al. 2018). Because the immune infiltration status is a reliable predictor of immunotherapy outcome, it becomes of paramount importance, when treating a tumour, to investigate its microenvironment as well (Duan et al. 2020).

1.2.3 The Immunosuppressive Tumour Microenvironment

Beyond the already demanding task of targeting a disease with such genetic instability and self-like properties, one of the main concerns in the field of adoptive cell transfer for cancer

therapy is the immunosuppressive microenvironment established and maintained in and around the tumour site to evade immunosurveillance.

Although every cancer is different in its driving pathways and relationship with the surroundings, several are the players of the microenvironment other than the cancer cells themselves: from stromal cells, like fibroblasts, endothelial cells and pericytes, to innate and adaptive immune cells, like macrophages, DCs, NK cells, Tregs and T cells in general.

In terms of the anti-cancer immune response, the paradigm is represented by CD8 T cells, T_H1 CD4 T cells and NK cells. T cells, both CD8 and CD4 of the T_H1 type, are considered the most desirable source of anti-cancer immunity due to their adaptive nature and the ability to recognise huge repertoires of antigens. Their stringent selection in the thymus entails a balanced recognition of 'self' and 'foreign'; in addition, they are tightly regulated *in situ* by a system of co-stimulatory and co-inhibitory receptors for a finely tuned response, with a range of cytokines (e.g. IFN-γ, TNF-α).

Thanks to their ability to screen MHC-presented peptides, they are the only component of the immune system proficient in intracellular scrutiny; this allows detection of altered cellular programs typical of cancer, without relying on surface antigens. Clonal expansion following activation allows rapid up-scaling of the immune response and their immunological memory formation prevents relapse. Conventional T cells, however, rely on antigen presentation and MHC expression to function.

On the other hand, NK cells are cytotoxic lymphocytes of the innate immune system, capable of MHC-independent responses against tumours based on a strategic set of receptors that recognise cellular stress signals (e.g. NKG2D) (Bauer et al. 1999) and distinguish 'self' from

'foreign' (e.g. KIRs) (Iannello et al. 2008). Crucially, they can target MHC-negative cells, thereby limiting tumour escape by MHC downregulation. Upon activation, they secrete cytotoxic cytokines, such as IFN-γ and perforin (Wilk and Blish 2018).

It has been increasingly shown that the anti-cancer immunity firmly relies on the coordination of CD4, CD8, and APCs, rather than a compartmentalised effort by a single cell subset (Spitzer et al. 2017). This is demonstrated by the significant link between clinical outcome and presence of tertiary lymphoid structures (TLS) at the tumour site, as recently reviewed by Munoz-Erazo et al. (2020). TLSs, in fact, act as hubs for the anti-cancer response and facilitate communication between APCs and effector cells, promoting their priming and maturation. In this context, while T and NK cells are the quintessential effectors, DCs are considered the most proficient APCs and therefore the essential orchestrator of the immune response against tumours. However, many are the ways in which the tumour can disrupt this equilibrium (Alfei, Ho, and Lo 2021).

1.2.4 Mechanisms of Immunosuppression

Tolerogenic cytokines, such as TGF-β and IL-10, are found in higher proportion in the cancer microenvironment; they can be secreted by the tumour itself or by third parties, such as Tregs. Overall, they impart an immunosuppressive program, by inducing anergy on activated T cells and polarising naïve T cells into iTregs. In addition, TGF-β was shown to cause CCR7 downregulation on DCs, ablating their ability to home back to the lymph nodes and prime the adaptive immune response (Imai et al. 2012).

Meanwhile, tumour downregulation of certain chemokine ligands contribute to reduced immune trafficking, such as in the case of reduced CCL4 and CCL5, shown to impair DC infiltration (Khuu et al. 2007). On the other hand, tumour upregulation of CD47 and other "do not eat me" signals are able to disrupt activation of anti-tumour pathways, like the cGAS-STING pathway for malignant DNA sensing (Huang et al. 2020).

Checkpoint receptors on the T cell surface (e.g. PD-1) have the function to dampen the immune response upon threat clearance; however, upregulation of their ligands (e.g. PD-L1, PD-L2) in the tumour microenvironment has been shown to be a key mechanism of immuno suppression (Chen et al. 2019).

Other cytokines, such as IL-6, G-CSF and GM-CSF, and chemoattractants, such as CXCR2 and CXCR4 ligands, are known to mobilise immature myeloid cells from the bone marrow and blood monocytes and recruit them to the site, resulting in their polarisation to immunosuppressive phenotypes, such as myeloid derived suppressor cells (MDSCs) or M2 polarised macrophages (Marvel and Gabrilovich 2015).

1.2.5 MDSCs

Polarised myeloid cells (i.e. MDSCs) represent a valuable resource for the tumour. They can perpetuate inflammation via IL1-β and TNF-α and ROS production, thereby increasing the rate of tumour proliferative pathways (e.g. NF-κB) and malignant progression. They can express metalloproteinases (e.g.MMP8 and MMP9) and angiogenic factors (VEGF), hence remodelling the extracellular matrix and supporting tumour invasion of adjacent tissues. Finally, they are

key suppressors of T cell responses, achieved by nutrient depletion in the microenvironment (F Veglia, Sanseviero, and Gabrilovich 2021).

Human MDSCs lack a unique marker of identification. Instead, Bronte, Gabrilovich and colleagues agreed on a phenotypic strategy which defines monocytic (M)-MDSCs as $CD14^{+}$, $CD33^{+}$, $CD11b^{+}$, $HLA\text{-}DR^{low}$, and granulocytic (G)-MDSCs as $CD15^{+}$, $CD33^{+}$, $CD11b^{+}$ (Bronte et al. 2016). As for their function, the main feature distinguishing MDSCs from other states of myeloid polarisation is the ability to markedly suppress T cell proliferation.

Whether or not addressed as MDSCs, cells sharing the phenotype defined above appeared in multiple articles and were described as an expanding population in the peripheral blood of patients with cancer. These ranged from 'defective DCs' reported in head and neck lung and breast cancer by Almand et al. (2001), to the heterogeneous phenotypes characterised in lung cancer (Sangaletti et al. 2021), gastric cancer (Oya, Hayakawa, and Koike 2020) neuroblastoma (Frosch, Leontari, and Anderson 2021) and glioma (Grabowski et al. 2021), including a recent multi-centre collaborative effort (Cassetta et al. 2020).

While these cells have a role in ending acute inflammation after threat clearance and promoting wound healing, in cancer they effect is highly damaging.
MDSCs can be recruited and expanded under tumour-derived GM-CSF and G-CSF signals and maintained under environmental T_H2 cytokines (e.g. IL-4, IL-13) (Dolcetti et al. 2010; Gabrilovich, Ostrand-Rosenberg, and Bronte 2012).
It has been shown that arginine depletion by upregulation of arginase or inducible nitric oxide synthase (iNOS) is sufficient for myeloid cells to cause local suppression of T cell proliferation

(Van de Velde et al. 2017). However, there are multiple other mechanisms they include to perpetuate immunosuppression: tryptophan degradation by expression of indoleamine 2,3 deoxygenase (IDO), upregulation of PD-1 ligands (PD-L1, PD-L2), production of immunoregulatory by-products such as NO and kynurenine and cytokines such as IL-6 and IL-10 (Murray, 2016). Despite the short life-span, the constant stream of recruitment from the bone marrow determines their enduring effects.

Crucially, these cells are shown to be a decisive element for the success of the anti-cancer immune response, be it endogenous or adoptive (Arina and Bronte 2015).
A recent phase I/II trial on an optimised third generation anti-GD2 CAR T cell against neuroblastoma reported compelling positive results in terms of initial tumour reduction; however, a key mechanism of therapy resistance involving MDSCs consistently prevented sustained disease regression and favoured relapses (Tumino et al. 2021).
In addition, several studies, including Heczey and colleagues (2017), highlight the expansion of a population of myeloid cells in the PBMCs of neuroblastoma patients, creating a strongly immunosuppressive niche and correlating with prognosis of high-risk disease, metastasis and response to therapy (Asgharzadeh et al. 2012; Pistoia et al. 2013).

Multiple therapeutic strategies aimed at the blockade of their recruitment (e.g. CXCR2 blockade) or their suppressive functions (e.g. arginase inhibitors, IDO inhibitors, COX2 inhibitors) are currently been tested in pre-clinical models or early phase trials (F Veglia, Sanseviero, and Gabrilovich 2021). Nevertheless, the identification of a viable therapeutic strategy to target their expansion represents one of the key priorities in oncology.

1.2.6 Nutrients Restriction in the Tumour Microenvironment

The fast-paced proliferative state of the tumour and its poor vascularisation determine a nutrient-poor TME with intense competition for essential carbon sources.
Low glucose levels in the TME have been shown to affect T cell IFN-γ production and effector functions (Chih-Hao Chang et al. 2013; Ho et al. 2015). Indeed, nutrient availability has also been linked to epigenetic regulation of T cell exhaustion (Franco et al. 2020).
Conversely, $FoxP3^+$ Tregs can function in environments poor in glucose and high in lactate (Angelin et al. 2017). Therefore, the nutrient scarce nature of the TME dictates a selective pressure.

In addition to glucose, certain amino acids are also found in limited availability in the TME. Amino acids are a fundamental component of life and their role exceeds protein synthesis; they take part in ATP production, redox balance, nucleotide synthesis and epigenetic modifications. Proliferation and immune effector functions heavily rely on amino acid availability, as demonstrated by the prompt upregulation of amino acid transporters and amino acid sensing machinery upon T cell activation (Kelly and Pearce 2020; Marchingo et al. 2020).

Indeed, tumours and other pro-tumour cells (i.e. MDSCs) in the TME employ the depletion of essential and conditionally essential amino acids as an immunosuppressive strategy. Typical examples are depletion of L-tryptophan and L-arginine, achieved by increased activity of their catabolic enzymes, i.e. indoleamine 2,3-dioxygenase (IDO) for L-tryptophan, iNOS and arginase for L-arginine. IDO expression is a negative prognostic marker for several cancers,

e.g. oesophageal adenocarcinoma and NSCLC, and it is usually associated with increased T cell exhaustion signatures (Loeser et al. 2020; Ludovini et al. 2021).

1.2.7 Arginine Depletion and T Cell Function

L-arginine is a semi essential amino acid, assimilated mainly through diet, and the precursor for protein and polyamine biosynthesis. L-arginine can be catalysed by NOS into L-citrulline and nitric oxide (NO), or alternatively by arginase (Figure 6).

Arginase is the first of five enzymes of the urea cycle, hydrolysing L-arginine into L-ornithine and urea. The enzyme exists in two isoforms: the cytosolic arginase 1 and the mitochondrial arginase 2. Despite differing in size (322 and 354 amino acid respectively), arginase 1 and arginase 2 catalyse the same biochemical reaction and share comparable kinetics (Wu and Morris 1998). Nonetheless, the expression patterns of the two isoforms are distinct: arginase 1 is mainly found in hepatic cells as part of the ammonia detoxification strategy and within activated myeloid cells for immunomodulating purposes; arginase 2 seems to be more ubiquitously expressed to oversee intracellular L-arginine homeostasis (Bronte and Zanovello 2005). In fact, the role of arginase 2 is attributed to the downstream synthesis of proline and polyamines (putrescine, spermidine and spermine).

Increased arginase 2 expression was shown to characterise the immunosuppressive TME of acute myeloid leukaemia (AML) and neuroblastoma and L-arginine depletion from the microenvironment was shown to be the main cause behind the immune failure in those cancers (Mussai et al. 2013, 2015).

High consumption of L-arginine via expression of arginase 1 was the first trait associated with T cell suppression by MDSCs (Raber, Ochoa, and Rodríguez 2012). It is well established that an L-arginine-poor microenvironment leads to impaired T cell activation and proliferation. In fact, low L-arginine culturing conditions were shown to induce abnormal expression of the CD3-ζ chain of the TCR and cyclin D-dependent cell cycle arrest. (Zea et al. 2004; Rodriguez, Quiceno, and Ochoa 2006). More recently, this was found to be coordinated by the cellular nutrient sensing machinery Rictor/mTORC2 (Van de Velde et al. 2017).

To sustain a post-stimulation clonal expansion, T cells need biosynthetic precursors. In this regard, L-ornithine plays an important upstream role, by providing the first step into the synthesis of polyamine (e.g. putrescine, spermidine and spermine) catalysed by ornithine decarboxylase (ODC). Polyamines in particular have recently been found useful precursors of hypusine and are important for adequate transcription and translation activity (Casero, Murray Stewart, and Pegg 2018).

By using a ^{3}H-labelled L-arginine and tracing it into L-ornithine and the polyamine synthetic pathways, Geiger et al. (2016) showed that upon activation, T cells increase considerably the uptake of L-arginine for polyamine synthesis.

A further proof of the importance of polyamines in T cell function is that Wang et al. (2011) found that supplementing polyamines reverses the effects of L-glutamine starvation.

Ultimately, from a tumour's perspective, L-arginine metabolism is crucial beyond the suppressive effects on the T cells. Tumour cells commonly rely on exogenous L-arginine, given that its synthesis is dispendious in energy. Indeed, L-arginine depletion has been hypothesised as a therapeutic approach in cancers that show L-arginine auxotrophy. This is

the case for cancers defective in argininosuccinate 1 (ASS1) or ornithine transcarbamylase (OTC), and therefore not able to convert L-citrulline and L-ornithine back into L-arginine respectively, such as acute lymphoblastic leukaemia, hepatocellular carcinoma, melanoma among others (Fultang et al. 2016; De Santo et al. 2018).

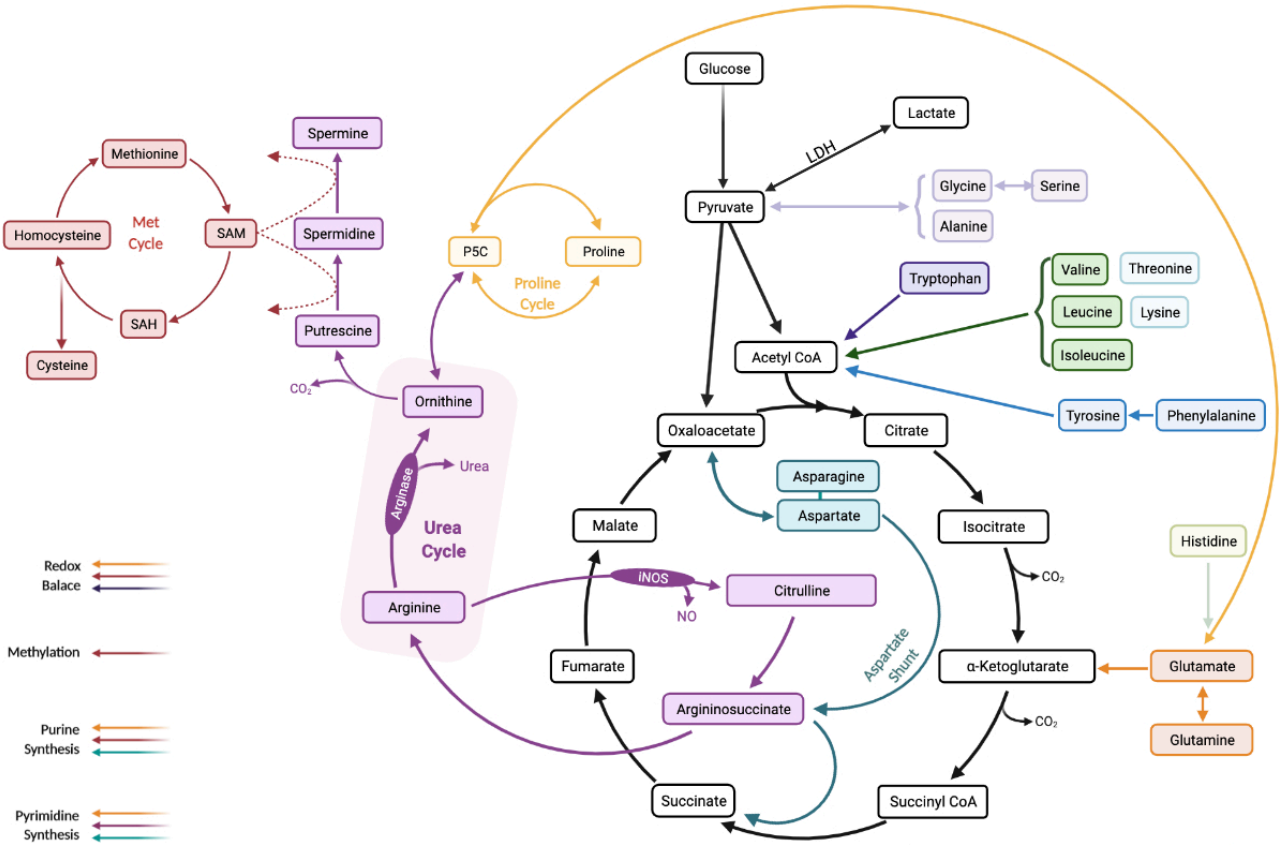

Figure 6: Schematic overview of the main pathways around L-Arginine metabolism.

L-arginine catabolism by arginase can support different pathways, including L-proline cycle, polyamine synthesis and TCA cycle. Created using BioRender.

1.3 Cancer Immunotherapy

The field of cancer immunotherapy has been object of an exponential growth over the past 20 years, as the role of the immune system in the treatment of cancer consolidated its importance. Milestones, like the approval of anti-CTLA-4 as the first checkpoint blockade therapy and the first in human CAR-T cell therapy, completely revolutionised the therapeutic landscape. Cancer immunotherapy is based on the use of cytokines, monoclonal antibodies and immune cells to reshape and modulate the anti-cancer immune response.
For the purpose of this thesis, we will focus our attention on cell-based therapies, in particular chimeric antigen receptor-T cells.

1.3.1 Cell-Based Therapies

Due to their relative abundance in the peripheral blood and their *in vitro* resilience, T cells are particularly suited to be engineered to acquire tumour specificity. In addition, T cells present the tools required for a successful and enduring cancer clearance: the ability to produce a wide range of cytotoxic and cytolytic products (e.g. TNFα, IFN-γ, perforin and granzymes), a proliferative programme induced upon activation and a life-long memory of the antigen.
Depending on the specific tumour antigen to be targeted, T cells can be engineered to express a synthetic TCR, useful for the detection of intracellular immunogenic peptides in a MHC-restricted fashion, such as in the case of NY-ESO-1-specific TCRs (Rapoport et al. 2015). Alternatively, they can be engineered to bear a chimeric antigen receptor (CAR), able to detect surface antigens independent of MHC presentation.

While most studies rely on lentiviral or retroviral platforms for the delivery of the transgenes, the utility of transposon systems has also been shown (Magnani et al. 2020).

At the moment, cell-based therapies propose to start from the patients' own T cells, obtained from the peripheral blood by leukapheresis, transduced with the gene encoding the novel receptor, expanded *ex vivo* and finally re-infused into the patient.

Leukapheresis and *ex vivo* GMP protocols represent a limiting factor and a manufacturing challenge in this therapeutic context. Therefore, researchers are working on the development of 'off the shelf' allogeneic CAR-T cells, using different gene editing technologies to produce readily available T cells from universal donors, with limited risk for graft-versus-host disease (Depil et al. 2020; Li et al. 2020).

1.3.2 Chimeric Antigen Receptor-T Cells

The first account of chimeric antigen receptor (CAR)-T cells engineering dates back to 1989 (Gross, Waks, and Eshhar 1989) and the field has since seen a huge expansion.

The conceptual design of a chimeric antigen receptor usually includes two key elements: an antigen-binding domain, obtained by fusing the variable regions of the heavy and light chains of an antibody, termed scFv; linked to a signalling domain, derived from the intracellular portion of the TCR, i.e. the CD3ζ chain, allowing activation signalling upon scFv engagement (Figure 7).

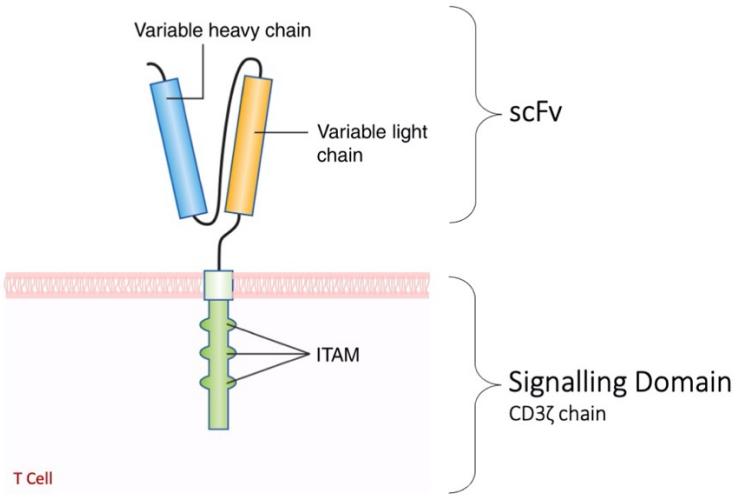

Figure 7: Structure of a basic chimeric antigen receptor.

CAR-T cells bear synthetic receptors made up of an antibody-derived scFv, as antigen binding region, and a TCR-derived CD3ζ chain, as signalling domain. Adapted from: Tokarew et al. 2019.

1.3.3 CAR Design

The original relatively simple framework of a CAR has been enriched and explored over time in several pre-clinical and clinical investigations in order to improve its function. An example of these adjustments is the inclusion of a variety of co-stimulatory sequences to compensate for the lack of co-stimulation at the tumour site and allow optimal signalling for the activation of the cell. The most common co-stimulatory molecules used in CAR T cell design are: CD28, 4-1BB, OX40 and CD27 (C. Imai et al. 2004; Maher et al. 2002; Song et al. 2012). Interestingly, the choice of co-stimulatory signal seems to have an impact on the long-term fate of the re-infused cells, their metabolic program, phenotype and persistence. Comparing different co-stimulatory molecules, several groups showed that CD28 co-stimulation yielded a population of engineered cells that expanded more rapidly, while 4-1BB signalling showed an improved

long term survival. In fact, CD28 co-stimulation was associated to a more glycolytic metabolism, whereas 4-1BB was characterised by higher mitochondrial involvement (Kawalekar et al. 2016; Majzner et al. 2020).

A further aspect having an impact on CAR performance are hinges and spacers. Despite not having a direct role in signalling, these sequences aim to distance the scFv domain from the T cell membrane and can be crucial for CAR mobility and interaction with the targets (Hudecek et al. 2015). Certain antigens might be found out of the reach radius of the receptor and an elongated molecule could represent a valuable improvement. Guest et al. (2005) analysed four CARs, directed at four different antigens, and found that in two cases (i.e. anti-neural cell adhesion molecule and anti-5T4 CARs) the spacer region was essential for optimal T cell activity; while, in the case of the anti-CD19 and anti-CEA (carcinoembryonic antigen) CARs, it had a detrimental effect.

Overall, the importance of CAR design cannot be overstated, as minimal changes to the structure lead to fundamental repercussions in terms of functionality and efficacy.

1.3.4 The Success in Haematological Malignancies

Adoptive transfer of CAR T cells was first successfully tested in human against B cell malignancies, as reported by Kochenderfer et al. (2012). The CAR was targeted at the CD19 marker, a surface molecule widely present on the B cell lineage, and it was combined to the CD3-ζ activation domain, as well as two co-stimulatory regions: CD28 and 4-1BB. The results of the first clinical trial using autologous anti-CD19 CAR T cells demonstrated their ability to

specifically recognise $CD19^+$ targets *in vivo* and maintain a long-term eradication of the malignancy: out of the 8 patients enrolled, 6 obtained an objective remission.
Several other studies went on to confirm these findings with similar success rates (Davila et al. 2014; Fesnak, June, and Levine 2016; Maude et al. 2014). These results, rightfully generating a substantial wave of enthusiasm, resulted in the FDA approval of anti-CD19 CAR-T cell therapies for B cell acute lymphoblastic leukaemia (B-ALL) and lymphoma in 2017 and 2018.

CD19 is not the only CAR-T cell target successfully developed. Other B cell-related targets have been tested, producing promising trial results. One is CD22, for which complete remission during trial was achieved by over 80% of patients in the highest treatment group (Fry et al. 2018). The second is a B cell maturation antigen (BCMA)-directed CAR for multiple myeloma patients, which elicited 85% objective responses in phase 1 (Raje et al. 2019).

Undoubtedly, some issues need to be further addressed: firstly, the management of the toxicity derived from cytokine release; secondly, the possibility of tumour-evasion via strategic antigen downregulation (Park et al. 2018). Nonetheless, CAR T cell therapy in the context of haematological malignancies has shown the ability to eradicate the disease and persist in some patients for over 10 years after T cell re-infusion; it therefore represents a successful therapeutic approach.

1.3.5 The Underwhelming Results in Solid Cancers

In clear divergence with the success in haematological malignancies, CAR-T cell therapy in solid tumours failed to obtain the stark results expected.

CAR-T cells in the solid TME have been reported to display underwhelming expansion and persistence (Heczey et al. 2017) and increased exhaustion (Long et al. 2015).

Solid tumours present an additional range of challenges compared to haematological malignancies. Firstly, the prevalence, distribution and density of the target antigen are often suboptimal in solid tumours; in fact, it has been shown through mathematical models and pre-clinical studies that there are specific antigen density thresholds required for optimal T cell engagement (James et al. 2010; Walker et al. 2017; Yoda et al. 2019).

Many target antigens are currently being explored for solid tumour targeting (Castellarin et al. 2018). The most clinical data so far has been obtained in the context the anti-EGFRvIII CAR, for the treatment of glioblastoma (Johnson et al. 2015); the anti-Mesothelin CAR, against the surface molecule overexpressed in pancreatic, ovarian and other cancers (Tanyi et al. 2015); the anti-GD2 CAR, developed against neuroblastoma neuroblastoma (Majzner et al. 2022); the anti-HER2 CAR, for Trastuzumab-resistant breast cancer, as well as melanoma and CNS tumours (Vitanza et al. 2021).

Nevertheless, even in presence of well consolidated solid tumour antigens, the results are remarkably poor. This is because, the tumour microenvironment creates a range of physical and immunological barriers impairing the anti-cancer immunity, including hypoxia and other metabolic checkpoints, such as amino acid depletion (Watanabe et al. 2018).

Following from this, our focus will move specifically to CAR-T cells targeting one of the most explored antigens in the field of solid tumour immunotherapy, the disialoganglioside GD2, as it epitomises the typical failure of CAR-T cell in solid cancers.

1.3.6 The Case Study of Anti-GD2 CAR-T Cell Therapy

GD2 represents one of the most valid solid tumour antigens; its first targeting with monoclonal antibodies dates back to 1987 (Cheung et al. 1987).
GD2 is a glycosphingolipid with limited expression on healthy tissue, but it is overexpressed by a range of tumours of neuroectodermal origin, e.g. neuroblastoma, melanoma and sarcomas (Dobrenkov et al. 2016; Kailayangiri et al. 2012). In $GD2^+$ tumours, its expression is uniform and substantial (Balis et al. 2018). In addition, it is found to enhance tumour proliferation, migration and invasiveness (Julien et al. 2013; Nazha, Inal, and Owonikoko 2020; Sujjitjoon et al. 2021), therefore reducing the likelihood of tumour escape with GD2-negative malignancy.

Despite the seemingly ideal conditions posed by this antigen, CAR-T cell therapies fail.
An example is given by the anti-GD2 CAR trial started by Pule et al. (2008) and subsequently followed up by Louis and colleagues (2011). In brief, of the 19 patients enrolled in the trial, only 11 (the 58%) had detectable CAR T cells in circulation in or after the 6th week from infusion. Of these, 3 patients achieved complete remission (CR): patient 1035, whose CAR T detection in the peripheral blood was among the highest at the 6 week time point; patient 1290, for whom the engineered cells were recorded until week 48; patient 1144, whose cells were circulating almost 4 years after having received the therapy (Figure 8 identifies the 3 patients with complete remissions).

What can be deduced from these data is that anti-GD2 CAR immunotherapy has the potential ability to eradicate $GD2^+$ tumours. Secondly, CAR T cell persistence in the peripheral blood is a valuable indicator of positive clinical outcome and it reflects expansion and efficacy.

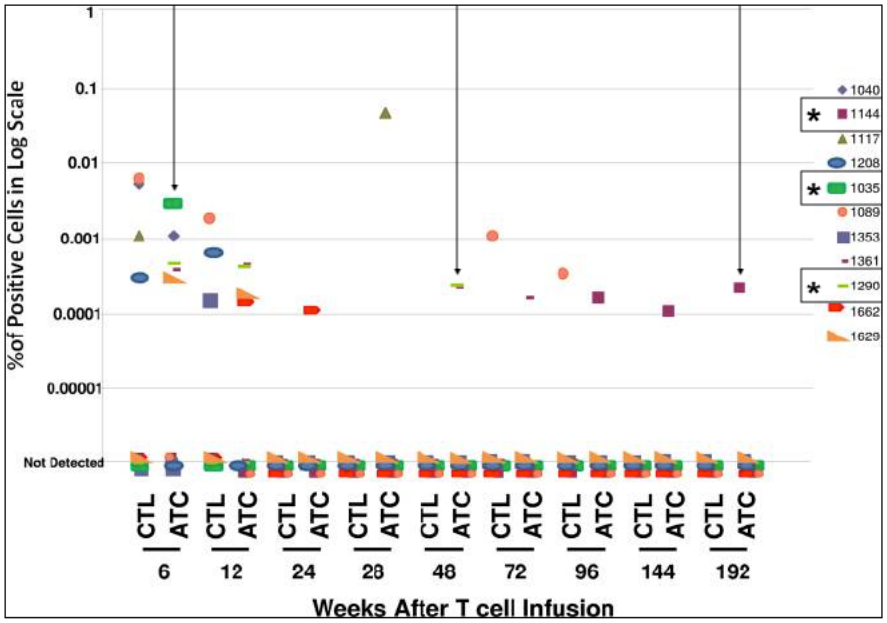

Figure 8: Long-term analysis of anti-GD2 CAR-T cell persistence in clinical trial NCT00085930.
Persistence of activated CAR-T cells (ATC) or EBV-specific CAR-T cell (CTL) in the peripheral blood of neuroblastoma patients. Detection was obtained by real-time quantitative PCR. Patient IDs are shown on the right. Adapted from (Louis et al. 2011)

Neuroblastoma, as well as other solid cancers, has the ability to recruit copious amounts of inflammatory myeloid cells, which are demonstrated to promote relapse and metastatic disease (Asgharzadeh et al. 2012). Moreover, Fultang, et al. (2019) were able to pinpoint the reciprocal relationship between tumour and microenvironment, demonstrating the ability of the myeloid cells-derived IL-1β and TNF-α to induce tumour expression of arginase 2, thereby depleting the microenvironment of L-arginine and perpetuating a T cell exclusion zone.
In conclusion, only by addressing the challenges of the tumour microenvironment, CAR-T cells will be able to perform their anti-cancer programme.

1.4 Options for Improved CAR-T Cell Therapy

1.4.1 Addressing CAR-T Cell Safety

Cell therapies are undoubtedly a powerful cytotoxic tool when acting according to their purpose. The side-effects are substantial, but most times they are medically manageable. However, on-target off-tumour toxicity is an eventuality to always consider, given it goes beyond the choice of the target itself and involves CAR design, therapeutic regimen and patient selection. For instance, an interesting case is presented by the two CD19-directed CAR-T cell trials by Juno, JCAR015 and JCAR017: despite sharing the same CAR scFv, the outcomes were markedly different, with JCAR015 having to be stopped due to fatal neurotoxicity. This was due to relatively minor differences in co-stimulatory domains used (CD28 and 4-1BB respectively), CD8 to CD4 T cell ratio (fixed in JCAR017 but not in JCAR015) and disease indication (ALL and lymphoma respectively)(Poh, 2018).

The growing need to address safety issues and potential long term on-target and off-target toxicity of cell-based immunotherapies led to the development of several CAR-T cell depletion strategies, normally in-built into the CAR construct itself in the form of suicide genes.
An example is represented by the integration of inducible caspase 9 (iCasp9), which enables the cell to initiate apoptosis upon patient administration of a small-molecule drug (Di Stasi et al. 2011), or the herpes simplex virus thymidine kinase (HSV-TK), which provide the cells with antiviral medication sensitivity (Ciceri et al. 2009).
Similarly, other research groups have investigated highly efficient antibody-based depletion mechanism, relying on the autologous immune response (NK cells, phagocytic cells and

complement) to neutralise the engineered cells. This is the case of the functionally inert truncated EGFR (EGFRt), shown to be consistently targeted by the anti-EGFR mAb cetuximab with consequent ablation of the CAR-T cells *in vivo* (Paszkiewicz et al. 2016).
Other suicide genes conferring susceptibility to antibody depletion have been investigated, such as CD20 to be targeted with the anti-CD20 rituximab (Serafini et al. 2004; Griffioen et al. 2009) and a short tag derived from human c-Myc, recognisable by a Myc-specific Ab (Kieback et al. 2008).

These systems provide a valuable opportunity for the pharmacological control of cell therapies. Nonetheless, a comprehensive analysis of all indexed CAR-based clinical trials in 2020 evidenced that only 49 out of the 501 active trials at the time (9.8%) included a safety system within the CAR construct (MacKay et al. 2020). This might be a reflection of the manufacturing challenge represented by the transduction of larger constructs.

1.4.2 Addressing CAR-T Cell Challenges Within the Microenvironment

One of the shortcomings of current CAR-T cell therapies is trafficking and persistence at the tumour site due to lack of environmental stimulation. One solution proposed to transduce T cells to express a conditioning cytokine together with the CAR, such as the examples generated in the labs of Chmielewski and Abken, investigating both IL-12 and IL-18 secreting CAR-T cells preclinically (Chmielewski and Abken 2012, 2017). This type of 4th generation design has been named TRUCK (or T Cells Redirected for Universal Cytokine Killing) T cells. Similar modifications have been experimented in non-conventional T cells in order to obtain

an even greater TME resistance. This is the case of IL-15-secreting anti-GD2 CAR-iNKT cells currently awaiting results from the phase I trial (NCT03294954) (Xu et al. 2019).

The specific cytokine signature of certain tumours can also be exploited to the benefit of the engineered immunity. Pancreatic cancer is characterised by high levels of the T_H2 cytokine IL-4. Mohammed et al. (2017) proposed the use of a CAR-T cell with an inverted cytokine receptor with an IL-4 receptor exodomain associated to an IL-7 endodomain, modulating the effect of IL-4 signalling.

In a more pan-cancer approach, CAR-T cells expressing dominant-negative TGF-β receptor type 2 were shown to be safe and increasingly efficacious, inducing some complete responses (Bollard et al. 2018).

In other respects, CAR-T cell research has been developed to counteract exhaustion signals received from the TME. Reduced tumour growth and exhaustion resistance were observed by CAR-T cells overexpressing BATF (Seo et al. 2021) and c-Jun (Lynn et al. 2019).

In addition, CRISPR-Cas9 editing or deletion of PD-1 receptor showed the ability to overcome immunosuppression by PD-L1$^+$ tumours *in vivo* (Cherkassky et al. 2016; Ren et al. 2017) and seem to persist well in the first patients this has been tested on (Stadtmauer et al. 2020).

Besides strategies involving CAR-inbuilt mechanisms, a vast array of combination therapies to associate to CAR-T cell administration are being investigated. These include checkpoint blockade therapy and delivery of co-adjuvant cytokines, either delivered systemically or intra-tumourally (Agliardi et al. 2021).

1.5 Aims and Objectives

Overall, this thesis intends to build on the prior knowledge around the failure of CAR-T cell therapy in solid tumours and combine it to the knowledge generated within our laboratory regarding the immunosuppressive tumour microenvironment.

In particular, our study will be led by two distinct hypotheses:

1. We hypothesise that MDSCs can be targeted by an existing drug, Gemtuzumab Ozogamicin, which will ablate their ability to suppress T cells.

2. We hypothesise that by inducing constitutive expression of arginase in CAR-T cell, we provide a metabolic advantage that will result in increased persistence in the TME of solid tumours.

For what concerns the first hypothesis, we aim to:

- Characterise MDSCs across a range of solid cancers and assess the feasibility of repurposing Gemtuzumab Ozogamicin to selectively deplete MDSCs;

- Determine whether Gemtuzumab Ozogamicin treatment on MDSCs results in the rescue of the autologous and engineered immunity against cancer.

For what concerns the second hypothesis, we aim to:

- Modify an anti-GD2 CAR construct to contain and express arginase enzymes and investigate the effect of the modification in a cell line model of T cells;

- Translate the investigation of the modified anti-GD2 CAR into primary T cells and confirm whether the improved ability to catabolise L-arginine imparts an advantage for the anti-tumour immunity.

2. MATERIALS AND METHODS

2.1 Research Project Ethics

The study received ethical approval from the Regional Ethics Committee (REC: 10/H0501/39).

2.2 Cell Culture

2.2.1 Patient Samples

Blood samples were obtained from the Birmingham Children's Hospital or the HBRC Tissue Bank (Birmingham) in heparinised tubes from adult and paediatric patients of different cancer diagnosis: lung (n = 21), pancreas (n = 7), colon (n = 36), brain (n = 7), head and neck (n = 8), prostate (n = 10), breast (n = 12), melanoma (n = 5) Wilms' (n = 5), neuroblastoma (n = 31), Ewing's (n = 2), non-Hodgkin's lymphoma (n = 2), rhabdomyosarcoma (n = 2) at diagnosis, prior to treatment. They were processed within 24h of sample collection.

2.2.2 Cell Line Maintenance

The suspension cell line Jurkat (human T lymphocyte, ATCC) was used as a proof-of-concept model of T cells. They were routinely cultured in sterile T75 flasks in R10% medium (

Table 1) at 37°C, 5%CO_2 and passaged 1:10 when optimally confluent.
Similarly, neuroblastoma adherent cell lines SK-N-AS, LAN-1, IMR-32 and KELLY (ATCC) were maintained in sterile T75 flasks in R10%. At confluency, the culturing medium was removed and TrypLE (Gibco) was used to detach the cells from the flask. The cells were washed in

R10% and subcultured at a ratio of 1:10. Cell lines were routinely checked for Mycoplasma infection by PCR analysis (Sigma) and utilised between passage 3-12.

2.2.3 Preparation of PBMCs from Whole Blood

Peripheral blood mononuclear cells (PBMCs) were obtained from healthy aphaeresis cones provided by the NHSBT Blood Bank (Birmingham) or venous blood from patients or healthy controls and processed on the same day of collection. The blood products were diluted in RPMI to a suitable concentration and layered onto Lymphoprep (StemCell Technologies), at a volume ratio of 2:1. The tubes were centrifuged for 30 minutes at 800×g without brakes, to allow blood component separation by density gradient. The PBMC layer was gently collected, washed in RPMI and centrifuged at 300×g for 10 minutes, twice.

2.2.4 Magnetic Assisted Cell Sorting

Cell sorting of desired populations, unless specified otherwise, was obtained by magnetic-assisted cell sorting (MACS)..

In the case of MDSC isolation, freshly isolated PBMCs from patients or healthy donors were resuspended in sterile ice-cold phosphate-buffered saline (PBS) pH7.2 (Gibco), 0.5% bovine serum albumin (BSA) fraction V (Merk), 2mM EDTA (ThermoFisher) (80µl/10^7 cells) and CD14 (for M-MDSCs) or CD15 (for G-MDSCs) cells were magnetically labelled with the appropriate Miltenyi Biotec MicroBeads kit (20µl/10^7 cells). After 15 minutes on ice, the cells were washed in abundant buffer, spun for 5 minutes at 300xg and resuspended in 1ml of buffer to be passed through an LS magnetic column applied to a QuadroMACS Separator (all Miltenyi Biotec). Labelled CD14 and CD15 cells, strongly interacting with the magnetic column, were

finally released upon removal of magnetic field and used for downstream applications.
In the case of CAR-transduced cells, the CD34 tag was used as a sorting marker. Similarly to what described above, mixed populations of transduced T cells were resuspended in 80µl/10^7 cells of buffer and 10µl/10^7 cells of anti-human CD34 MicroBeads, labelling the CAR+ population. Following 15 minutes on ice, the cells were washed in abundant buffer, spun at 300xg for 5 minutes and resuspended in 1ml of buffer prior to being passed through an MS magnetic column, applied to a QuadroMACS Separator. Labelled CD34+ cells were released from the magnetic column upon removal from the magnetic field and used for downstream applications.

2.2.5 Fluorescence-Activated Cell Sorting

Fluorescence-activated cell sorting (FACS) was employed preferably to sort small and precise populations of cells, e.g. transduced CAR+ T cells.

Surface staining was performed using a 1:50 dilution of the antibody against the CAR-specific marker (anti-human CD34, Biolegend), conjugated to an APC fluorophore. The mixed population, suspended at a density of up to 1x107cells/ml of sterile FACS buffer, was run through a FACSAria II (BD Biosciences) and the selected cells collected according to the sorting gate P3 illustrated in Figure 9. The gate P3 was placed in order to collect the CD34 high population of T cells. The sorted cells were collected in sterile conditions and employed in downstream assays.

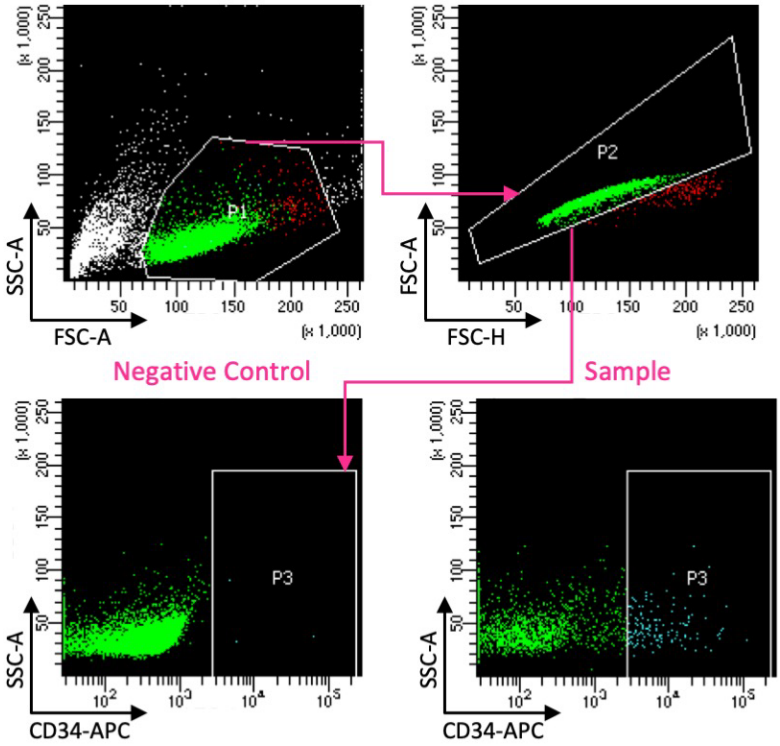

Figure 9: CD34⁺ population sorting strategy by FACS

Representative dotplots of the gating strategy employed to enrich CD34⁺ cells within a mixed T cell population. Transduced T cells were stained with anti-human CD34-APC antibody diluted 1:50 for 20 minutes at 4°C. The cells were subsequently washed by centrifugation with abundant FACS buffer, resuspended in a suitable volume to obtain a cell suspension of $2x10^6$ cells/ml and finally run on the BD FACSAria II cytometer. The cells of interest were selected from the morphology gate forward scatter (FSC) vs side scatter (SSC); single cells were selected from the hight vs area of the FSC and the CD34-high population (P3) was determined. Cells within the sorting gate P3 were collected for downstream applications.

2.2.6 *In vitro*-Derived MDSCs

In order to obtain *in vitro*-derived MDSCs, MACS-sorted populations of CD14⁺ cells obtained from the PBMCs of healthy leukocyte cones were plated at $1x10^6$ cells/ml/well in 24 well plates, in presence of 1:1 ratio of R10% and the culturing supernatants of a range of cancer cell lines, referred to as TCM. Polarisation was allowed to occur at 37°C, 5%CO_2 during the following 48 hours.

2.2.7 Patient-Derived MDSCs

MACS-sorted populations of $CD14^+$ cells were obtained from the PBMCs of cancer patients' blood and promptly used in downstream assays. They are also referred to as $CD33^+$ or MDSCs, because of their CD33 expression and ability to suppress T cells later confirmed.

2.2.8 Gemtuzumab Ozogamicin Treatment

In vitro-derived and patient-derived MDSCs were seeded in 24 well plates at a density of maximum $1x10^6$ cells/ml in R10% and weretreated with 1µg/ml of Gemtuzumab Ozogamicin for 24 hours at 37°C, 5% CO_2, unless otherwise stated in the specific figure legends.

2.2.9 Primary Tumour Digestion and Tumour Conditioned Media

Primary neuroblastoma or glioblastoma tumours were occasionally received from the Birmingham Children's Hospital or the HBRC Tissue Bank.

They were mechanically broken down using a scalpel and incubated with type IV collagenase (Thermo Fisher) for up to 1 hour at 37°C, 5% CO_2. They were further mechanically digested by applying pressure on a strainer and gently stirred with the bottom of a syringe until a single cell suspension was obtained. After centrifugation the digested tumours were assessed for GD2 expression by flow cytometry. In case of GD2 presence, they were used *in vitro* as target cells in downstream assays; in case of GD2-negative neuroblastoma tumours, they were resuspended in a suitable volume of R10% and cultured for 48h at 37°C, 5% CO_2 in order to obtain tumour conditioned media (TCM).

2.2.10 Cryopreservation

Cell lines and T cells were cryopreserved in FBS, 10% DMSO (i.e. Freezing Medium) (Table 1). 5 to 15x10^6 of cells were spun at 300xg for 5 minutes, resuspended in Freezing Medium and transferred into cryovials (Nunc) to be promptly transported into -80°C storage using a Mr.Frosty freezing container.

When needed to be thawed, the cryovials were extracted from storage and brought to room temperature in a 37°C water bath. Once thawed, the cells were promptly washed by centrifugation in RPMI, to remove residual DMSO, and finally resuspended in the desired culturing medium.

2.2.11 Reagents

Table 1: Routine culturing media and assay media compositions

Cell Culture Media	Reagent	Concentration	Supplier
R10%	**RPMI-1640**	–	Sigma
	Fetal Bovine Serum (FBS)	10%	Sigma
	L-Glutamine	2mM	Gibco
	Penicillin/Streptomycin	100 U/mL	Gibco
	Sodium Pyruvate	1mM	Sigma
75% Arg Free Medium or **Low Arg Medium**	**SILAC RPMI-1640**	–	Gibco
	Dialysed Fetal Bovine Serum	10%	Gemini Biosciences Ltd
	L-Glutamine	2mM	Gibco
	Penicillin/Streptomycin	100 U/mL	Gibco
	Sodium Pyruvate	1mM	Sigma
	L-Lysine	200µM	Sigma
T Cell Medium	**RPMI-1640**	–	Sigma
	Fetal Bovine Serum (FBS)	10%	Sigma
	Human Serum	1%	TCS Biosciences
	L-Glutamine	2mM	Gibco
	Penicillin/Streptomycin	100 U/mL	Gibco
	Sodium Pyruvate	1mM	Sigma
	β-Mercaptoethanol	50µM	ThermoFisher
	HEPES	5mM	Gibco
	IL-2 (Proleukin)	100 U/ml	Novartis
Phoenix Ampho Medium	**DMEM**	–	Sigma
	Fetal Bovine Serum (FBS)	10% v/v	Sigma
	L-Glutamine	2mM	Gibco
	Sodium Pyruvate	1mM	Sigma
Freezing Medium	**Fetal Bovine Serum (FBS)**	–	Sigma
	Dimethyl Sulfoxide (DMSO)	10%	Sigma
GC-MS Medium	**SILAC RPMI-1640 Flex**	–	Gibco
	Dialysed Fetal Bovine Serum	10%	Gemini Biosciences Ltd
	L-Glutamine	2mM	Gibco
	D-Glucose	10mM	Sigma
	L-Lysine	200µM	Sigma
	L-Arginine U-13C6	500µM	CK Isotopes Ltd
Seahorse XF Medium	**XF RPMI (#103576-100)**	–	Agilent Technologies
	D-Glucose	5mM	Sigma
	L-Glutamine	2mM	Gibco
	Sodium Pyruvate	1mM	Sigma
	HEPES	5mM	Gibco

2.3 Retroviral Transduction of Human Lymphocytes

2.3.1 Retroviral Transfection of Packaging Cell Line

Phoenix AMPHO cell line (ATCC) was used as the retroviral packaging line, cultured in Phoenix antibiotic-free Ampho Medium (i.e. DMEM, 10% FBS, 200mM L-glutamine).

A new cryovial of cells was thawed and cultured for each transfection cycle, the Friday ahead of transfection week. The cells were split at confluency (generally on the following Monday) and seeded onto T150 flasks at $4x10^6$ cells/flask, one flask per transfection condition. Phoenix Ampho were expected to reach the optimal transfection confluence of 40-60% within the following 24 hours.

On transfection day, the transfection reagents were prepared as follows: 12µg/flask of CAR plasmid, 12µg/flask of pCL Ampho DNA, 120µl/flask FuGENE (Promega) in a total volume of 3.6ml/flask of OptiMEM (Gibco). The mixture was allowed to rest at room temperature for 30 min, before being seeded in the cell line flask, together with 9ml of fresh culturing medium. The supernatants were replaced 24h post-transfection, to avoid FuGENE toxicity on the packaging cell line and the flasks were incubated for further 24h, to allow retrovirus production.

2.3.2 T cell Activation

Peripheral blood mononuclear cells (PBMCs) obtained from leukocyte cones were collected with a Pasteur pipette, washed twice in RPMI and centrifuged at 300xg for 10 minutes, twice. The monocytic fraction (CD14+) of the PBMCs was depleted by MACS sorting, using CD14 MicroBeads (Miltenyi Biotec) as described above, in order to obtain a lymphocyte-rich

fraction for CAR transduction.

Once discarded the CD14+ population, the negative fraction was washed and resuspended in T cell medium (RPMI, 1% human serum (TCS Biosciences), 10% FBS, 200mM L-glutamine, 1% Penicillin Streptomycin). The cells were then activated in T150 flasks at a density of $1x10^6$/ml at 37°C, 5%CO_2 for 48h in presence of 300U/ml of IL-2 (Proleukin, Novartis), soluble anti-CD3 (OKT3) (eBioscence) and anti-CD28 (R&D) both at the concentration of 30ng/ml.

2.3.3 Retroviral Transduction of T Cells

The retroviral supernatants were harvested without disturbing the adherent Phoenix Ampho cells and centrifuged at 300xg to precipitate any cell or debris in suspension. The resulting retrovirus-rich supernatants were then plated in non-tissue culture-treated 6 well plates, previously coated overnight with 30µg/ml of Retronectin (Takara Clontech) in sterile PBS. The plated supernatants were subsequently centrifuged at high speed (2000xg) for 2 hours at 37°C, in order to allow the virus to form a complex with the plate-bound Retronectin. After centrifugation, the supernatants could be removed, as the retrovirus were immobilised onto the plates.

In the meantime, the activated primary T cells were harvested, washed by centrifugation and counted, in order to be resuspended in fresh T Cell Medium at a density of $1x10^6$cells/ml. The cells were subsequently added to the retrovirus-loaded plates in a total of 2 million cells/well and briefly centrifuged at 300xg for 5 minutes to allow contact with the Retronectin-retrovirus complex. The plates were incubated at 37°C, 5% CO2 overnight, before 4ml of fresh T cell medium was added to each well and then incubated for further 72h.

On the other hand, transduction of Jurkat cell lines was obtained without the requirement for T cell activation. In fact, the cells were harvested from the culturing flask, washed by centrifugation and plated at $0.5x10^6$cells/well in a total volume of 2ml of R10% medium, directly onto the retrovirus-coated plates. They were finally spun at 300xg for 5 minutes. The plates were incubated at 37°C, 5% CO2 overnight, before 4ml of fresh R10% was added to each well and then further incubated for 72h.

Transduction efficiencies were assessed by flow cytometry on the fourth day post-transduction by detecting the surface expression of the truncated CD34 marker.

2.4 T Cell Suppression Assay

2.4.1 By ^{3}H-Thymidine Incorporation

In order to assess the ability of MDCSs to suppress T cell proliferation, a T cell suppression assay was performed, using 96 well plates pre-coated with 3µg/ml of anti-CD3 (OKT3) antibody (eBioScience) and incubated at 4°C overnight.
Healthy allogeneic T cells (CD14- fraction of PBMCs from leukocyte cones) were plated at a density of $2x10^5$ cells/well, in a total volume of 200µl R10%, 0.1% β-mercaptoethanol (Thermo Fisher) and soluble anti-CD28 stimulation (2µg/ml) (eBioScience). In addition, GO-treated MDSCs (or untreated controls), were added to the wells at equal or decreasing ratios (e.g. T cells : MDSCs of 1 : 1, or 1 : 0.5). The co-cultures were incubated for 4 days at 37 °C, 5% CO_2, before 1µCi/well of ^{3}H-thymidine (Perkin Elmer) was added and further incubated

overnight. The proliferation was then determined based on ^{3}H-thymidine incorporation within the daughter cells' DNA and quantified using a TopCount NXT Scintillation Counter (Perkin Elmer) and expressed as counts per minute (cpm). T cell proliferation was then expressed as a percentage of the T cell proliferation obtained in absence of MDSCs, in the T cell alone control, using the formula:

Sample Proliferation (%) = Sample Proliferation (cpm) x 100 / T cells Alone (cpm)

2.5 CAR-T Cell Proliferation

2.5.1 By ^{3}H-Thymidine Incorporation

Sorted CAR-T cells were plated in 100µl/well Low Arg Medium or TCM from primary neuroblastomas for 4 days onto 96 well plates in presence of plate bound anti-CD3 and soluble anti-CD28 stimulation (3µg/ml and 2µg/ml respectively). Then, 100µl/well of R10% was added to the culture for further 4 days, after which ^{3}H-thymidine was added (1µCi/well) and further incubated overnight. Proliferation was determined using a TopCount NXT Scintillation Counter and increase in proliferation expressed relative to the GD2 control, using the formula:

ARG-CAR Proliferation (%) = ARG-CAR Proliferation (cpm) x 100 / GD2-CAR Proliferation (cpm).

2.5.2 By Flow Cytometry

Transduced GD2, GD2 ARG1 and GD2 ARG2 CAR-T cells were cultured in T Cell Media supplemented with 100µM L-Arginine for 5 days at 37°C, 5%CO_2. Cells were stained with

CD34-APC antibody (targeting the CAR) and PI viability stain. A fixed volume of sample was acquired for each group with a flow cytometer, as exemplified by the gating strategy in Figure 10. Counts of CAR-positive cells were then expressed as % proliferation relative to GD2 control, using the formula:

ARG-CAR Proliferation (%) = Events in ARG-CAR CAR+ Gate x 100 / Events in GD2-CAR CAR+ Gate.

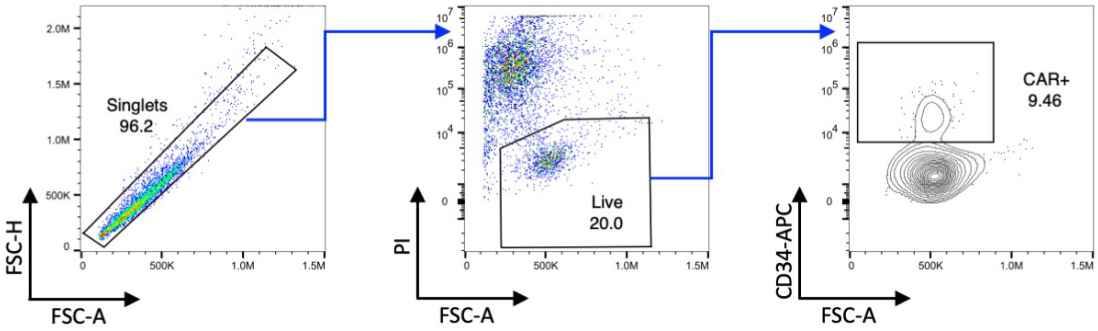

Figure 10: CAR-T cell proliferation by FACS gating strategy

After the necessary incubation period, the CAR-T cells were stained with anti-CD34 APC and propidium iodide (PI) and subsequently acquired by flow cytometry. Single cells were selected from the hight vs area of the forward scatter (FSC) to then further select the live cell population (PI-). Finally, the CD34 population within the live cells was determined.

2.5.3 By Antigen Stimulation

$GD2^+$ SK-N-MC cells were seeded onto plates and allowed to adhere for 1 hour in the incubator. Populations of GD2, GD2 ARG1 and GD2 ARG2 CAR-T cells were seeded at a ratio of 10:1 (effector:target) and incubated for a total of 5 days, before fresh $GD2^+$ SK-N-MC cells were added to the culture for further 4 days. Stained with CD34-APC and PI viability dye, the

samples were acquired by fixed volume with a flow cytometer and counts of CAR-positive cells were then expressed as % proliferation relative to GD2 control, using the formula: ARG-CAR Proliferation (%) = Events in ARG CAR+ Gate x100 / Events in GD2 CAR+ Gate.

2.6 Flow Cytometry

2.6.1 Surface Staining

$1x10^5$ to $3x10^5$ cells per sample were resuspended in FACS buffer (i.e. PBS, 5% FBS) and stained using a panel of desired fluorophore-conjugated antibodies from Table 2 at a concentration of 1:50. The cells were then incubated for 20min at 4°C, to avoid unspecific binding, then washed by centrifugation in abundant ice-cold buffer. The stained samples were then resuspended in 200µl of FACS buffer for acquisition on a Beckman Coulter CytoFLEX machine. Compensation beads (CompBeads, BD Biosciences) were prepared for each fluorophore used and acquired before the start of each experiment to allow the calculation of a compensation matrix and control for fluorophore interactions and false positives.
The viability of the sample was assessed including a propidium iodide (PI) live/dead staining, by adding 1:100 of PI working solution (1µg/ml) to the sample, 5 minutes before acquisition. A PI-only control sample was included among the compensations. Unstained cells samples were used to determine gating strategies after compensation calculation, such as Singlets, Live/Dead and population of interest, as explained in Figure 11.

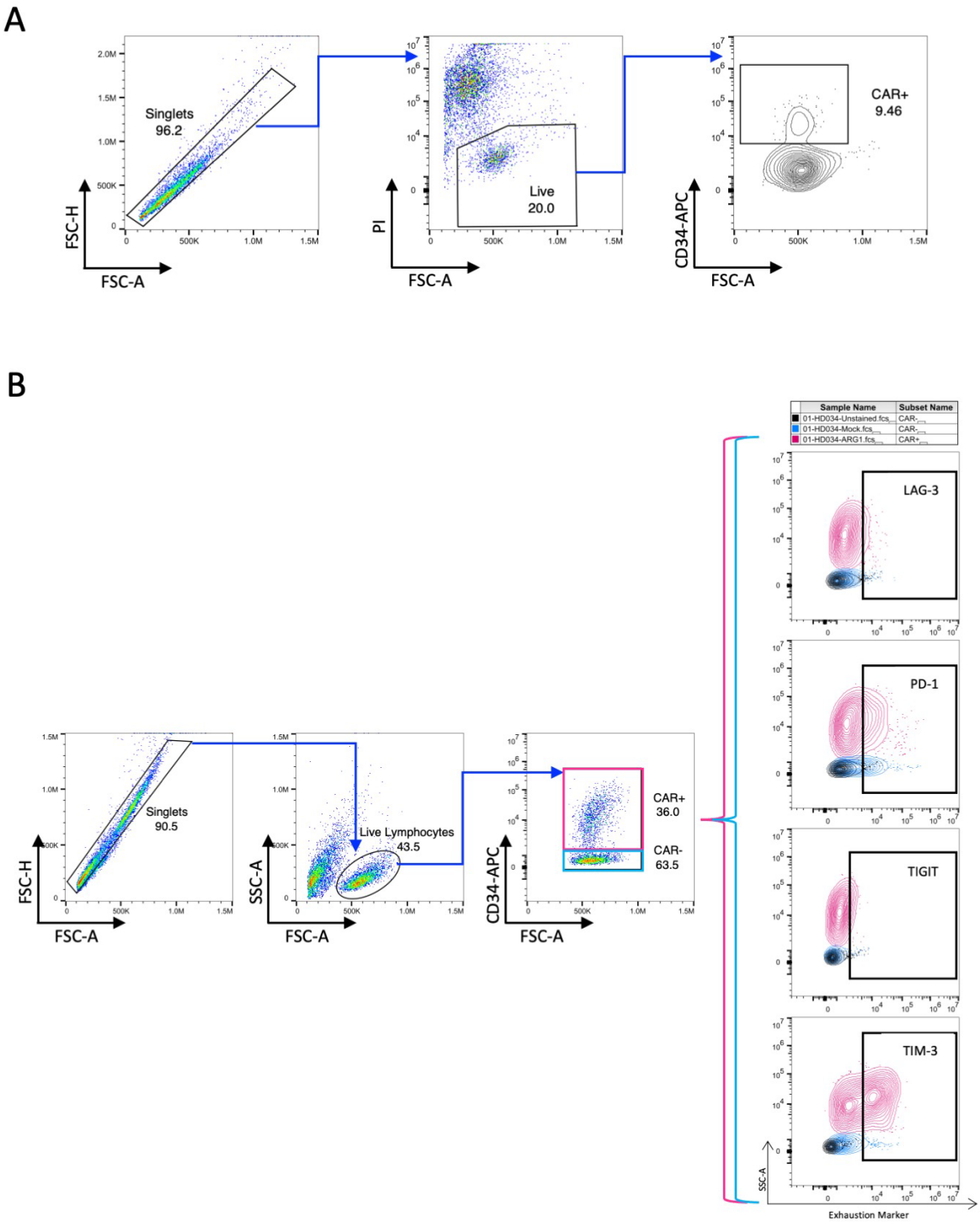

Figure 11: Gating strategy examples for the analysis of CAR-T cell assays and phenotypes by flow cytometry.

(A) Representative dotplots of Singlets selection on the forward scatter (FSC) height vs area plot; Live selection based on propidium iodide incorporation on the PI vs FSC plot; downstream selection of CAR+ cells. (B) Following Singlets identification, Live Lymphocytes were selected based on FSC and side scatter (SSC). CAR+ T cells were denoted by CD34 positivity in the CD34-APC vs FSC plot, while CAR- cells were used for Unstained or Mock downstream gating. Exhaustion markers (LAG3-FITC, PD1-PE, TIGIT-BV421, TIM3-PECy7) gates were defined based on the unstained sample and quantified as the positive % within the CAR+ or CAR- population.

2.6.2 Intracellular Staining

Intracellular staining steps were included in order to detect and quantify markers not available at the surface, such as intracellular proteins and transcription factors.
Upon staining with the required panel of antibodies against surface markers, the cells were fixed in 100µl of eBioscience Fixation Buffer for 20 minutes at 4°C, washed by centrifugation and resuspended in 200µl eBioscience Permeabilisation Buffer twice.
The subsequent staining steps for the detection of intracellular molecules was performed in Permeabilisation Buffer, incubating the required antibodies for 30 minutes at 4°C.

2.6.3 GO Internalisation Assay

Using an AlexaFluor Protein Labeling Kit (Life Technologies), Gemtuzumab Ozogamicin was covalently bound to an AlexaFluor-647 fluorophore.
The cells were treated at the concentration of 1µg/ml with GO-Alexa647, incubated on ice for 30 minutes to allow target binding and then incubated at 37°C for a range of time points (i.e. 0, 0.5, 1, 2, 4, 8 hours). The internalisation was stopped by placing the cells on ice for 10 minutes. The samples were washed by centrifugation and resuspended in a pH 2.2 stripping buffer (0.2M Glycine HCl) for 5 minutes to cleave the membrane-bound GO-Alexa 647. Cells were washed again and acquired on a flow cytometer using PI staining for live/dead gating (Figure 12).

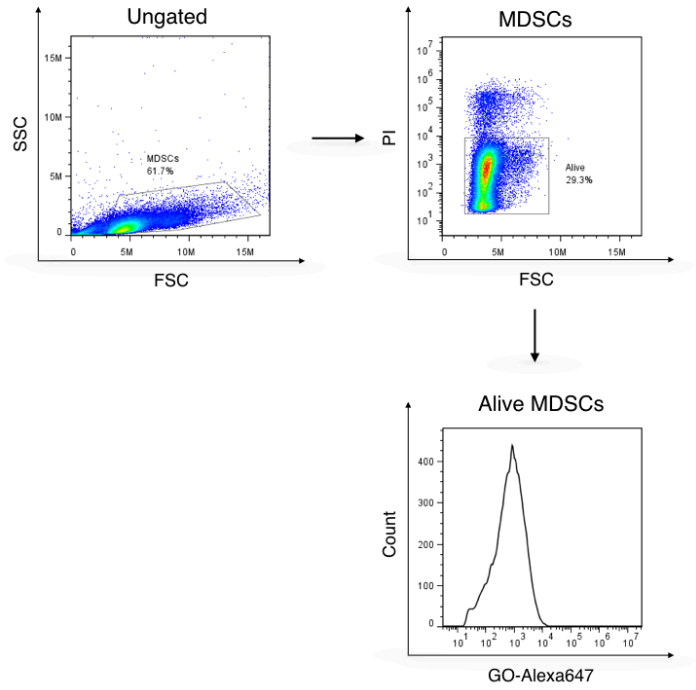

Figure 12: Drug Internalisation Assay Gating Strategy

The samples acquired by flow cytometry were firstly gated based on size (i.e. FSC vs SSC, top left dotplot example) to avoid the inclusion of debris; the live cells (i.e. PI- events, top right dotplot example) were then selected and GO-linked fluorescence (Alexa-647, bottom right) was recorded and compared across timepoints in the form of a histogram.

2.6.4 Reagents

Table 2: Antibodies routinely used for flow cytometry

Target Marker	Fluorophore	Species	Supplier
CD3	APC	Human	BioLegend
CD4	FITC	Human	BD
CD8	PE	Human	BD
CD14	FITC	Human	BioLegend
CD15	APC	Human	BioLegend
CD33	PE	Human	BioLegend
CD34	APC	Human	BioLegend
CD62L	PE	Human	BioLegend
CD69	PECy7	Human	BioLegend
PD1	PE	Human	BioLegend
TIM3	APCCy7	Human	BioLegend
LAG3	FITC	Human	BioLegend
TIGIT	BV421	Human	BioLegend
GD2	Alexa-647	Human	Invitrogen

2.7 Microscopy

2.7.1 Tissue Micro Array (TMA) Staining and Scoring

A tissue micro-array (TMA) of 200 cancer patients (n=40 non-small cell lung carcinoma, n=40 prostate adenocarcinoma, n=40 breast invasive ductal carcinoma, n=40 colon adenocarcinoma, and n=40 pancreas ductal adenocarcinoma and n=10 normal control tissues for each cancer) was provided by US Biomax. Deparaffinised samples were stained overnight at 4°C with anti-human CD33 (Abcam) on a Ventana Discovery Ultra, according to manufacturer's protocol. Antigen retrieval was achieved by heat-induction using cell conditioning 1 buffer (CC1) at a pH of 8.5 (Ventana). Tissues were additionally stained with haematoxylin and mounted in DPX (VWR). Secondary antibodies were added (Discovery anti-Rabbit HQ) and detection was obtained using the Novolink Polymer Detection System (RE7280-K, Leica).

CD33 isotype controls were included (Vector Labs). Antigen expression was evaluated on an Olympus BX51 microscope by independent pathologists. Immunostaining scores were assigned based on images obtained with Olympus DP70 camera and relative software, using the following parameters: score of 0 = negative, + = weak, ++ = moderate, +++ = strong.

2.7.2 Transmission Electron Microscopy

MDSCs from patients were treated with GO at 1μg/ml for 48h. After treatment the cells were centrifuged and the pellets fixed using 2.5% glutaraldehyde. After staining with 1% osmium tetroxide, the samples were dehydrated with EtOH and fixed in propylene oxide and resin at

60°C for 16h. 80nm thick sections were embedded onto copper slot grids and visualised by transmission electron microscopy (TEM).

2.7.3 Immunofluorescence

$1x10^4$ MDSCs were seeded onto glass coverslip inserts and treated with GO at 1µl/ml for 24 hours. They were stained with CD33-PE (BioLegend), washed and fixed in 2% paraformaldehyde for 20 minutes at RT, then permeabilised in 0.1% Triton X for 10 minutes. After blocking with PBS, 5% heat inactivated goat serum for 1 hour, they were stained intracellularly with 1:100 eFluor660-conjugated phospho-ATM (Ser 1981) (eBiosciences) abnd washed well. Air dried coverslips were mounted onto slides with SlowFade Gold mountant with DAPI (Thermo Fisher) and examined by confocal microscopy using the Zeiss LSM780 and images acquired with the Zen software.

2.8 Western Blot

2.8.1 Cell Lysate Preparation

Cell pellets were washed in PBS and lysed with 100µl of 1x RIPA buffer (Sigma) with protease inhibitor, incubated on ice for 30 minutes, vortexed occasionally. They were then spun for 20 minutes at 11,000xg and supernatants were collected. Laemmli buffer loading dye (Bio-Rad) was added to the samples at 1:4 ratio and incubated at 95°C for 5 minutes to allow denaturation.

2.8.2 Protein Quantification

The total protein concentration of the samples was determined by Bradford assay, adding 198µl of Bradford reagent to 2µl of sample, measured with a spectrophotometer at 595nm and values extrapolated from the standard curve generated with known concentrations of bovine serum albumin (BSA) (ThermoFisher) run alongside. Comparable amounts of protein were loaded for each sample.

2.8.3 Electrophoresis and Protein Transfer

Precast gels (4-20%) (Bio-Rad) were utilised and the loaded samples, together with a protein size ladder, were allowed to migrate at 150V for an hour. The separated proteins within the gel were subsequently transferred onto a PVDF membrane, using a Trans-Blot Turbo (Bio-Rad). Upon transfer the membrane was blocked in PBS, 5% BSA for 1 hour.

2.8.4 Protein Blotting

Primary antibodies (Table 3), diluted as per data sheet instruction in PBS, 5% BSA, were added overnight on a shaker at 4°C. The following day, the membrane was washed three times with PBS, 0.1% Tween 20 (PBS-T), before the appropriate horseradish peroxidase (HRP)-linked secondary antibody was added and allowed to bind on a shaker, at room temperature, for 1 hour. After the incubation, the membrane was washed thoroughly with PBS-T and developed with enhanced luminol-based chemiluminescent substrate, ECL (Promega), in order to detect the presence of HRP-derived signal with X-ray film exposure or ChemiDoc (Bio-Rad).

Table 3:Western blot antibodies

Target Marker		Antibody	Source Species	Supplier
Primary	**Arginase 1**	Arginase 1 mAb	Rabbit, Monoclonal	Cell Signalling Technologies
	Arginase 2	Arginase 2 mAb	Rabbit, Monoclonal	Cell Signalling Technologies
	β-Actin	β-Actin mAb	Mouse, Monoclonal	Cell Signalling Technologies
	CAT-1	Anti-SLC7A1/CAT-1	Rabbit, Polyclonal	Peprointech
Secondary	**Rabbit**	Anti-Rabbit HRP-linked	Goat	Cell Signalling Technologies
	Mouse	Anti-Mouse HRP-linked	Horse	Cell Signalling Technologies

2.9 Enzyme Activity Assessment

2.9.1 Arginase Activity Assay

Cells were counted, washed in PBS and pelleted, 0.5-1x10^6 cells per sample.

Cell pellets were lysed in 50µL of lysis buffer containing 0.1% Triton X-100 and protease inhibitors. The samples were incubated at 37°C for 30 minutes, vortexing every 10 minutes, then centrifuged at 11,000xg in order to discard the cell pellet and collect the lysates.

Arginase enzyme activation was achieved by incubation at 56°C for 10 minutes with addition of 50µl of Tris-HCl (25mM) and 10µl $MnCl_2$ (10mM) to 50µl of sample (all Sigma).

100µl L-arginine (0.5M, Sigma) was subsequently added to the samples and incubated at 37°C for 2 hours to allow its enzymatic conversion into urea and L-ornithine.

L-arginine hydrolysis was stopped with an acidic mixture of H_2SO_4 : H_3PO_4 : H_2O at the ratio of 1:3:7. The standard curve was obtained by serial dilution of urea (Sigma) in water (range 10mg/ml to 0.78µg/ml), with addition of 50µl TRIS-HCl, 10µl $MnCl_2$, 100µl L-arginine.

The converted urea was quantified by adding 40µl of 9% α-isonitrosopropriophenone (Sigma) in EtOH, incubated at 100°C for 30 minutes or until colour development. The samples were

cooled on ice for 10 minutes and then spun at 11,000xg for 5min to allow debris to precipitate. 200µl of supernatant from each sample and standard were transferred to a flat bottom 96 well plate for reading on a spectrophotometer at 540 nm. The concentrations obtained were normalised by cell number.

2.10 Cytokine Production

2.10.1 ELISA

Plasma from healthy donors or cancer patients were obtained from the peripheral blood, by centrifuging the collection tubes at 300xg for 5 minutes and collecting them from the very top layer. Samples were stored at -80°C until experiment day. Supernatants from cell cultures were obtained by centrifugation of the cells in suspension at 300xg for 5 minutes, in order to exclusively collect the cell-free media portion. Samples were plated appropriately diluted onto coated ELISA half area plates (Corning) following manufacturer's instructions. All ELISA kits utilised were BioLegend, excluding the TGF-β1 and TNF-α, which were purchased from R&D Systems. Colour change intensities were detected at 450nm on a spectrophotometer.

2.11 Target Recognition

2.11.1 Antigen Stimulation of CAR-Jurkat

Different $GD2^+$ cell lines were seeded onto plates and allowed to establish a monolayer of adherent cells for 1 hour. Mock, GD2, GD2 ARG1 and GD2 ARG2 CAR-Jurkat cells were added to the culture alone or at a different effector (E) to target (T) ratios (i.e.: 1:1, 10:1, 100:1) and incubated in R10% for 48 hours. The cells were then harvested and stained to be acquired on a flow cytometer for expression of GD2, to allow tumour out-gating, and CD69, to measure Jurkat activation.

2.11.2 Target Lysis by Flow Cytometry

Co-culture between GD2+ cell lines (target) and CAR-T cells (effector) were established in flat bottom 96 well plates, at an effector:target ratio of 10:1 in R10% medium (unless otherwise specified) for 48 hours.

Plates were then centrifuged to discard supernatant, resuspended in FACS buffer and surface-stained for key markers (e.g. CD34, GD2). After being washed, the wells were resuspended with suitable amounts of FACS buffer with PI live/dead stain and acquired by flow cytometry. Compensation of the fluorescent signals were achieved using single stained samples. Gates were established using unstained control and target or effector alone controls.

2.12 Transcriptomics Analysis

2.12.1 MDSC RNA Sequencing

G-MDSCs and M-MDSCs were isolated from the peripheral blood of cancer patients (head and neck, prostate, lung, breast, and melanoma, n = 3 per type) based on the guidelines published by (Bronte et al. 2016), i.e. immunophenotyping by flow cytometry and T cell immunosuppression assay by ^{3}H-Thymidine incorporation assay (see 2.4.1). The cells were MACS-sorted, using CD14 and CD15 MicroBeads for M-MDSCs and G-MDSCs respectively. RNA was then extracted with a Qiagen RNeasy Plus, DNAse treated and the samples were prepared using the Illumina TruSeq RNA Sample Preparation Kit v2. The sequencing was performed on the Illumina HiSeq2000 platform using TruSeq v3 chemistry, over 76 cycles. Reads were aligned to GRCh37 human genome using STAR RNA-Seq aligner software. Normalisation and differential expression of M-MDSCs versus G-MDSCs was performed using DESeq2 R Bioconductor package.

2.12.2 CAR-T cell RNA Sequencing

Sets of unmodified and modified CAR-Jurkat were cultured in Low Arg Medium for 48h, before RNA extraction.

GD2, GD2 ARG1 and GD2 ARG2 CAR-T cells and mock controls from n=3 human healthy donors were pre-conditioned in Low Arg Media for 4 days in presence of CD3/CD28 stimulation; R10% medium was subsequently added and cells were incubated for further 4 days. On day 9, pure populations of CAR-T cells were selected by FACS and RNA promptly extracted with an RNeasyPlus Kit (Qiagen) and DNAse treated.

Libraries were prepared using a Lexogen QuantSeq 3' mRNA-Seq Library Prep Kit FWD for Illumina and sequenced on the NextSeq 500 platform (Illumina) over 150 cycles.

2.13 Gas Chromatography-Mass Spectrometry (GC-MS)

2.13.1 Sample Culturing

Pure populations of transduced Jurkat cells were cultured for 48h in Low Arg medium prior to seeding at 1.5 x10^6 cells/well onto a 12-well plate in 1ml of GC-MS medium (Table 1), inclusive of 500µM of uniformly labelled L-Arginine, i.e.$^{13}C_6$-Arginine. Cells were further cultured for 24h at 37°C, 5% CO_2.

2.13.2 Folch Extraction

The samples were gently washed twice with saline solution and extracted with 500µL of -20°C methanol (Fisher Scientific), 200µL of ice-cold distilled water with D6-glutaric acid standard (2,5µg/ml) and 500µL of -20°C chloroform (Fisher Scientific). The phases were allowed to naturally separate on a rocker, on ice, for 10 minutes, before being centrifuged at 14,000xg for 10 minutes at 4°C.

The upper phase, comprising of methanol and polar metabolites (e.g. amino acids) was transferred into a clean safe-lock eppendorf and dried in a speedvac at 45°C for 3h, while the middle phase (i.e. proteins and nucleic acids) was used for protein quantification by Bradford assay and the lower phase (i.e. chloroform and lipids) discarded.

2.13.3 Derivatisation

Dried samples were derivatized using a two-step protocol: first, they were resuspended in 40µl/sample of 2% methoxamine hydrochloride (Sigma) in pyridine (Honeywell) and incubated for 1h at 60°C; then, 50µl/sample of N-(tert-butyldimethylsilyl)-N-methyl-trifluoroacetamide (MTBSTFA) with 1% tert-butyldimethylchlorosilan (t-BDMCS) (Restek) and incubated at 60°C for 1h. Derivatised samples were centrifuged at maximum speed for 1 minute and transferred to glass vials for analysis by gas chromatography-mass spectrometry (GC-MS).

2.13.4 Intracellular Metabolites Abundance and L-Arginine Tracing

An Agilent 7890B GC equipped with a polydimethylsiloxane column (Rxi-5ms, Restek) connected to a 5977A MSD (Agilent Technologies) was used for analysis of the derivatized polar metabolites. Compound detection was carried out in scan mode and analyte ion counts were normalized to the internal standard. A natural abundance correction was performed, and Mass Isotopomer Distributions (MIDs) calculated using in-house MATLAB scripts (courtesy of the Tennant Lab). Data was normalized to protein amount.

2.14 Bioenergetic Analysis by Seahorse XF

2.14.1 Mitochondrial Stress Assay

Pure populations of Mock, GD2, GD2-ARG1 and GD2-ARG2 transduced Jurkat cells were cultured for 48h in Low Arg Medium prior to Seahorse XF analysis. Cells were counted and seeded at the optimised density (Plitzko and Loesgen 2018) of 1x105 cells/well on to CellTak-coated Seahorse XFe96 cell culture microplates (Agilent Technologies) in 175µl/well of Seahorse Medium (e.g. RPMI, 5mM glucose, 2mM L-Glutamine and 1mM sodium pyruvate, 5mM HEPES) (Table 1).

Following a cell-stabilising incubation of 1 hour at 37°C in a non-CO_2 incubator and XFe96 sensor cartridge calibration, the plate was transferred to the Seahorse XFe96 chamber for the assay. Baseline oxygen consumption rates (OCR) and extracellular acidification rates (ECAR) were measured for 4 cycles consisting of a mix and measure cycles. Injections of 2µg/ml oligomycin, 3µM BAM15 and rotenone + antimycin A (both 2µM) were performed in sequence, allowing for 3 measurement cycles between injections. Injection of BAM15 as a mitochondrial uncoupler was preferred over FCCP, due to its increased specificity (Kenwood et al. 2014). Quantification of parameters was obtained using Seahorse Analytics.

2.15 *In vivo* Experiment

2.15.1 Lentiviral production of CAR-T cells

Anti-GD2 CAR T cells were generated from the same construct sequences using a lentiviral platform and 3 healthy donors by ProMab Biotechnology. Transduced cells, CAR^+ between 10 and 15%, were cryopreserved until injection in animals.

2.15.2 Animal Study

The animal study was conducted by Axis Bio.

All protocols used in this study have been approved by the Axis Bio Animal Welfare and Ethical Review Committee, and all procedures were carried out under the guidelines of the Animal (Scientific Procedures) Act 1986.

48 female Balb/c nude mice aged 8-10 weeks were used for the study. Tumour cells KELLY ($2.5x10^6$/mouse), 1:1 in Matrigel, were implanted subcutaneously onto the flank. When tumours reached an average of 10-15 mm^3, animals were randomised into the groups. Cyropreserved T cells were thawed in RPMI, washed and centrifuged at 400xg to collect the cell pellet. The cells were resuspended in PBS+2% FCS and prepared in 200µl/mouse for injection. Tumour volume and body weight were monitored. At sacrifice, tumours were harvested and processed to a single cell suspension and cryopreserved until delivered to us.

2.15.3 qPCR

RNA was extracted from digested tumour tissues with RNeasy Mini Kit (Qiagen)

First strand cDNA synthesis was performed using SuperScript™ III Reverse Transcriptase

(ThermoFisher) following the manufacturer's instructions. RT-Q-PCR was performed using the FAST SYBR Green Master Mix and the Applied Biosystems 7500 Fast Real-Time PCR system (ThermoFisher). Gene specific primer sequences were: GAPDH (Forward:5'-CCAGCCGAGCCACATCGCTC-3' Reverse:5'-ATGAGCCCCAGCCTTCTC-3'). CAR specific primers targeting the spacer region of the GD2 CAR (Forward: ACTCCAAACTCACCGTGGAC, Reverse: TTTTTGCCGGGTGAGAGTGA). Gene expression data is represented as normalised cycle thresholds relative to sample internal controls (Δct).

2.16 Statistical Analysis

Statistical analysis, data elaboration and figures were conducted on a Prism 8 platform (GraphPad Software Inc); the statistical approach is specified in the relative figure legends.

3. TARGETING MYELOID DERIVED SUPPRESSOR CELLS FOR IMPROVED CANCER IMMUNOTHERAPY

3.1 Overview

MDSCs are a heterogeneous population of myeloid cells able to condition the surrounding environment and suppress T cell function. In cancer, their role has been central for about two decades and their negative impact widely characterised (Veglia, Sanseviero, and Gabrilovich 2021). For this reason, there is a pressing need for clinically available solutions to selectively target this population, eliminate their pro-tumour activity and, finally, release the breaks on the anti-cancer immune response.

Differently from the murine counterpart, M-MDSCs (defined as $CD11b^{+}$, $CD14^{+}$, $HLA\text{-}DR^{low}$) and G-MDSCs (defined as $CD11b^{+}$, $CD15^{+}$) lack the expression of a univocal marker to allow their direct identification; this, in turn, impacts the ability to specifically target MDSCs in a clinical setting.

3.1.1 CD33 Surface Receptor

CD33 is a common marker for immature cells of the myeloid lineage and, as such, it is expressed on MDSCs and could represent an attractive target.

CD33 is a sialic acid-binding immunoglobulin-like lectin (Siglec), a family of membrane proteins with varied roles in cellular adhesion and cell-to-cell communication. In particular, human CD33 (or Siglec 3) is thought to have an inhibitory role, due to the presence of two tyrosine-based inhibitory motifs (ITIMs) in its intracellular portion; however, due to the lack of

equivalent receptors in mice, the understanding of its function is yet to be elucidated (Laszlo, Estey, and Walter 2014). The expression pattern of CD33 is restricted to the early stages of myelocyte development and is absent in non-haematopoietic tissues. As such, it can be found on myeloid multipotent precursors, immature monocytic and granulocytic cells and blood circulating monocytes, while it is downregulated in mature and tissue resident cells.

3.1.2 Gemtuzumab Ozogamicin

Pfizer's Mylotarg (i.e. Gemtuzumab Ozogamicin) is a CD33-directed monoclonal antibody conjugated to a calicheamicin molecule, a potent enediyne antitumour antibiotic derived from Micromonospora echinospora (Maiese et al. 1989).

Approved by the United States Food and Drug Administration (FDA) in 2000 for the treatment of acute myeloid leukaemia (AML), Gemtuzumab is able to bind the CD33-expressing cells via the mAb moiety and deliver intracellularly the calicheamicin toxin, which is activated upon hydrolysis of the pH-sensitive linker once in the lysosome. The toxin, which binds to the minor groove of the DNA helix at specific consensus sequences (TCCT), causes repeated double strand breaks, eventually leading to death.

3.2 Objectives

In this chapter, we characterised MDSCs across a range of different solid cancers and investigated the ability of Gemtuzumab Ozogamicin to selectively deplete MDSCs to restore the anti-cancer immunity.

3.3 Results

The data presented in this chapter has been published in the following article:

Fultang*, Panetti*, et al. 2019. *MDSC targeting with Gemtuzumab ozogamicin restores T cell immunity and immunotherapy against cancers*. EBioMedicine. (Full Article in Appendix 8.1)

3.3.1 Transcriptomics profiles of M-MDSCs and G-MDSCs

To overcome the lack of a specific surface marker to identify MDSCs, we intended to investigate their transcriptomic profiles and screen for potential therapeutic targets.
We isolated M-MDSCs and G-MDSCs from the peripheral blood of treatment-naïve head and neck (n=3), melanoma (n=3), lung (n=3) and breast cancer patients at diagnosis, based on the expression of the immunophenotypic consensus markers, $CD11b^{+}CD14^{+}$ for M-MDSCs and $CD11b^{+}CD15^{+}$ for G-MDSCs, as represented in Figure 13A. The enriched populations were further analysed to confirm their functional characteristics, the ability to suppress T cell proliferation (Figure 13B). Samples satisfying both the immunophenotypic and functional conditions were prepared for downstream RNA sequencing.

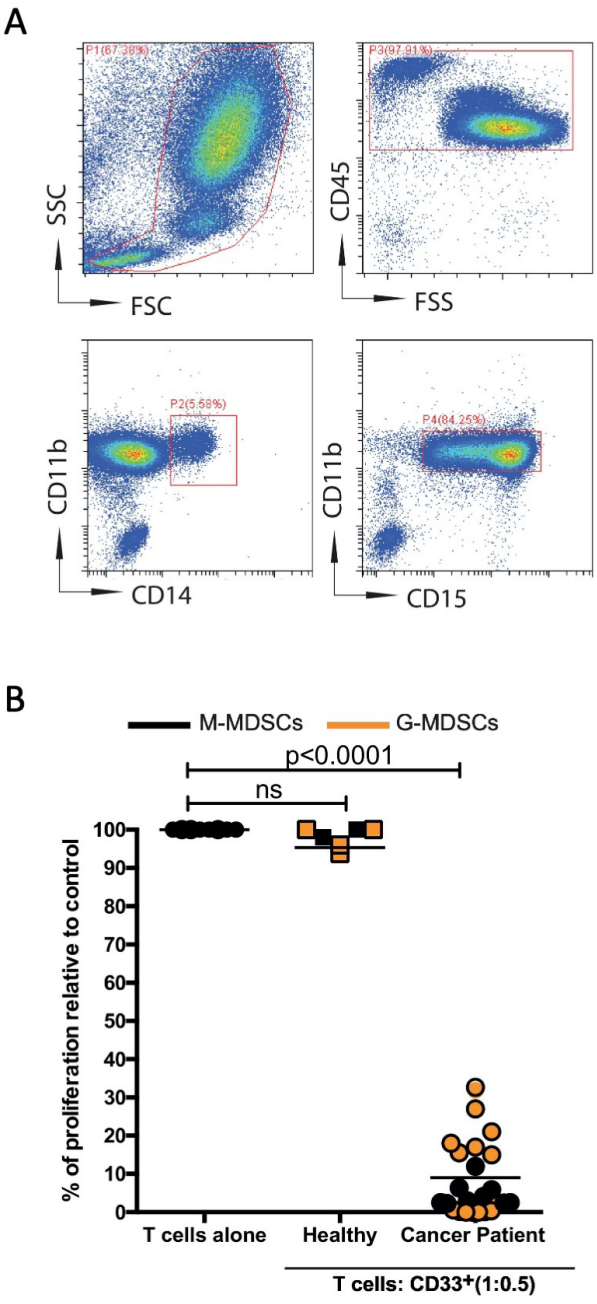

Figure 13: M-MDSCs and G-MDSCs were isolated from cancer patients.

M-MDSCs and G-MDSCs were isolated from cancer patients (n=3 breast cancer, n=3 head and neck cancer, n=3 lung cancer and n=3 melanoma) and selected based on the immunophenotype consensus and suppressive ability. (A) Representative flow cytometry gating strategy of M-MDSCs as CD11b+, CD14+ and G-MDSCs as CD11b+, CD15+. (B) Confirmation of their suppressive ability by allogeneic T cell ^{3}H-thymidine incorporation assay. Shown as proliferation relative to T cells alone control. Statistical analysis: Mann-Whitney test.

Transcriptome sequencing of M-MDSCs and G-MDSCs from the 12 patients was obtained, revealing a striking segregation between the granulocytic and the monocytic MDSC subtypes, as illustrated by the principal component analysis (PCA) in Figure 14A, based on the transcript per million (TPM) of the entire dataset. While some differences were highlighted across donors (PC2 axis, with a 3% variance), the most visible clustering was recorded between the two MDSC populations, with a variance of 85% (PC1).

The top 300 differentially expressed genes between M-MDSCs and G-MDSCs were then represented as a heatmap (Figure 14B), in order to identify potential markers to selectively target the two subsets. Interestingly, three different surface molecules, targets of known immunotoxins, were found to be overexpressed by the M-MDSC cohort: these were CD74, CD86 and CD33. Of these, CD33 was considered the most appealing candidate, due to the extensive clinical history and the range of therapeutic options already available. In fact, human CD33 had been targeted successfully and safely in the context of acute myeloid leukaemia for the past two decades (Brinkman-Van der Linden et al. 2003; Lamba et al. 2017). We therefore decided to investigate further the feasibility of surface CD33 as a therapeutic target of M-MDSCs in the context of cancer.

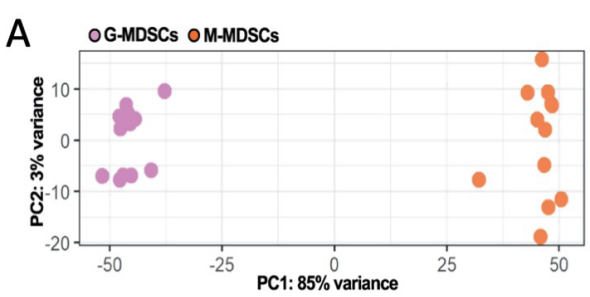
A
G-MDSCs
M-MDSCs
PC2: 3% variance
10
0
-10
-20
-50
-25
0
25
50
PC1: 85% variance

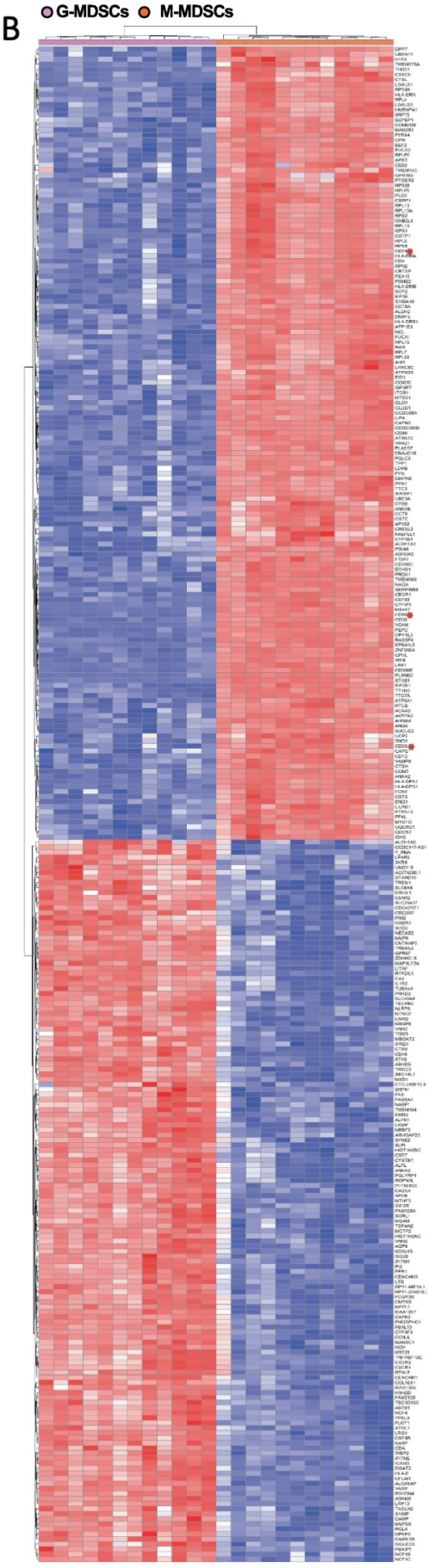
B
G-MDSCs
M-MDSCs

Figure 14: mRNA-sequencing of M-MDSCs and G-MDSCs to identify potential therapeutic targets.
MDSCs from cancer patients (breast, head and neck, lung and melanoma, n=12, 3 for each diagnosis) isolated following immunophenotype consensus and suppressive ability were used to generate an mRNA-sequencing library of M-MDSCs and G-MDSCs. (A) Principal component analysis (PCA) plot representing each donor's G-MDCSs and M-MDSCs variance based on their transcript abundance. (B) Heatmap of the top 300 genes differentially expressed between M-MDSCs and G-MDSCs across the 12 cancer patients. Statistical analysis by Noyvert B., CRUK funded biostatistician at the University of Birmingham.

3.3.2 MDSCs Prevalence in the Solid Tumour Landscape

MDSC presence within the TME of solid cancers was next assessed with a tumour micro-array (TMA) examining CD33 expression in 200 tissues from non-small cell lung carcinoma (n=40), prostate adenocarcinoma (n=40), breast invasive ductal carcinoma (n=40), colon adenocarcinoma (n=40) and pancreatic adenocarcinoma (n=40)compared to healthy controls for each tissue type (n=10) (Figure 15A and B).

Antigen expression on the immunohistochemistry sections was assessed by pathologists and the relative abundance of $CD33^+$ cells within the representative image frames from each sample was quantified (Figure 16A). Indeed, the proportion of $CD33^+$ cells found within these tissues was significantly increased in the tumour microenvironment of lung ($p=0.020$), prostate ($p=0.023$), pancreatic ($p=0.011$) and breast cancers ($p=0.025$) compared to their normal tissue controls.

Furthermore, the intensity of the CD33 signal was scored with the Olympus DP70 software and assigned "-" when negative, "+" when weak, "++" when moderate and "+++" when strong. Again,the majority of the tumour tissues analysed reached the highest intensity score (Figure 16B), confirming the relevance of such marker in the tumour microenvironment . No significant difference was observed in $CD33^+$ prevalence nor intensity between tumoural and

healthy colon tissues; healthy colon, in fact, presents with a high baseline level of $CD33^{+}$ cells.

We therefore excluded this cancer subtype from our analysis.

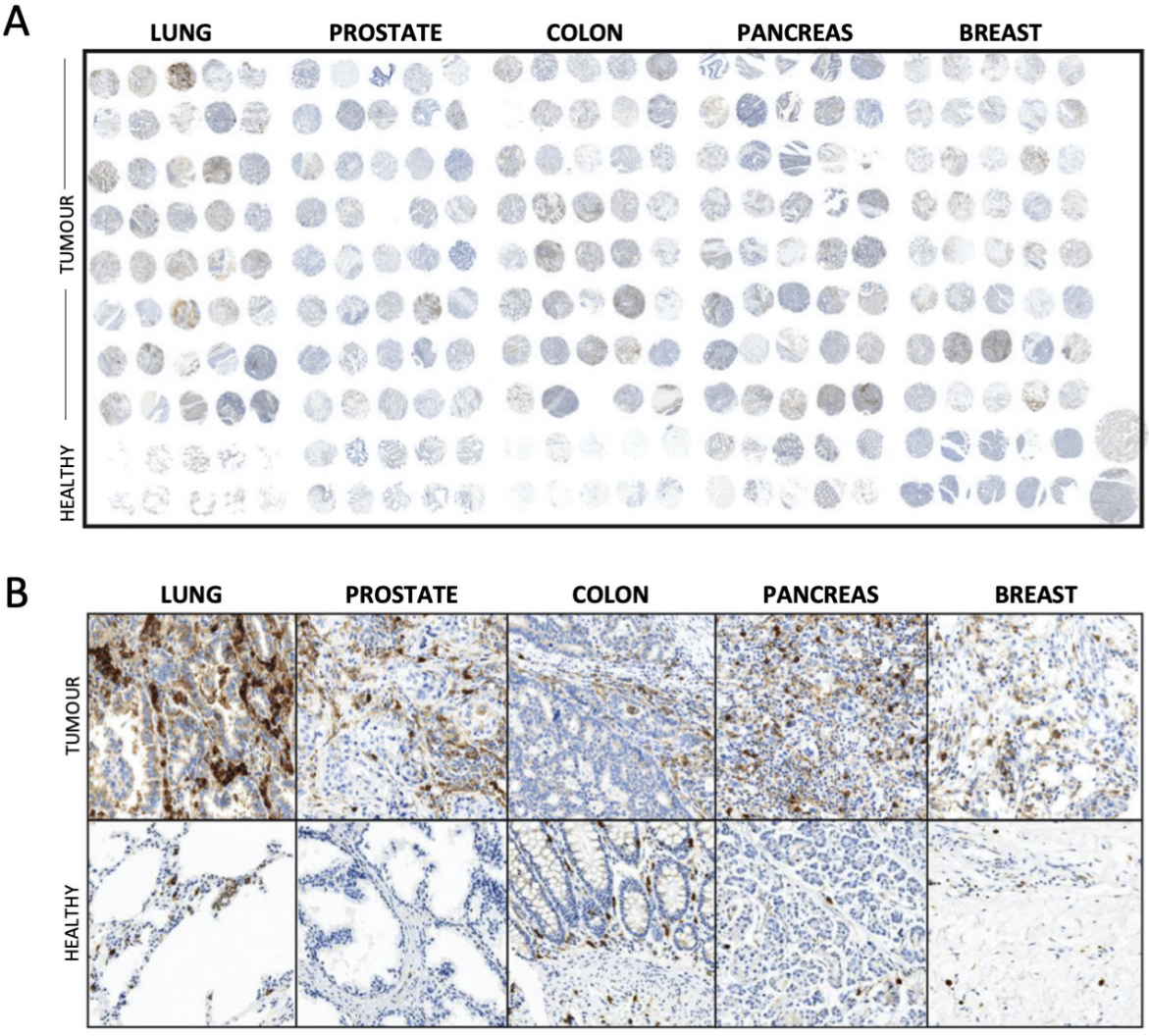

Figure 15: Immunohistochemical analysis of CD33 expression in the tumour stroma.

Tissue micro-array comprising of 200 samples was sourced from US Biomax and stained with haematoxylin and CD33 to investigate the prevalence of the marker in n=40 non-small cell lung carcinoma, n=40 prostate adenocarcinoma, n=40 breast invasive ductal carcinoma, n=40 colon and n=40 pancreatic adenocarcinoma with n=10 healthy control for each tissue. (B) Representative magnification of the stained tumour (top panel) and healthy tissues (bottom panel) for each of the tissue types.

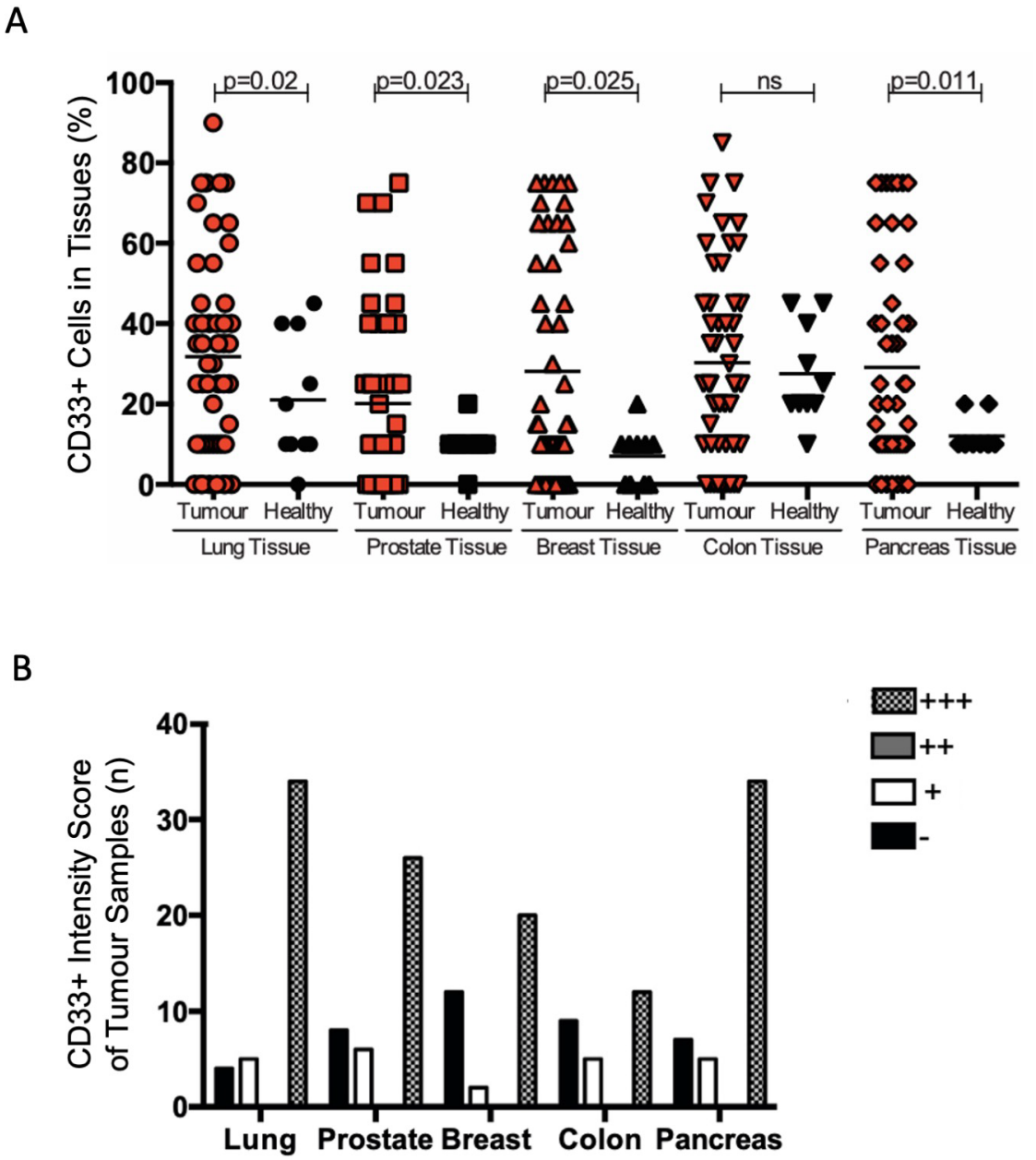

Figure 16: CD33 prevalence and intensity within the tumour tissue.

(A) CD33$^+$ cells in tumour stroma (red) or healthy tissue (black) were quantified by an expert pathologist using 400X magnification frames of the tissue. Shown as geometric mean; n=40 per tumour type and n=10 per healthy control type. Statistical analysis: unpaired t test. (B) Intensity score of CD33$^+$ signal within the tumour tissues as detected by the Olympus DP70 software. n=40 per tumour type. Scored as: "-" for negative, "+" for weak, "++" for moderate and "+++" for strong.

We next proceeded by staining the peripheral blood of cancer patients.
Evaluation of the whole blood by flow cytometry reflected the findings of the tissue: CD33-expressing cells were more abundant in the peripheral blood of cancer patients compared to healthy individuals ($p<0.0001$) (Figure 17A). In addition, CD33 intensity was found to be greater in M-MDSCs compared to G-MDSCs, confirming the results of the RNA sequencing (Figure 17B).

As a requirement for the definition of MDSCs, their suppressive ability *ex vivo* needed to be assessed. Healthy T cells were stimulated with anti-CD3/CD28 antibodies in presence or absence of $CD33^+$ cells from healthy donors or cancer patients. The extent of T cell proliferation was detected on day 5 by ^3H-thymidine incorporation.
Indeed, we observed a significantly reduced proliferation when T cell were cultured together with the $CD33^+$ cells obtained from cancer patients ($p<0.0001$). On the other hand, the proliferation was unaffected when T cells were cultured with $CD33^+$ cells from healthy donors (Figure 17C). The ability to suppress T cell proliferation is an established hallmark of MDSCs. Thus, we were able to conclude that, due to the polarisation received within the TME, patient-derived $CD33^+$ cells are indeed MDSCs.

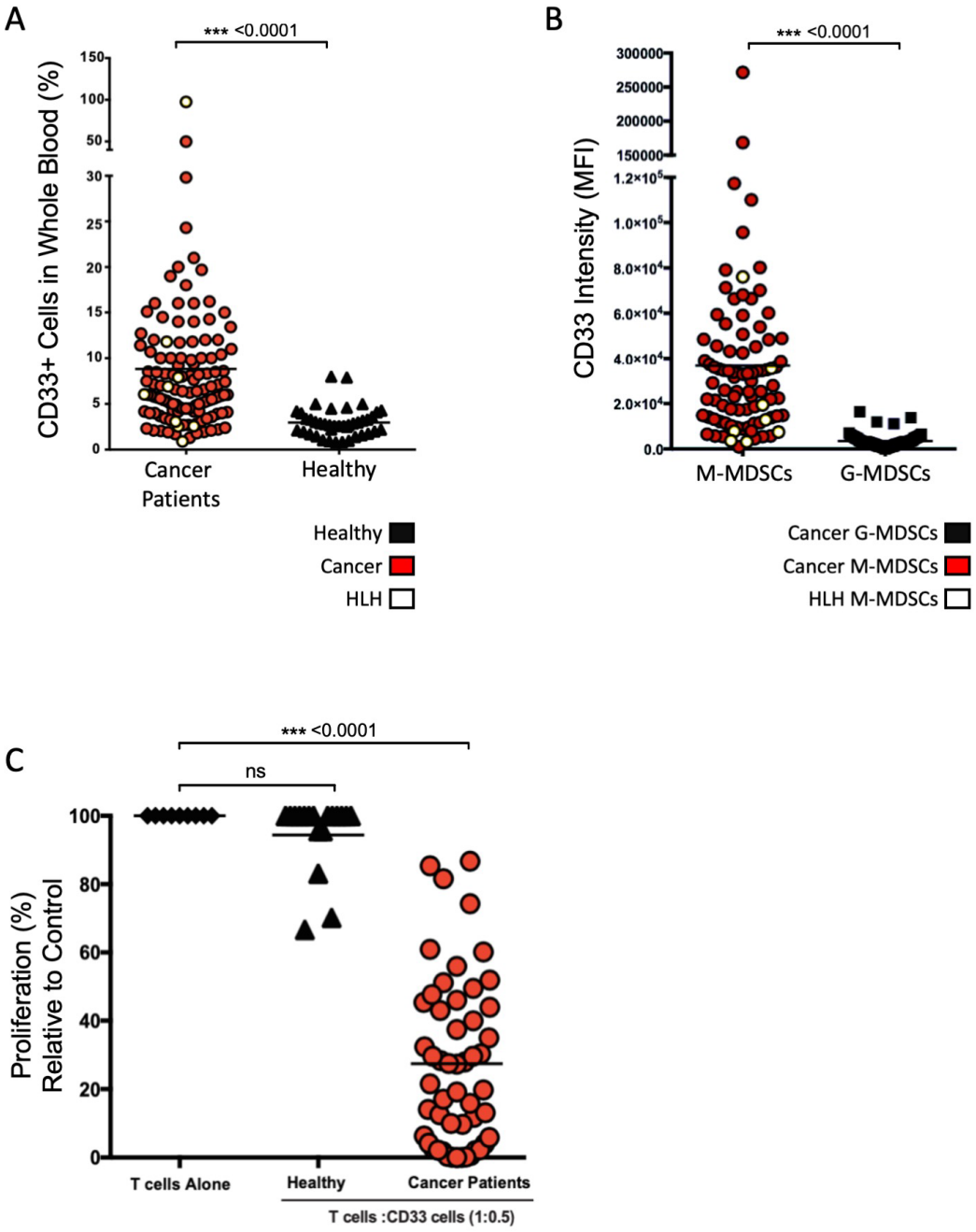

Figure 17: Peripheral blood analysis of CD33^{+} cell.

Peripheral blood of cancer patients and healthy controls was lysed and stained to assess (A) CD33 expression between cancer patients and healthy individuals; (B) intensity of the staining signal (MFI) for M-MDSCs and G-MDSCs. Cancer patients (red) n=81, acquired HLH (white) n=9; healthy (black) n=39. (C) ^{3}H-Thymidine incorporation assay of CD3/28 stimulated T cells in co-culture with CD33+ cells from healthy donors (black, n=17) or cancer patients (red, n=49). Statistical analysis: Mann-Whitney test. Disclosure: the graphs include some patients processed by co-author Dr Livingstone Fultang.

3.3.3 MDSCs Perpetuate Immunosuppression at a Systemic Level

The repercussions of MDSC expansion are known to impact the immunity of the organism on different levels (Groth et al. 2019). Therefore, we proceeded by investigating whether MDSC presence appeared in association with other signs of immune dysfunction.

First, we decided to evaluate the relative proportion of T cells in the peripheral blood of cancer patients (Figure 18A). We found that the percentage of circulating $CD3^+$ T cells was significantly lower in cancer patients than in healthy controls ($p<0.0001$).

This prompted us to further assess whether sorted T cells from cancer patients were able to proliferate to the same extent of healthy T cells when stimulated with anti-CD3/28 antibodies. We found no overall significant difference in T cells proliferation between cancer patients and healthy donors, with a high variance within the patient cohort (Figure 18B). Because the proliferation rates did not give a qualitative account of the T cell subsets involved, we thought it was important to elucidate whether the cancer patients presented a normal ratio of CD4 and CD8 T cells within the whole blood. We found that the CD4:CD8 ratio of cancer patients was drastically increased compared to healthy controls ($p=0.0246$). In fact, while the healthy controls exhibited a CD4:CD8 of 1.8 (and in agreement with the literature (Garrido-Rodríguez et al. 2021), patients displayed a mean CD4:CD8 of 5.3 (Figure 18C).

T cell exhaustion is commonly thought to be one of the main causes for the failure of the anti-cancer immunity. The analysis of the most common exhaustion markers on the patient-derived peripheral blood T cells was recorded. No significant difference was found in the expression of PD-1, LAG-3, TIM-3 and TIGIT in the T cells from cancer patients compared to healthy individuals (Figure 18D).

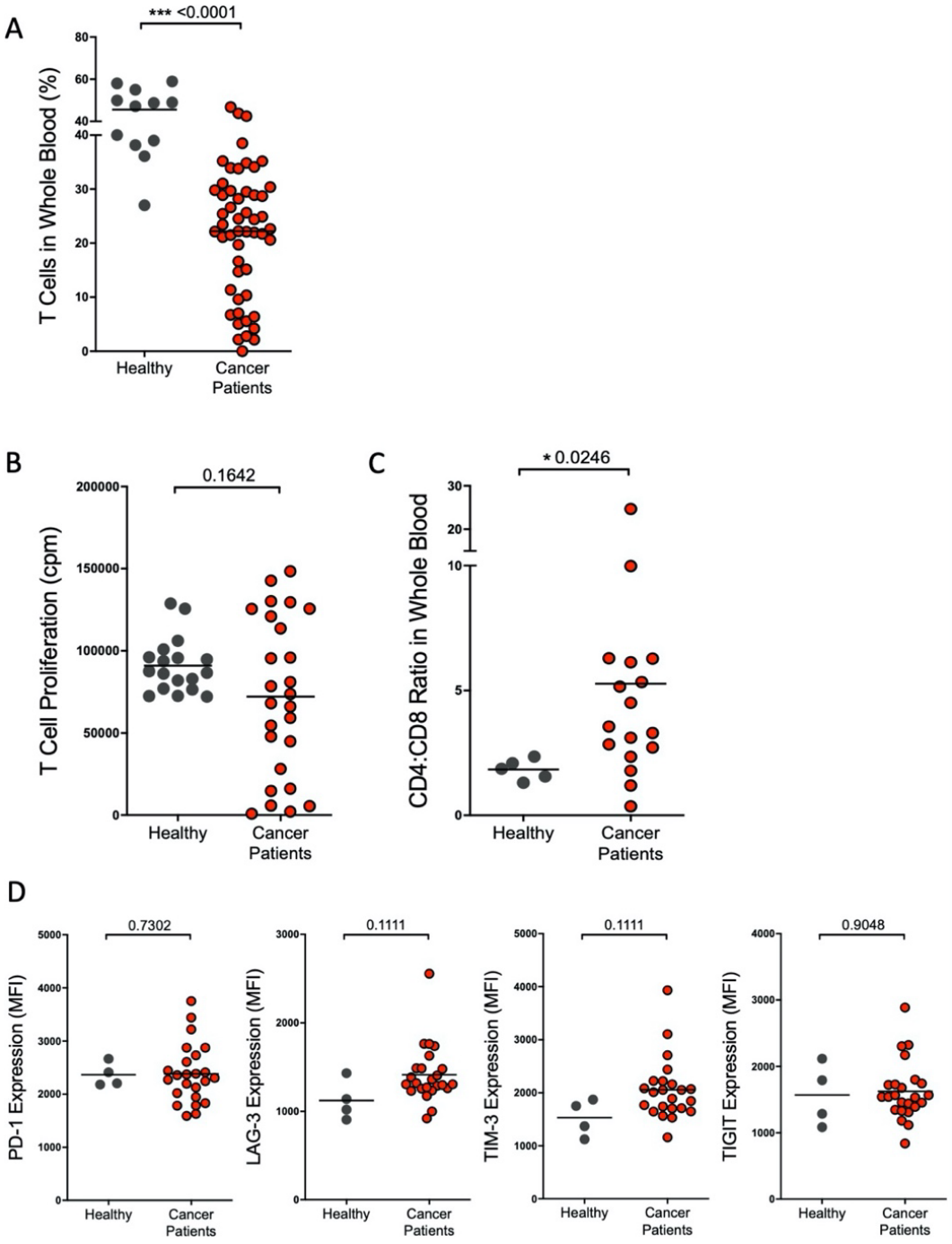

Figure 18: Functional and phenotypic investigation of cancer patients T cells.

(A) Whole blood staining of $CD3^+$ T cells in healthy and cancer patients. (B) Sorted $CD3^+$ T cells from peripheral blood of patients and healthy controls were plated in a proliferation assay, stimulated with CD3 and CD28 mAb for 4 days. ^{3}H-Thymidine incorporation was evaluated on day 5 and shown as counts per minute (cpm). (C) Flow cytometric analysis of $CD4^+$ and $CD8^+$ proportion within the $CD3^+$ population of T cells, represented as CD4:CD8 ratio. (D) Exhaustion phenotyping of $CD3^+$ cells shown as median fluorescent intensity (MFI) of PD-1, LAG-3, TIGIT and TIM-3. Cancer patients: red; healthy: black; bars are the mean. Statistical analysis: Mann-Whitney test.

The presence of tolerogenic cytokines in the TME is a hallmark of immunosuppression and MDSCs have been shown to perpetuate the production of pro-tumour signalling molecules (F Veglia, Sanseviero, and Gabrilovich 2021). We proceeded to analyse the plasma of patients for the most common pro-tumour molecules by ELISA.

Significantly raised amounts of TGF-β were recorded in the plasma of cancer patients, with a 6.25-fold increase compared to healthy control ($p<0.0001$) (Figure 19A). The pro-angiogenic vascular endothelial growth factor (VEGF) also was markedly raised in patients' plasma, whilst remaining mostly undetected in healthy individuals ($p<0.0001$) (Figure 19B). Similarly, we observed higher IL-6 levels in cancer patients, while being below detection in the healthy cohort ($p<0.0003$) (Figure 19D). Finally, no significant difference was found in G-CSF and IL-10 concentrations in the plasma between the two groups (Figure 19C and E).

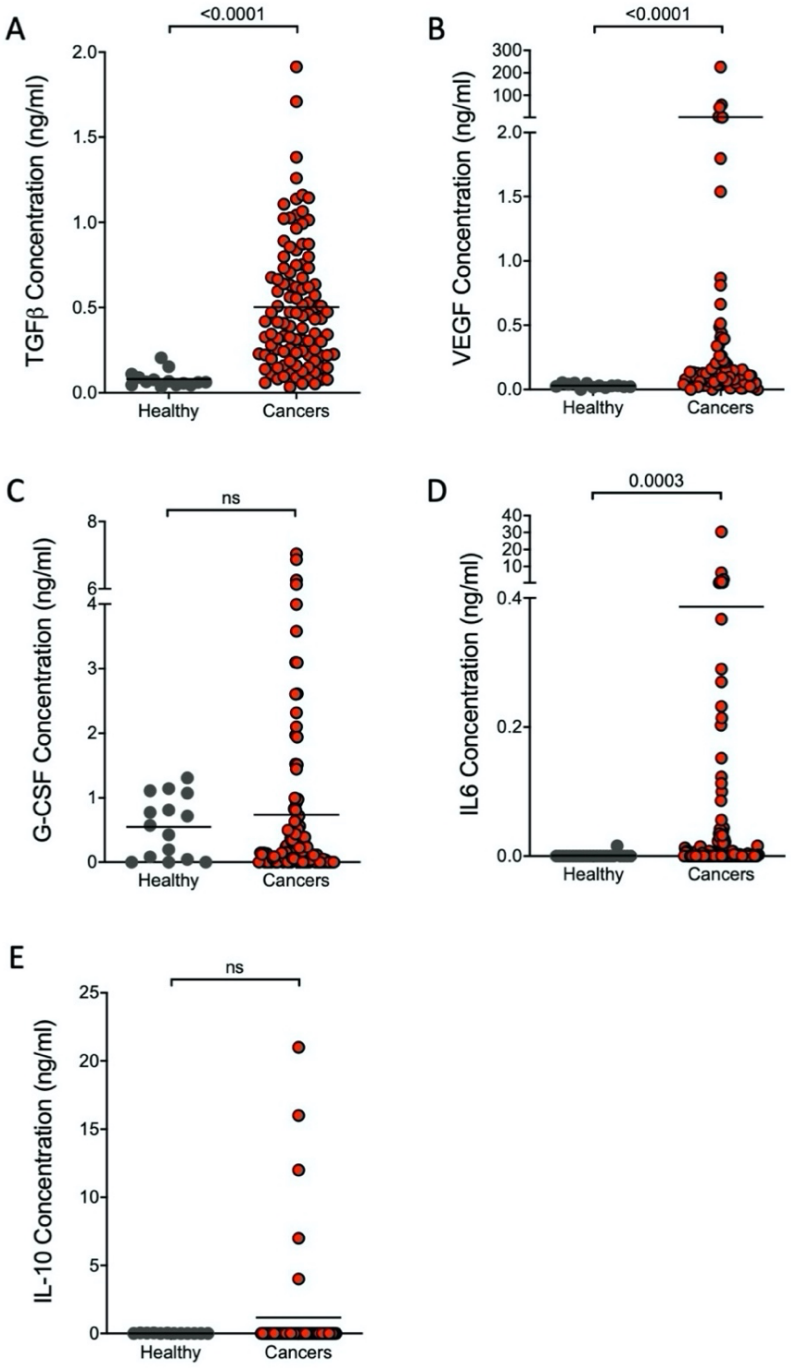

Figure 19: Plasma analysis of common cytokines within the tumour microenvironment.

Plasma samples from patients and healthy donors were collected from the peripheral blood, centrifuged at 500xg and cryopreserved. Cytokine quantification was performed by ELISA. (A) Tumour growth factor β (TGF-β); (B) vascular endothelial growth factor (VEGF); (C) granulocyte-colony stimulating factor (G-CSF); (D) interleukin-6 (IL6); (E) IL-10. Healthy (black): n≥15, cancer patients (black): n≥106; bars show the mean. Statistical analysis: Mann-Whitney test.

3.3.4 Therapeutic Opportunities to Contrast MDSC-Derived Inhibition

After having confirmed the expansion of $CD33^{+}$ in cancer patients and having seen the pro-tumour microenvironment promoted by these cells, we proceeded with the investigation of an MDSC depleting strategy based on CD33 targeting.

CD33 is a sialic acid-binding immunoglobulin-like lectin (Siglec), a membrane protein capable of internalisation (Laszlo, Estey, and Walter 2014). The expression pattern of CD33 is restricted to the early stages of myelocyte development and is absent in non-haematopoietic tissues. As such, it can be found on myeloid multipotent precursors, immature monocytic and granulocytic cells and blood circulating monocytes, while it is downregulated in mature and tissue resident cells.

More importantly, CD33 is the target of an existing immunoconjugate, Gemtuzumab Ozogamicin (GO), developed to treat acute myeloid leukaemia (AML). It consists of a CD33-directed monoclonal antibody conjugated to a calicheamicin molecule, a potent enediyne antitumour antibiotic derived from Micromonospora echinospora (Maiese et al. 1989), which binds to the minor groove of the DNA helix at specific consensus sequences (TCCT) and causes repeated double strand breaks.

Therefore, we decided to investigate whether GO could be repurposed to target MDSCs.

We previously showed that M-MDSCs displayed a higher CD33 intensity compared to G-MDSCs; for the continuation of the study we focussed our attention on M-MDSCs as they represented a more suitable target for the therapy.

First, we assessed whether MDSCs were able to internalise Gemtuzumab Ozogamicin.

Using *in vitro*-derived MDSCs and fluorescently labelled GO, we incubated the cells with the

drug for a range of increasing timepoints (from 15 minutes to 8 hours). Importantly, a low pH stripping step followed each incubation timepoint, to eliminate the fluorescent signal derived from surface-bound GO and guarantee the detection of the internalised drug exclusively. Indeed, we showed that MDSCs were able to internalise GO.

After exclusion of PI-negative cells (Figure 20A), an overlay of consecutive timepoints displayed the histogram increasingly shifting to the right due to internalised GO fluorescence (Figure 20B), starting within 15 minutes of incubation and progressively increasing until the longest incubation time of 8 hours. The internalisation curve was also generated (R^2=0.9981) to show that the steepest rate was obtained during the first 30 minutes of drug treatment (Figure 20C).

Furthermore, we investigated the implications of GO internalisation within the cells. It is known that the calicheamicin toxin carried by GO is capable of causing DNA double strand breaks. In the confocal microscopy image in Figure 20D, we were able to show phosphorylation of ATM serine/threonine kinase due to GO treatment. This is consistent with the induction of a DNA-damage response, as phosphorylation of ATM is necessary for the initiation of the homologous recombination repair pathway upon double strand break.

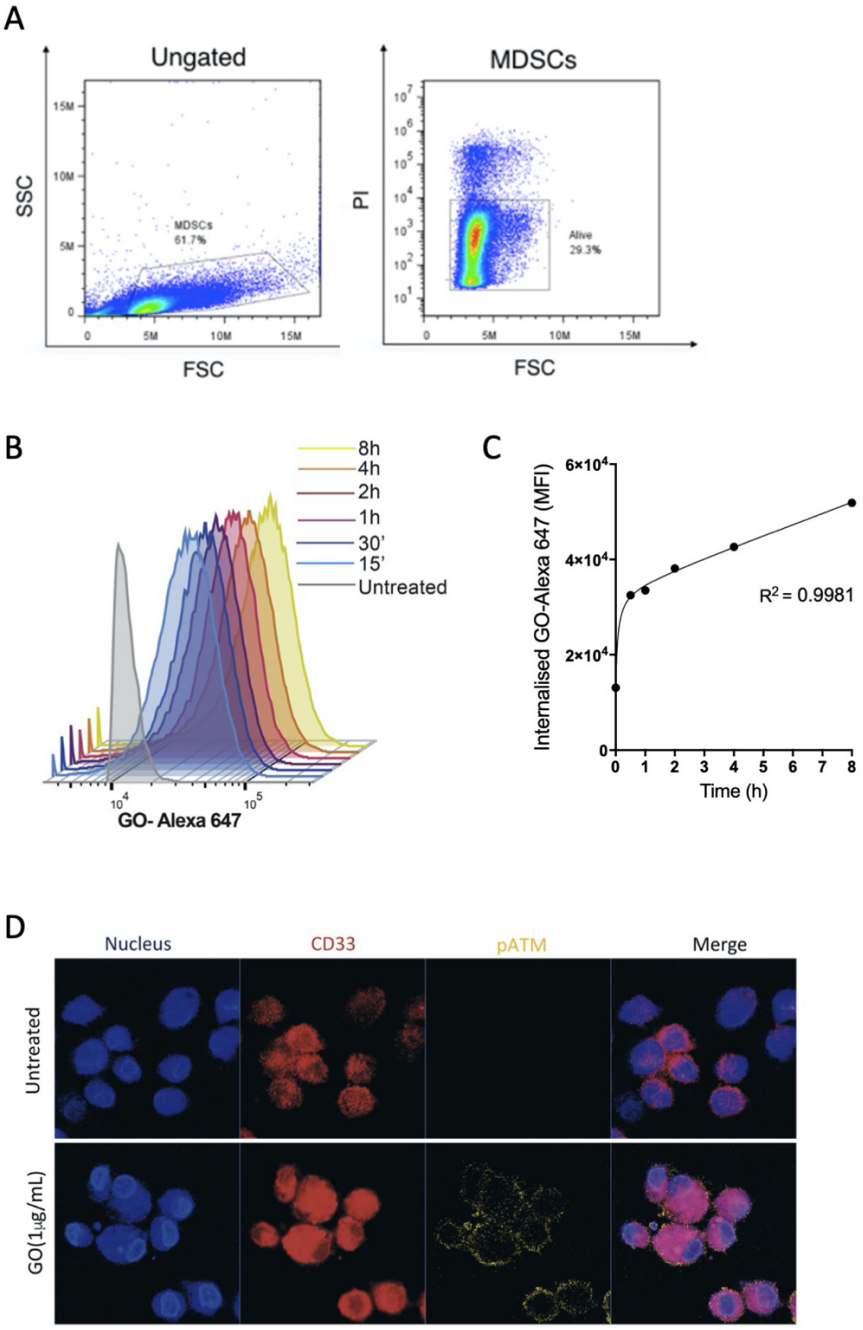

Figure 20: Gemtuzumab Ozogamicin is internalised by MDSCs and causes DNA damage.

In vitro-derived MDSCs were incubated with 1µg/ml of fluorescently labelled GO to monitor drug internalisation kinetics. Treatment timepoints of 15', 30', 1h, 2h, 4h, 8h, were followed by low pH-stripping steps to clear surface bound, not internalised fluorescence. Gating strategy of PI-negative cells (A), internalisation represented as histograms of Alexa-647 fluorescence (B) and kinetic curve (C) of one representative experiment. Patient-derived MDSCs were treated with 1µg/ml GO for 24h and subsequently stained with CD33-PE (red), DAPI (nucleus) (blue) and p-ATM-eFluor660 (yellow) and subsequently visualised by confocal microscopy (D). This image was obtained by, and used with the permission of, the co-author Dr Livingstone Fultang.

Extensive DNA damage accumulation, with failure of prompt repair, eventually leads to cell death by apoptosis. In order to further explore the effects of GO treatment on MDSCs, treated and untreated MDSCs samples from cancer patients were visualised with a transmission electron microscope after 48 hours of incubation at 1µg/ml GO. Indeed, the images in Figure 21 captured a cell morphology consistent to that of apoptotic cells, with visible presence of nuclear fragmentation, chromatin condensation, membrane blebbing and formation of apoptotic bodies.

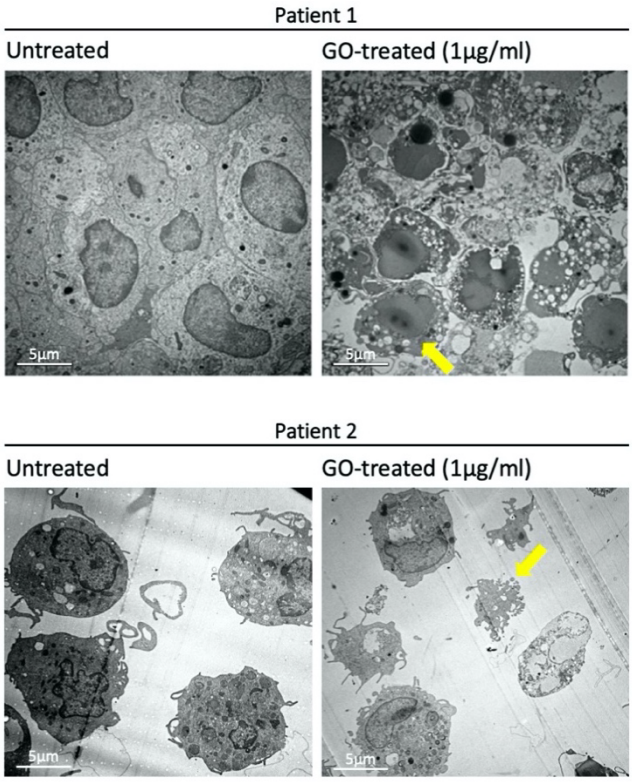

Figure 21: Gemtuzumab Ozogamicin treatment induces death of MDSCs

Patient-derived $CD33^+$ cells were enriched by MACS separation using the CD14 marker from the peripheral blood, treated with 1µg/ml of GO or untreated for 48h. They were then prepared for visualisation by transmission electron microscopy (TEM): fixed in 2.5% glutaraldehyde, stained with 1% osmium tetroxide, dehydrated with ethanol and embedded in propylene oxide and resin. 80nm thick sections were used for imaging. Yellow arrows point at typical apoptotic features, such as blebbing membranes and apoptotic bodies.

3.3.5 Gemtuzumab Ozogamicin Selectively Targets MDSCs

Seen that the therapeutic strategy we proposed relied on GO being auxiliary to the anti-cancer immunity, we deemed necessary to confirm whether GO had an impact on the viability of $CD33^+$ cells exclusively.

For this reason, we incubated PBMCs from patients at increasing concentrations of GO for 48 hours and assessed their viability by flow cytometry, using CD33 and PI staining.

Indeed, GO-mediated $CD33^+$ cell death was visible from the concentration of 0.25µg/ml, with a target death of about 25%, up to 75% of $CD33^+$ clearance at 2µg/ml (Figure 22A and B).

No decrease in viable CD33-negative cells was observed at any of the drug concentrations tested, therefore confirming the ability to specifically target the $CD33^+$ population with GO, without compromising the CD33-negative portion of the PBMCs.

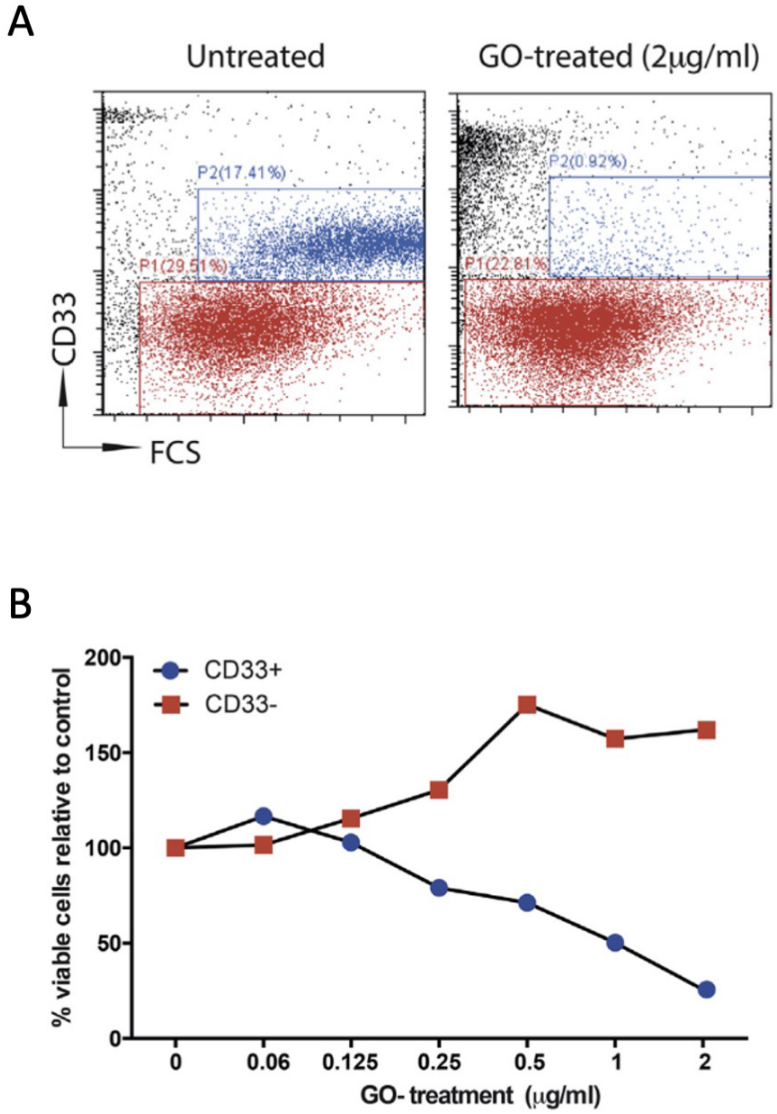

Figure 22: Gemtuzumab Ozogamicin specifically targets CD33$^+$ cells.

PBMCs from a cancer patient were treated with increasing concentrations of GO (0, 0.06, 0.125, 0.25, 0.5, 1 and 2µg/ml) for 48 hours and viability was assessed by flow cytometry based on CD33 staining. Results are shown as % of PI-negative cells, for CD33$^+$ (blue) and CD33$^-$ (red). Example dotplots are shown for untreated and treated cells (A); while the titration curve is shown in (B). Graph show a representative experiment of n=2.

We next wanted to demonstrate that MDSC targeting could be achieved in a range of cancer-induced MDSCs, both from cell line and primary patients.

In vitro-polarised MDSCs were derived from the TCM of a range of cancer cell lines and incubated with the drug. The cells were then acquired by flow cytometry after 48 hours of GO treatment and PI^- percentages were measured. In Figure 23A, we showed a substantial decrease in viability of *in vitro*-derived MDSCs, as a consequence of GO treatment, with MDSCs viability being reduced to an average of 33% at the concentration of 1µg/ml ($p=0.0015$) and below 20% at the concentration of 2 µg/ml ($p<0.0001$). This outcome was consistent across different polarisation media, albeit with a degree of variation.

Similarly, we repeated the treatment on MDSCs directly obtained from the peripheral blood of cancer patients. Again, $CD33^+$ cells showed a remarkable decrease in viability due to GO treatment, with an average of 51% of viable cells after 48 hours in presence of 1µg/ml of GO, down to 33.5% at the increased drug concentration of 2µg/ml ($p=0.0387$) (Figure 23B).

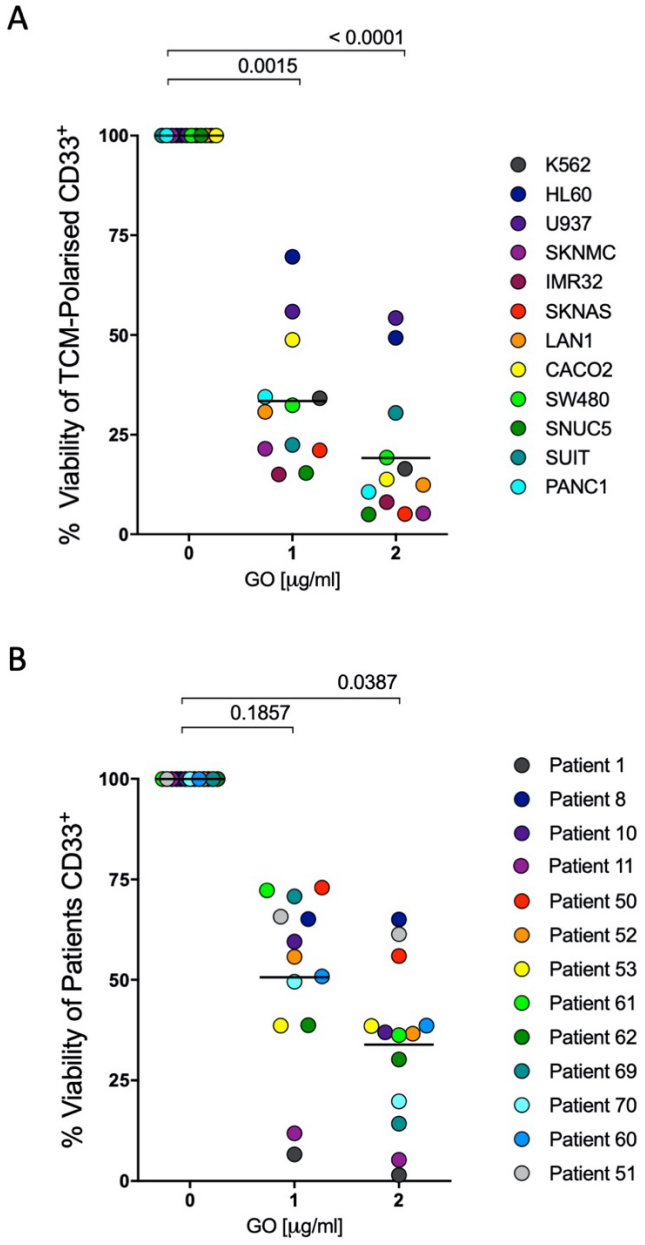

Figure 23: GO treatment kills *in vitro*- and patient-derived MDSCs.

$CD33^+$ cells polarised for 48h in the supernatant of different cancer cell lines (i.e. TCM) were harvested and treated at increasing concentrations of GO (0, 1 or 2µg/ml) for 48h and their viability was assessed by flow cytometry with PI staining (A). Similarly, cancer patients-derived $CD33^+$ cells were sorted from peripheral blood, treated at with GO (0, 1 or 2µg/ml) for 48h and assessed by flow cytometry with propidium iodide staining (B). Bars representative of the mean. Statistical analysis: Mann-Whitney test; n=12 (A) and n=13 (B). Disclosure: the graphs A and B include some donors processed by co-author Dr Livingstone Fultang.

3.3.6 Gemtuzumab Ozogamicin Treatment on MDSCs Rescues T Cell Proliferation

Next, we wanted to investigate whether as a consequence of MDSC depletion, T cell proliferation could be restored.

In order to achieve this, CD3/CD28 stimulated T cells from healthy donors were cultured with MDSCs, untreated or previously treated with 1µg/ml GO for 24 hours. The resulting proliferation was measured by ^{3}H-thymidine incorporation on day 5 and represented as a percentage of cell proliferation relative to T cell alone control (Figure 24).

Indeed, we observed that activated T cells in presence of MDSCs displayed a marked reduction in proliferation, compared to the T cell alone control ($p \leq 0.0001$). On the other hand, upon Gemtuzumab Ozogamicin treatment on the MDSCs, the T cell proliferation was rescued, from an average of 31.4% to an average of 65.3% of the T cell control (100%).

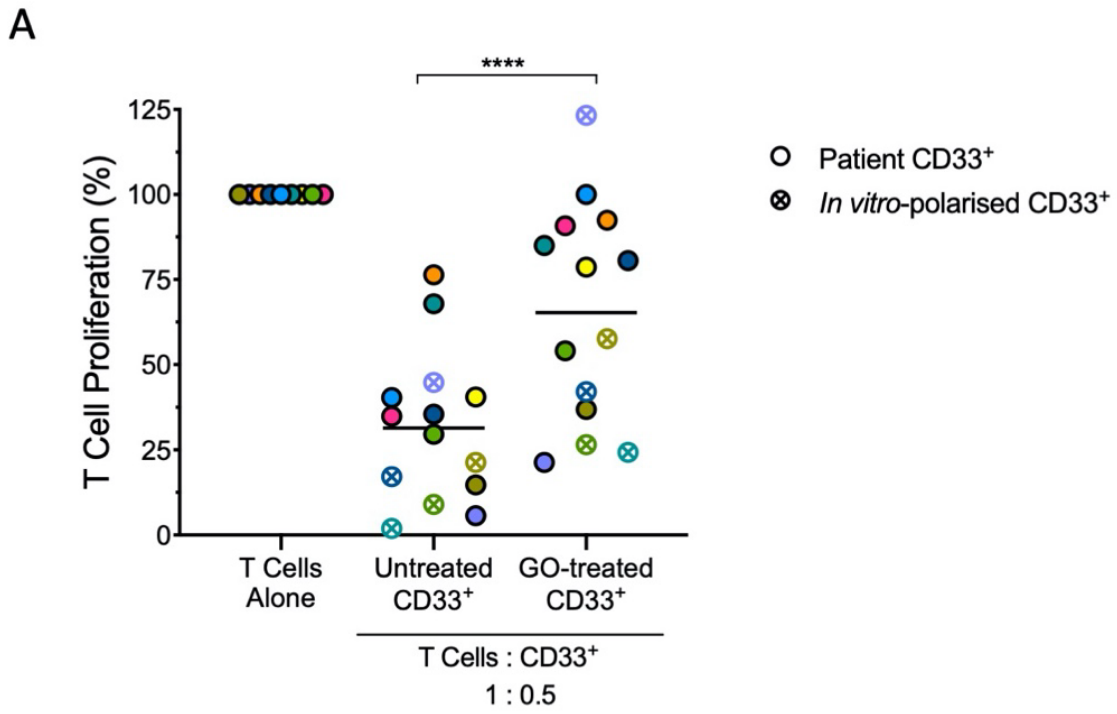

Figure 24: Allogeneic T cell proliferation is rescued upon MDSC treatment with GO.

T cells from healthy donors were plated in a ^{3}H-thymidine incorporation assay, with CD3/CD28 stimulation, in presence of untreated or GO-treated (1µg/ml for 24h) CD33^{+} cells and the proliferation was assessed on day 5. Matching symbols represent independent biological repeats; coloured circles for patient-derived CD33^{+} MDSCs (n=9), crossed circles for *in vitro*-polarised MDSCs (n=5). Bar representative of the mean. Statistical analysis: paired t test; **** $p \leq 0.0001$.

3.3.7 CAR-T Cell Antigen Targeting Ability is Restored by GO

We have previously discussed how the immunosuppressive tumour microenvironment negatively affects cancer immunotherapy. In particular, we wanted to assess whether MDSC depletion could benefit cancer-specific engineered T cells and their function. In order to do so, we retrovirally transduced anti-GD2 CAR-T cells, relying on a previously reported CAR construct used to target GD2^{+} tumours such as neuroblastoma (Pule et al. 2008), as will be

described in the chapters ahead.

$GD2^+$ Neuroblastoma (NB) cell line SK-N-AS was labelled with carboxyfluorescein succinimidyl ester (CFSE) and plated with *in vitro*-derived MDSCs, GO-treated or untreated; anti-GD2 CAR-T cells were added in co-culture at a ratio of 1:1 to MDSCs for 48 hours.

Equal volumes of samples were subsequently acquired by flow cytometry to assess tumour viability in the different conditions (Figure 25A and B).

Live NB cells were found to reach the highest value when in co-culture with untreated MDSCs (mean = 96,400 counts/ml) compared to NB alone (mean = 81,500 counts/m) or GO-treated MDSCs (mean = 73,200 counts/ml, p=0.0187).

Crucially, when in presence of untreated MDSCs, the anti-GD2 CAR-T cells were found impaired in tumour killing, only marginally reducing NB viability to an average of 60,000 counts/ml; on the other hand, GO treatment allowed CAR-T cells to significantly reduce tumour burden to an average of 36,400 counts/ml (p=0.0296).

In fact, we confirmed a significant decrease in live MDSCs within the GO treatment group (p=0.0061), coupled with an increase in live CAR-T cells compared to the untreated control (p=0.0190) (Figure 25 Cand D).

Overall, we were able to demonstrate that Gemtuzumab Ozogamicin treatment resulted in MDSC ablation and improved tumour targeting by CAR-T cells.

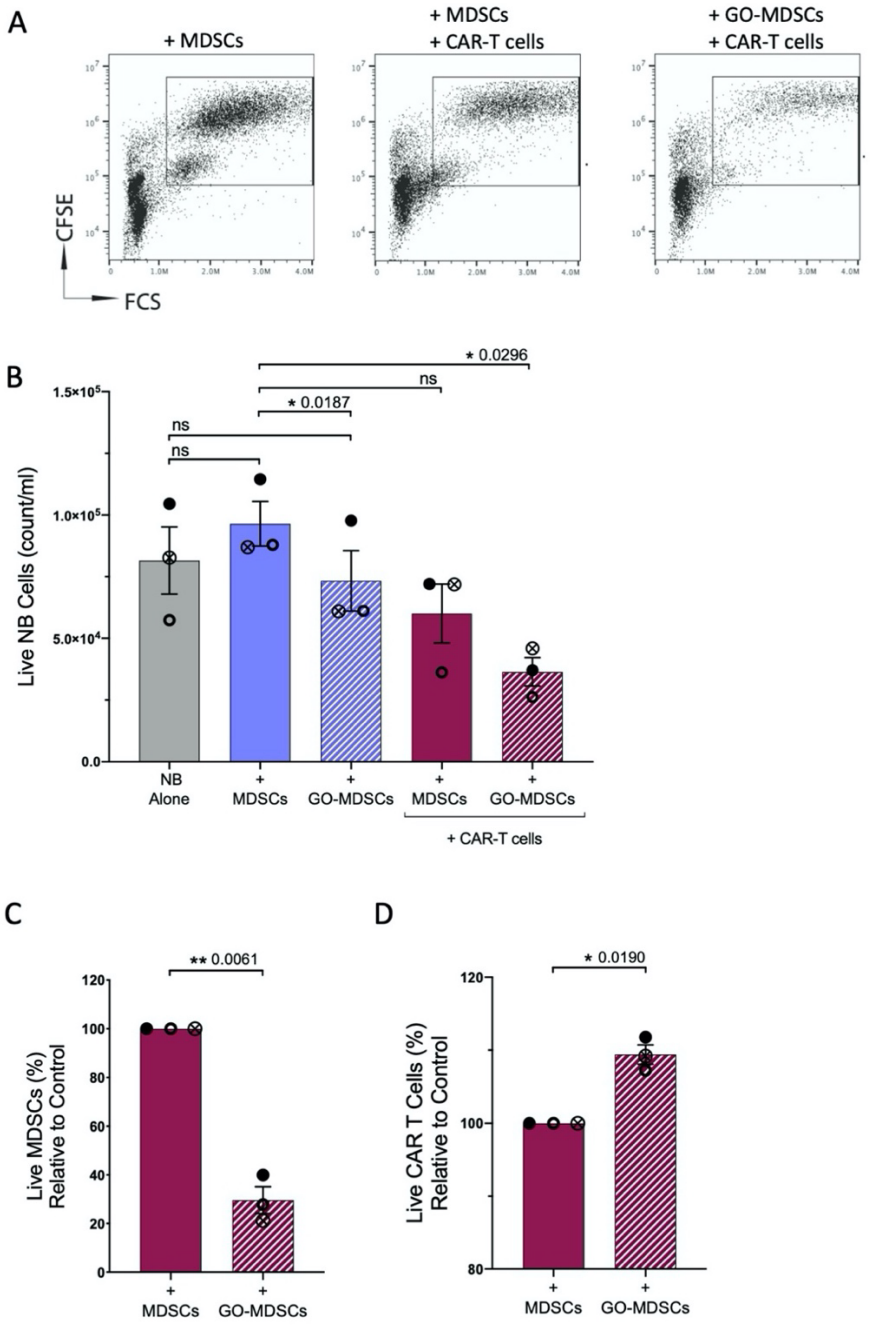

Figure 25: Gemtuzumab Ozogamicin rescues CAR-T cell efficacy from MDSC inhibition.

48h co-cultures were established with: CFSE-labelled GD2^{+} neuroblastoma (NB) cell line (SK-N-AS), *in vitro*-polarised MDSCs, treated or untreated with GO for 24h at 1µg/ml; anti-GD2 CAR-T cells. Populations were seeded at a ratio of NB : MDSC : CAR-T cells of 0.5 : 1 : 1. The co-cultures were assessed by flow cytometry 48h later: cell death was identified by PI staining, CAR-T cells by CD3 staining, MDSCs by CD14 staining. (A) Representative dotplot of the assay conditions; (B) Live NB (PI-negative/CFSE+) counts/ml; (C) live MDSCs relative to untreated control (PI-/CD14+); (D) live CAR-T cells relative to untreated control (PI-/CD3+). Shown as mean ± SEM, n=3 biological repeats. Statistical analysis: paired t test.

3.4 Discussion

Previously we stressed the urgence to address MDSC expansion and immunosuppression in the tumour microenvironment to enable the adequate performance of the natural anti-cancer immunity, as well as the engineered T cells. In fact, MDSC expansion represents a common denominator across solid tumour types for their ability to establish a *de facto* immune-privileged site around the tumour.

Here, we hypothesised that the repurposed use of Gemtuzumab Ozogamicin can strategically affect immature myeloid cells with pro-tumour effects, i.e. MDSCs and, consequently, help the autologous and the engineered immunity to endure the immunosuppressive microenvironment and implement anti-tumour activity. Gemtuzumab Ozogmicin was originally developed to target the sialic acid-binding receptor CD33 present on the surface of AML blasts; indeed, due to their myeloid origin and immature nature, CD33 is also extensively expressed on MDSCs, as confirmed by our RNA sequencing data.

Because CD33 intensity was found to be higher on M-MDSCs, compared to G-MDSCs, we decided to focus our investigation on M-MDSCs, as the therapy was more likely to be of benefit.

We have assessed the prevalence of $CD33^+$ cells in the tissues from a range of solid tumour types, as well as in the peripheral blood. The $CD33^+$ burden was convincingly higher in cancer patients compared to healthy controls. Crucially, $CD33^+$ cells obtained from patients were able to significantly inhibit the proliferation of allogeneic healthy T cells when in co-culture *in vitro*, while $CD33^+$ cells from healthy individuals did not interfere with the proliferative ability of T cells.

Moreover, as anticipated in the literature, these cells contributed to perpetuate an immunosuppressive milieu at a systemic level, characterised by a combination of raised tolerogenic cytokines (e.g. TGFβ), angiogenic factors (e.g. VEGF) and myeloid-driven inflammation (i.e. IL-6) in the plasma. This suggested that the immunosuppression within the TME was capable of extending beyond the tumour site, as confirmation of the potent nature of MDSC immunosuppression.

A reduced prevalence of T cells in circulation was also noticed, which additionally showed an abnormal CD4 to CD8 proportion balance. This has for long been shown to be descriptive of the immunological state of certain conditions, including cancer (Amadori et al. 1995). Although we are not able to discriminate whether the higher CD4:CD8 ratio was due to an excess of CD4 or a deficiency of CD8, these data suggested an overall skewed immunological homeostasis, most likely to the advantage of the tumour and its immunosuppressive microenvironment.

Unfortunately, only a limited number of therapeutic options to address MDSCs have been making their way into the clinic, due to the critical lack of a specific surface marker and the broad range of mechanisms in which they condition the TME.

Several strategies aim to block specific pathways; examples are cyclooxygenase 2 (COX2) inhibitors to prevent downstream PGE_2 (Fujita et al. 2011), small-molecule CXCR2 inhibitors to hinder MDSC recruitment (Greene et al. 2020), or arginase inhibitors to counteract MDSC-dependent L-arginine depletion (Steggerda et al. 2017).

Although these novel treatments might prove useful in circumscribing the specific MDSC-driven pro-tumour pathways, they represent single-pronged solutions to tackle a highly

versatile and dynamic population of cells. For this reason, we believe that a thorough and specific ablation of this expanded cell subset represents the most desirable way forward.

MDSC depletion was previously shown to be achievable by standard chemotherapy (Welters et al. 2016); however, this serves as a short term effect only, due to the prompt renewal ability of the cells. Furthermore, chemotherapy collaterally affects the viability of the anti-tumour immune response, undermining its synergistic potential in co-administration with immunotherapies.

Other immunotoxin directed to potential MDSC targets highlighted by the RNA sequencing data have been developed, e.g. CD74 (Chang et al. 2005) and CD86 (Otten et al. 2003); however, their exploration remains immature (Moek et al. 2017).

For this reason, CD33 targeting represents the most MDSC-selective and clinically investigated target available at this point in time.

Novel bispecific (BiTE) and trispecific (TriKE) engagers have been developed, to cross link effector cells to MDSCs; an example is GBT-3550, engaging CD16 on NK cells and CD33 (Sarhan et al. 2018). Despite giving promising results in AML and myelodysplastic syndrome (MDS), this NK cell-dependent therapeutic approach might prove challenging in the context of a solid tumour for its reliance on NK cell activity.

In this therapeutic landscape, Gemtuzumab Ozogamicin represents an interesting opportunity to shape the solid tumour microenvironment: it has been vastly tested on cancer patients, its side effects and management thereof are known and predictable, and it targets specifically MDSCs, without compromising other immune cells nor relying on their function.

Overall the toxicity profile of Gemtuzumab Ozogamicin treatment of AML in adults and

paediatric malignancies has been shown to be manageable, with side effects including myelosuppression, veno-occlusive disease and tumour lysis syndrome (Duncan et al. 2018).

Indeed, our work confirmed the ability of the MDSC CD33 receptor to bind and promptly internalise the agent, allowing the DNA-damaging calicheamicin moiety to be released intracellularly and induce cell death. Importantly, we showed that no consequence was observed on CD33-negative cells, such as T cells, highlighting the specificity of the treatment. Moreover, we demonstrated the rescue of allogeneic T cell proliferation as a direct consequence of MDSC targeting, with an over 2-fold improvement in proliferation compared to the untreated sample.

Enhanced CAR-T cell tumour killing upon Gemtuzumab Ozogamicin treatment was also observed. Interestingly, MDSC presence showed to increase NB viability; effect that was subsequently ablated by GO treatment. Whether this reciprocal tumour-immune system reinforcement axis is linked to what was described by Fultang et al. (2019), involving myeloid cell-derived TNF-α and IL1-β, it remains not confirmed.

In conclusion, we believe that the value of the therapeutic approach here presented lies in its pan-cancer and clinic-ready applicability, allowing to modulate the hostile TME of a wide range of solid cancers and restore the anti-cancer immune response, whether natural or genetically engineered.

Ultimately, further assessments will be executed during the phase II trial currently recruiting, GOTHAM, to determine the best administration strategies to maximise its effect and minimise toxicity (ISRCTN89158144, https://doi.org/10.1186/ISRCTN89158144).

Furthermore, we anticipate great interest in exploring combination approaches with other immunotherapies, such as checkpoint blockade and CAR-T cell therapy.

4. A MODEL FOR THE STUDY OF A MICROENVIRONMENT-RESISTANT CAR CONSTRUCT

4.1 Overview

In light of what was discussed in 1.3.5 and beyond, CAR-T cell therapies tested in solid tumours encounter considerable hurdles that prevent a successful cancer clearance. A key example is the consistently underwhelming results of anti-GD2 CAR-T cell therapy in neuroblastoma: both the approach and the target have been shown to be safe, however T cell expansion and long-term persistence remain poor (Louis et al. 2011), even when combined with PD-1 blockade (Heczey et al. 2017). The TME is thought to have a definite impact on immunity and, as such, also the engineered one. In fact, in their Phase I clinical trial, Heczey and colleagues (2017) documented an expansion of a myeloid population ($CD33^+$, $CD11b^+$, $CD163^+$) in the PBMCs of patients upon anti-GD2 CAR-T cell infusion, despite lymphodepletion regimen. The authors suggested this population as being the limiting factor to immunotherapy efficacy.

4.1.1 The Immunosuppressive Microenvironment of Neuroblastoma

Neuroblastoma has been known to create a strongly immunosuppressive niche, characterised by infiltration of myeloid pro-inflammatory cells, clearly correlating with prognosis of high-risk disease and metastasis (Asgharzadeh et al. 2012; Pistoia et al. 2013). Mussai et al. (2015) have previously demonstrated how this is achieved via the overexpression of arginase 2 by the

neuroblastoma cells and consequent depletion of L-arginine from the surroundings, a known mechanism of T cell suppression already discussed (1.2.7). Furthermore, neuroblastoma showed to interact and polarise infiltrating myeloid cells, in order to establish a pro-inflammatory milieu rich in IL1β and TNFα, which in turn promoted a feedback loop to enhance arginase 2 expression in the cancer cells (Livingstone Fultang, Gamble, et al. 2019). This reciprocal tumour-immune system reinforcement axis was partially subverted by depletion of L-arginine with a recombinant arginase (i.e. BCT-100), an agent currently undergoing clinical trial (PARC, NCT03455140).

4.1.2 Arginase 1 and Arginase 2

Arginase is one of five enzymes of the urea cycle, hydrolysing L-arginine into L-ornithine and urea. Ubiquitously found in the mitochondria of living organisms, from bacteria to vertebrates, it first appeared in its cytosolic form in ureotelic animals, implicating an alternative scope for arginine and ornithine metabolism to that of the urea cycle (Dzik 2014). Mainly, the urea-independent role of arginase is attributed to the downstream synthesis of proline and polyamines (putrescine, spermidine and spermine), the latter useful precursors of hypusine and important for adequate transcription and translation activity (Casero, Murray Stewart, and Pegg 2018).

The cytosolic arginase 1 and the mitochondrial arginase 2, despite differing in size (322 and 354 amino acid respectively), catalyse the same biochemical reaction and share comparable kinetics (Wu and Morris 1998). Nonetheless, the expression patterns of the two isoforms are also distinct: while arginase 1 is mainly found in hepatic cells as part of the ammonia

detoxification strategy and within activated myeloid cells for immunomodulating purposes, arginase 2 seems to be more ubiquitously expressed to oversee intracellular L-arginine homeostasis (Bronte and Zanovello 2005).

In addition, the different subcellular compartmentalisation could also elicit different downstream effects of the enzymes, with several studies attempting to pinpoint the causes of the so-called “arginine paradox”, for which theoretically arginine-saturated environments still respond to arginine supplementation (Caldwell et al. 2018; Elms et al. 2013).

4.1 Objectives

In the previous chapter, we investigated a (CAR-)T cell-adjuvant approach to deplete myeloid suppressive cells in the TME and enable (CAR-)T cell effectiveness.

Here, we proposed an alternative method to intrinsically alter the CAR-T cell metabolism, in order to resist and thrive within the nutrient-poor microenvironment of the solid tumour and, ultimately, to execute the anti-cancer program for which CAR-T cells were created.

Given the positive results of recombinant arginase treatment on neuroblastoma *in vitro* (Fultang et al. 2019), we hypothesised that CAR-T cells constitutively expressing arginase, not only would be capable to promptly metabolise environmental L-arginine for downstream use, but also they would deplete L-arginine at the interface with the tumour.

For the first phase of this investigation, we will employ a model of T cell, the Jurkat cell line, to allow for cell-dispendious optimisations and techniques. The cell line was established from T cell acute lymphoblastic leukaemia and has been widely used to study T cell activation and

TCR signalling (Abraham and Weiss 2004).In this chapter, we aim to:

- engineer anti-GD2 CAR-Jurkat cells, constitutively expressing arginase 1 and arginase 2;

- validate the CAR and enzyme presence and functionality;

- investigate the impact of arginase expression on Jurkat biology and metabolism.

4.2 Results

4.2.1 CAR Construct Design

The retroviral vector MP71 (Schambach et al. 2000) was employed for expression of the transgenes, shown in Figure 26, and flanked by long terminal repeat (LTR) sequences.
Briefly, at the foundation of this study is the anti-GD2 scFv derived from the monoclonal antibody 14.G2a, previously used (Pule et al. 2008; Rossig et al. 2002).
In addition, the CAR features are: a truncated CD34 (CD34t) tag, added for detection and purification purposes (Philip et al. 2014; Zhan et al. 2013), co-expressed but separated upon translation by the F2A self-cleaving peptide; a CD8-derived signal peptide to mediate membrane localization of the CAR; a CD3 ζ-chain signalling domain and 4-1BB co-stimulation, linked to the scFv via a CH2CH3 spacer; a CD8-derived hinge sequence, to facilitate CAR binding to the target and appropriate conformation (Hudecek et al. 2015; Long et al. 2015).
Equivalent anti-GD2 CAR backbone (hereon referred to simply as GD2) was utilised to obtain GD2 ARG1 and GD2 ARG2 CARs, with the incorporation of codon-optimised human arginase 1 or 2 enzymes respectively, following a P2A cleavage site.
Full DNA and protein sequences of the transgenes can be found in the Appendix (8).

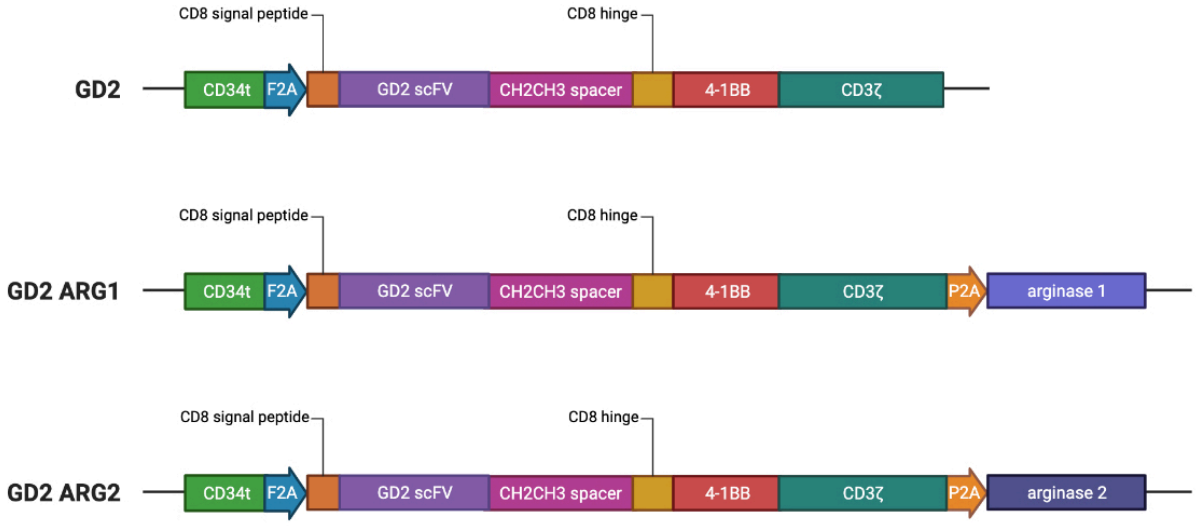

Figure 26: Structure and design of the novel anti-GD2 chimeric antigen receptors (CARs).

The anti-GD2 CAR backbone (GD2) consisting of: truncated CD34 (CD34t) for sorting and detection, F2A cleavage site, CD8 signal peptide for localisation, GD2 recognition domain (scFv from 14.G2a mAb), CH2CH3 spacer region and CD8-derived hinge for spatial plasticity, 4-1BB co-stimulation and CD3-ζ chain signalling domain. Arginase 1 or arginase 2 enzyme sequences were added following P2A cleavage site, to obtain GD2 ARG1 and GD2 ARG2 CARs.

4.2.2 Retroviral Titre and Transduction of the Novel Constructs

CAR-containing vectors were transfected into Phoenix AMPHO retrovirus cell line and viral titres were measured 24 hours post-transfection (Figure 27A). The average titres, measured with QuickTitre Retrovirus Quantitation Kit (Cell Biolabs), were comprised between 80µg/ml and 110µg/ml, with GD2 ARG2 recording the highest average viral load. Harvested retroviruses were then used to transduce Jurkat cell likes.

CAR detection was performed by flow cytometry using the CD34 tag present in the CAR, with Mock-transduced cells of each individual experiment representing 0% efficiency (Figure 27B). The CAR was shown to be expressed in all the transduced samples, with efficiencies on day 4 post-transduction exceeding 20% (Figure 27C).

Successfully engineered Jurkat cells were isolated by positive selection and population purity was checked by flow cytometry on the CAR-Jurkat cells for downstream experiments (Figure 27D).

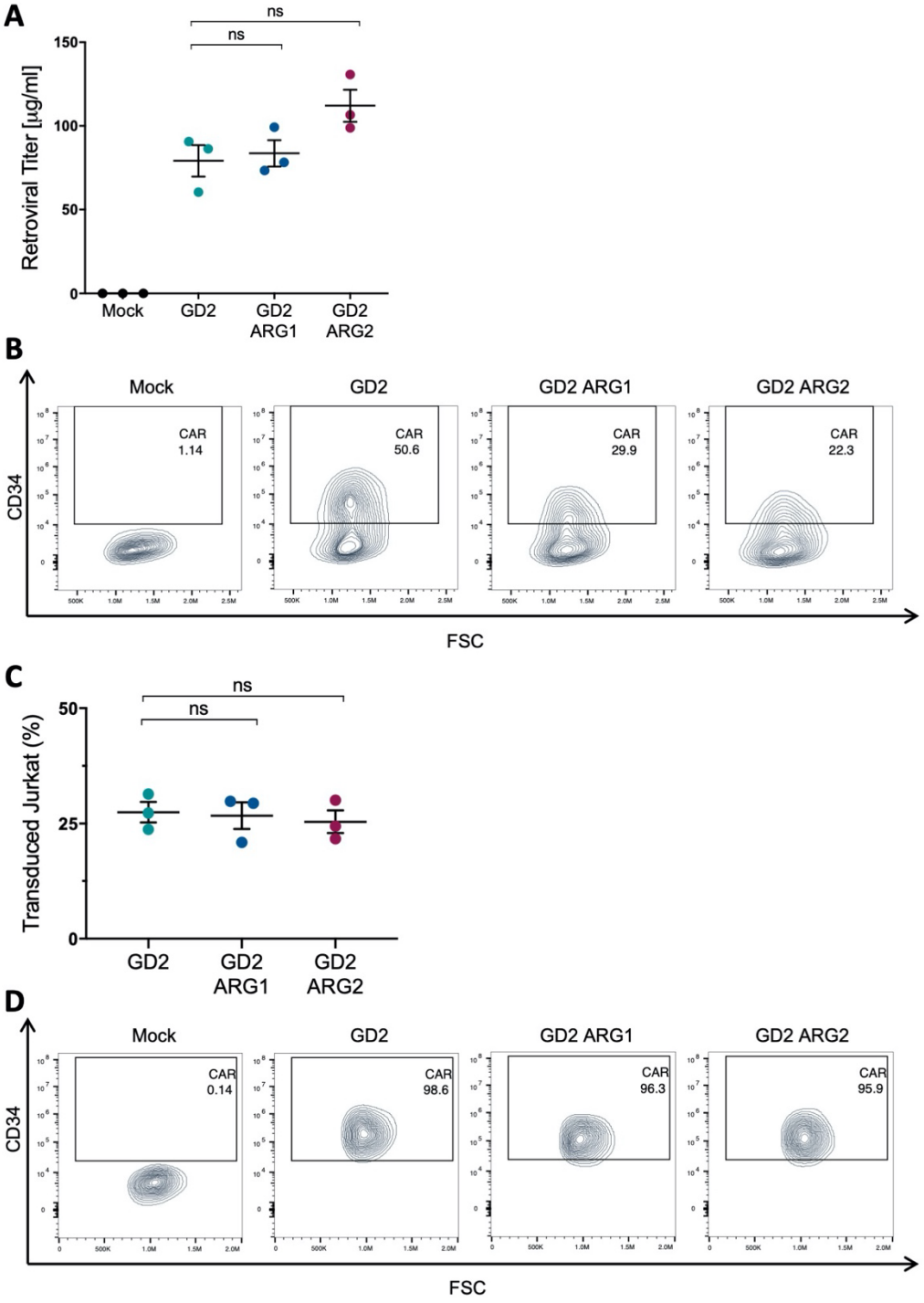

Figure 27: Retrovirus production and transduction of Jurkat cells with GD2, GD2 ARG1 and GD2 ARG2 CARs.
Retroviral titres were measured by viral nucleic acid content in the supernatants after 24h for transfected and untransfected (i.e. Mock) Phoenix AMPHO (n=3) using a QuickTitre Retrovirus Quantitation Kit (Cell Biolabs) (A). Transduction efficiencies of CAR constructs in Jurkat cells based on CD34t detection with CD34 mAb by flow cytometry compared to Mock-transduced cells; representative flow cytometry gating (B) and summary data (C). After isolation of CAR+ cells, purity was confirmed by flow cytometry (D). Results in A and C are shown as mean ± SEM of n=3. Statistical analysis: paired t test.

4.2.3 Expression and Function of ARG1 and ARG2 in the Engineered Cells

We next sought to assess arginase 1 and 2 enzyme expression within the transduced cells. As confirmed by western blot (Figure 28A) with β-actin as a loading control, arginase 1 was expressed by the GD2 ARG1 cells, while undetected in all other transduced or Mock cells (Figure 28B). We found baseline expression of arginase 2 in all Jurkat samples; however, the enzyme was overexpressed by 1.4-fold in the GD2 ARG2 cells compared to control, as confirmed by densitometry (Figure 28C).

In human, most extracellular L-arginine is imported inside the cell by cationic amino acid transporter (CAT) 1. The presence of such plasma membrane transporter is key to guarantee availability of substrate for arginase 1 and 2. Therefore, CAT1 expression was also assessed by western blot and confirmed to be equally expressed across all the samples (Figure 28A).

Although the presence of the translated arginases was confirmed, it was essential to prove its functionality. Lysed CAR-Jurkat samples were tested in an enzyme activity assay and the production of urea resulting from the hydrolysis of L-arginine was quantified colourimetrically. Urea conversion rates were further translated into enzymatic activity units per cell (Canè and Bronte 2020).

Consistent with the protein expression, we observed an increased arginase activity, within the arginase-transduced Jurkat samples. In particular, when compared to the GD2 control CAR, GD2 ARG1 showed a 6.7-fold increase ($p=0.0020$) and GD2 ARG2 a 2.5-fold increase in enzyme activity ($p=0.0156$) (Figure 28D).

This data proved that both the GD2 ARG1 and GD2 ARG2 CAR constructs successfully delivered functional enzymes within the cells and allowed their constitutive expression.

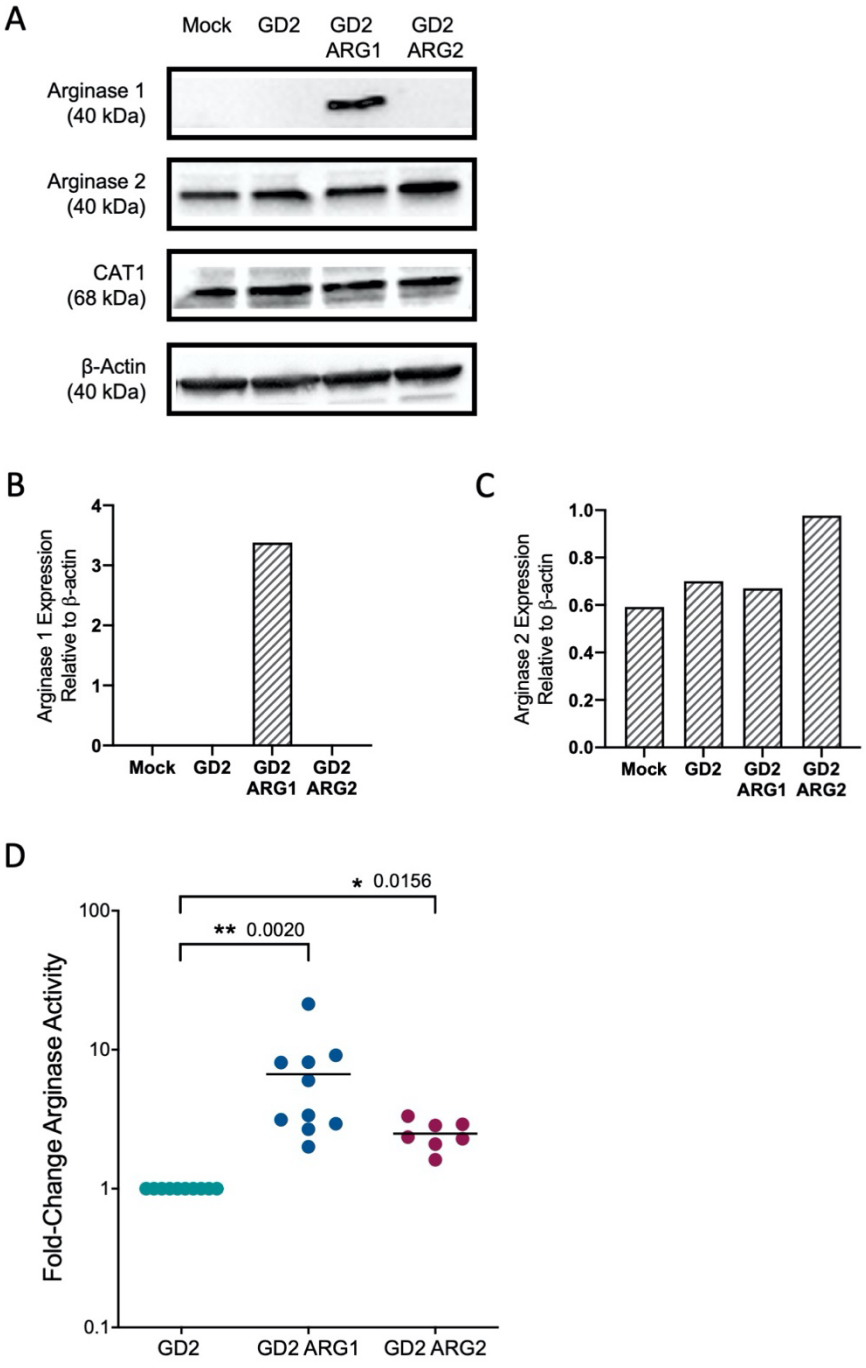

Figure 28: Arginase 1 and arginase 2 expression and functionality in CAR-transduced Jurkat cells.

Protein expression analysis by western blot of arginase 1, arginase 2 and the L-arginine transporters CAT1 in CAR-engineered or Mock Jurkat cells, with β-actin as loading control (A). Densitometric analysis of arginase 1 and arginase 2 protein expression relative to β-actin control (B, C). Arginase activity assay of the GD2 ARG1 and GD2 ARG2 vs control GD2 Jurkat, expressed as fold-change activity (mU/million cells) (n=7) (D). Statistical analysis: Willcoxon test.

4.2.4 Neuroblastoma Recognition *In Vitro*

To test whether the CAR-engineered Jurkat cells were able to recognize the antigen *in vitro*, we co-cultured $GD2^+$ neuroblastoma cell lines with CAR-Jurkat for 48 hours at different effector (E) to target (T) ratios (i.e.: 1:1, 10:1, 100:1). The cells were then acquired with a flow cytometer and expression of the T cell activation marker CD69 was measured.

Prior to the experiment, the presence of the target antigen GD2 was confirmed by flow cytometry (Figure 29A).

As displayed in Figure 29B, Jurkat cells presented a baseline expression of CD69 even in absence of target across all samples. Nonetheless, we were able to detect marked upregulation of CD69 in response to $GD2^+$ target cells across all the CAR-transduced samples. Antigen dilution corresponded to a decreased level of CD69, consistent to a dose-response effect. Antigen recognition was still appreciable at the lowest antigen titration of 1:100 (E:T), where the ΔMFI was still significantly higher than in absence of antigen ($p=0.0094$ for GD2, $p=0.0165$ for GD2 ARG1, $p=0.0033$ for GD2 ARG2).

With these data we could conclude that the anti-GD2 CARs introduced in Jurkat cells were able to successfully recognise the GD2 antigen on the tumour surface and induce downstream signalling through their CD3ζ-chain domain.

We did not detect any significant difference in activation marker expression between the GD2 ARG1 or GD2 ARG2 samples, compared to the GD2 control. Hence, co-expression of the enzymes arginase 1 or arginase 2 did not affect the functionality of the chimeric antigen receptor.

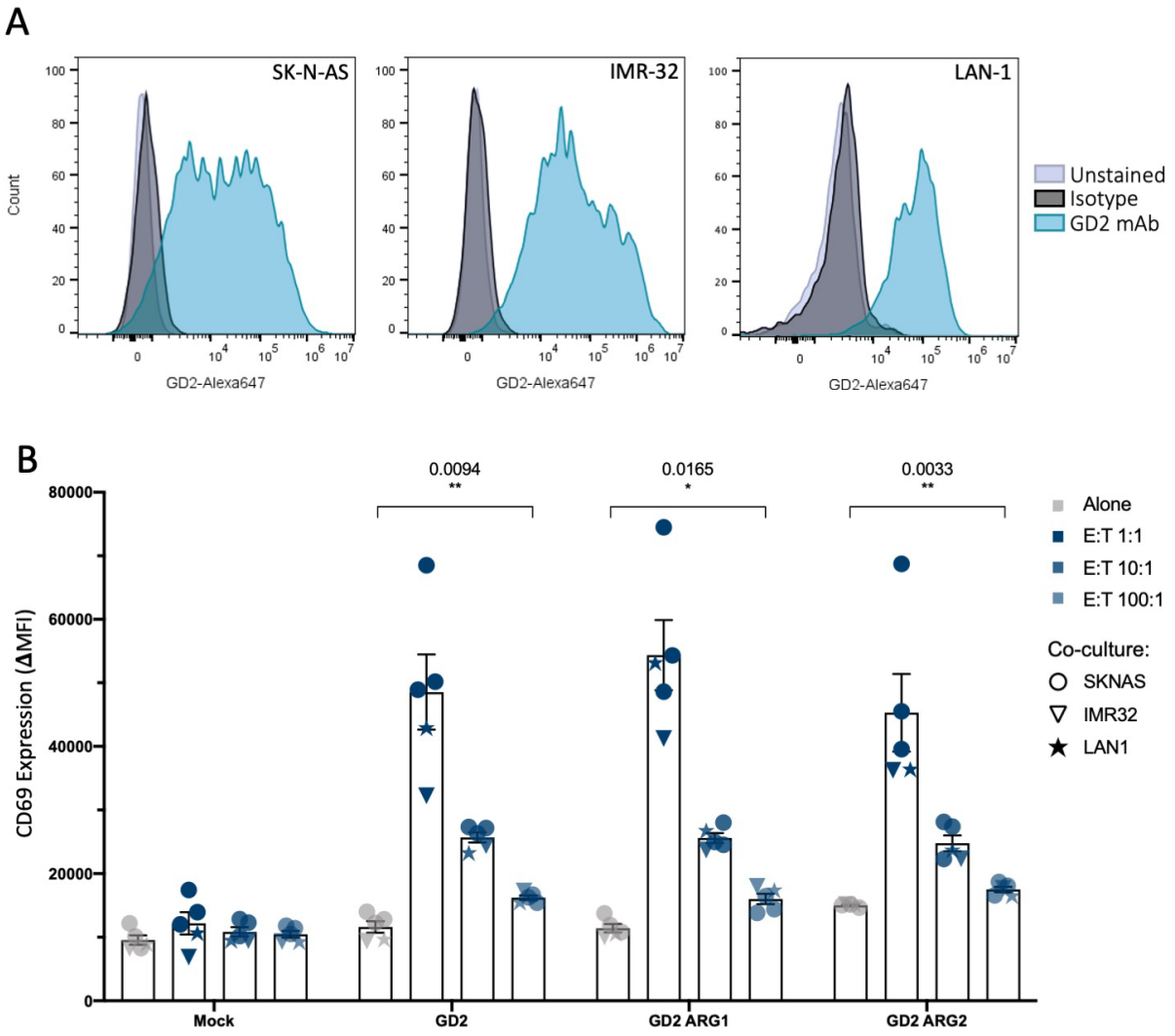

Figure 29: CAR-Jurkat recognise GD2+ neuroblastoma in vitro.

Neuroblastoma cell lines (SK-N-AS, IMR-32, LAN-1) expression of target antigen GD2 was routinely confirmed by flow cytometry prior to coculture experiments (A). Neuroblastoma cell lines were plated and allowed to adhere for 2h before CAR-Jurkat addition and 48h incubation. Co-culture were set up with (blue) or without (grey) target antigen at different effector to target (E:T) ratios of 1:1, 10:1, 100:1 (B). Resulting CD69 expression was measured by flow cytometry as median fluorescent intensity, subtracted of unstained (ΔMFI). Symbols represent cell line type; colour shading represents antigen dilution. Shown as mean ±SEM of n=5 independent experiments. Statistical analysis: paired t test.

4.2.5 Assessment of Cellular Bioenergetics

Glucose breakdown into pyruvate (i.e. glycolysis) followed by oxidative phosphorylation (OxPhos) in the mitochondria (i.e. respiration) is the most convenient source of ATP to fuel the cell's energy demand; albeit it requires availability of oxygen.

Rapidly growing cells, such as activated T cells, are known to heavily rely on glycolysis with fermentation of pyruvate into lactate, i.e. aerobic glycolysis or Warburg effect (Lunt and Vander Heiden 2011).

T cell performance is closely associated to bioenergetics and L-arginine has been implicated in the modulation of T cell responses, as previously discussed in 1.2.7.

Therefore, we decided to interrogate the CAR-Jurkat models with a real-time metabolic flux assay using a Seahorse XF Analyzer, to understand whether the introduction of ectopic arginases within the cells altered their bioenergetic profile.

Figure 30 describes the pathways measured by the Seahorse platform and the output of the assay, which relies on the simultaneous measurement of extra-cellular acidification rate (ECAR) (mpH/min) and oxygen consumption rate (OCR) (pmol/min), as means to quantify glycolysis and OxPhos respectively.

A set of injections of different electron transport chain inhibitors (e.g. oligomycin, BAM15, Rotenone + Antimycin A) constitutes the Mito Stress assay, enabling us to determine specific metabolic parameters: the basal ECAR, glycolytic capacity and maximal ECAR for glycolysis; the basal respiration, maximal respiration, ATP production, spare respiratory capacity, non-mitochondrial oxygen consumption and proton leak for OxPhos, as previously defined (Kolev et al. 2015; Jones et al. 2019).

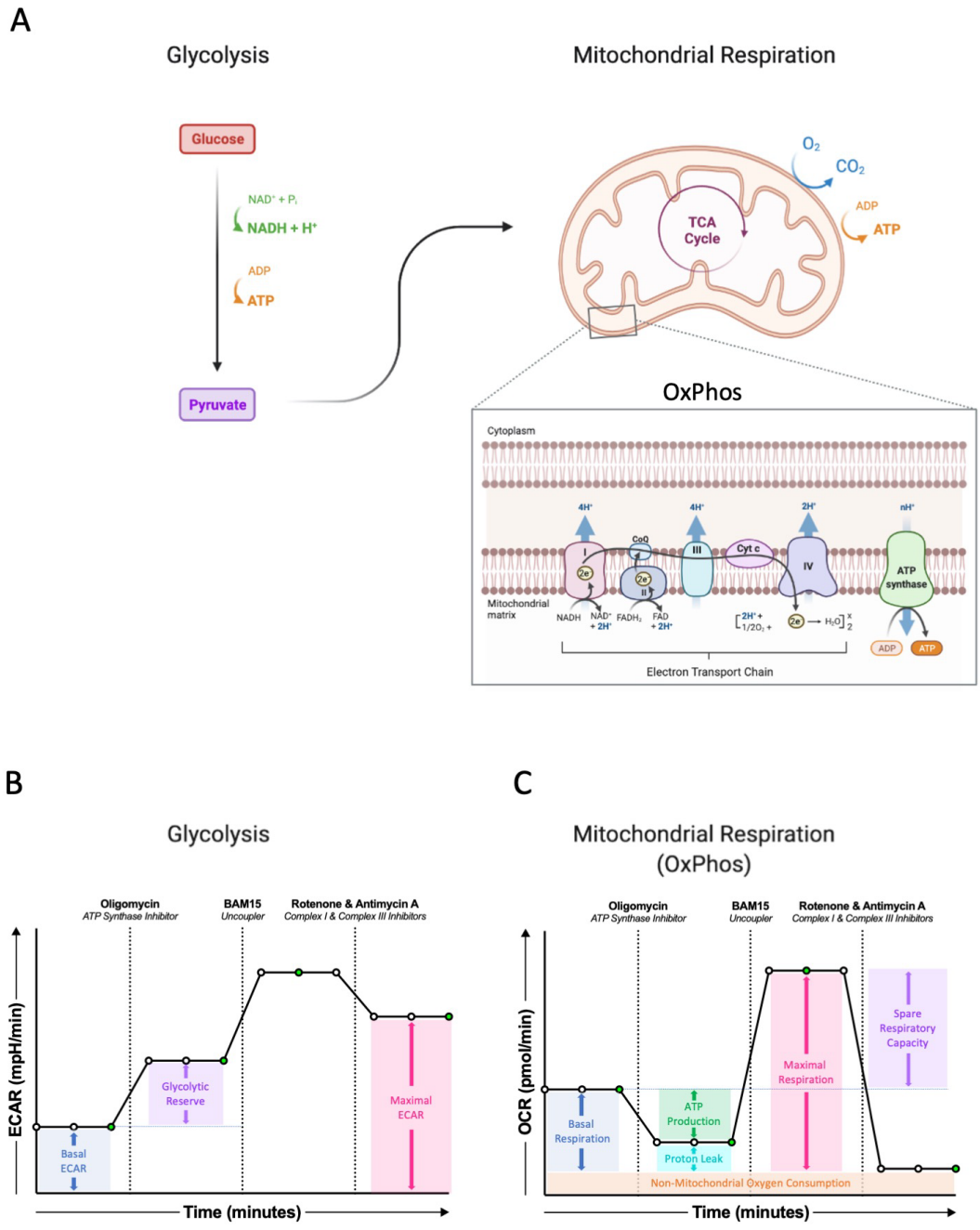

Figure 30: Overview of glycolysis and mitochondrial respiration (or OxPhos) and their parameters.

(A) Glycolysis is the cellular process of breaking down glucose into pyruvate. In presence of O_2, pyruvate is fully oxidised to CO_2 by the TCA cycle in the mitochondria to generate ATP, a process known as mitochondrial respiration, via oxidative phosphorylation (OxPhos). Glycolysis and OxPhos can be measured in real-time by the Seahorse XF Analyzer as the rates of extra-cellular acidification (ECAR) and oxygen consumption (OCR) respectively. During a Mito Stress assay, the staggered injection of specific inhibitors allows the calculation of several glycolytic (B) and OxPhos (C) parameters at the measure points marked in green.

Mock-, GD2-, GD2 ARG1- and GD2 ARG2-engineered Jurkat cells were cultured for 48h in Low L-Arg Medium to mimic the tumour microenvironment and then plated for the Mito Stress assay. The representative OCR over time curve showed the trend for both the arginase-containing CAR-Jurkats to consume oxygen at a higher rate throughout the assay (Figure 31A). Higher basal respiration characterised the GD2 ARG1 sample compared to the GD2 control ($p = 0.0273$), while the same trend was not significant in the case of GD2 ARG2 (Figure 31B). A pronounced spike in OCR followed BAM15 injection, denoting the maximal respiration capacity of the samples. This was significantly increased for both the arginase-containing Jurkat cells compared to control ($p=0.0483$ for GD2 ARG1, $p=0.0098$ for GD2 ARG2) (Figure 31C). Increased spare respiratory capacity was observed only in the GD2 ARG2 sample ($p=0.0175$) (Figure 31D), while GD2 ARG1 was characterised by an increase in ATP production ($p=0.0427$), proton leak ($p=0.0097$) and non-mitochondrial oxygen consumption ($p=0.0103$) compared to the GD2 control (Figure 31E-G).

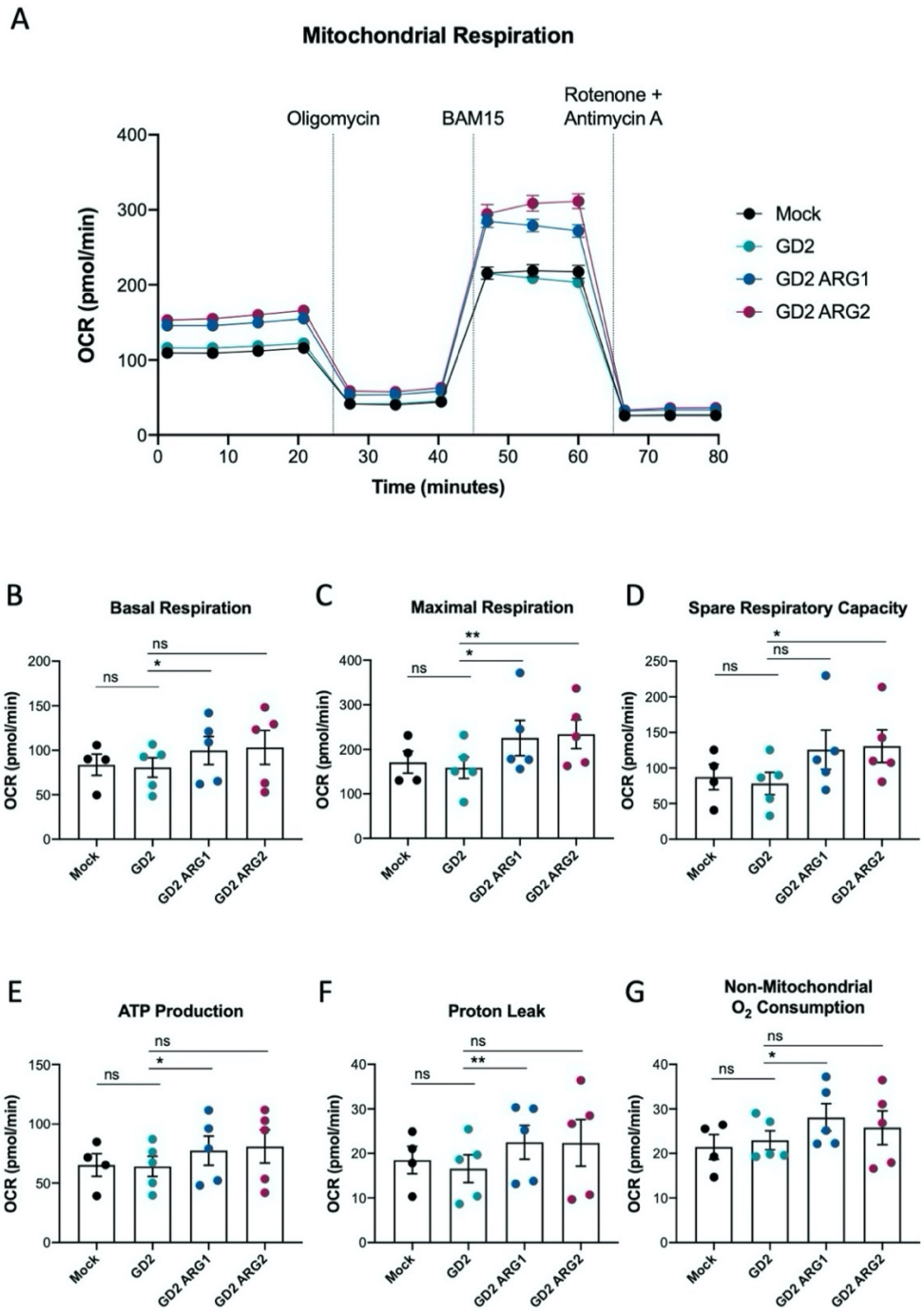

Figure 31: Mitochondrial respiration assessment of different CAR-Jurkat cells under mitochondrial stress.

Mock-, GD2-, GD2 ARG1- and GD2 AGR2-transduced Jurkat cell lines were assessed with a Mito Stress test on a Seahorse XF Analyzer platform (A). Oxygen consumption rate (OCR) was recorded as measure of oxidative phosphorylation (OxPhos); oligomycin, BAM15 and rotenone and antimycin A were injected to inhibit steps of respiration. OxPhos parameters were calculated and compared: basal respiration (B), maximal respiration (C), spare respiratory capacity (D), ATP production (E), proton leak (F) and non-mitochondrial O_2 consumption (G). Results shown as mean ± SEM of n=5 independent experiments. Statistical analysis: t test, * $p \leq 0.05$, ** $p \leq 0.01$.

At the same time, ECAR was measured. Similarly to what was seen for OCR, both the arginase-containing CAR-Jurkat cells seemed to have increased rates compared to control, as shown in the representative ECAR over time plot (Figure 32A).

Interestingly, before the oligomycin injection, there was no statistical difference in basal ECAR across the CAR-Jurkat samples (Figure 32B). However, upon mitochondrial challenge, the GD2 ARG2 sample displayed greater maximal ECAR ($p=0.0097$) and glycolytic capacity ($p=0.0305$) than control (Figure 32C and D).

To further highlight whether there was a change in glycolytic or oxidative reliance across samples, the ratio between basal OCR and basal ECAR was calculated as previously described (Keuper et al. 2019). In this instance, no change was observed in the OCR/ECAR ratio across the four samples (Figure 32E).

In order to quantify the total ATP production flux of the cells (JATP), the method advised by Louie et al. (2020) was used to correct and convert ATP production. Glycolysis-derived ATP (JATPglyc) and OxPhos-derived ATP (JATPmito) were summed to obtain total JATP and the results are shown in (Figure 32E). GD2 ARG1 and GD2 ARG2 displayed a raised, albeit not significant, JATPglyc and JATPmito compared to control.

Finally, no difference between Mock-transduced and GD2 control CAR-transduced Jurkat was observed in any of the parameters measured during the Mito Stress assay, indicating that there were no metabolic alterations due to the transduction protocol alone.

Overall, these data showed evidence for a role of arginase in cellular bioenergetics.

In addition, due to the different signatures observed between the GD2 ARG1 and GD2 ARG2 Jurkat, we can conclude that arginase 1 and arginase 2 present effects on the bioenergetics distinct to one another.

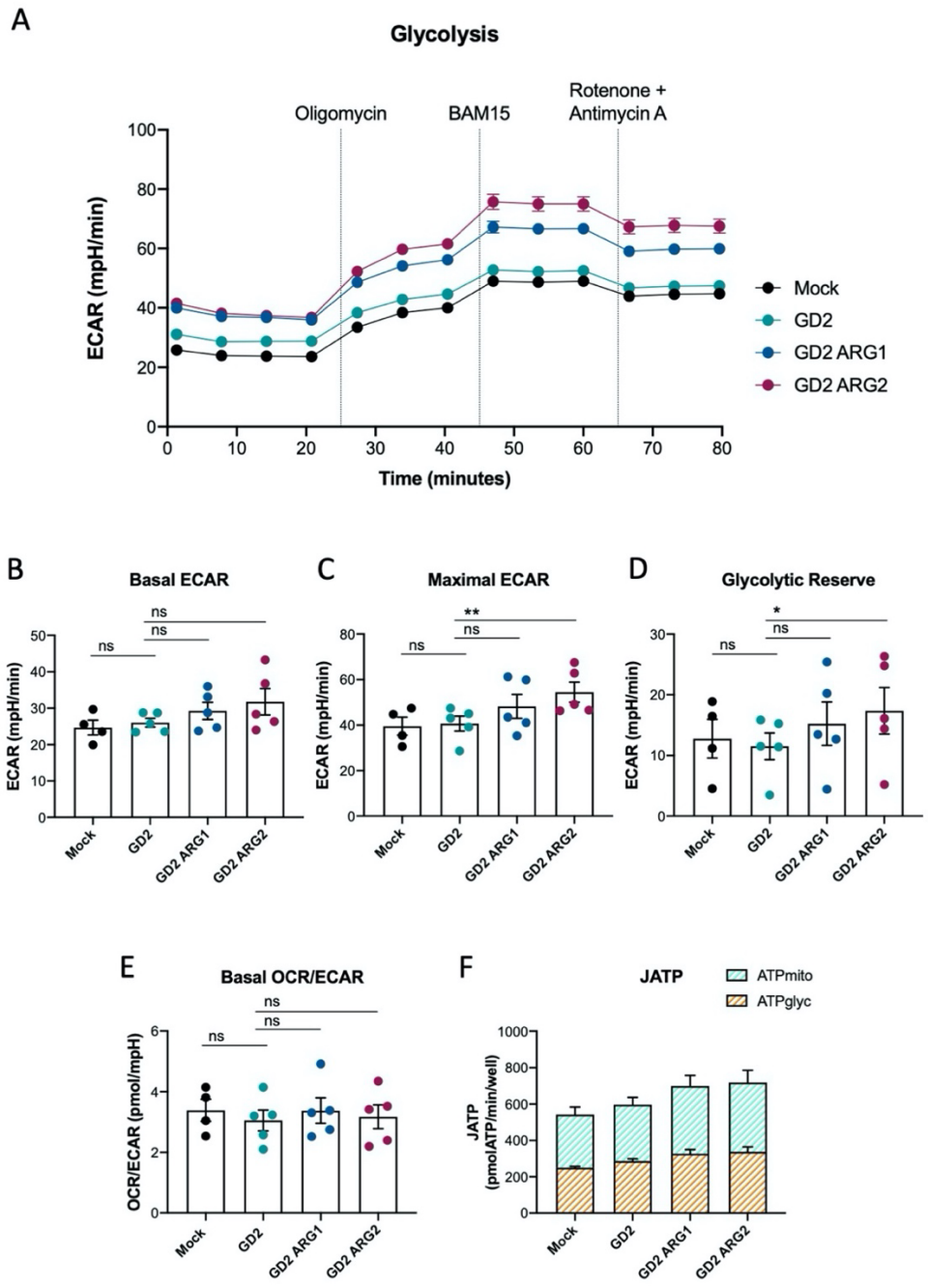

Figure 32: Glycolytic rate analysis of the different CAR-Jurkat cells under mitochondrial stress.

Mock-, GD2-, GD2 ARG1- and GD2 AGR2-transduced Jurkat cell lines were assessed with a Mito Stress test on a Seahorse XF Analyzer platform (A). Extra-cellular acidification rate (ECAR) was recorded as measure of glycolysis; oligomycin, BAM15 and rotenone and antimycin A were injected to inhibit steps of respiration. Glycolytic parameters were calculated and compared: basal ECAR (B), maximal ECAR (C), glycolytic reserve (D). OCR/ECAR ratio was obtained from respective basal values (E). Total ATP production rate (JATP) was calculated as sum of glycolytic ATP (ATPglyc) and OxPhos-derived ATP (ATPmito), following Louie et al. 2020 (F). Results are represented as mean ± SEM of n=5 independent experiments. Statistical analysis: t test, * $p \leq 0.05$, ** $p \leq 0.01$.

4.2.6 Transcriptome Analysis of CAR-Jurkat Cells by RNASeq

The phenotypic differences observed in the mitochondrial stress response after insertion of arginase 1 and arginase 2 within the cells suggested to investigate the transcriptome of the transduced Jurkat samples by mRNA sequencing, to understand what pathways and transcription programmes could be found changed in the enzyme-modified cells.

Pure populations of GD2, GD2 ARG1 and GD2 ARG2 CAR-Jurkat cells were pre-conditioned in Low Arg Medium for 48h and subsequently harvested for RNA extraction and mRNA library preparation; sequencing was then obtained on a NextSeq 500 platform.

We decided to focus the attention on the genes involved in cellular metabolism and bioenergetics, i.e. the glucose metabolism hallmarks, from the Molecular Signatures Database (www.MSigDB.org) (Liberzon et al. 2015) (Figure 33).

Several changes in cellular processes emerged from this overview. Firstly, genes encoding key glycolytic enzymes, such as hexokinase 2 (HK2) enolase (ENO1) and lactate dehydrogenase (LDHA), were shown to have a decreased expression in the GD2 ARG1 and GD2 ARG2 samples compared to GD2. Conversely, the monocarboxylate transporter 4 encoded by *SLC16A3* seemed to have a reduced expression in the GD2 and GD2 ARG1 samples, while it was upregulated in GD2 ARG2.

Another aspect emerged from the data is the upregulation of the hexosamine biosynthetic pathway in both the arginase-containing CAR-Jurkat, given by the expression patterns of *GFPT1*. In fact, *GFPT1* encodes for the first and rate-limiting enzyme of the hexosamine pathway, catalysing the conversion of glucose into glucosamine 6-phosphate and therefore committing glucose to the hexosamine fate.

Further to the pathways mentioned so far, a group of genes involved in the aspartate/malate shuttle seemed to display a distinct pattern of expression across the CAR constructs assessed; these were *GOT1* and *GOT2*, *MDH1* and *MDH2*, and the mitochondrial membrane transporters of malate and aspartate *SLC25A10* and *SLC25A13*.

In particular, *GOT1* was upregulated in the GD2 ARG1 sample, while *GOT2* in the GD2 ARG2 sample. Furthermore, the genes encoding for malate dehydrogenase, the enzyme catalysing the reaction step downstream of GOT, were also characterised by different expressions: *MDH1* was found to be downregulated in both GD2 ARG1 and GD2 ARG2 cell, while *MDH2* was overexpressed exclusively in the GD2 ARG2 cells.

The upregulation of the mitochondrial transporters for malate and aspartate *SLC25A10* (in both GD2 ARG1 and GD2 ARG2) and *SLC25A13* (only in GD2 ARG1) was also observed.

Lastly, two genes required for the maintenance of the cellular redox balance were highlighted for their differential expression: *GLRX,* encoding for the glutathione oxidoreductase enzyme was upregulated in the GD2 ARG1 sample, while *IDH1*, i.e isocitrate dehydrogenase, was overexpressed in the GD2 ARG2 sample. Both gene products promote the restoration of the NADP:NADPH ratio of the cells.

In conclusion, the transcriptomic signatures described a different metabolic transcription programme, both between GD2 and the arginase-expressing cells, and between the GD2 ARG1 and GD2 ARG2 samples.

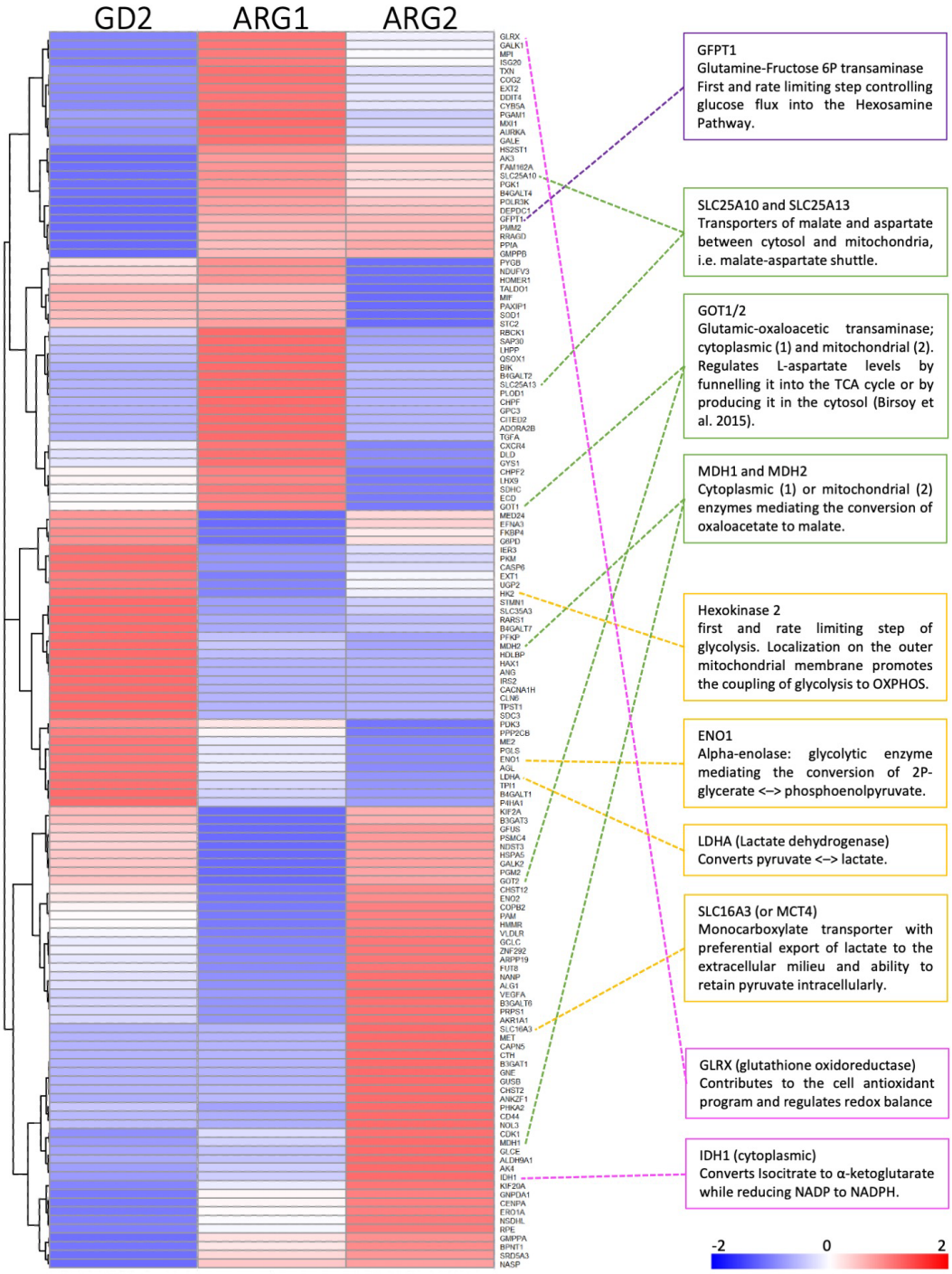

Figure 33: Gene expression heatmap of glucose metabolism within CAR-Jurkat samples

Heatmap resulting from the RNASeq of GD2, GD2 ARG1 and GD2 ARG2 CAR-Jurkat samples to investigate patterns of gene expression within the glucose metabolic pathways. Gene set enrichment analysis based on MSigDB's Hallmark_Glycolysis gene set (Liberzon et al. 2015), represented as $\log_2$Fold-change. Highlighted pathways/functions: hexosamine biosynthesis pathway (purple), aspartate-malate shuttle (green), glycolysis (yellow) and redox balance (pink).

4.2.7 Intracellular Metabolite Analysis and L-Arg Tracing of the Novel Engineered Cells

It has previously been shown that L-arginine uptake in activated T cells is necessary beyond protein synthesis and instead it is funnelled into the production of the downstream metabolites L-ornithine, L-proline and spermidine (Geiger et al. 2016).

As summarised in the diagram in Figure 34, L-arginine metabolism crosses paths with several key cellular pathways within the cytoplasm and mitochondria: the urea cycle and the downstream polyamine production; nitric oxide (NO) production via NOS with its ubiquitous biological impacts; the TCA cycle via the L-aspartate shunt; the proline cycle and downstream glutamate reservoir; finally, the L-methionine cycle, involved in polyamine synthesis, DNA methylation and the one-carbon metabolism (Choudhari et al. 2013).

Given the differences in bioenergetic rates and transcriptomic signatures, we sought to investigated whether the constitutive expression of arginase 1 and arginase 2 could alter the biochemical reactions of the cells.

We proceeded with the analysis by GC-MS of the intracellular metabolites of the CAR-Jurkat cells. The cells were conditioned in Low L-Arg Medium for 48 hours, prior to 24-hour culture in GC-MS Medium for the downstream extraction and analysis.

Unfortunately, our GC-MS protocol did not allow for the detection of L-arginine, L-ornithine, L-citrulline or polyamine (putrescine, spermidine, spermine), due to their difficult to distinguish pattern of fragmentation. Nonetheless, we were able to obtain an overview of the intracellular abundance of TCA cycle and glycolytic intermediates, as well as amino acids.

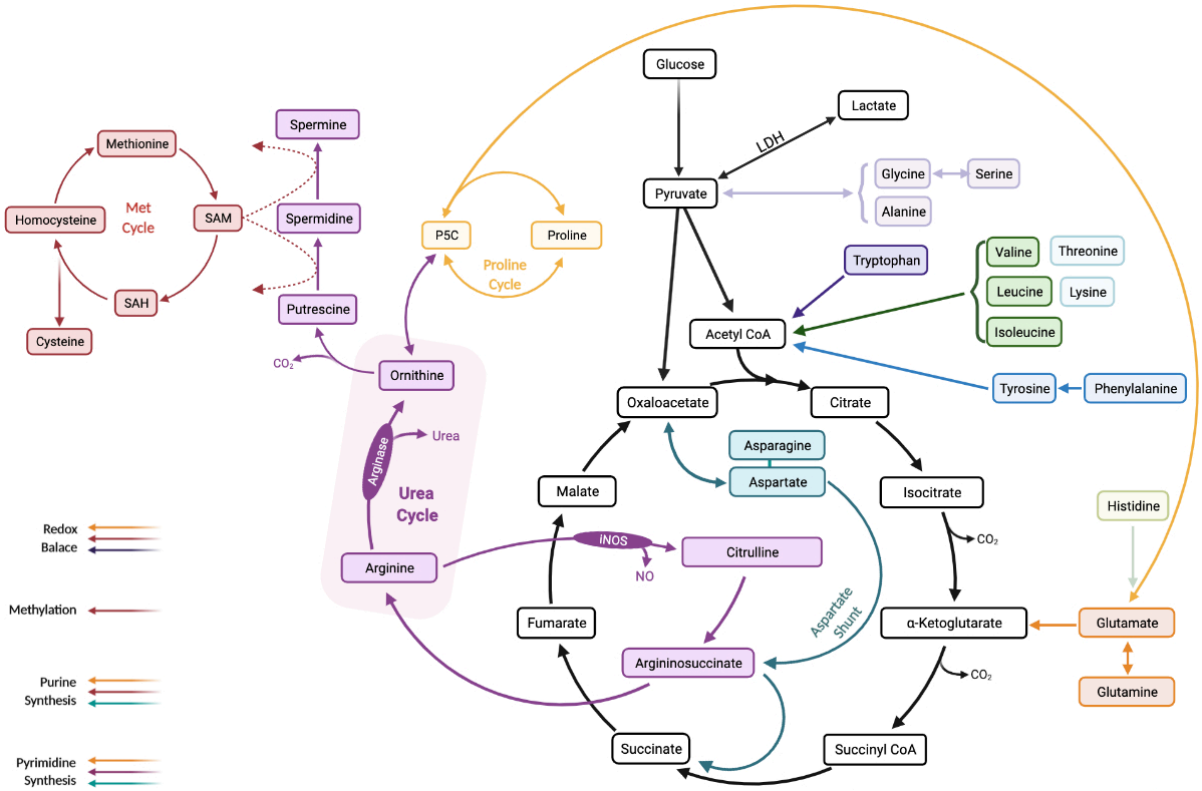

Figure 34: L-Arginine metabolism and its intersections with the intracellular pathways.

L-arginine metabolism crosses path with multiple cellular activities: the urea cycle (purple), the TCA cycle (black) via the L-aspartate shunt (teal), the proline biosynthesis (yellow), the methionine cycle (red); hence, L-arginine is involved, directly or indirectly, in protein, purine and pyrimidine biosynthesis, as well as DNA methylation and cellular redox balance.

An overview of the key metabolites and their prevalence is given in the heatmap in Figure 35, which highlights the overall changes within the arginase-containing samples compared to the GD2 control. Generally, it appeared that most intracellular metabolites were raised in the arginase 1 CAR-Jurkat, with the exclusion of the TCA cycle intermediates; on the other hand, the arginase 2 CAR-Jurkat presented a less stark divergence to the control.

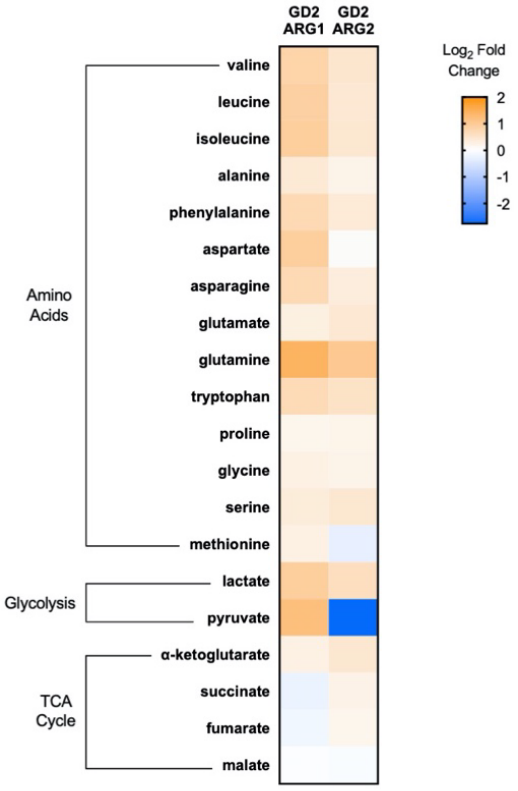

Figure 35: Overview of the intracellular metabolite abundance of CAR-Jurkat cells detected by GC-MS.

CAR-Jurkat cells pre-conditioned in Low Arg Medium for 48h, were cultured in GC-MS medium replete of nutrients for 24h; polar metabolites were subsequently extracted and derivatised before being analysed by GC-MS and normalised by protein concentration. A heatmap of the most relevant metabolites for GD2 ARG1 and GD2 ARG2 is shown as log_2 fold-change of the GD2 control. Results from 3 independent experiments.

In Figure 36, the key glycolytic and TCA cycle metabolites are illustrated.

The GD2 ARG1 CAR-Jurkat presented a significantly increased concentration of the glycolytic end-products pyruvate ($p = 0.028$) and lactate ($p = 0.006$), as well as the TCA cycle intermediate α-ketoglutarate ($p = 0.017$).

No difference was found in the downstream TCA metabolites succinate, fumarate and malate.

GD2 ARG2 also showed higher levels of lactate ($p = 0.026$); however, no significant rise in pyruvate or TCA metabolite levels were found compared to the control. This highlights a first underlying difference between the effects of the two arginase isoforms on cellular metabolism.

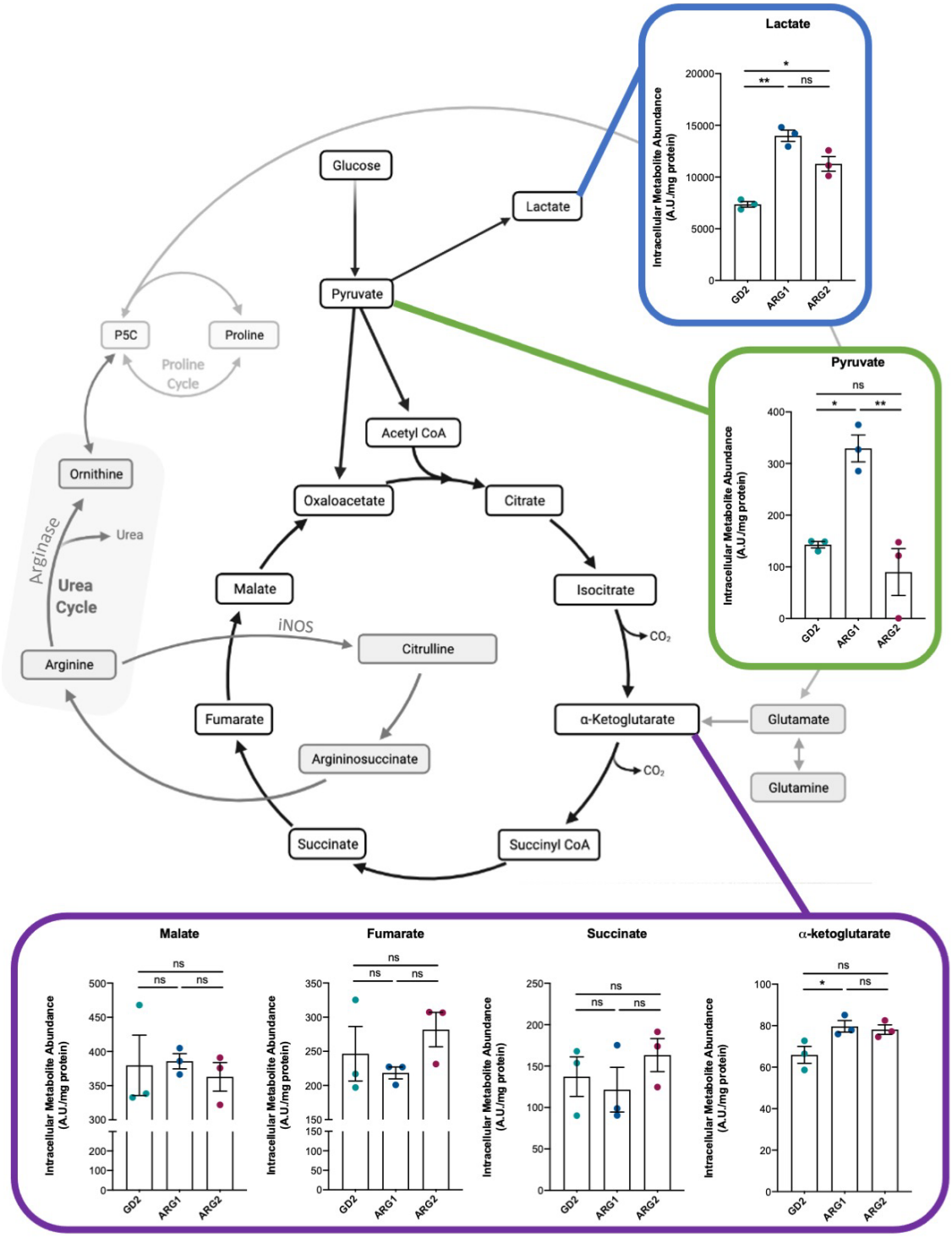

Figure 36: Intracellular glycolytic and TCA cycle metabolite abundances of CAR-Jurkat cells.

CAR-Jurkat cells pre-conditioned in L-Arg Low microenvironment for 48h, were cultured in GC-MS medium replete of nutrients for 24h; polar metabolites were subsequently extracted and derivatised before being analysed by GC-MS and normalised by protein concentration. Selected metabolites are shown as mean ± SEM of 3 independent experiments. Statistical analysis: paired t test; * $p \leq 0.05$, ** $p \leq 0.01$.

For what concerns the intracellular amino acid pool (Figure 37), we observed a marked arginase 1-linked increase in most amino acids: valine ($p = 0.016$), leucine ($p = 0.013$), isoleucine ($p = 0.014$), glycine ($p = 0.032$), alanine ($p = 0.030$), phenylalanine ($p = 0.016$), tyrosine ($p = 0.012$), tryptophan ($p = 0.015$), glutamine ($p = 0.003$), glutamate ($p = 0.011$); asparagine ($p = 0.036$) and aspartate ($p = 0.030$).

Interestingly, despite most amino acids being moderately raised also in the GD2 ARG2 sample, only glutamate ($p = 0.038$) was found at significantly higher concentration compared to GD2 control.

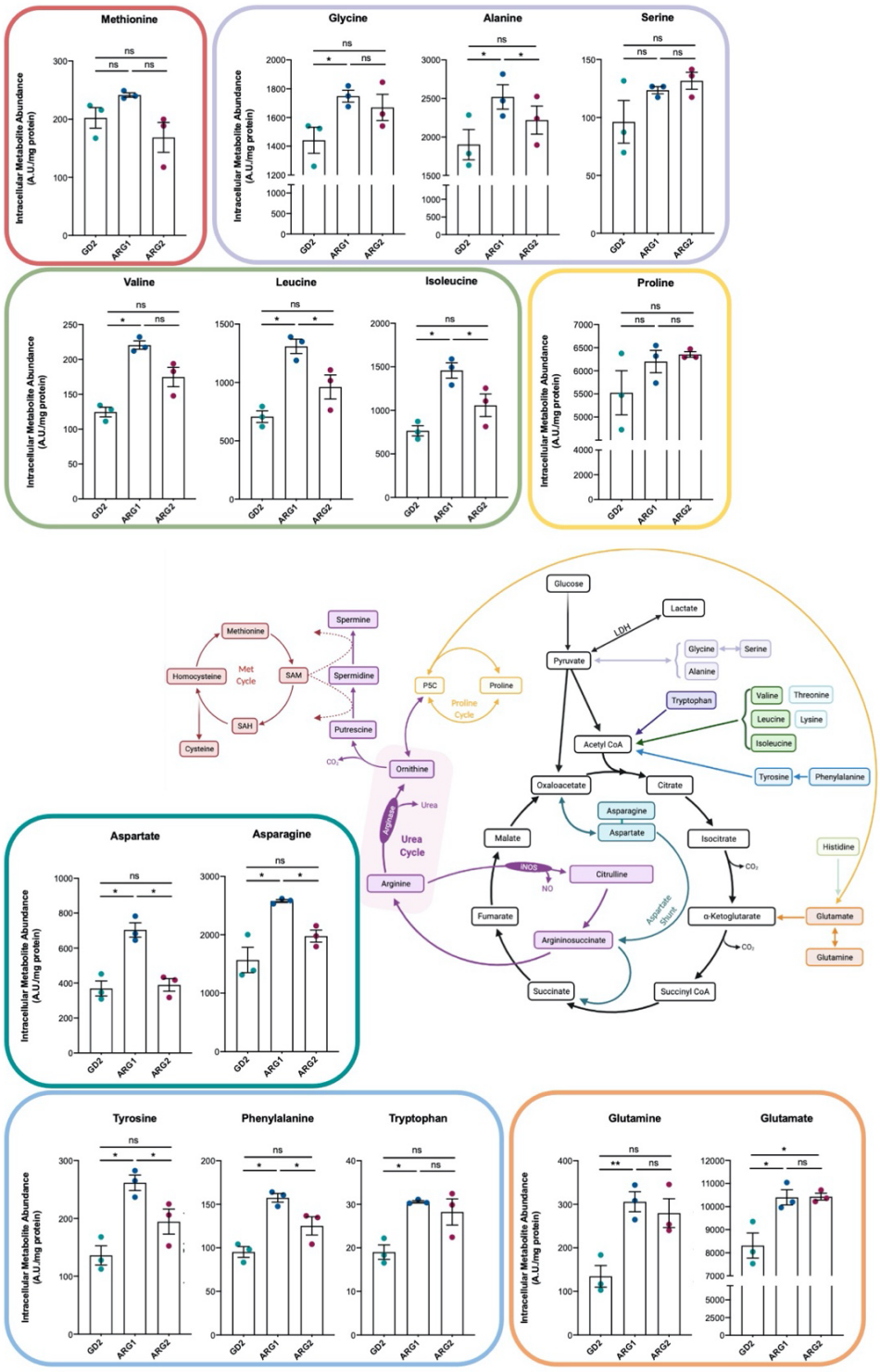

Figure 37: Intracellular amino acid abundance of CAR-Jurkat cells detected by GC-MS.

CAR-Jurkat cells pre-conditioned in L-Arg Low microenvironment for 48h, were cultured in GC-MS medium replete of nutrients for 24h; polar metabolites were subsequently extracted and derivatised before being analysed by GC-MS and normalised by protein concentration. Selected amino acids are shown as bar charts, mean ± SEM. Results from 3 independent experiments. Statistical analysis: paired t test; * $p \leq 0.05$, ** $p \leq 0.01$.

While this type of output informed us on the relative prevalence of metabolites within the different samples, the explanation for such build-up (or depletion) can either be due to the increased upstream production or to the decreased downstream consumption. In the attempt to better understand the flux of the metabolic pathways involved, we conducted a tracing analysis and followed the intracellular fate of L-arginine.

The different CAR-Jurkat cells were incubated in GC-MS medium supplemented with uniformly labelled L-arginine (U-$^{13}C_6$ L-Arginine) for 24h before extraction and downstream acquisition by GC-MS. Normalised results were represented depending on the number of labelled ^{13}C atoms present in the particular metabolite, with m+0 meaning that no ^{13}C was detected and m+1, m+2, … m+x, indicating 1, 2, … x ^{13}C were detected.

The tracing analysis revealed only a negligible contribution of L-arginine-derived carbons into lactate (m+1) and such contribution did not significantly vary across the CAR-Jurkat samples (Figure 38).

On the other hand, about 60% of the total pyruvate within the GD2 ARG2 cells contained ^{13}C, with the most abundant isotopomer being m+1; while only 20% of the total pyruvate pool contained ^{13}C in the GD2 control. No ^{13}C labelling was observed in the GD2 ARG1 sample.

For what concerns the metabolism downstream of pyruvate, α-ketoglutarate presented even levels of ^{13}C incorporation throughout all the isotopomers and across all samples; while no evident incorporation of L-arginine was detected in other TCA cycle intermediates such as succinate, fumarate and malate (Supplementary 1).

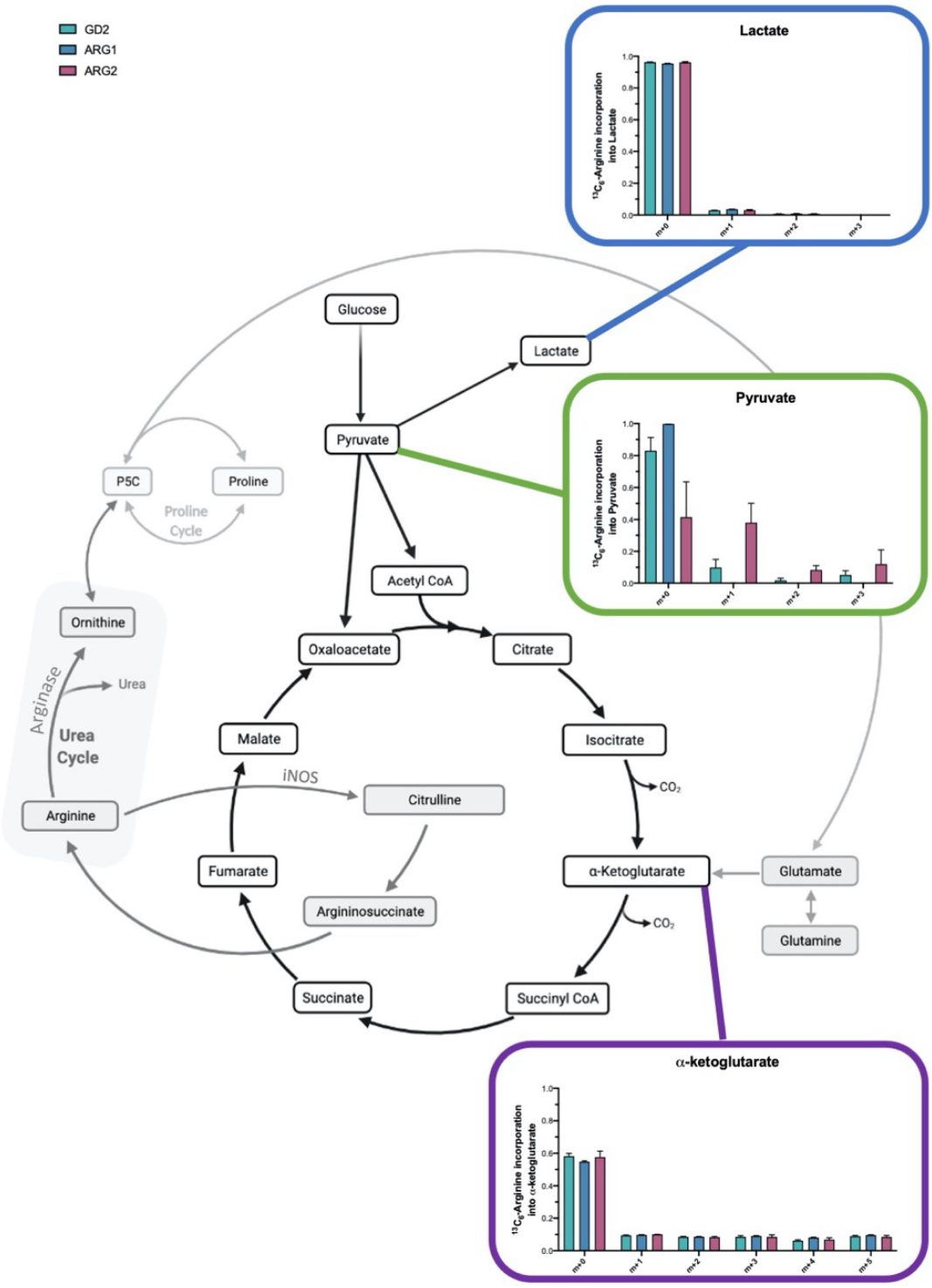

Figure 38: Incorporation of L-arginine into glycolytic and TCA cycle metabolites.

Upon preconditioning in L-arg low microenvironment (48h), CAR-Jurkat cells were incubated with uniformly labelled $^{13}C_6$ L-Arginine for 24h; polar metabolites were extracted and read on a GC-MS. Incorporation of L-arginine was detected in lactate (blue box), pyruvate (green box) and α-ketoglutarate (purple box). Results are normalised by total metabolite abundance and ^{13}C isotopomer distribution is noted as "m+x".

We next wanted to assess whether we could detect any ^{13}C labelling within amino acids. We found that about 15% of the total proline (m+5), as well as a limited amount of glutamate (m+5), were labelled and therefore originated directly from L-arginine hydrolysis (Figure 39). However, we did not observe a marked difference in labelling as a consequence of CAR-Jurkat type.

Overall, these findings suggest that most of the labelled L-arginine introduced in the cultures was likely incorporated within metabolites outside of our detection range or detection window.

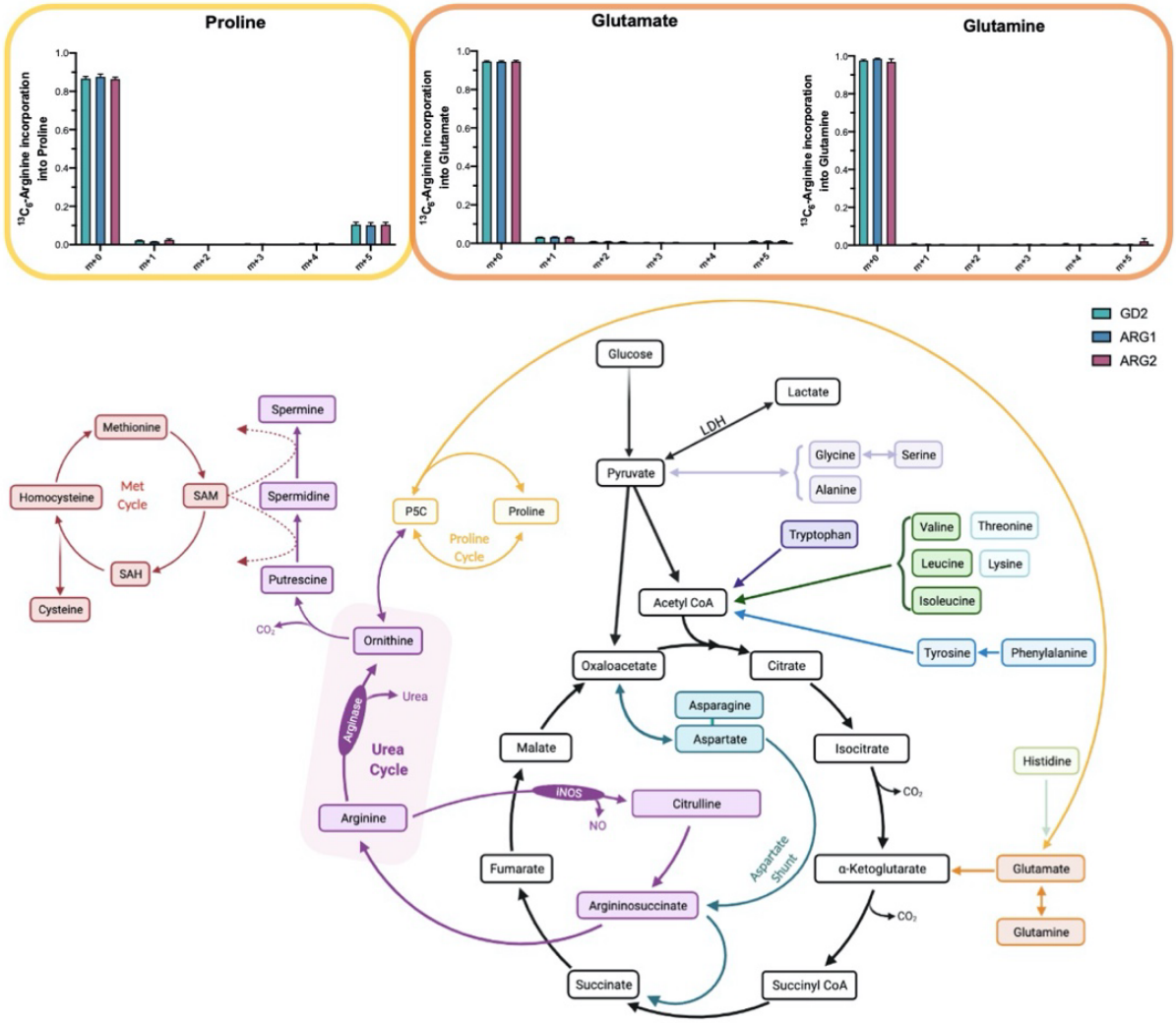

Figure 39: Incorporation of L-arginine into amino acids.

Upon preconditioning in L-arg low microenvironment (48h), CAR-Jurkat cells were incubated with uniformly labelled $^{13}C_6$ L-Arginine for 24h; polar metabolites were extracted and read on a GC-MS. Incorporation of L-arginine was detected in several amino acids. Results are normalised by total metabolite abundance and ^{13}C isotopomer distribution is noted as "m+x".

4.3 Discussion

The results presented so far illustrated how we were able to design and deliver a set of modified CAR constructs within Jurkat T cells. They were shown to be viable and express stable CAR molecules on their surface.

Jurkat cells do not have the ability to be cytotoxic; therefore, we could not rely on target killing to prove antigen recognition. Instead, in order to assess the anti-GD2 CAR functionality, we measured the T cell activation marker CD69 in response to GD2 antigen encounter. This method was previously utilised by Duong et al. (2013) and then Bloemberg et al. (2020) as a mean to assess target recognition when using Jurkat for TCR screening. Indeed, the transduced Jurkats were able to upregulate the CD69 activation marker even at the lowest antigen concentration, demonstrating the CAR's ability to trigger signalling.

The enzyme expression was also confirmed in both AGD2 ARG1 and GD2 ARG2. While arginase 1 was solely expressed by the GD2 ARG1 CAR-Jurkat sample, the mitochondrial isoform arginase 2 was endogenously present to a certain degree in the cell line prior to transduction, in agreement with previous literature (Martí i Líndez et al. 2019). Nonetheless, GD2 ARG2 CAR-Jurkat cells presented an enhanced arginase 2 protein expression compared to GD2. In addition, when assessing the enzyme activity, both GD2 ARG1 and GD2 ARG2 exhibited a significantly increased L-arginine hydrolysis compared to control, despite the underlying presence of endogenous arginase within Jurkat.

The improved rate of L-arginine hydrolysis confirmed the relevance of the metabolic modification we propose.

Interestingly, when comparing the two enzyme isoforms, arginase 1 showed an increased L-

arginine catabolic activity compared to arginase 2, potentially related to their marginally different affinity for the amino acid (Bascur et al. 1966).

T cell performance has been shown to be linked to bioenergetics. Glycolysis with fermentation to lactate (i.e. aerobic glycolysis or Warburg effect) is known to fuel T cell activation (Lunt and Vander Heiden 2011), despite being less convenient in terms of ATP gain. Long lived antigen-experienced cells present a heightened metabolism even when at rest and retain permanent metabolic modifications to enable efficient response upon re-stimulation (Gubser et al. 2013; Jones et al. 2019). Geiger and colleagues (2016) found evidence of L-arginine-induced metabolic alteration in activated T cells, including a shift from glycolysis to OxPhos, which promoted cell resilience and survival in arginine-replete conditions.
While no appreciable change in pathway of choice was observed, as indicated by the constant OCR/ECAR ratio, our metabolic analysis of the modified Jurkat also pointed towards changes in cellular bioenergetics caused by L-arginine metabolism.
Overall, we observed higher metabolic rates between the arginase-expressing CARs and the GD2 control. In addition, our analysis revealed two distinct phenotypes for arginase 1 and arginase 2.

The GD2 ARG1 cells were characterised by raised OxPhos levels at baseline, underpinning a higher energy demand at time 0. In this model, we also found an increased proton leak rate, as well as a heightened non-mitochondrial oxygen consumption rate compared to control; the latter, a parameter generally linked to ROS production. Proton leak, in turn, is likely a consequence of ROS, as it is thought to be a protective mechanism (Cheng et al. 2017).

Interestingly, ROS production in T cells has been shown to be necessary for cell function (Kuwabara et al. 2021).

On the other hand, the GD2 ARG2 sample did not present a significantly altered bioenergetic profile at baseline. Instead, it was characterised by elevated levels of spare glycolytic and mitochondrial capacities, a phenotype associated to metabolic fitness, as it facilitates maintenance of ATP homeostasis and rapid adaptation to metabolic changes (Keuper et al. 2014). In fact, T cells are required to promptly surge their glycolytic rates upon activation, not just to support ATP production, but also to enable biosynthesis of cytokines and acquisition of effector function (Chang et al. 2013; Menk et al. 2018). In parallel, increased spare respiratory capacity is a hallmark of long lived, central memory T cells (van der Windt et al. 2012).

Overall, based on the results obtained so far, we can suggest that the highest mitochondrial fitness was observed in the Jurkat cells metabolising L-arginine via mitochondrial arginase, i.e. GD2 ARG2, rather than the cytosolic isoform. However, further analysis is required to determine whether the GD2 ARG2 CAR could indeed be supporting increased effector function or the formation of immunological memory thanks to the mitochondrial reservoir.

Transcriptomic analysis revealed changes in a range of metabolic pathways, one of which was the aspartate/malate shuttle and the distinct pattern of expression of *GOT1* and *GOT2*, *MDH1* and *MDH2*, and the mitochondrial membrane transporters of malate and aspartate *SLC25A10* and *SLC25A13*. Birsoy et al. 2015, in a study that investigated the link between mitochondrial electron transport chain and cell proliferation, pointed towards the key role of mitochondrial aspartate sysnthesis and its fundamental player, GOT1. Specifically, in normal

condition GOT1 was found to use up aspartate in order to transfer electrons to mitochondria (i.e. aspartate –> oxaloacetate); however, the enzyme was also able to reverse the direction of its reaction and produce aspartate in the cytosol when needed, becoming an asset for aspartate homeostasis and, ultimately, cell proliferation.

What appeared interesting from the transduced Jurkat transcriptomic data was that, only in presence of cytosolic arginase (i.e. ARG1), the cytosolic protein encoded by *GOT1* was upregulated; while, only in presence of mitochondrial arginase (i.e. ARG2), the expression of the mitochondrial GOT2 gene was overexpressed. This indicated a close link between arginine catabolism and aspartate homeostasis.

Furthermore, malate dehydrogenase (MDH), the enzyme catalysing the reaction step downstream of GOT (i.e. oxaloacetate –> malate), was also shown to vary across samples. This time, while cytoplasmic MDH1 was found to be downregulated in both GD2 ARG1 and GD2 ARG2 cell (but not in GD2), mitochondrial MDH2 was overexpressed exclusively in the GD2 ARG2 cells.

The upregulation of the mitochondrial transporters for malate and aspartate *SLC25A10* (in both GD2 ARG1 and GD2 ARG2) and *SLC25A13* (only in GD2 ARG1) was also observed, contributing to the picture of an increasingly active aspartate-malate shuttle in conjunction with arginase expression.

Overall, these findings translated into the following patterns: in presence of mitochondrial arginase 2 activity, both *GOT2* and *MDH2* were overexpressed to result in increased flux of malate –> oxaloacetate –> aspartate; on the other hand, in presence of cytoplasmic arginase 1, aspartate homeostasis was instead obtained by GOT1 alone, in the reaction oxaloacetate

<–> aspartate, while both malate and aspartate could be replenished by its transportation from the mitochondria via SLC25A10 and SLC25A13.

Several antioxidant cellular strategies were activated in the GD2 ARG1 CAR-Jurkat. For example, the upregulation of the glutathione oxidoreductase gene expression (*GLRX*), a pivotal enzyme in cellular redox balance; the aspartate-malate shuttle, which involves the translocation of electrons between cytosol and mitochondria; the increased proton leak across the mitochondrial membrane measured by Seahorse.

In addition, the increased presence of LDH substrates pyruvate and lactate, could underlie a higher LDH activity; this could explain the augmented non-mitochondrial O_2 consumption of the GD2 ARG1 sample, given the ability of the enzyme to produce H_20_2 (Wu et al. 2021). Indeed, lactate production and LDH activity are not only known to be a direct correlation of rapid cell proliferation (Grist et al. 2018); but also an essential step for the restoration of the NAD^+/NADH balance of glycolysis (Rogatzki et al. 2015).

Interestingly, a publication by Tauffenberger et al. (2019) established an overall protective effect of LDH against oxidative stress: in fact, the peroxide production was demonstrated to benefit the cell through a hormetic mechanism.

In terms of biosynthetic activity, it is essential for the cell to produce abundant macromolecules to support cell division; amino acids represent important precursors not only for protein synthesis, but also nucleic acids and lipids. In particular, aspartate and glutamine are carbon and nitrogen sources for purine and pyrimidine biosynthesis, while glutamine and the branched chain amino acids valine, leucine and isoleucine can contribute to lipogenesis via acetyl-CoA (Yoneshiro et al. 2019).

Of the 20 proteinogenic amino acids, only four are directly implicated in the production of non-essential amino acids, namely glutamine, glutamate, methionine and phenylalanine (Lieu et al. 2020).

From this viewpoint, the GD2 ARG1 CAR-Jurkat presented the most advantageous intracellular landscape: the increased abundance of all the aforementioned amino acids guarantees a larger pool of biosynthetic precursors compared to control. Interestingly, we recorded a similar, albeit mitigated and not always significant, increase in most amino acids within the GD2 ARG2 sample as well, confirming the arginase-driven phenotype. However, cytosolic arginase was found to be dominant in this context.

In addition, the upregulation of the hexosamine pathway committing step encoded by *GFPT1* in both GD2 ARG1 and GD2 ARG2 reinforced the picture of a cellular programme with biosynthetic propensity. The hexosamine pathway's downstream product, UDP-GlcNAc, is essential for protein glycosylation. This seemed to align with the attempt to decrease glycolytic flux while prioritising protein synthesis.

Another element linked to arginase expression was the increase in glycolytic end-product availability: both pyruvate and lactate in the GD2 ARG1, while only lactate in the GD2 ARG2 Jurkat. While pyruvate is seen as an undiscussed asset to cellular bioenergetics for its prompt accessibility and diverse fate, lactate still represents a grey ground. For years it was thought to be a mere waste product of glycolysis; only recently it became a more multifaceted metabolite, with implications in ROS damage protection, redox balance, epigenetic modifications (i.e. histone lactylation) and intracellular signalling, as previously mentioned (Rogatzki et al. 2015; Pucino et al. 2019; Zhang et al. 2019). Hence, it remains challenging to

establish the meaning of lactate build-up seen in the modified CAR-Jurkat.
Furthermore, it is common to believe that lactate is promptly exported in the extracellular space by the monocarboxylate transporter (MCT) family in order for it to take part in the lactate shuttle at an organism level (Brooks 2009). Our extraflux analysis by Seahorse, however, does not support the hypothesis of an increase in extracellular lactate, as the baseline ECAR measurements remained unchanged across the samples. In conclusion, raised intracellular lactate could indicate either a function for it in the intracellular space to achieve NAD:NADH balance, or an inhibition at a transporter level.
In this respect, upregulation of the pyruvate/lactate MCT4 transporter gene *SLC16A3* was observed in the arginase 2 cohort, prompting the interpretation that increased lactate export might be required in those cells. Interestingly, the MCT4 isoform is thought to be particularly efficacious for the export of lactate in the extracellular milieu, while preserving the intracellular pyruvate pool to allow for lactate dehydrogenase-mediated fermentation of pyruvate and consequent re-establishment of the redox balance (Halestrap 2013).

Regardless, further investigations into the fate of intracellular lactate are required in order to appreciate the whole picture.

The Jurkat model represented a valuable platform for the early evaluation of the metabolic consequences of arginase introduction in T cells, as it guaranteed a constant and high cell throughput for downstream analysis by Seahorse and GC-MS; nonetheless, it remains a leukaemia-derived cell line with several discrepancies from primary T cells.
First and foremost, the 'cancerous programme' of this cell line might be intrinsically skewed towards glycolysis and ROS generation. Secondly, due to their efficient proliferation rate and

robust nature, it is challenging to detect small changes in cell division due to CAR transduction. Furthermore, Jurkat cells fail to produce the range of cytokines of a T cell and instead limit their repertoire to a constitutive pro-survival IL-2 secretion; similarly, they are not conventionally proficient in exhaustion marker regulation (Abraham and Weiss 2004). These aspects inevitably limit our understanding on the interaction between the tumour microenvironment and the CAR-Jurkat cells and how this affects cell phenotype.

Finally, our objective is to build an anti-cancer CAR T cell able to lyse tumour cells upon CAR signalling. So far, although we demonstrated antigen-specific CAR engagement with CD69 upregulation, it was not possible to demonstrate target lysis.

Hence, further investigations in primary T cells are needed in order to complement our findings and translate them into relevant observations within the context of the anti-cancer immunity.

5. THE STUDY OF A MICROENVIRONMENT-RESISTANT CAR-T CELL FOR CANCER IMMUNOTHERAPY

5.1 Overview

The insights gained using the Jurkat model confirmed that we were able to transduce modified anti-GD2 CAR constructs able to endow the cells with constitutive arginase expression. The arginase-expressing samples were characterised by altered metabolic signatures and increased intracellular concentrations of biosynthetic precursors and substrates for ATP production.

We next progressed by testing our hypothesis in primary T cells from healthy donors.

5.2 Objectives

In this chapter, we aim to:

- engineer anti-GD2 CAR-T cells, constitutively expressing arginase 1 and arginase 2;
- validate the CAR and enzyme presence and functionality;
- investigate the impact of arginase expression on T cell function in vitro;
- assess CAR-T cell therapy success in a tumour xenograft of neuroblastoma.

5.3 Results

5.3.1 Transduction of the Novel Constructs into Primary T Cells

Phoenix AMPHO cell lines were used to produce the retroviruses for transduction, as previously described. Healthy T cells were activated with anti-CD3/CD28 and 48 hours later incubated with the retrovirus at 37°C, 5% CO_2 for 4 days. Transduction efficiency was then monitored by flow cytometry.

T cells were able to undergo gene transfer and successfully express the CAR with the truncated CD34 detection tag, as shown in the representative donor flow cytometry plot in Figure 40A. Mock-transduced cells of each donor instructed the gating strategy.
Overall, donor variation seemed to have an impact on transduction efficiency; nonetheless, the main predictor of transduction efficiency was the CAR construct type, with the GD2 generally providing the highest transduction yield (mean: 8.1%), followed by GD2 ARG1 (mean: 6.4%) and GD2 ARG2 (mean: 4.9%) (Figure 40B). CAR-positive cells were subsequently isolated to a pure population and utilised in downstream experiments (Figure 40C).

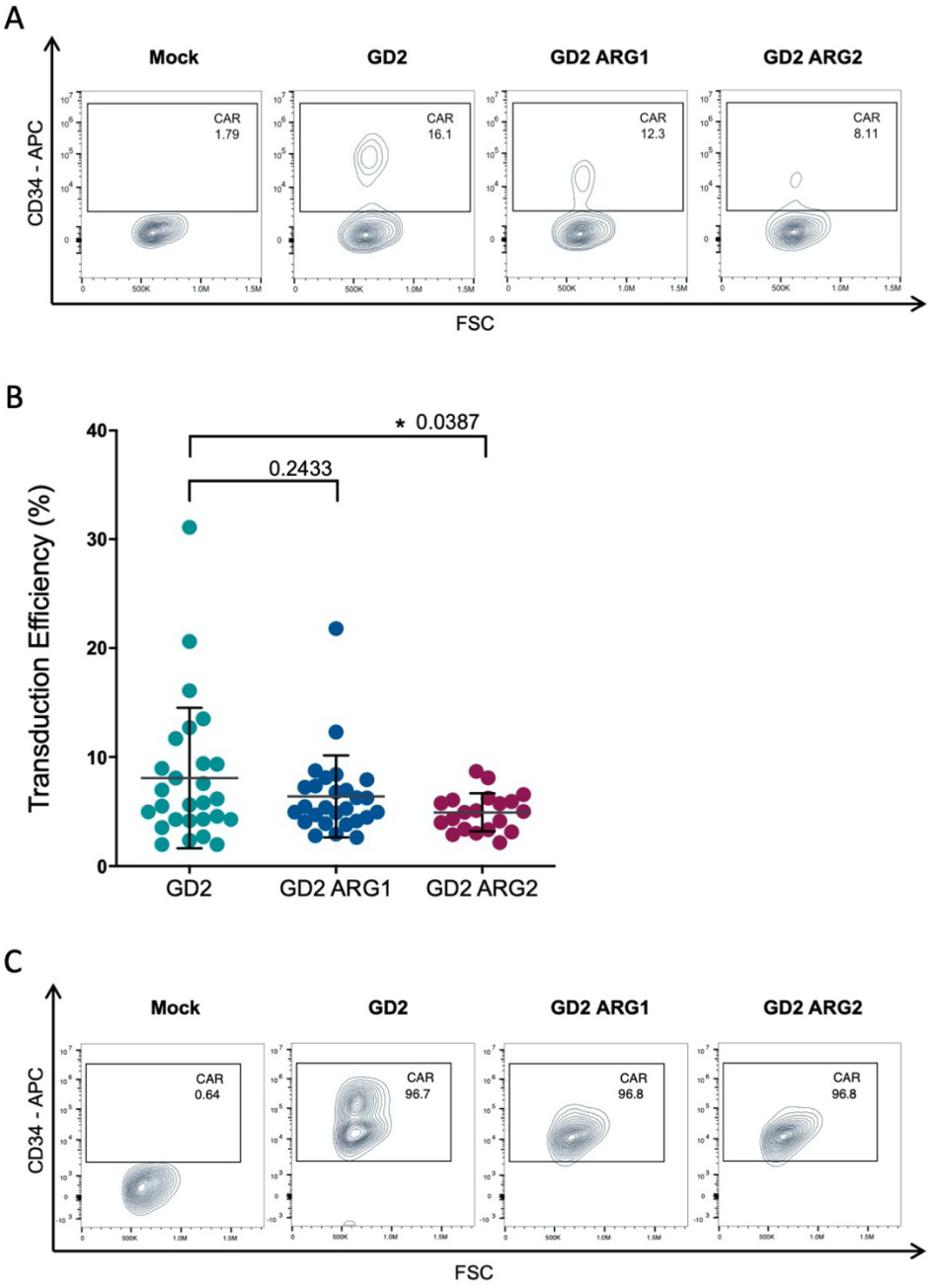

Figure 40: Transduction of human primary T cells with anti-GD2, anti-GD2 ARG1 and anti-GD2 ARG2 CARs.

T cells sorted from healthy donors' peripheral blood were activated for 48h with anti-CD3/CD28 and incubated with CAR-carrying retroviruses. Transduction efficiencies were recorded by flow cytometry utilising the truncated CD34 detection tag co-expressed with the CAR gene. Mock-transduced cells from each donor are used to set the CAR gate. (A) Flow cytometry plot of the GD2, GD2 ARG1 and GD2 ARG2 CAR-T cells generated from a single representative donor. (B) Transduction efficiency summary of all transduced donors (n≥20), shown as mean ± SEM; statistical analysis: paired t test. (C) Flow cytometry plot of a representative donor to monitor cell population purity after CAR-T cell sorting.

5.3.2 Expression and Function of Arginase 1 and Arginase 2 in the Engineered Cells

To confirm arginase expression in the transduced CAR-T cells, western blots were performed on the cell lysates.

By using β-actin as loading control, we measured arginase 1 and arginase 2 expression in the GD2, GD2 ARG1 and GD2 ARG2 samples. An underlying basal level of expression of the enzymes within T cells was observed; nonetheless, the densitometry of the blots confirmed a 4-fold increase of arginase 1 and a 2-fold increase of arginase 2 in the GD2 ARG1 and GD2 ARG2 CAR-T cells respectively, compared to GD2 control (Figure 41A and B).

Additionally, we confirmed that the key transporter of L-arginine across the plasma membrane, CAT-1, was present in all samples (Figure 41C).

Beyond enzyme presence, its functionality was also assessed by performing an arginase activity assay, as previously described.

L-arginine hydrolysis was measured colourimetrically and arginase activity determined. A significant fold-change increase in the GD2 ARG1 ($p=0.0312$) samples compared to GD2 controls was observed; at the same time the increase in arginase activity seen in the GD2 ARG2 sample was not statistically significant in this instance ($p=0.1250$) (Figure 41D).

So far, we could conclude that the transduction of primary T cells with anti-GD2 CARs containing arginase enzymes was possible and yielded a population of cells with detectable levels of functional enzymes and enhanced ability to hydrolyse L-arginine.

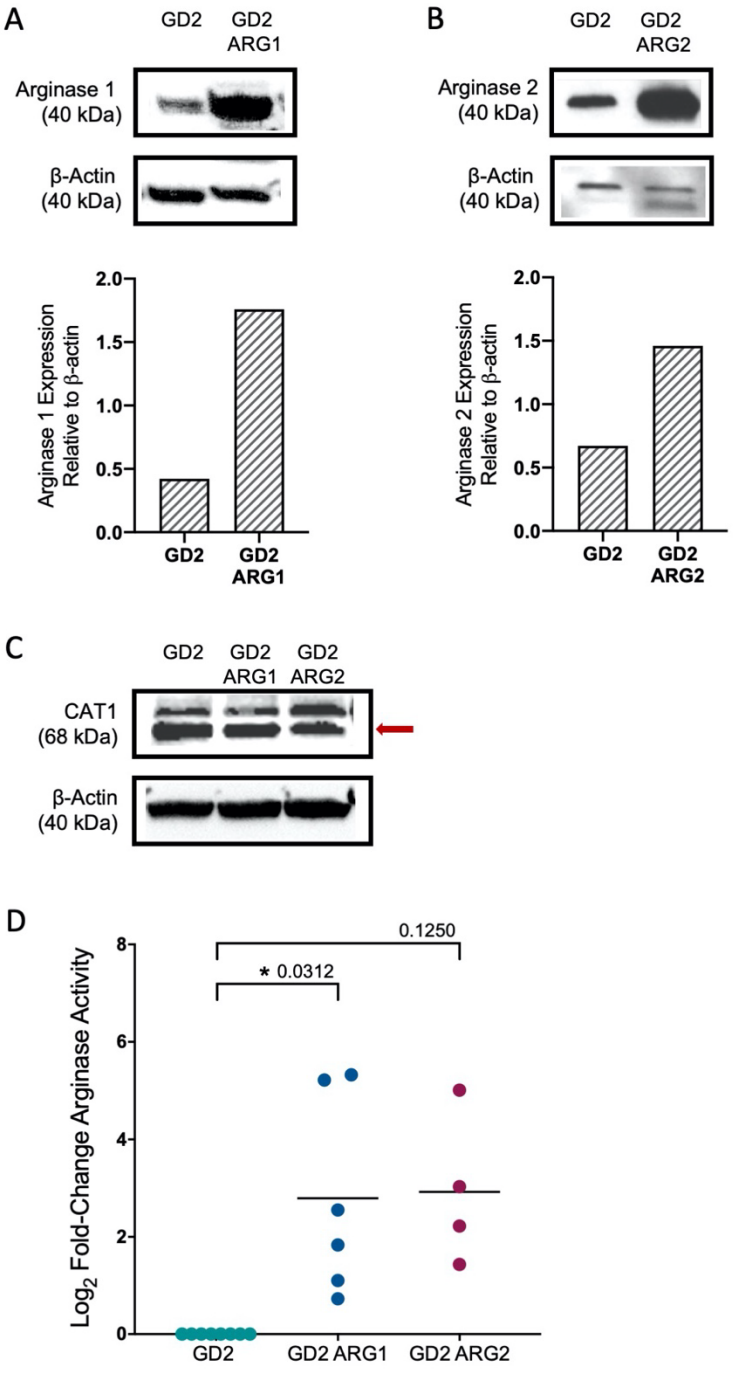

Figure 41: Protein expression and activity in primary CAR-T cells.

Lysates of sorted GD2, GD2 ARG1 and GD2 ARG2 CAR-T cells were analysed by western blot for protein expression of arginase 1, arginase 2 and CAT1, with β-actin used as loading control. Immunoblotting with relative densitometry of arginase 1 (A) and arginase 2 (B), representative of 3 experiments. CAT-1 protein expression in the transduced cells, as indicated by arrow (C). Cell lysates were assessed for arginase activity calculated in mU/10^6 cells and represented as $\log_2$ fold-change of the GD2 control CAR construct (D). Statistical analysis: Willcoxon test, n≥4.

5.3.3 GD2 Targeting *In Vitro*

Having based our constructs DNA sequence on an existing and well tested anti-GD2 CAR, we expected the receptor to appropriately target the GD2 antigen. Nonetheless, we wanted to confirm CAR-T cells targeting of the GD2 antigen.

Transduced CAR-T cells were seeded in co-culture with an adherent monolayer of $GD2^+$ cells for 48h; the cells were subsequently harvested and stained for acquisition on a flow cytometer.

As exhibited in Figure 42, the target cells were able to thrive when cultured alone or with Mock-transduced cells; conversely, a reduction in the $GD2^+$ population was observed in presence of functional anti-GD2 CARs, consistent with CAR-mediated killing of the targets. In particular, when quantifying the live tumour cell population in the GD2, GD2 ARG1 and GD2 ARG2 samples, they were found to be reduced to an average of respectively 63%, 57% and 34% compared to the Mock sample.

A certain degree of variation between donors was observed; nonetheless, we can conclude that all the CAR-T cells were able to kill $GD2^+$ targets cells in a coculture setting.

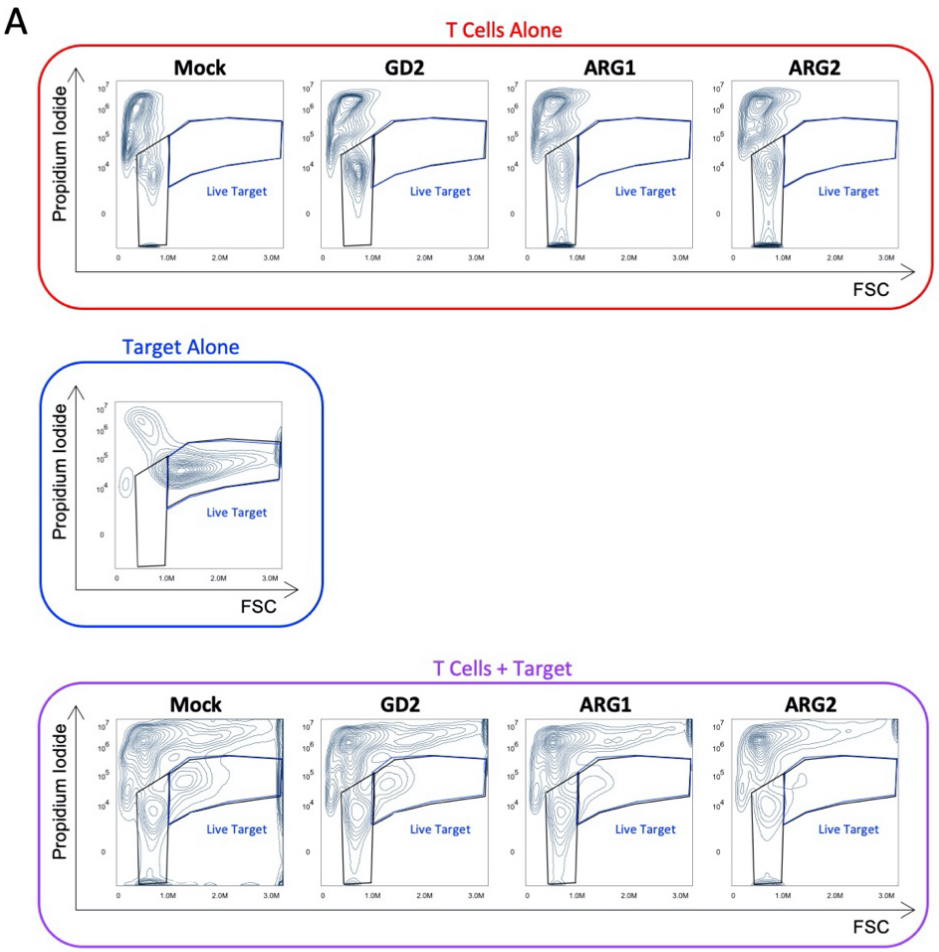

Figure 42: *In vitro* targeting of GD2^{+} targets by flow cytometry.

GD2^{+} SK-N-MC cell lines were seeded to form a monolayer and cultured for 48h in presence or absence of Mock, GD2, GD2 ARG1 and GD2 ARG2 CAR-T cells. (A) Representative flow cytometry gating strategy of the co-cultures, using PI viability stain and scatter-based gates to quantify target death. (B) Summary of SK-N-MC viability in co-culture of n≥4 independent experiments. Bars represent mean ± SEM. Statistical analysis: paired t test.

5.3.4 Gene Expression Patterns Characterising the Arginase CAR-T Cells

In order to gain a deeper understanding on the alterations derived from the introduction of constitutive arginase enzymes within T cells, we proceeded with the transcriptome sequencing of transduced T cells from 3 different healthy donors.

The transduced T cells were pre-conditioned for 4 days in Low Arg Medium, in presence of CD3/CD28 stimulation; R10% was then added to the cultures and the cells incubated for 4 further days. Pure populations of GD2, GD2 ARG1 and GD2 ARG2 CAR-T cells were processed for RNA extraction; sequencing was obtained on a NextSeq 500 platform.

A heatmap representing the top 100 differentially expressed genes between the GD2 ARG1 samples and the GD2 controls from the three donors is shown in Figure 43A, as $\log_2$ of fold-change. Of the 100 entries determining the diverging phenotype between the two CAR constructs, GD2 and GD2 ARG1, the most significantly altered genes ($p \leq 0.05$) are represented in Figure 43B, ordered by adjusted p value.

Of these, some seemed to be particularly relevant in the context of our study. Firstly, the expression of *TOB1,* a cell growth suppressor gene, was found downregulated in the arginase 1-transduced cells compared to control ($p = 0.00013$). Secondly, *C2CD2L,* encoding for a lipid membrane organising protein, was upregulated in the GD2 ARG1 cohort. Thirdly, the upregulation of *MT-ND4*, encoding for a subunit of the NADH dehydrogenase, and *FASTKD2*, a mitochondrial regulator of bioenergetic balance.

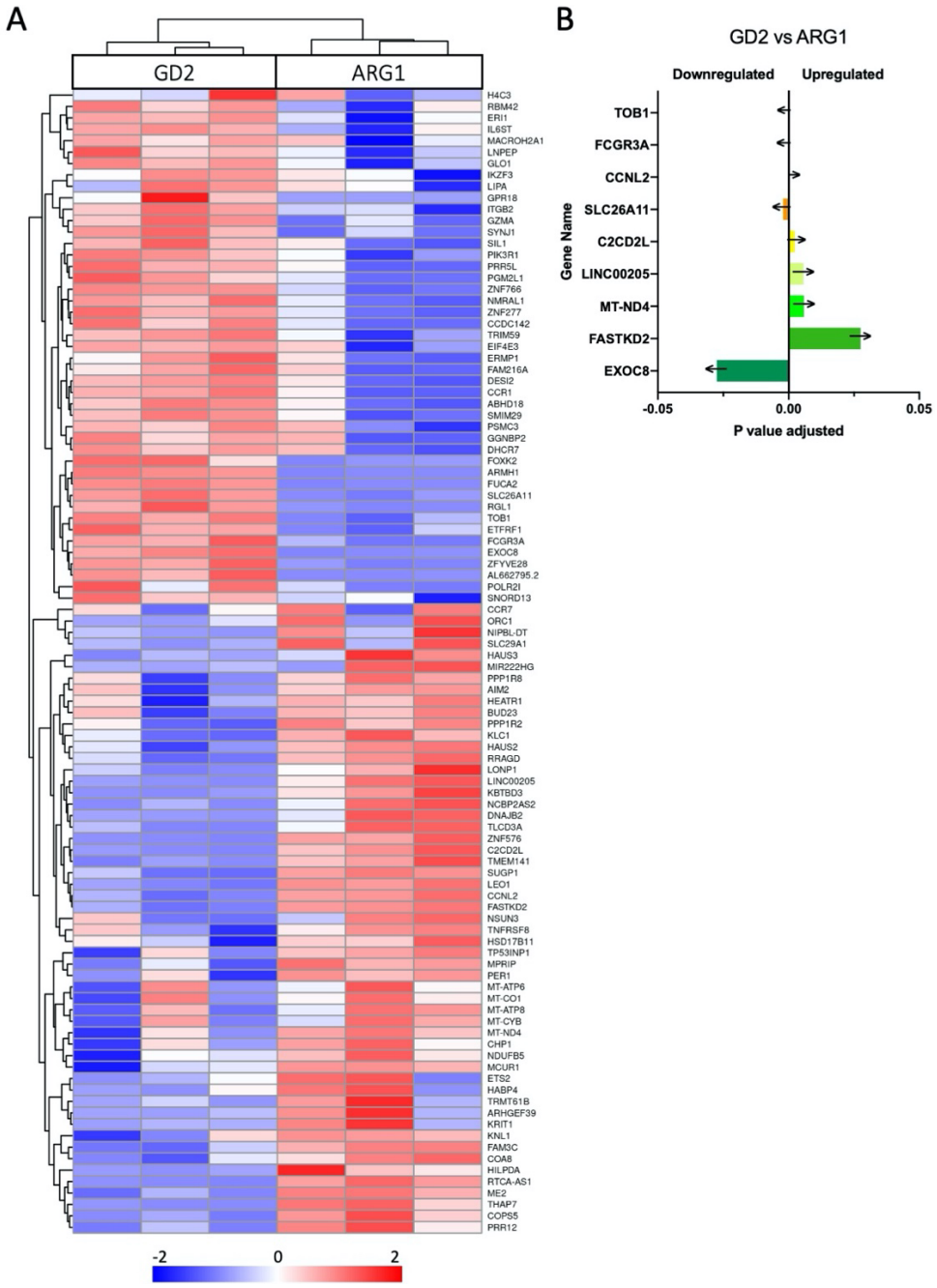

Figure 43: Heatmap of the top 100 genes differentially expressed between GD2 and GD2 ARG1 CAR-T cells.

Transduced T cells from 3 healthy donors were activated with anti-CD3/CD28 in Low Arg Medium for 4 days, then cultured in R10% for further 4 days. CAR^+ cells were then sorted by FACS, RNA extracted and library prepared for sequencing on a NextSeq 500 platform. RNASeq data is displayed as heatmap of the top 100 differentially expressed genes between the GD2 and GD2 ARG1 constructs as $\log_2$ of fold-change of GD2 control (A). Significantly changed gene expressions between GD2 ARG1 and control, with adjusted p value ≤0.05, are additionally shown in order of significance (B). Statistical analysis by CRUK Birmingham Centre bioinformaticians Noyvert B. and Pan Y.

Similarly, the comparison between arginase 2-transduced cells and GD2 controls was also performed and the top 100 differentially expressed genes are shown in the heatmap in Figure 44A. Of these, the entries scoring an adjusted p value below 0.05 were additionally represented in Figure 44B.

Like in the GD2 ARG1 sample, the mitochondrial NADH dehydrogenase gene *MT-ND4*, appeared to be markedly upregulated in the GD2 ARG2 CAR-T cells.

The gene encoding for the killer cell lectin like receptor B1 (*KLRB1)* was also found as one of the most significantly altered genes upon ectopic expression of arginase 2. Interestingly, this receptor, also known as CD161, has been described on the surface of tumour infiltrating Th17 cells and thought to have a homing function for this subset of anti-tumour lymphocytes (Zhao et al. 2013). In parallel, the lymph node homing receptor CCR7 displayed significant upregulation in the GD2 ARG2 cells, compared to control.

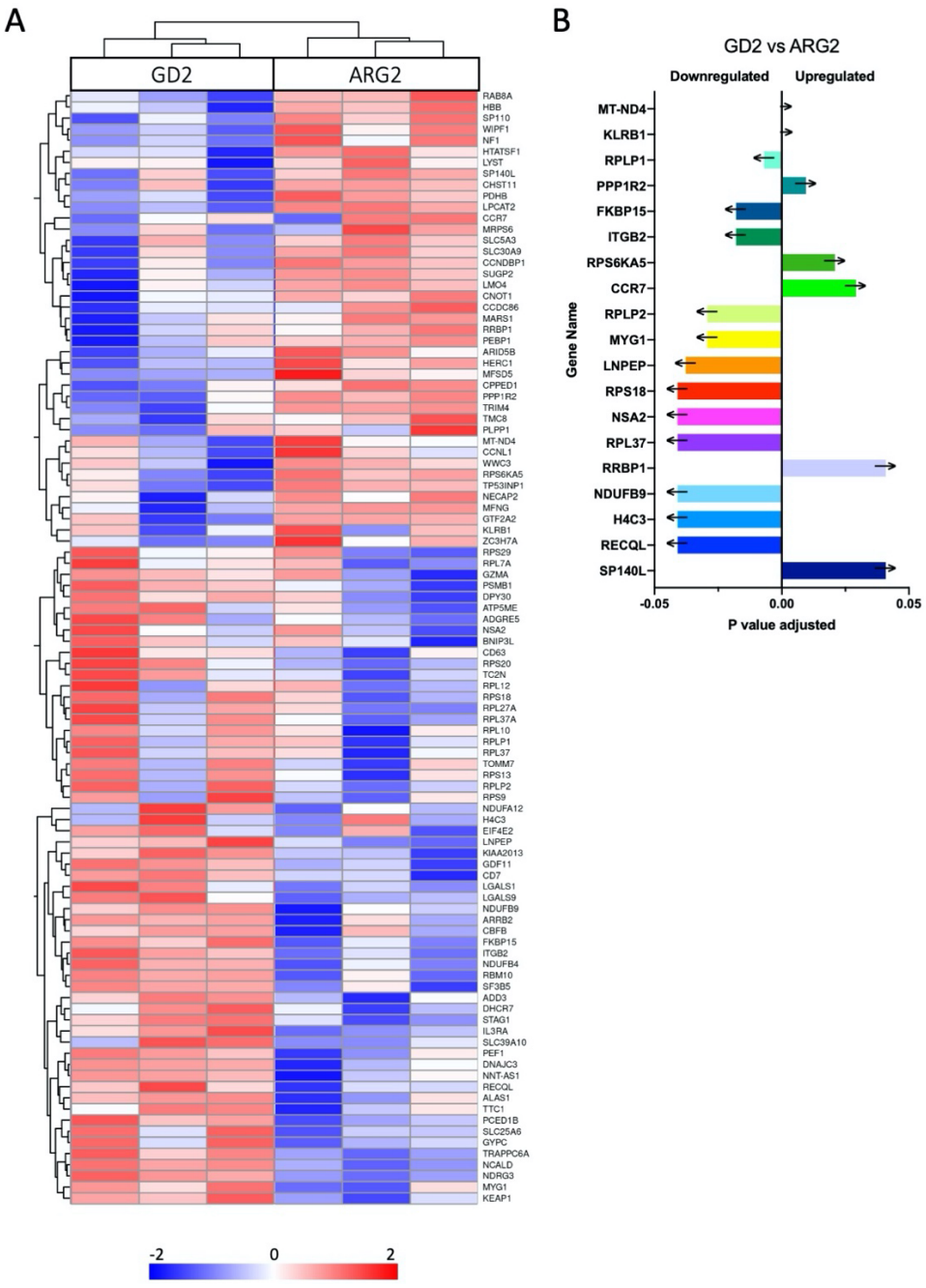

Figure 44: Heatmap of the top 100 genes differentially expressed between GD2 and GD2 ARG2 CAR-T cells.

Transduced T cells from 3 healthy donors were activated with anti-CD3/CD28 in Low Arg Medium for 4 days, then cultured in R10% for further 4 days. CAR^+ cells were then sorted by FACS, RNA extracted and library prepared for sequencing on a NextSeq 500 platform. RNASeq data is displayed as heatmap of the top 100 differentially expressed genes between the GD2 and GD2 ARG2 constructs as $\log_2$ of fold-change of GD2 control (A). Significantly changed gene expressions between GD2 ARG2 and control, with adjusted p value ≤0.05, are additionally shown in order of significance (B). Statistical analysis by CRUK Birmingham Centre bioinformaticians Noyvert B. and Pan Y.

5.3.5 Proliferation Advantage of the Novel CAR-T Cells

The ability to proliferate after reinfusion is key in implementing the anti-cancer program. We proceeded to investigate whether the novel feature, shown to alter the CAR-T cell transcriptome, endowed the CAR T cells with a proliferative advantage in a range of environmental conditions.

We began the assessment by measuring the anti-CD3/CD28-driven proliferation of CAR-T cells pre-conditioned in Low Arg Medium or primary neuroblastoma tumour-conditioned media (TCM) for 4 days, to mimic the microenvironment at the tumour site. T cell proliferation was quantified using ^{3}H-labelled thymidine incorporation on the 9th day (Figure 45A).

We observed an increased proliferation in the arginase-containing CAR-T cells compared to the GD2 control, with an average 2-fold improvement for GD2 ARG1 ($p < 0.0001$) and 2.7-fold for GD2 ARG2 ($p < 0.0001$).

Moreover, proliferating T cells are known to secrete cytokines in the surroundings upon activation, such as INF-γ. We therefore measured the concentration of INF-γ in the endpoint supernatants by ELISA to assess whether there was a difference (Figure 45B). Indeed, the GD2 ARG1 cohort presented a modest but significant increase in INF-γ production (mean = 7.2 ng/ml) compared to GD2 control (mean = 6.1 ng/ml) ($p = 0.0208$). INF-γ concentration did not overall change for the GD2 ARG2 samples.

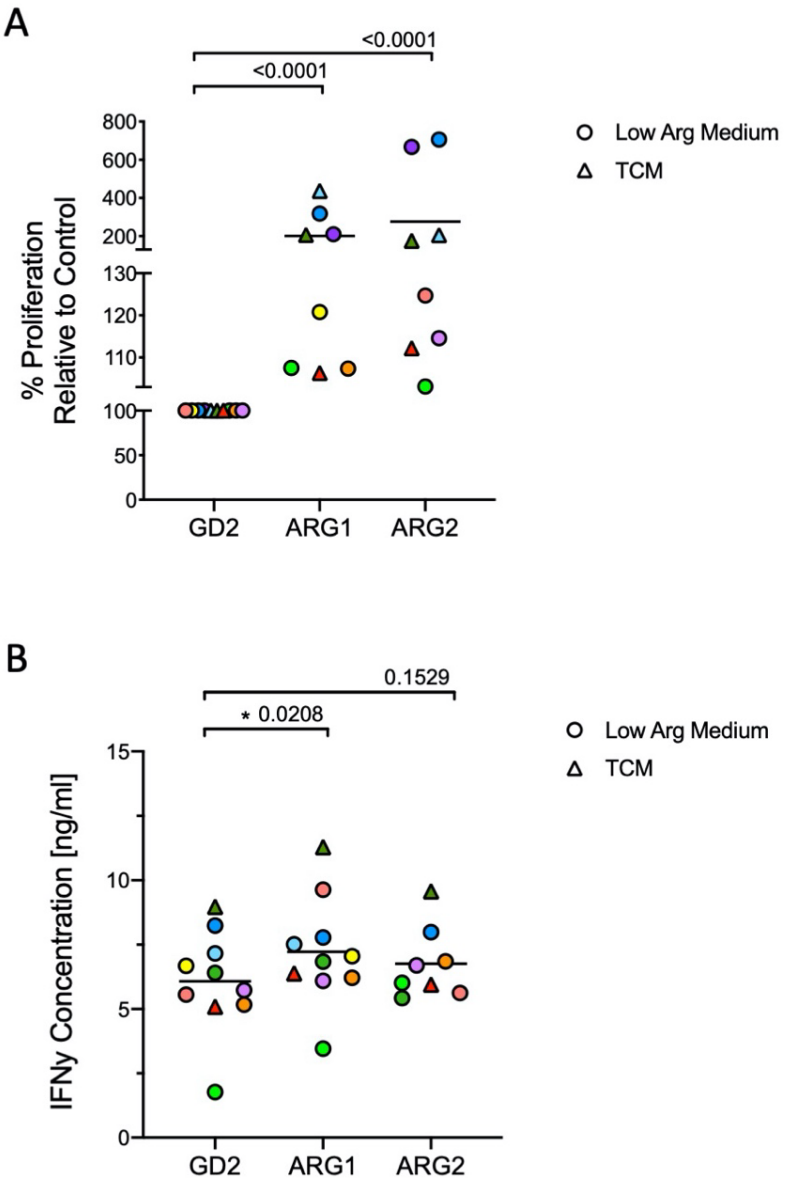

Figure 45: Analysis of primary CAR-T cells' proliferation ability *in vitro*.

Sorted GD2, GD2 ARG1 and GD2 ARG2 CAR-T cells were pre-conditioned in Low Arg Medium (circle) or tumour conditioned media (TCM) from primary neuroblastomas (triangle) for 4 days in presence of CD3/CD28 mAb stimulation; 1 volume of R10% was added for further 4 days; proliferation was quantified via detection of ^{3}H-thymidine incorporation on the 9th day (A). INF-γ production was quantified by ELISA in the supernatants (B). T cell donors are colour-matched; n≥8. Statistical analysis: Mann-Whitney test (A) and paired t test (B).

Next, we wondered how the improved ability to hydrolyse L-arginine would affect CAR-T cell expansion within an arginine-rich microenvironment.

Equal amounts of CAR^+ T cells were cultured in T Cell Medium (Table 1) supplemented with L-arginine (100µM). The cells were acquired by flow cytometry on day 5, after being stained with anti-CD34 mAb and propidium iodide (PI) viability stain.

As shown in Figure 46, the percentage of live CAR^+ cells relative to GD2 control was found increased in both the arginase 1 and arginase 2-expressing groups (p=0.0022 and p=0.0048 respectively).

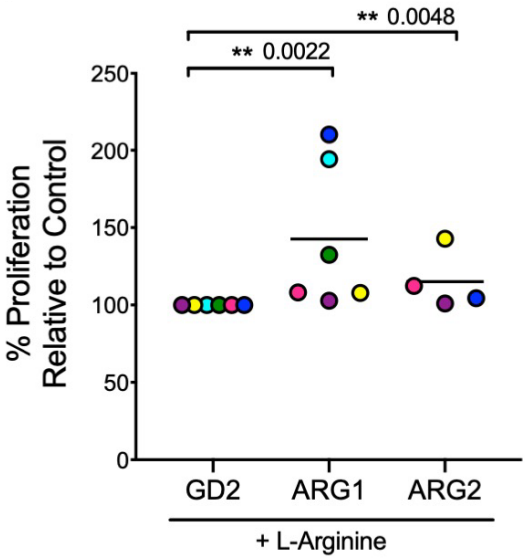

Figure 46: CAR-T cell proliferation in L-Arg-replete conditions

Transduced GD2, GD2 ARG1 and GD2 ARG2 CAR-T cells were cultured in T Cell Media (R10%, 1% human serum, 100U/ml IL-2, 50µM β-mercaptoethanol, 5mM HEPES) supplemented with 100µM L-Arginine for 5 days at 37°C, 5%CO_2. Cells were stained with CD34 fluorescent marker and PI viability stain and acquired with a flow cytometer. CAR^+ proliferation % relative to control was measured. Donors are colour-matched; n≥4. Statistical analysis: Mann-Whitney test.

Furthermore, we wanted to assess expansion as a direct consequence of CAR stimulation. In order to do so, a $GD2^+$ cell line was plated and allowed to adhere; pure populations of CAR-T cells were then added to the assay at a ratio of 10:1 effector:target. CAR-T cells were re-challenged with target cells on day 5 and proliferation was measured by flow cytometry on day 9, based on live $CD34^+$ counts and expressed as a percentage relative to GD2 control (Figure 47).

Antigen-driven stimulation resulted in a consistently improved expansion of the GD2 ARG1 sample over GD2 ($p = 0.0286$), averaging a 16% increase in final cell number. In this instance, arginase 2 did not show a significant proliferative advantage.

All together, these data indicated a role for arginase in CAR-T cell proliferation.

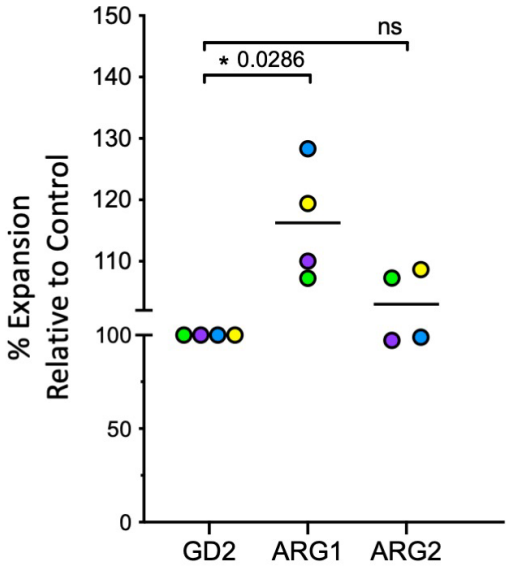

Figure 47: Antigen-stimulated expansion of GD2, GD2 ARG1 and GD2 ARG2 CAR-T cells.

$GD2^+$ SK-N-MC cells were allowed to adhere on plates before pure GD2, GD2 ARG1 and GD2 ARG2 CAR-T cells were seeded at a ratio of 10:1 (effector:target) and incubated for a total of 9 days. Same amounts of fresh target cells were added on day 5. Proliferation was measured by flow cytometry, using CD34 staining and PI viability dye, and displayed as % relative to GD2 control. Donors are colour-matched; n=4. Statistical analysis: Mann-Whitney test.

5.3.6 CAR-T Cell Exhaustion

T cell exhaustion has been shown to be one of the main causes of anti-tumour inefficacy (McLane, Abdel-Hakeem, and Wherry 2019). This state of hypo-responsiveness is generally seen in the context of chronic infections, as well as cancer, and is characterised by surface upregulation of several inhibitory receptors: programmed cell death 1 (PD-1), lymphocyte activation gene 3 (LAG-3), T-cell immunoglobulin and mucin domain 3 (TIM-3), and T-cell immunoglobulin and immunoreceptor tyrosine-based inhibitory motif domain (TIGIT) among others.

We progressed our CAR-T cell analysis with the investigation of their exhaustion state 14 days after the transduction process, maintained in T Cell Medium, to understand whether the constitutive expression of arginases had an effect on the cell's upregulation of key immune checkpoint molecules.

We observed no significant difference in PD-1, LAG-3, TIM-3 or TIGIT expression levels between the GD2 control and the GD2 ARG1 or the GD2 ARG2 CAR-T cells (Figure 48A-E).

In addition, while we found no significant difference between CAR-engineered T cells and Mock in PD-1, LAG-3 and TIGIT, TIM-3 expression was significantly decreased in the untransduced cells (i.e. Mock).

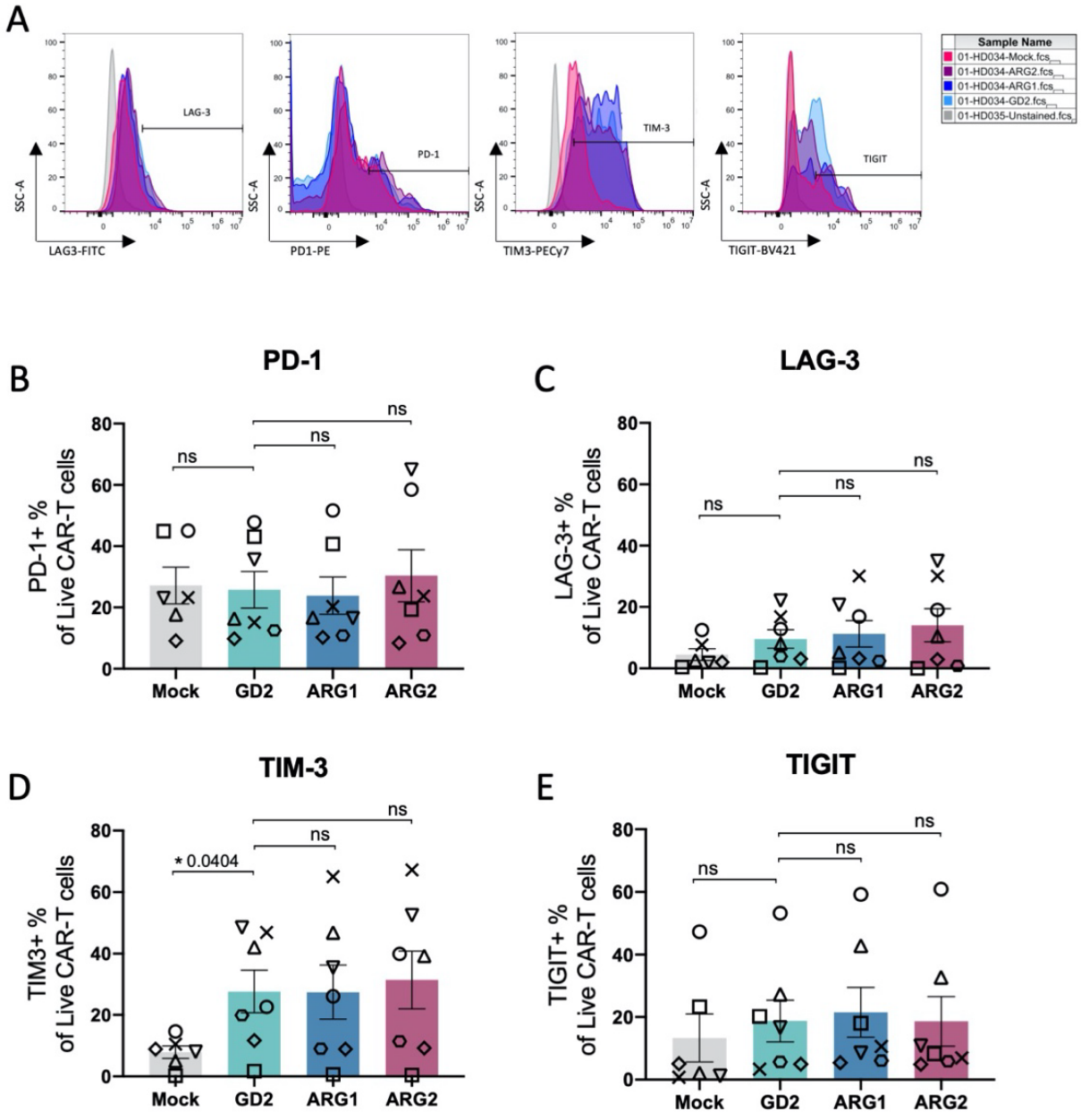

Figure 48: Exhaustion markers assessment of the engineered T cells.

On day 14 following transduction, Mock, GD2, GD2 ARG1 and GD2 ARG2 CAR-T cells were assessed for surface expression of common exhaustion markers (PD-1, LAG-3, TIM-3 and TIGIT) by flow cytometry. Gated on the live CAR^+ populations (or CAR^- for Mock), a representative set of overlayed histograms is shown in (A). The percentage of cells positive for PD-1 (A), LAG-3 (B), TIM-3 (C) and TIGIT (D) were recorded for n≥6 donors and represented as mean ± SEM. Donors are symbol-matched. Statistical analysis: paired t test.

Further to this, we then measured the same checkpoint molecules on the CAR-T cells, 14 days post-transduction and after GD2-driven stimulation, to understand how the expression patterns of PD-1, LAG-3, TIM-3 and TIGIT compared to the ones just shown.

No significant change was found on PD-1, LAG-3 or TIGIT expression across the different CAR types. On the other hand, GD2 ARG2 displayed a significantly reduced TIM-3 expression compared to GD2 control ($p = 0.0451$) (Figure 49A-D).

Untransduced Mock samples presented a significant decrease in LAG-3 ($p = 0.0307$) and TIGIT ($p = 0.0271$) expression, compared to the CAR-transduced cells.

So far, these data suggested that arginase 2 had an effect in the downregulation of TIM-3 expression during antigen-driven CAR stimulation.

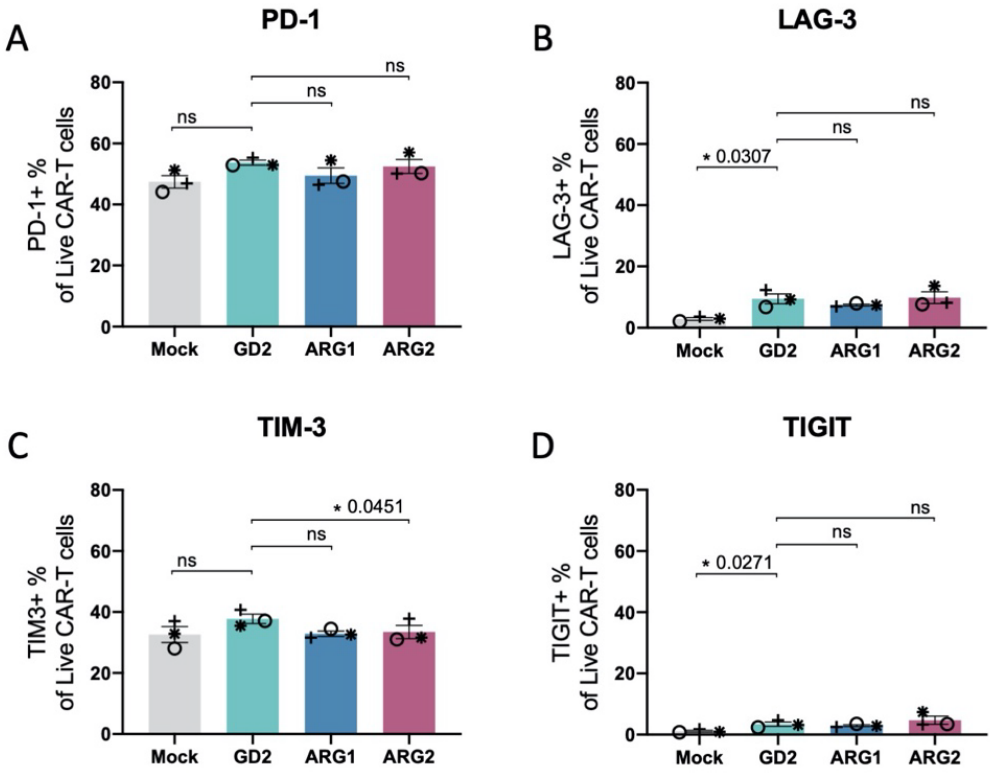

Figure 49: Exhaustion markers assessment of the engineered T cells upon antigen challenge.

On day 14 following transduction, after repeated antigen challenge with $GD2^+$ SK-N-MC on day 5 and day 10, Mock, GD2, GD2 ARG1 and GD2 ARG2 CAR-T cells were assessed for surface expression of common exhaustion markers (PD-1, LAG-3, TIM-3 and TIGIT) by flow cytometry. Gated on the live CAR^+ populations (or $CD3^+$ for Mock), the percentage of cells positive for PD-1 (A), LAG-3 (B), TIM-3 (C) and TIGIT (D) were recorded. Donors are symbol-matched. Shown as mean ± SEM; n=3. Statistical analysis: paired t test.

5.3.7 Neuroblastoma Targeting *In Vivo*

In order to assess the anti-tumour potential of the novel CAR-T cells within an *in vivo* tumour model, $2.5x10^6$ $GD2^+$ KELLY cells (1:1 in Matrigel) were implanted onto the flank of balb/c nude mice. Upon tumour establishment (volume ≥ 10-15 mm^3) the mice were randomised into treatment groups of 12 mice each, which included vehicle controls, GD2, GD2 ARG1 and GD2 ARG2 CAR-T cells. On day 0, they received a single injection of intravenous CAR-T cells

($2.5x10^6$/mouse). The CAR-T cells were supplied by ProMab Biotechnology and produced using a lentiviral platform. Transduction efficiencies and CAR^+ percentage was confirmed to be between 10% and 15% of the final infusion product, which was cryopreserved until injection. The anti-GD2 specificity of the CAR transduced with lentivirus was confirmed in a previous study (Fultang et al. 2020). Each CAR construct was transduced in 3 human healthy donors, and each donor was assigned to 4 mice in each treatment group.
The *in vivo* protocol (Figure 50A) was fully executed by an external company, Axis Bioservices, under the guidelines of the Animal (Scientific Procedures) Act 1986. *Post-mortem* tissues were received to conduct downstream analyses.

Monitoring of tumour volume and body weight occurred consistently to the end of the experiment. In particular, body weight on day 24 revealed no change across the different treatment groups, as shown in Figure 50B. Tumour volumes increased along time and the individual curves of tumour growth rates were plotted for the GD2 ARG1 cohort (Figure 50C) and GD2 ARG2 cohort (Figure 50D) alongside GD2 controls.

Prior to CAR-T cell injection, on day 0, tumour engraftment was confirmed based on size and randomised treatment groups presented comparable starting tumour volumes (Figure 50E). On the other hand, endpoint tumour volumes (day 24) showed a significant arginase-dependent tumour shrinkage (Figure 50F). We could therefore conclude that both GD2 ARG1 and GD2 ARG2 conferred a significantly improved ability to control the tumour in vivo to the standard GD2 CAR-T cells ($p = 0.0014$ and $p = 0.0266$ respectively).

Further analysis by qPCR revealed substantial CAR-T cell infiltration within the tumour tissue of CAR-T cell treated mice, shown in Figure 50G. We observed no significant difference in CAR infiltration between the GD2 standard CAR-T cells and the arginase-modified ones.

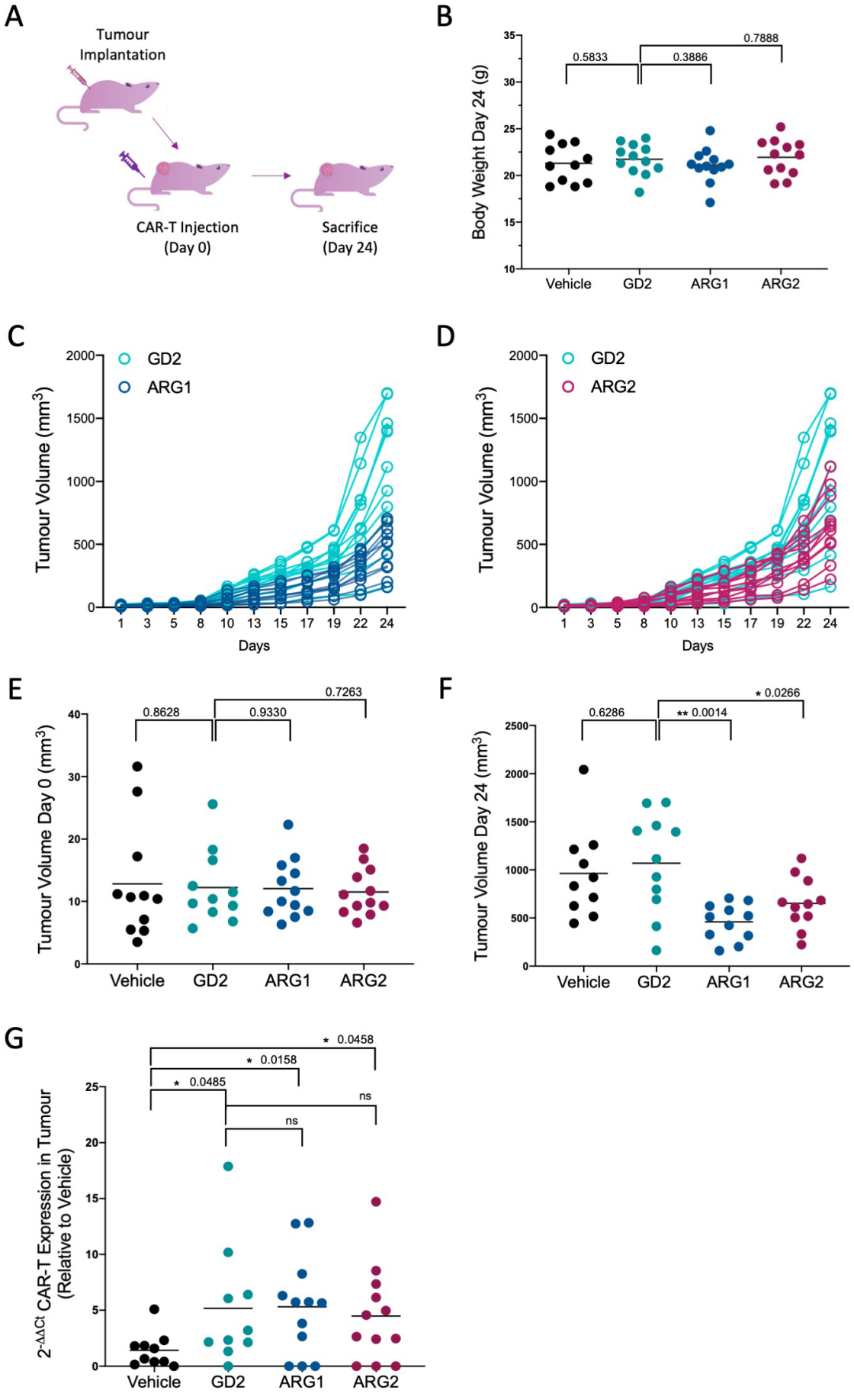
A
Tumour Implantation
CAR-T Injection (Day 0)
Sacrifice (Day 24)
B
Body Weight Day 24 (g)
0.5833
0.3886
0.7888
Vehicle
GD2
ARG1
ARG2
C
GD2
ARG1
Tumour Volume (mm3)
Days
D
GD2
ARG2
Tumour Volume (mm3)
Days
E
Tumour Volume Day 0 (mm3)
0.8628
0.9330
0.7263
Vehicle
GD2
ARG1
ARG2
F
Tumour Volume Day 24 (mm3)
0.6286
** 0.0014
* 0.0266
Vehicle
GD2
ARG1
ARG2
G
2-ΔΔCt CAR-T Expression in Tumour (Relative to Vehicle)
* 0.0485
* 0.0158
* 0.0458
ns
ns
Vehicle
GD2
ARG1
ARG2

Figure 50: In vivo tumour model to assess the efficacy of standard and enzyme-modified CAR-T cells.

Balb/c nude mice were inoculated subcutaneously with neuroblastoma xenografts ($2.5x10^6$ KELLY cells, 1:1 in Matrigel) and tumours were allowed to grow to 10-15mm^3. GD2, GD2 ARG1 and GD2 ARG2 CAR-T cells from 3 different human donors were delivered by single iv injection ($2.5x10^6$/mouse), together with vehicle control. Schematic illustration of the *in vivo* experimental procedure (A). Body weight on day 24 (B); individual tumour volumes from day 0 (CAR-T cell inoculation) to day 24 (sacrifice): GD2 vs ARG1 (C) and GD2 vs ARG2 (D). Tumour volume at day 0 (E) and day 24 (F). Post-mortem CAR-T cell detection by qPCR relative to vehicle control in tumour tissue (G). Data in (G) were obtained by, and are shown with the permission of, Fultang LFK. Bars represent mean; dots are individual mice. Statistical analysis: unpaired t-test.

5.4 Discussion

The work included in this chapter demonstrated the ability to successfully transduce human primary T cells with anti-GD2 CAR constructs containing arginase 1 or arginase 2 enzymes. The engineered cells were able to stably express the transgene and, as expected, they acquired the ability to specifically target and kill $GD2^+$ cells. The novel CAR-T cells displayed a significantly increased amount of active arginase protein compared to the GD2 control. Transcriptomic profiles based on three T cell donors revealed interesting alterations in the cell programmes due to arginase expression. An example is the expression of TOB1, a cell growth suppressor gene known to inhibit T cell proliferation and cytokine production (Ezzeddine et al. 2007), which was found downregulated in the arginase 1-transduced cells compared to control.

On the other hand, arginase 2 showed increased gene expression of tumour trafficking and homing molecules, such as CD161 and CCR7.

CD161, in particular, has previously been observed in tumour infiltrating lymphocytes with a T_H17 phenotype (Zhao et al. 2013). While our cytokine profiling of the modified CAR-T cells was limited to INF-γ production, it could be interesting to expand the phenotypic characterisation further and verify whether arginase expression is involved in the differentiation process of T cells subsets.

Both GD2 ARG1 and GD2 ARG2 CAR-T cells seemed to have a significant proliferative advantage in the context of arginine-rich microenvironments, as well as in restricted arginine availability. GD2 ARG1 also displayed a statistically significant increase in IFN-γ production in the restricted L-arginine environment.

During antigen-driven proliferation, arginase 1 conferred a more successful phenotype than arginase 2. These proliferation assays were in fact co-cultures of neuroblastoma cell lines and CAR-T cells, in which substantial competition for nutrients and amino acids was likely to occur. Indeed, CAR-T cell performance in this context could have been determined by the different subcellular localisation of the enzymes, i.e. cytoplasmic for ARG1 and mitochondrial for ARG2. In fact, in the tug of war between T cells and cancer cells for environmental L-arginine, the cytoplasmic isoform offered a spatio-temporal advantage over arginase 2 in obtaining the substrate.

We found no difference in the expression of the common exhaustion markers (PD-1, LAG-3, TIM-3 and TIGIT) between modified and standard CAR-T cells, with the exclusion of a significant downregulated TIM-3 within the GD2 ARG2 CAR-T cells stimulated by GD2 antigen. This will need to be confirmed with further experiments.

As a further point on the importance of enzyme localisation, arginase 1, but not arginase 2, has been shown to have negative control over iNOS translation (Lee et al. 2003). In turn, lower NO levels are known to promote S-nitrosylation of the arginase 1 cysteine residues, which further increase its enzymatic activity (Caldwell et al. 2018; Santhanam et al. 2007). Therefore, we could argue that arginase 1 subcellular localisation has the ability to dictate an increased rate of L-arginine catabolism and explain the difference in phenotype observed between GD2 ARG1 and GD2 ARG2 cells.

CAR-T cell numbers were a limiting factor for most assays; the sorting steps were found to affect cell viability and deliver suboptimal yields. For this reason, it was not possible to include metabolomic and bioenergetic analyses on the primary samples to confirm the findings of the

Jurkat model. Transcriptomics, on the other hand, was useful in highlighting an arginase-linked upregulation of *MT-ND4,* an NADH oxidase involved in the electron transport chain, potentially denoting a raised mitochondrial activity in the GD2 ARG1 and GD2 ARG2 samples, consistent to what was previously found in the Jurkat model.

Another limitation for the study was determined by the nature of the target antigen. In fact, there is no industrial availability of the disialoganglioside GD2 up to date. For this reason, many of the *in vitro* assays relied on its expression on adherent cells lines, known to be fluctuating in levels, adding a further layer of complication to the experiments.
A potential solution to overcome this problem could be represented by the purification of the antigen from sera, as proposed by Schulz et al. (1984) or cell lines. Interestingly, despite antigen shedding was shown in a remarkable proportion of primary neuroblastomas (Ladisch S et al. 1987), we failed to detect the antigen in the supernatants of the cell lines we tested (IMR-32, LAN-1, SK-N-AS, SK-N-MC).
Nevertheless, we did show that the modified CAR-T cells were able to recognise, become activated and kill the encountered target *in vitro,* to the same extent of the parent GD2 CAR.

Although aligned to the results from other research groups (Thomas et al. 2016), the extent of tumour killing seen with the anti-GD2 CAR was always found substandard, compared to other CAR specificities routinely used in our laboratory (e.g. anti-CD33 CAR).
A possible explanation is linked to the antigen and its expression. Indeed, mathematical models, as well as pre-clinical studies, have shown the existence of an antigen density threshold for optimal T cell engagement (James et al. 2010; Walker et al. 2017; Yoda et al. 2019). Despite the GD2 positivity of the target cells was routinely confirmed by flow

cytometry at the start of each experiment, we were not able to control the GD2 status during the experiment, nor its density or availability.

With all probability, the most effective way to show the advantage acquired upon arginase introduction in CAR-T cells is through the *in vivo* experiment.

The Kelly xenograft model of neuroblastoma on balb/c background is a fast-growing model; in addition, our protocol allowed the tumours to engraft to a size between 10 and 15 mm^3, prior to CAR-T cell injection. This warranted the establishment of an immunosuppressive niche, similar to what CAR-T cells would find in a patient.

The standard GD2 CAR failed to control tumour growth effectively, resulting in a tumour volume comparable to vehicle on day 24. On the other hand, both GD2 ARG1 and GD2 ARG2 engineered T cells displayed enhanced tumour control from day 10 onwards, culminating with a markedly significant difference on day 24. Surprisingly, equal levels of all CAR-T cells were found expressed in the tumour tissue, as a testament of the fact that tumour trafficking did not represent the central issue behind therapy failure. Instead, T cell effector functions were successfully modulated by arginase expression *in vivo*, consistent to what we observed during the *in vitro* investigations.

Whether this is due to the L-arginine depletion strategy operated by the T cells on the tumour, or whether the effects of increased arginase activity on T cell metabolism favoured a more responsive phenotype, it remains to be determined.

To conclude, in this chapter we successfully expanded our knowledge on the arginase-expressing CAR-T cells previously investigated using the Jurkat model, and now in the context of primary cells. Despite the intrinsic difference between Jurkat and T cells, most of the

findings could be aligned in suggesting an advantage derived from arginase expression within T cells, which could counteract the immunosuppressive microenvironment of L-arginine-avid tumours.

6. FINAL CONCLUSIONS

6.1 Overview

The field of tumour immunology has seen an exceptional expansion in the past two decades, and CAR-T cells represent a remarkable leap forward for cancer treatment. However, only in a small subset of cases CAR-T cells are as efficacious as we hoped.

MDSCs have been found to be one of the leading reasons for CAR-T cell therapy failure in solid tumours, with MDSC expansion and their negative impact on prognosis being documented across cancer types.

One of the most characterised means of T cell immunosuppression exploited by MDSCs, as well as by some tumours, is L-arginine depletion by arginase. T cells require this semi essential (but conditionally essential) amino acid to sustain their proliferation, protein synthesis and polyamine production. L-arginine starvation was shown to impair TCR expression and stop cell cycle progression.

In this thesis we delved into the investigation of two main angles for the improvement of cancer immunotherapy. Firstly, we assessed the repurposing of an existing immunoconjugate, Gemtuzumab Ozogamicin, to selectively deplete MDSCs from the TME and peripheral blood of patients by exploiting their CD33 marker. Secondly, by utilising a standard CAR-T cell directed at the GD2 antigen, we proposed the introduction of metabolic alterations to render the CAR-T cell more resilient in the immunosuppressive TME. In particular, we designed arginase-expressing CAR-T cells to counteract and compete with the L-arginine-catabolising tumour and therefore present an advantage once at its interface.

Crucially, we believe that the particular value of the two individual approaches we proposed is the pan-cancer relevance. In fact, while we focused our investigation on the anti-GD2 CAR system, the concept of introducing arginase within CAR-T cells can be applied to any CAR construct, against any target. This was shown to be the case in a previous study from our group, in which ASS1- and OTC-expressing CAR-T cells were tested on CARs with different scFv specificities (Fultang et al. 2020).

For what concerns MDSC depletion, not only we showed the positive effect of Gemtuzumab Ozogamicin across different cancer types; its use will be beneficial in rare and fatal conditions, such as in haemophagocytic lymphohistiocytosis or macrophage activation syndrome, which often appear as a consequence of cancer and for which there are no specific treatments available, other than cytokine blockade (Marsh et al. 2017). This will be one of the main objects of the clinical trial GOTHAM.

6.2 Findings Summary

The evaluation of a range of solid tumours confirmed the increased prevalence of MDSCs in the tumour tissue and blood of a range of cancer patients. As a consequence of MDSC expansion, T cells were found in reduced proportions and with an unbalanced representation of the CD4 and CD8 subsets. Increased TGF-β, VEGF and IL-6 in the plasma confirmed the establishment of a pro-tumour microenvironment extended at a systemic level.

We showed that CD33 was widely expressed on M-MDSCs and G-MDSCs, albeit the intensity was higher in M-MDSCs. Hence, Gemtuzumab Ozogamicin could be internalised by the cells and induce DNA damage. Importantly, this was found to affect the $CD33^+$ portion of cells exclusively, whilst leaving unharmed the CD33-negative cells.

Indeed, GO treatment impaired the MDSC immunosuppressive ability and T cell proliferation was rescued *in vitro* as a consequence of targeted MDSC depletion.

Finally, when anti-GD2 CAR-T cells were incubated with $GD2^+$ target cells in presence of MDSCs, tumour killing was defective. Gemtuzumab Ozogamicin treatment on MDSCs was found decisive in subverting MDSCs' pro-tumour effect and enabling CAR-T cell effector function on the targets.

Overall, our data showed the feasibility and benefit of selective MDSC depletion using an extensively tested agent, which has the potential to impact the therapeutic outcome for many.

In addition to MDSC depletion, we proposed that the nutrient-poor tumour microenvironment could be reshaped by the introduction of constitutive arginase within CAR-T cells for effective immunotherapy.

Indeed, the metabolic studies conducted using a Jurkat cell line model of CAR-T cell revealed significant difference in bioenergetic signatures between the modified and the control CAR. The arginase-expressing samples displayed increased metabolic flexibility, given the higher respiration rates observed. Arginase 1 was characterised by an increased overall ATP production, while arginase 2 was shown to upregulate the glycolytic flux as well.

With the analysis of the different intracellular metabolite abundances by GC-MS, we observed a generalised increase in intracellular amino acid availability, such as glutamate in both GD2 ARG1 and GD2 ARG2, while a wider range of metabolites was raised in GD2 ARG1 (e.g. the branched chain amino acids, aspartate, glycine,…). As evidence of the higher metabolic rates in the modified cells, pyruvate (in GD2 ARG1) and lactate (in both) were found more prevalent.

When moving the study onto primary cells we could confirm the relevance of the metabolic alterations observed in Jurkat. In fact, both the arginase-expressing CAR-T cells displayed a marked increase in proliferation in different L-arginine microenvironments, from the low L-arginine condition, to the primary tumour-derived TCM and the supplementation of L-arginine.

Interestingly, the antigen dependent proliferation seemed to favour the arginase 1 genotype, adding to the underlying difference we have seen between the effects of the arginase isoforms. whether this is linked to the increased IFN-γ production also associated to the GD2 ARG1 CAR, it needs to be investigated.

Importantly, these findings were confirmed by the *in vivo* experiment, which showed a significantly improved tumour control by the both arginase-expressing CARs.

6.3 Future Work

The work presented in this thesis helped answer some of the questions concerning the feasibility and benefit of the therapeutic strategies proposed. Nevertheless, they opened new avenues of investigation to be pursued.

From a clinical standpoint, GO represents a potential asset to many therapeutic regimens, across many cancer types. Yet, some work will need to be done in order to define which patient groups will receive the most benefit from the therapy. This includes pre-treatment investigations on the myeloid burden, the systemic cytokine milieu, the identification of gene signatures at diagnosis that might entail a substantial MDSC-derived immunosuppression (Grzywa et al. 2020). For the little we could tell from the immunohistochemistry of tumour tissues, for example, colon cancer appeared to be the least CD33-expanded tumour type compared to healthy tissue controls among those analysed. This might be a potential indication of a less Gemtuzumab-responding cohort.

Similarly, having showed differences in G-MDCS and M-MDSC CD33 staining intensity, understanding whether this parameter affects the efficacy of the treatment in the patient will be of paramount importance.

Overall, many of these points will be address by the phase II trial, GOTHAM, which aims to test Gemtuzumab Ozogamicin treatment on a range of solid tumour.

Always from a clinical perspective, the benefit of a metabolically enhanced CAR-T cell over the standard one needs to be assessed, what elements could help us determine which patients will gain the most benefit from an arginase CAR.

We showed that endogenous arginase is upregulated in T cells upon activation to a degree that varies from donor to donor. Whether this could be a discriminant in choosing what patients should receive an arginase-expressing CAR will have to be assessed.
Furthermore, learning from the studies relative to the recombinant arginases, such as BCT-100, and the literature on L-arginine starvation as a cancer treatment, the choice of tumour type (or tumour subset) could make a substantial difference in modified-CAR-T cell therapy outcome. For example, it is well known that L-arginine auxotrophic cancers rely greatly on exogenous arginine due to their deficient expression of ASS1 (Fultang et al. 2016). As a consequence, these cancers respond well to L-arginine depleting strategies.
Therefore, we anticipate that ASS1-negative cancer subtypes will show increased susceptibility to arginase-expressing CAR-T cells.

Recently, Badeaux et al. (2021) assessed the synergistic effect of arginine depletion and checkpoint inhibition, showing increased $CD8^+$ infiltration and overall enhanced tumour targeting. This was thought to be related to increased MHC expression and antigen presentation, as well as increased M1-polarised macrophage, due to L-arginine starvation. In light of this, it would be extremely interesting to investigate whether the arginase-modified CAR-T cells would help re-shape the microenvironment *in vivo* in the same way Badeaux et al. describe, i.e. higher MHC expression on tumour and immune cells, higher M1 macrophage infiltration. It would be extremely interesting to understand how much of what changes in the microenvironment can be attributed to L-arginine depletion alone and how much of it applies to our “live L-arginine depletion” approach.

With a more biology-oriented outlook, the repercussions of constitutive arginase activity within Jurkat and T cells were shown to include increased metabolism and intracellular metabolite abundance. However, for technical reasons, we were not able to execute L-arginine tracing into the metabolites of arguably highest interest, e.g. L-citrulline, L-ornithine, spermine, spermidine and putrescine. In fact, we detected low to no levels of ^{13}C incorporation by GC-MS on the metabolites included by our analysis.

This leaves us wondering whether we missed the highest L-arginine-derived metabolites, i.e. the products of the polyamine synthesis route. Recently, we understood that the technical challenges of L-arginine tracing could be overcome by using a UHPLC-MS/MS method developed by Zhang et al. (2019) to simultaneously detect and quantify polyamines and their precursors. Further investigations in this respect could provide valuable biological answers on the pathways fuelled by increased L-arginine hydrolysis.

Finally, our work included some RNA sequencing to obtain a snapshot of the cells' transcriptome; indeed, the gene signatures highlighted elements to draw apart the effects of arginase 1 and 2 on CAR-T cells. Of particular interest, is the highly significant upregulation of CCR7 and CD161 on the GD2 ARG2 samples, denoting the induction of a different CAR-T cell phenotype. As mentioned previously, CD161 was linked to tumour infiltration of T_H17 cells and linked to improved prognosis Zhao et al. (2013).

Further validation of these targets on GD2 ARG2 is necessary in order to confirm their relevance; nonetheless, following this trail could help elucidate the relationship between arginase 2 and the differentiation of T cell memory phenotypes and specific cytokine signatures.

Similarly, given the raised metabolic rates already detected by Seahorse in both the arginase 1 and arginase 2 CAR-Jurkat, it would be important to follow up the investigation further in T cells. In fact, T cell phenotype has been shown to be important in the therapeutic outcome. As highlighted in Dimeloe et al. (2016), there are other elements that can help discriminate T cell memory from short-lived subsets. These are differences in mitochondrial content, electron transport chain expression and cytosolic GAPDH. Investigation of these parameters, in association with the canonical markers (e.g. CD45RA, CD45RO, CCR7, CD62) could provide valuable insights in the phenotype of the arginase-expressing CAR-T cells.

7. REFERENCES

Abraham, Robert T, and Arthur Weiss. 2004. "Jurkat T Cells and Development of the T-Cell Receptor Signalling Paradigm." *Nature Reviews Immunology* 4(4): 301–8. https://doi.org/10.1038/nri1330.

Acuto, Oreste, and Frédérique Michel. 2003. "CD28-Mediated Co-Stimulation: A Quantitative Support for TCR Signalling." *Nature Reviews Immunology* 3(12): 939–51. https://doi.org/10.1038/nri1248.

Agliardi, Giulia et al. 2021. "Intratumoral IL-12 Delivery Empowers CAR-T Cell Immunotherapy in a Pre-Clinical Model of Glioblastoma." *Nature communications* 12(1): 444. https://pubmed.ncbi.nlm.nih.gov/33469002.

Alfei, Francesca, Ping-Chih Ho, and Wan-Lin Lo. 2021. "DCision-Making in Tumors Governs T Cell Anti-Tumor Immunity." *Oncogene* 40(34): 5253–61. https://doi.org/10.1038/s41388-021-01946-8.

Almand, Bond et al. 2001. "Increased Production of Immature Myeloid Cells in Cancer Patients: A Mechanism of Immunosuppression in Cancer." *The Journal of Immunology* 166(1): 678 LP – 689. http://www.jimmunol.org/content/166/1/678.abstract.

Amadori, Alberto et al. 1995. "Genetic Control of the CD4/CD8 T-Cell Ratio in Humans." *Nature medicine* 1(12): 1279–83.

Angelin, Alessia et al. 2017. "Foxp3 Reprograms T Cell Metabolism to Function in Low-Glucose, High-Lactate Environments." *Cell Metabolism* 25(6): 1282-1293.e7.

Arina, Ainhoa, and Vincenzo Bronte. 2015. "Myeloid-Derived Suppressor Cell Impact on Endogenous and Adoptively Transferred T Cells." *Current Opinion in Immunology* 33: 120–25. https://www.sciencedirect.com/science/article/pii/S0952791515000357.

Asgharzadeh, Shahab et al. 2012. "Clinical Significance of Tumor-Associated Inflammatory Cells in Metastatic Neuroblastoma." *Journal of Clinical Oncology* 30(28): 3525–32. https://doi.org/10.1200/JCO.2011.40.9169.

Badeaux, Mark D et al. 2021. "Arginase Therapy Combines Effectively with Immune Checkpoint Blockade or Agonist Anti-OX40 Immunotherapy to Control Tumor Growth." *Cancer Immunology Research* 9(4): 415–29. https://doi.org/10.1158/2326-6066.CIR-20-0317.

Balis, Frank M et al. 2018. "GD2 as a Circulating Tumor Biomarker (CTB) for Neuroblastoma (NBL)." *Journal of Clinical Oncology* 36(15_suppl): 10538. https://doi.org/10.1200/JCO.2018.36.15_suppl.10538.

Bascur, Luz, Julio Cabello, Marta Véliz, and Adriana González. 1966. "Molecular Forms of Human-Liver Arginase." *Biochimica et Biophysica Acta (BBA) - Enzymology and Biological*

Oxidation 128(1): 149–54. https://www.sciencedirect.com/science/article/pii/0926659366901512.

Bauer, Stefan et al. 1999. "Activation of NK Cells and T Cells by NKG2D, a Receptor for Stress-Inducible MICA." *Science* 285(5428): 727–29.

Bekkering, Siroon et al. 2018. "Metabolic Induction of Trained Immunity through the Mevalonate Pathway." *Cell* 172(1–2): 135-146.e9. https://doi.org/10.1016/j.cell.2017.11.025.

Beutler, Bruce. 2004. "Innate Immunity: An Overview." *Molecular Immunology* 40(12): 845–59.

Blees, Andreas et al. 2017. "Structure of the Human MHC-I Peptide-Loading Complex." *Nature* 551(7681): 525–28. http://dx.doi.org/10.1038/nature24627.

Bollard, Catherine M et al. 2018. "Tumor-Specific T-Cells Engineered to Overcome Tumor Immune Evasion Induce Clinical Responses in Patients With Relapsed Hodgkin Lymphoma." *Journal of Clinical Oncology* 36(11): 1128–39. https://doi.org/10.1200/JCO.2017.74.3179.

Boshoff, Chris, and Robin Weiss. 2002. "Aids-Related Malignancies." *Nature Reviews Cancer* 2(5): 373–82. https://doi.org/10.1038/nrc797.

Brinkman-Van der Linden, E C M et al. 2003. "CD33/Siglec-3 Binding Specificity, Expression Pattern, and Consequences of Gene Deletion in Mice." *Molecular and Cellular Biology* 23(12): 4199–4206. https://doi.org/10.1128/MCB.23.12.4199-4206.2003.

van den Broek, M E et al. 1996. "Decreased Tumor Surveillance in Perforin-Deficient Mice." *Journal of Experimental Medicine* 184(5): 1781–90. https://doi.org/10.1084/jem.184.5.1781.

Bronte, Vincenzo et al. 2016. "Recommendations for Myeloid-Derived Suppressor Cell Nomenclature and Characterization Standards." *Nature communications* 7: 12150.

Bronte, Vincenzo, and Paola Zanovello. 2005. "Regulation of Immune Responses by L-Arginine Metabolism." *Nature Reviews Immunology* 5(8): 641–54. https://doi.org/10.1038/nri1668.

Brooks, George A. 2009. "Cell–Cell and Intracellular Lactate Shuttles." *The Journal of physiology* 587(23): 5591–5600.

Burkhardt, Janis K., Esteban Carrizosa, and Meredith H. Shaffer. 2008. "The Actin Cytoskeleton in T Cell Activation." *Annual Review of Immunology* 26(1): 233–59.

Burkhart, Deborah L, and Julien Sage. 2008. "Cellular Mechanisms of Tumour Suppression by the Retinoblastoma Gene." *Nature Reviews Cancer* 8(9): 671–82. https://doi.org/10.1038/nrc2399.

Burnet, F M. 1970. "The Concept of Immunological Surveillance." In *Progress in Tumor*

Research, , 1–27. https://www.karger.com/DOI/10.1159/000386035.

Burrows, Scott R, Jamie Rossjohn, and James McCluskey. 2006. "Have We Cut Ourselves Too Short in Mapping CTL Epitopes?" *Trends in Immunology* 27(1): 11–16. https://doi.org/10.1016/j.it.2005.11.001.

Caldwell, R William et al. 2018. "Arginase: A Multifaceted Enzyme Important in Health and Disease." *Physiological reviews* 98(2): 641–65. https://pubmed.ncbi.nlm.nih.gov/29412048.

Canè, Stefania, and Vincenzo Bronte. 2020. "Chapter Eleven - Detection and Functional Evaluation of Arginase-1 Isolated from Human PMNs and Murine MDSC." In *Tumor Immunology and Immunotherapy – Cellular Methods Part B*, eds. Lorenzo Galluzzi and Nils-Petter B T - Methods in Enzymology Rudqvist. Academic Press, 193–213. https://www.sciencedirect.com/science/article/pii/S0076687919303027.

Caruso, Roberta, Neil Warner, Naohiro Inohara, and Gabriel Núñez. 2014. "NOD1 and NOD2: Signaling, Host Defense, and Inflammatory Disease." *Immunity* 41(6): 898–908.

Casero, Robert A, Tracy Murray Stewart, and Anthony E Pegg. 2018. "Polyamine Metabolism and Cancer: Treatments, Challenges and Opportunities." *Nature Reviews Cancer* 18(11): 681–95. https://doi.org/10.1038/s41568-018-0050-3.

Cassetta, Luca et al. 2020. "Differential Expansion of Circulating Human MDSC Subsets in Patients with Cancer, Infection and Inflammation." *Journal for ImmunoTherapy of Cancer* 8(2): e001223. http://jitc.bmj.com/content/8/2/e001223.abstract.

Castellarin, Mauro et al. 2018. "Driving Cars to the Clinic for Solid Tumors." *Gene therapy* 25(3): 165–75.

Chang, Chien-Hsing et al. 2005. "Effective Therapy of Human Lymphoma Xenografts with a Novel Recombinant Ribonuclease/Anti-CD74 Humanized IgG4 Antibody Immunotoxin." *Blood* 106(13): 4308–14.

Chang, Chih-Hao et al. 2013. "Posttranscriptional Control of T Cell Effector Function by Aerobic Glycolysis." *Cell* 153(6): 1239–51. https://doi.org/10.1016/j.cell.2013.05.016.

Chen, Shuming et al. 2019. "Mechanisms Regulating PD-L1 Expression on Tumor and Immune Cells." *Journal for ImmunoTherapy of Cancer* 7(1): 305. http://jitc.bmj.com/content/7/1/305.abstract.

Cheng, Jiali et al. 2017. "Mitochondrial Proton Leak Plays a Critical Role in Pathogenesis of Cardiovascular Diseases." *Advances in experimental medicine and biology* 982: 359–70. https://pubmed.ncbi.nlm.nih.gov/28551798.

Cherkassky, Leonid et al. 2016. "Human CAR T Cells with Cell-Intrinsic PD-1 Checkpoint Blockade Resist Tumor-Mediated Inhibition." *The Journal of clinical investigation* 126(8): 3130–44. https://pubmed.ncbi.nlm.nih.gov/27454297.

Cheung, N K et al. 1987. “Ganglioside GD2 Specific Monoclonal Antibody 3F8: A Phase I Study in Patients with Neuroblastoma and Malignant Melanoma.” *Journal of Clinical Oncology* 5(9): 1430–40. https://doi.org/10.1200/JCO.1987.5.9.1430.

Chmielewski, Markus, and Hinrich Abken. 2012. “CAR T Cells Transform to Trucks: Chimeric Antigen Receptor–Redirected T Cells Engineered to Deliver Inducible IL-12 Modulate the Tumour Stroma to Combat Cancer.” *Cancer Immunology, Immunotherapy* 61(8): 1269–77. https://doi.org/10.1007/s00262-012-1202-z.

———. 2017. “CAR T Cells Releasing IL-18 Convert to T-Bet^{High} FoxO1^{Low} Effectors That Exhibit Augmented Activity against Advanced Solid Tumors.” *Cell Reports* 21(11): 3205–19. https://doi.org/10.1016/j.celrep.2017.11.063.

Choudhari, Sheetal Korde et al. 2013. “Nitric Oxide and Cancer: A Review.” *World Journal of Surgical Oncology* 11(1): 118. https://doi.org/10.1186/1477-7819-11-118.

Ciceri, Fabio et al. 2009. “Infusion of Suicide-Gene-Engineered Donor Lymphocytes after Family Haploidentical Haemopoietic Stem-Cell Transplantation for Leukaemia (the TK007 Trial): A Non-Randomised Phase I–II Study.” *The Lancet Oncology* 10(5): 489–500. https://doi.org/10.1016/S1470-2045(09)70074-9.

Clemente, Claudio G et al. 1996. “Prognostic Value of Tumor Infiltrating Lymphocytes in the Vertical Growth Phase of Primary Cutaneous Melanoma.” *Cancer* 77(7): 1303–10. https://doi.org/10.1002/(SICI)1097-0142(19960401)77:7%3C1303::AID-CNCR12%3E3.0.CO.

Coley, W.B. 1893. “The Treatment of Malignant Tumors by Repeated Inoculations of Erysipelas. With a Report of Ten Original Cases.” *The American journal of the Medical Sciences* 105(5): 487–511.

Dann, Sara M., and Lars Eckmann. 2007. “Innate Immune Defenses in the Intestinal Tract.” *Current Opinion in Gastroenterology* 23(2): 115–20.

Davies, M A, and Y Samuels. 2010. “Analysis of the Genome to Personalize Therapy for Melanoma.” *Oncogene* 29(41): 5545–55. https://doi.org/10.1038/onc.2010.323.

Davila, Marco et al. 2014. “Efficacy and Toxicity Management of 19-28z CAR T Cell Therapy in B Cell Acute Lymphoblastic Leukemia.” *Science Translational Medicine* 6(224): 224ra25-224ra25. https://doi.org/10.1126/scitranslmed.3008226.

Depil, S et al. 2020. “‘Off-the-Shelf’ Allogeneic CAR T Cells: Development and Challenges.” *Nature Reviews Drug Discovery* 19(3): 185–99. https://doi.org/10.1038/s41573-019-0051-2.

Derbinski, Jens, Antje Schulte, Bruno Kyewski, and Ludger Klein. 2016. “Promiscuous Gene Expression in Medullary Thymic Epithelial Cells Mirrors the Peripheral Self.” *Journal of Immunology* 196(7): 2915–22.

Dighe, Anand S., Elizabeth Richards, Lloyd J. Old, and Robert D. Schreiber. 1994. “Enhanced in

Vivo Growth and Resistance to Rejection of Tumor Cells Expressing Dominant Negative IFNγ Receptors." *Immunity* 1(6): 447–56.

Dimeloe, Sarah et al. 2016. "The Immune-Metabolic Basis of Effector Memory CD4⁺ T Cell Function under Hypoxic Conditions." *The Journal of Immunology* 196(1): 106 LP – 114. http://www.jimmunol.org/content/196/1/106.abstract.

Dobrenkov, Konstantin et al. 2016. "GD2/GD3 Expression: Companion Diagnostic for Ganglioside-Targeted Immunotherapy against Pediatric Solid Tumors." *Journal of Clinical Oncology* 34(15_suppl): 10567. https://doi.org/10.1200/JCO.2016.34.15_suppl.10567.

Dolcetti, Luigi et al. 2010. "Hierarchy of Immunosuppressive Strength among Myeloid-derived Suppressor Cell Subsets Is Determined by GM-CSF." *European journal of immunology* 40(1): 22–35.

Duan, Qianqian, Hualing Zhang, Junnian Zheng, and Lianjun Zhang. 2020. "Turning Cold into Hot: Firing up the Tumor Microenvironment." *Trends in Cancer* 6(7): 605–18. https://doi.org/10.1016/j.trecan.2020.02.022.

Duncan, Christine et al. 2018. "Veno-Occlusive Disease Characteristics in Pediatric Patients with Acute Myeloid Leukemia Receiving Gemtuzumab Ozogamicin before Allogeneic Stem Cell Transplant." *Biology of Blood and Marrow Transplantation* 24(3): S302.

Dunn, Gavin P et al. 2002. "Cancer Immunoediting: From Immunosurveillance to Tumor Escape." *Nature Immunology* 3(11): 991–98. https://doi.org/10.1038/ni1102-991.

Dzik, Jolanta Maria. 2014. "Evolutionary Roots of Arginase Expression and Regulation." *Frontiers in Immunology* 5: 544. https://www.frontiersin.org/article/10.3389/fimmu.2014.00544.

Elms, Shawn et al. 2013. "Insights into the Arginine Paradox: Evidence against the Importance of Subcellular Location of Arginase and ENOS." *American Journal of Physiology-Heart and Circulatory Physiology* 305(5): H651–66. https://doi.org/10.1152/ajpheart.00755.2012.

Encyclopædia Britannica. "Immunoglobulins." *Encyclopædia Britannica*.

Eren, Metin I, Anne Chao, Wen-Han Hwang, and Robert K Colwell. 2012. "Estimating the Richness of a Population When the Maximum Number of Classes Is Fixed: A Nonparametric Solution to an Archaeological Problem." *PLOS ONE* 7(5): e34179. https://doi.org/10.1371/journal.pone.0034179.

Ezzeddine, Nader et al. 2007. "Human TOB, an Antiproliferative Transcription Factor, Is a Poly(A)-Binding Protein-Dependent Positive Regulator of Cytoplasmic MRNA Deadenylation." *Molecular and cellular biology* 27(22): 7791–7801. https://pubmed.ncbi.nlm.nih.gov/17785442.

Ferrara, Napoleone. 2009. "Vascular Endothelial Growth Factor." *Arteriosclerosis, Thrombosis, and Vascular Biology* 29(6): 789–91. https://doi.org/10.1161/ATVBAHA.108.179663.

Fesnak, Andrew D, Carl H June, and Bruce L Levine. 2016. “Engineered T Cells: The Promise and Challenges of Cancer Immunotherapy.” *Nature Reviews Cancer* 16(9): 566–81. https://doi.org/10.1038/nrc.2016.97.

Forthal, Donald N. 2015. “Functions of Antibodies.” *Antibodies for Infectious Diseases* 2(4): 23–48.

Franco, Fabien et al. 2020. “Metabolic and Epigenetic Regulation of T-Cell Exhaustion.” *Nature Metabolism* 2(10): 1001–12. https://doi.org/10.1038/s42255-020-00280-9.

Frosch, Jennifer, Ilia Leontari, and John Anderson. 2021. “Combined Effects of Myeloid Cells in the Neuroblastoma Tumor Microenvironment.” *Cancers* 13(7): 1743. https://pubmed.ncbi.nlm.nih.gov/33917501.

Fry, Terry J et al. 2018. “CD22-Targeted CAR T Cells Induce Remission in B-ALL That Is Naive or Resistant to CD19-Targeted CAR Immunotherapy.” *Nature Medicine* 24(1): 20–28. https://doi.org/10.1038/nm.4441.

Fujita, Mitsugu et al. 2011. “COX-2 Blockade Suppresses Gliomagenesis by Inhibiting Myeloid-Derived Suppressor Cells.” *Cancer research* 71(7): 2664–74.

Fultang, L, A Vardon, C De Santo, and F Mussai. 2016. “Molecular Basis and Current Strategies of Therapeutic Arginine Depletion for Cancer. PG - 501-9 LID - 10.1002/Ijc.30051 [Doi].” (1097-0215 (Electronic)).

Fultang, Livingstone, Laura D Gamble, et al. 2019. “Macrophage-Derived IL1β and TNFα Regulate Arginine Metabolism in Neuroblastoma.” *Cancer Research* 79(3): 611 LP – 624. http://cancerres.aacrjournals.org/content/79/3/611.abstract.

Fultang, Livingstone, Silvia Panetti, et al. 2019. “MDSC Targeting with Gemtuzumab Ozogamicin Restores T Cell Immunity and Immunotherapy against Cancers.” *EBioMedicine* 47: 235–46. https://doi.org/10.1016/j.ebiom.2019.08.025.

Fultang, Livingstone et al. 2020. “Metabolic Engineering against the Arginine Microenvironment Enhances CAR-T Cell Proliferation and Therapeutic Activity.” *Blood* 136(10): 1155–60. https://doi.org/10.1182/blood.2019004500.

Gabrilovich, Dmitry I, Suzanne Ostrand-Rosenberg, and Vincenzo Bronte. 2012. “Coordinated Regulation of Myeloid Cells by Tumours.” *Nature Reviews Immunology* 12(4): 253–68. https://doi.org/10.1038/nri3175.

Galili, U, F Vanky, L Rodriguez, and Eva Klein. 1979. “Activated T Lymphocytes within Human Solid Tumors.” *Cancer Immunology, Immunotherapy* 6(3): 129–33. https://doi.org/10.1007/BF00205536.

Galon, Jérôme et al. 2006. “Type, Density, and Location of Immune Cells Within Human Colorectal Tumors Predict Clinical Outcome.” *Science* 313(5795): 1960 LP – 1964. http://science.sciencemag.org/content/313/5795/1960.abstract.

Garrido-Rodríguez, V et al. 2021. “Immunological Features beyond CD4/CD8 Ratio Values in Older Individuals. PG - 13443-13459 LID - 10.18632/Aging.203109 [Doi].” (1945-4589 (Electronic)).

Gattinoni, Luca et al. 2011. “A Human Memory T Cell Subset with Stem Cell-like Properties.” *Nature Medicine* 17(10): 1290–97.

Gaud, Guillaume, Renaud Lesourne, and Paul E Love. 2018. “Regulatory Mechanisms in T Cell Receptor Signalling.” *Nature Reviews Immunology* 18(8): 485–97. https://doi.org/10.1038/s41577-018-0020-8.

Geiger, Roger et al. 2016. “L-Arginine Modulates T Cell Metabolism and Enhances Survival and Anti-Tumor Activity.” *Cell* 167(3): 829-842.e13. http://dx.doi.org/10.1016/j.cell.2016.09.031.

Gerlach, Carmen et al. 2016. “The Chemokine Receptor CX3CR1 Defines Three Antigen-Experienced CD8 T Cell Subsets with Distinct Roles in Immune Surveillance and Homeostasis.” *Immunity* 45(6): 1270–84. https://doi.org/10.1016/j.immuni.2016.10.018.

Germain, Ronald N. 2002. “T-Cell Development and the CD4–CD8 Lineage Decision.” *Nature Reviews Immunology* 2(5): 309–22. https://doi.org/10.1038/nri798.

Giraldo, Nicolas A, and Claire Germain. 2016. “Dieu-Nosjean_et_al-2016-Immunological_Reviews.” 271: 260–75.

Grabowski, Matthew M et al. 2021. “Immune Suppression in Gliomas.” *Journal of Neuro-Oncology* 151(1): 3–12. https://doi.org/10.1007/s11060-020-03483-y.

Greene, Sarah et al. 2020. “Inhibition of MDSC Trafficking with SX-682, a CXCR1/2 Inhibitor, Enhances NK-Cell Immunotherapy in Head and Neck Cancer Models.” *Clinical Cancer Research* 26(6): 1420–31.

Griffioen, Marieke et al. 2009. “Retroviral Transfer of Human CD20 as a Suicide Gene for Adoptive T-Cell Therapy.” *Haematologica* 94(9 SE-Brief Reports): 1316–20. https://haematologica.org/article/view/5358.

Grist, James T et al. 2018. “Extracellular Lactate: A Novel Measure of T Cell Proliferation.” *The Journal of Immunology* 200(3): 1220 LP – 1226. http://www.jimmunol.org/content/200/3/1220.abstract.

Gross, Gideon, Tova Waks, and Zelig Eshhar. 1989. “Expression of Immunoglobulin-T-Cell Receptor Chimeric Molecules as Functional Receptors with Antibody-Type Specificity.” *Proceedings of the National Academy of Sciences* 86(24): 10024–28.

Groth, Christopher et al. 2019. “Immunosuppression Mediated by Myeloid-Derived Suppressor Cells (MDSCs) during Tumour Progression.” *British Journal of Cancer* 120(1): 16–25. http://dx.doi.org/10.1038/s41416-018-0333-1.

Gubser, Patrick M. et al. 2013. “Rapid Effector Function of Memory CD8+ T Cells Requires an

Immediate-Early Glycolytic Switch." *Nature Immunology* 14(10): 1064–72.

Guest, Ryan D et al. 2005. "The Role of Extracellular Spacer Regions in the Optimal Design of Chimeric Immune Receptors: Evaluation of Four Different ScFvs and Antigens." *Journal of Immunotherapy* 28(3). https://journals.lww.com/immunotherapy-journal/Fulltext/2005/05000/The_Role_of_Extracellular_Spacer_Regions_in_the.5.aspx.

Hanahan, Douglas et al. 2011. "Hallmarks of Cancer: The Next Generation." *Cell* 144(5): 646–74. http://www.ncbi.nlm.nih.gov/pubmed/21376230 (April 11, 2017).

Hanahan, Douglas, and Judah Folkman. 1996. "Patterns and Emerging Mechanisms of the Angiogenic Switch during Tumorigenesis." *Cell* 86(3): 353–64. https://doi.org/10.1016/S0092-8674(00)80108-7.

Hartman, D J et al. 2012. "Mutant Allele-Specific Imbalance Modulates Prognostic Impact of KRAS Mutations in Colorectal Adenocarcinoma and Is Associated with Worse Overall Survival." *International Journal of Cancer* 131(8): 1810–17. https://doi.org/10.1002/ijc.27461.

Haynes, Barton F et al. 2000. "The Role of the Thymus in Immune Reconstitution in Aging, Bone Marrow Transplantation, and HIV-1 Infection." *Annual Review of Immunology* 18(1): 529–60. https://doi.org/10.1146/annurev.immunol.18.1.529.

Heczey, Andras et al. 2017. "CAR T Cells Administered in Combination with Lymphodepletion and PD-1 Inhibition to Patients with Neuroblastoma." *Molecular Therapy* 25(9): 2214–24. https://www.sciencedirect.com/science/article/pii/S1525001617302307.

Heil, Florian et al. 2013. "#11.15Species-Specific Recognition of Single-Stranded RNA via Toll-like Receptor 7 and 8." *Science (New York, N.Y.)* 303(5663): 1526–29. papers3://publication/doi/10.1126/science.1093620.

Ho, Ping Chih et al. 2015. "Phosphoenolpyruvate Is a Metabolic Checkpoint of Anti-Tumor T Cell Responses." *Cell* 162(6): 1217–28. http://dx.doi.org/10.1016/j.cell.2015.08.012.

Hozumi, N., and S. Tonegawa. 1976. "Evidence for Somatic Rearrangement of Immunoglobulin Genes Coding for Variable and Constant Regions." *Proceedings of the National Academy of Sciences of the United States of America* 73(10): 3628–32.

Huang, Can-Yu, Zi-Han Ye, Mu-Yang Huang, and Jin-Jian Lu. 2020. "Regulation of CD47 Expression in Cancer Cells." *Translational Oncology* 13(12): 100862.

Hudecek, Michael et al. 2015. "The Nonsignaling Extracellular Spacer Domain of Chimeric Antigen Receptors Is Decisive for <Em>In Vivo</Em> Antitumor Activity." *Cancer Immunology Research* 3(2): 125 LP – 135. http://cancerimmunolres.aacrjournals.org/content/3/2/125.abstract.

Iannello, Alexandre, Olfa Debbeche, Suzanne Samarani, and Ali Ahmad. 2008. "Antiviral NK Cell Responses in HIV Infection: I. NK Cell Receptor Genes as Determinants of HIV Resistance and Progression to AIDS." *Journal of Leukocyte Biology* 84(1): 1–26.

Imai, C et al. 2004. “Chimeric Receptors with 4-1BB Signaling Capacity Provoke Potent Cytotoxicity against Acute Lymphoblastic Leukemia.” *Leukemia* 18(4): 676–84. https://doi.org/10.1038/sj.leu.2403302.

Imai, K et al. 2012. “Inhibition of Dendritic Cell Migration by Transforming Growth Factor-B1 Increases Tumor-Draining Lymph Node Metastasis.” *Journal of Experimental & Clinical Cancer Research* 31(1): 1–9.

James, Scott E et al. 2010. “Mathematical Modeling of Chimeric TCR Triggering Predicts the Magnitude of Target Lysis and Its Impairment by TCR Downmodulation.” *The Journal of Immunology* 184(8): 4284 LP – 4294. http://www.jimmunol.org/content/184/8/4284.abstract.

Janeway, Charles A., P. Travers, M. Walport, and et al. 2001. “The Major Histocompatibility Complex and Inflammation.” In *Immunobiology: The Immune System in Health and Disease*, New York: Garland Science. https://www.ncbi.nlm.nih.gov/books/NBK27156/.

Janssen, Edith M. et al. 2003. “CD4+ T Cells Are Required for Secondary Expansion and Memory in CD8+ T Lymphocytes.” *Nature* 421(6925): 852–56.

Joglekar, Alok V, and Guideng Li. 2021. “T Cell Antigen Discovery.” *Nature Methods* 18(8): 873–80. https://doi.org/10.1038/s41592-020-0867-z.

Johnson, Laura et al. 2015. “Rational Development and Characterization of Humanized Anti–EGFR Variant III Chimeric Antigen Receptor T Cells for Glioblastoma.” *Science Translational Medicine* 7(275): 275ra22-275ra22. https://doi.org/10.1126/scitranslmed.aaa4963.

Jones, Nicholas et al. 2019. “Akt and STAT5 Mediate Naïve Human CD4+ T-Cell Early Metabolic Response to TCR Stimulation.” *Nature Communications* 10(1): 152–60. http://dx.doi.org/10.1038/s41467-019-10023-4.

Kailayangiri, S et al. 2012. “The Ganglioside Antigen GD2 Is Surface-Expressed in Ewing Sarcoma and Allows for MHC-Independent Immune Targeting.” *British Journal of Cancer* 106(6): 1123–33. https://doi.org/10.1038/bjc.2012.57.

Kaldjian, Eric P et al. 2001. “Spatial and Molecular Organization of Lymph Node T Cell Cortex: A Labyrinthine Cavity Bounded by an Epithelium-like Monolayer of Fibroblastic Reticular Cells Anchored to Basement Membrane-like Extracellular Matrix.” *International Immunology* 13(10): 1243–53. https://doi.org/10.1093/intimm/13.10.1243.

Kawalekar, Omkar U. et al. 2016. “Distinct Signaling of Coreceptors Regulates Specific Metabolism Pathways and Impacts Memory Development in CAR T Cells.” *Immunity* 44(2): 380–90. http://dx.doi.org/10.1016/j.immuni.2016.01.021.

Kelly, Beth, and Erika L Pearce. 2020. “Amino Assets: How Amino Acids Support Immunity.” *Cell Metabolism* 32(2): 154–75. https://doi.org/10.1016/j.cmet.2020.06.010.

Kenwood, Brandon M et al. 2014. “Identification of a Novel Mitochondrial Uncoupler That

Does Not Depolarize the Plasma Membrane." *Molecular Metabolism* 3(2): 114–23. https://www.sciencedirect.com/science/article/pii/S2212877813001233.

Keuper, Michaela et al. 2014. "Spare Mitochondrial Respiratory Capacity Permits Human Adipocytes to Maintain ATP Homeostasis under Hypoglycemic Conditions." *The FASEB Journal* 28(2): 761–70. https://doi.org/10.1096/fj.13-238725.

———. 2019. "Preadipocytes of Obese Humans Display Gender-Specific Bioenergetic Responses to Glucose and Insulin." *Molecular Metabolism* 20: 28–37. https://www.sciencedirect.com/science/article/pii/S2212877818310469.

Khuu, Ciera H, Roberto M Barrozo, Tsonwin Hai, and Steven L Weinstein. 2007. "Activating Transcription Factor 3 (ATF3) Represses the Expression of CCL4 in Murine Macrophages." *Molecular immunology* 44(7): 1598–1605.

Kieback, Elisa et al. 2008. "A Safeguard Eliminates T Cell Receptor Gene-Modified Autoreactive T Cells after Adoptive Transfer." *Proceedings of the National Academy of Sciences of the United States of America* 105(2): 623–28. https://pubmed.ncbi.nlm.nih.gov/18182487.

Kinzler, Kenneth W, and Bert Vogelstein. 1998. "Landscaping the Cancer Terrain." *Science* 280(5366): 1036 LP – 1037. http://science.sciencemag.org/content/280/5366/1036.abstract.

Kochenderfer, James N et al. 2012. "B-Cell Depletion and Remissions of Malignancy along with Cytokine-Associated Toxicity in a Clinical Trial of Anti-CD19 Chimeric-Antigen-Receptor–Transduced T Cells." *Blood* 119(12): 2709–20. https://doi.org/10.1182/blood-2011-10-384388.

Kolev, Martin et al. 2015. "Complement Regulates Nutrient Influx and Metabolic Reprogramming during Th1 Cell Responses." *Immunity* 42(6): 1033–47. https://doi.org/10.1016/j.immuni.2015.05.024.

Krasinskas, Alyssa M et al. 2013. "KRAS Mutant Allele-Specific Imbalance Is Associated with Worse Prognosis in Pancreatic Cancer and Progression to Undifferentiated Carcinoma of the Pancreas." *Modern Pathology* 26(10): 1346–54. https://doi.org/10.1038/modpathol.2013.71.

Krummel, M F, and J P Allison. 1995. "CD28 and CTLA-4 Have Opposing Effects on the Response of T Cells to Stimulation." *Journal of Experimental Medicine* 182(2): 459–65. https://doi.org/10.1084/jem.182.2.459.

Kubsch, Sebastian, Edith Graulich, Jürgen Knop, and Kerstin Steinbrink. 2003. "Suppressor Activity of Anergic T Cells Induced by IL-10-Treated Human Dendritic Cells: Association with IL-2- and CTLA-4-Dependent G1 Arrest of the Cell Cycle Regulated by P27Kip1." *European Journal of Immunology* 33(7): 1988–97. https://doi.org/10.1002/eji.200323600.

Kuwabara, Taku et al. 2021. "SATB1-Dependent Mitochondrial ROS Production Controls TCR

Signaling in CD4 T Cells." *Life Science Alliance* 4(11): e202101093. http://www.life-science-alliance.org/content/4/11/e202101093.abstract.

Ladisch S et al. 1987. "Shedding of GD2 Ganglioside by Human Neuroblastoma." (0020-7136 (Print)).

Lal, Neeraj et al. 2018. "KRAS Mutation and Consensus Molecular Subtypes 2 and 3 Are Independently Associated with Reduced Immune Infiltration and Reactivity in Colorectal Cancer." *Clinical cancer research : an official journal of the American Association for Cancer Research* 24(1): 224–33. https://pubmed.ncbi.nlm.nih.gov/29061646.

Lamba, Jatinder K et al. 2017. "CD33 Splicing Polymorphism Determines Gemtuzumab Ozogamicin Response in de Novo Acute Myeloid Leukemia: Report from Randomized Phase III Children's Oncology Group Trial AAML0531." *Journal of Clinical Oncology* 35(23): 2674.

Laszlo, George S, Elihu H Estey, and Roland B Walter. 2014. "The Past and Future of CD33 as Therapeutic Target in Acute Myeloid Leukemia." *Blood reviews* 28(4): 143–53.

Lederman, By Seth et al. 1992. "From the Departments of *Medicine and TPathology, Columbia University, New York, New York 10032." 175(April): 47–49.

Lee, James et al. 2003. "Translational Control of Inducible Nitric Oxide Synthase Expression by Arginine Can Explain the Arginine Paradox." (0027-8424 (Print)): 4843–48.

Lee, Kyung-Mi et al. 1998. "Molecular Basis of T Cell Inactivation by CTLA-4." *Science* 282(5397): 2263 LP – 2266. http://science.sciencemag.org/content/282/5397/2263.abstract.

Lengauer, Christoph, Kenneth W Kinzler, and Bert Vogelstein. 1998. "Genetic Instabilities in Human Cancers." *Nature* 396(6712): 643–49. https://doi.org/10.1038/25292.

Li, Yingrui et al. 2020. "DNT Cell-Based Immunotherapy: Progress and Applications." *Journal of Cancer* 11(13): 3717–24. https://www.jcancer.org/v11p3717.htm.

Liberzon, Arthur et al. 2015. "The Molecular Signatures Database Hallmark Gene Set Collection." *Cell Systems* 1(6): 417–25. https://doi.org/10.1016/j.cels.2015.12.004.

Lieu, Elizabeth L, Tu Nguyen, Shawn Rhyne, and Jiyeon Kim. 2020. "Amino Acids in Cancer." *Experimental & Molecular Medicine* 52(1): 15–30. https://doi.org/10.1038/s12276-020-0375-3.

Liew, Pei Xiong, and Paul Kubes. 2019. "The Neutrophil's Role during Health and Disease." *Physiological Reviews* 99(2): 1223–48.

Loeser, Heike et al. 2020. "Indoleamine 2,3-Dioxygenase (IDO) Expression Is an Independent Prognostic Marker in Esophageal Adenocarcinoma" ed. Ravirajsinh Jadeja. *Journal of Immunology Research* 2020: 2862647. https://doi.org/10.1155/2020/2862647.

Long, Adrienne H et al. 2015. "4-1BB Costimulation Ameliorates T Cell Exhaustion Induced by

Tonic Signaling of Chimeric Antigen Receptors." *Nature Medicine* 21(6): 581–90. https://doi.org/10.1038/nm.3838.

Louie, Maggie C et al. 2020. "Total Cellular ATP Production Changes With Primary Substrate in MCF7 Breast Cancer Cells ." *Frontiers in Oncology* 10. https://www.frontiersin.org/article/10.3389/fonc.2020.01703.

Louis, Chrystal U. et al. 2011. "Antitumor Activity and Long-Term Fate of Chimeric Antigen Receptor-Positive T Cells in Patients with Neuroblastoma." *Blood* 118(23): 6050–56.

Ludovini, Vienna et al. 2021. "High PD-L1/IDO-2 and PD-L2/IDO-1 Co-Expression Levels Are Associated with Worse Overall Survival in Resected Non-Small Cell Lung Cancer Patients." *Genes* 12(2).

Lunt, Sophia Y, and Matthew G Vander Heiden. 2011. "Aerobic Glycolysis: Meeting the Metabolic Requirements of Cell Proliferation." *Annual Review of Cell and Developmental Biology* 27(1): 441–64. https://doi.org/10.1146/annurev-cellbio-092910-154237.

Lynn, Rachel C et al. 2019. "C-Jun Overexpression in CAR T Cells Induces Exhaustion Resistance." *Nature* 576(7786): 293–300. https://doi.org/10.1038/s41586-019-1805-z.

Macián, Fernando, Sin-Hyeog Im, Francisco J García-Cózar, and Anjana Rao. 2004. "T-Cell Anergy." *Current Opinion in Immunology* 16(2): 209–16. http://www.sciencedirect.com/science/article/pii/S0952791504000160.

MacKay, Matthew et al. 2020. "The Therapeutic Landscape for Cells Engineered with Chimeric Antigen Receptors." *Nature Biotechnology* 38(2): 233–44. https://doi.org/10.1038/s41587-019-0329-2.

Magnani, Chiara F et al. 2020. "Sleeping Beauty–Engineered CAR T Cells Achieve Antileukemic Activity without Severe Toxicities." *The Journal of Clinical Investigation* 130(11): 6021–33. https://doi.org/10.1172/JCI138473.

Maher, John et al. 2002. "Human T-Lymphocyte Cytotoxicity and Proliferation Directed by a Single Chimeric TCRζ /CD28 Receptor." *Nature Biotechnology* 20(1): 70–75. https://doi.org/10.1038/nbt0102-70.

Maiese, W M et al. 1989. "Calicheamicins, a Novel Family of Antitumor Antibiotics: Taxonomy, Fermentation and Biological Properties." *The Journal of antibiotics* 42(4): 558–63.

Majzner, Robbie G et al. 2020. "Tuning the Antigen Density Requirement for CAR T-Cell Activity." *Cancer Discovery* 10(5): 702–23. https://doi.org/10.1158/2159-8290.CD-19-0945.

———. 2022. "GD2-CAR T Cell Therapy for H3K27M-Mutated Diffuse Midline Gliomas." *Nature* 603(7903): 934–41. https://doi.org/10.1038/s41586-022-04489-4.

Marchingo, Julia M, Linda V Sinclair, Andrew J M Howden, and Doreen A Cantrell. 2020. "Quantitative Analysis of How Myc Controls T Cell Proteomes and Metabolic Pathways

during T Cell Activation." *Elife* 9: e53725.

Marsh, Rebecca A et al. 2017. "Salvage Therapy for Refractory Hemophagocytic Lymphohistiocytosis: A Review of the Published Experience." *Pediatric Blood & Cancer* 64(4): e26308.

Martí i Líndez, Adrià Arnau et al. 2019. "Mitochondrial Arginase-2 Is a Cell-Autonomous Regulator of CD8+ T Cell Function and Antitumor Efficacy." *JCI Insight* 4(24).

Marusina, Alina I et al. 2017. "CD4+ Virtual Memory: Antigen-Inexperienced T Cells Reside in the Naïve, Regulatory, and Memory T Cell Compartments at Similar Frequencies, Implications for Autoimmunity." *Journal of Autoimmunity* 77: 76–88. http://www.sciencedirect.com/science/article/pii/S0896841116302414.

Marvel, Douglas, and Dmitry I Gabrilovich. 2015. "Myeloid-Derived Suppressor Cells in the Tumor Microenvironment: Expect the Unexpected." *The Journal of Clinical Investigation* 125(9): 3356–64. https://doi.org/10.1172/JCI80005.

Maude, Shannon L et al. 2014. "Chimeric Antigen Receptor T Cells for Sustained Remissions in Leukemia." *New England Journal of Medicine* 371(16): 1507–17. https://doi.org/10.1056/NEJMoa1407222.

McLane, Laura M, Mohamed S Abdel-Hakeem, and E John Wherry. 2019. "CD8 T Cell Exhaustion During Chronic Viral Infection and Cancer." *Annual Review of Immunology* 37(1): 457–95. https://doi.org/10.1146/annurev-immunol-041015-055318.

Mebius, Reina E, and Georg Kraal. 2005. "Structure and Function of the Spleen." *Nature Reviews Immunology* 5(8): 606–16. https://doi.org/10.1038/nri1669.

Medzhitov, Ruslan, and Charles A Janeway Jr. 2000. "How Does the Immune System Distinguish Self from Nonself?" *Seminars in Immunology* 12(3): 185–88. http://www.sciencedirect.com/science/article/pii/S1044532300902306.

Micalizzi, Douglas S, Susan M Farabaugh, and Heide L Ford. 2010. "Epithelial-Mesenchymal Transition in Cancer: Parallels Between Normal Development and Tumor Progression." *Journal of Mammary Gland Biology and Neoplasia* 15(2): 117–34. https://doi.org/10.1007/s10911-010-9178-9.

Michie, Colin A., Angela McLean, Christopher Alcock, and Peter C.L. Beverley. 1992. "Lifespan of Human Lymphocyte Subsets Defined by CD45 Isoforms." *Nature* 360(6401): 264–65.

Moek, K L, D J A de Groot, E G E de Vries, and R S N Fehrmann. 2017. "The Antibody–Drug Conjugate Target Landscape across a Broad Range of Tumour Types." *Annals of Oncology* 28(12): 3083–91. https://doi.org/10.1093/annonc/mdx541.

Mohammed, Somala et al. 2017. "Improving Chimeric Antigen Receptor-Modified T Cell Function by Reversing the Immunosuppressive Tumor Microenvironment of Pancreatic Cancer." *Molecular Therapy* 25(1): 249–58. https://doi.org/10.1016/j.ymthe.2016.10.016.

Mombaerts, Peter et al. 1992. “RAG-1-Deficient Mice Have No Mature B and T Lymphocytes.” *Cell* 68(5): 869–77. https://doi.org/10.1016/0092-8674(92)90030-G.

Munoz-Erazo, Luis, Janet L Rhodes, Valentine C Marion, and Roslyn A Kemp. 2020. “Tertiary Lymphoid Structures in Cancer – Considerations for Patient Prognosis.” *Cellular & Molecular Immunology* 17(6): 570–75. https://doi.org/10.1038/s41423-020-0457-0.

Murray, Peter J. 2016. “Amino Acid Auxotrophy as a System of Immunological Control Nodes.” *Nature immunology* 17(2): 132–39.

Mussai, Francis et al. 2013. “Acute Myeloid Leukemia Creates an Arginase-Dependent Immunosuppressive Microenvironment. PG - 749-58 LID - 10.1182/Blood-2013-01-480129 [Doi].” (1528-0020 (Electronic)).

———. 2015. “Neuroblastoma Arginase Activity Creates an Immunosuppressive Microenvironment That Impairs Autologous and Engineered Immunity.” *Cancer Research* 75(15): 3043 LP – 3053. http://cancerres.aacrjournals.org/content/75/15/3043.abstract.

Naing, A et al. 2019. “Phase I Study of the Arginase Inhibitor INCB001158 (1158) Alone and in Combination with Pembrolizumab (PEM) in Patients (Pts) with Advanced/Metastatic (Adv/Met) Solid Tumours.” *Annals of Oncology* 30: v160. https://www.sciencedirect.com/science/article/pii/S0923753419586628.

Nazha, Bassel, Cengiz Inal, and Taofeek K Owonikoko. 2020. “Disialoganglioside GD2 Expression in Solid Tumors and Role as a Target for Cancer Therapy.” *Frontiers in oncology* 10: 1000. https://pubmed.ncbi.nlm.nih.gov/32733795.

Nelson, Brad H. 2008. “The Impact of T-Cell Immunity on Ovarian Cancer Outcomes.” *Immunological Reviews* 222(1): 101–16. https://doi.org/10.1111/j.1600-065X.2008.00614.x.

Nizzoli, Giulia et al. 2013. “Human CD1c+ Dendritic Cells Secrete High Levels of IL-12 and Potently Prime Cytotoxic T-Cell Responses.” *Blood* 122(6): 932–42.

Otten, Henderikus G et al. 2003. “Preclinical Evaluation of Anti-CD86 Immunotoxin in Rhesus Monkeys: Analysis of Systemic Toxicity, Pharmacokinetics, and Effect on Primary T-Cell Responses.” *Cancer Immunology, Immunotherapy* 52(9): 569–75.

Oya, Yukiko, Yoku Hayakawa, and Kazuhiko Koike. 2020. “Tumor Microenvironment in Gastric Cancers.” *Cancer science* 111(8): 2696–2707. https://pubmed.ncbi.nlm.nih.gov/32519436.

Park, Jae H et al. 2018. “Long-Term Follow-up of CD19 CAR Therapy in Acute Lymphoblastic Leukemia.” *New England Journal of Medicine* 378(5): 449–59. https://doi.org/10.1056/NEJMoa1709919.

Paszkiewicz, Paulina J et al. 2016. “Targeted Antibody-Mediated Depletion of Murine CD19 CAR T Cells Permanently Reverses B Cell Aplasia.” *The Journal of clinical investigation* 126(11): 4262–72. https://pubmed.ncbi.nlm.nih.gov/27760047.

St. Paul, Michael, and Pamela S Ohashi. 2020. “The Roles of CD8⁺ T Cell Subsets in Antitumor Immunity.” *Trends in Cell Biology* 30(9): 695–704. https://doi.org/10.1016/j.tcb.2020.06.003.

Philip, Brian et al. 2014. “A Highly Compact Epitope-Based Marker/Suicide Gene for Easier and Safer T-Cell Therapy.” *Blood* 124(8): 1277–87. https://doi.org/10.1182/blood-2014-01-545020.

Pistoia, Vito et al. 2013. “Immunosuppressive Microenvironment in Neuroblastoma .” *Frontiers in Oncology* 3: 167. https://www.frontiersin.org/article/10.3389/fonc.2013.00167.

Plitzko, Birte, and Sandra Loesgen. 2018. “Measurement of Oxygen Consumption Rate (OCR) and Extracellular Acidification Rate (ECAR) in Culture Cells for Assessment of the Energy Metabolism.” *Bio-protocol* 8(10): e2850. https://doi.org/10.21769/BioProtoc.2850.

Poh, Alissa. 2018. “JCAR015 in ALL: A Root-Cause Investigation.” *Cancer Discovery* 8(1): 4 LP – 5. http://cancerdiscovery.aacrjournals.org/content/8/1/4.3.abstract.

Pucino, Valentina et al. 2019. “Lactate Buildup at the Site of Chronic Inflammation Promotes Disease by Inducing CD4+ T Cell Metabolic Rewiring.” *Cell metabolism* 30(6): 1055–74.

Pule, Martin A. et al. 2008. “Virus-Specific T Cells Engineered to Coexpress Tumor-Specific Receptors: Persistence and Antitumor Activity in Individuals with Neuroblastoma.” *Nature Medicine* 14(11): 1264–70.

Raber, Patrick, Augusto C Ochoa, and Paulo C Rodríguez. 2012. “Metabolism of L-Arginine by Myeloid-Derived Suppressor Cells in Cancer: Mechanisms of T Cell Suppression and Therapeutic Perspectives.” *Immunological Investigations* 41(6–7): 614–34. https://doi.org/10.3109/08820139.2012.680634.

Raje, Noopur et al. 2019. “Anti-BCMA CAR T-Cell Therapy Bb2121 in Relapsed or Refractory Multiple Myeloma.” *New England Journal of Medicine* 380(18): 1726–37. https://doi.org/10.1056/NEJMoa1817226.

Rapoport, Aaron P et al. 2015. “NY-ESO-1–Specific TCR–Engineered T Cells Mediate Sustained Antigen-Specific Antitumor Effects in Myeloma.” *Nature Medicine* 21(8): 914–21. https://doi.org/10.1038/nm.3910.

Ren, Jiangtao et al. 2017. “Multiplex Genome Editing to Generate Universal CAR T Cells Resistant to PD1 Inhibition.” *Clinical Cancer Research* 23(9): 2255–66. https://doi.org/10.1158/1078-0432.CCR-16-1300.

Renan, Michael J. 1993. “How Many Mutations Are Required for Tumorigenesis? Implications from Human Cancer Data.” *Molecular Carcinogenesis* 7(3): 139–46. https://doi.org/10.1002/mc.2940070303.

Rodriguez, Paulo C, David G Quiceno, and Augusto C Ochoa. 2006. “L-Arginine Availability Regulates T-Lymphocyte Cell-Cycle Progression.” *Blood* 109(4): 1568–73.

https://doi.org/10.1182/blood-2006-06-031856.

Rogatzki, Matthew J, Brian S Ferguson, Matthew L Goodwin, and L Bruce Gladden. 2015. "Lactate Is Always the End Product of Glycolysis ." *Frontiers in Neuroscience* 9: 22. https://www.frontiersin.org/article/10.3389/fnins.2015.00022.

Rossig, Claudia et al. 2002. "Epstein-Barr Virus–Specific Human T Lymphocytes Expressing Antitumor Chimeric T-Cell Receptors: Potential for Improved Immunotherapy." *Blood* 99(6): 2009–16. https://doi.org/10.1182/blood.V99.6.2009.

Rothenberg, Ellen V. 2019. "Programming for T-Lymphocyte Fates: Modularity and Mechanisms." *Genes and Development* 33(17–18): 1117–35.

Saeed, Sadia et al. 2014. "Epigenetic Programming of Monocyte-to-Macrophage Differentiation and Trained Innate Immunity." *Science* 345(6204): 1251086. http://science.sciencemag.org/content/345/6204/1251086.abstract.

Sallusto, Federica, Charles R Mackay, and Antonio Lanzavecchia. 1997. "Selective Expression of the Eotaxin Receptor CCR3 by Human T Helper 2 Cells." *Science* 277(5334): 2005 LP – 2007. http://science.sciencemag.org/content/277/5334/2005.abstract.

Sangaletti, S et al. 2021. "Myeloid Cell Heterogeneity in Lung Cancer: Implication for Immunotherapy." (1432-0851 (Electronic)).

Sansom, Stephen N. et al. 2014. "Population and Single-Cell Genomics Reveal the Aire Dependency, Relief from Polycomb Silencing, and Distribution of Self-Antigen Expression in Thymic Epithelia." *Genome Research* 24(12): 1918–31.

Santhanam, Lakshmi et al. 2007. "Inducible NO Synthase–Dependent S-Nitrosylation and Activation of Arginase1 Contribute to Age-Related Endothelial Dysfunction." *Circulation Research* 101(7): 692–702. https://doi.org/10.1161/CIRCRESAHA.107.157727.

De Santo, Carmela et al. 2018. "The Arginine Metabolome in Acute Lymphoblastic Leukemia Can Be Targeted by the Pegylated-Recombinant Arginase I BCT-100." *International Journal of Cancer* 142(7): 1490–1502.

Sarhan, Dhifaf et al. 2018. "161533 TriKE Stimulates NK-Cell Function to Overcome Myeloid-Derived Suppressor Cells in MDS." *Blood advances* 2(12): 1459–69.

Schambach, Axel et al. 2000. "Context Dependence of Different Modules for Posttranscriptional Enhancement of Gene Expression from Retroviral Vectors." *Molecular Therapy* 2(5): 435–45. https://doi.org/10.1006/mthe.2000.0191.

Schulz, Gregor et al. 1984. "Detection of Ganglioside GD2 in Tumor Tissues and Sera of Neuroblastoma Patients." *Cancer Research* 44(12 Part 1): 5914–20. https://cancerres.aacrjournals.org/content/44/12_Part_1/5914.

Schwartz, Ronald H. 2003. "T Cell Anergy." *Annual Review of Immunology* 21(1): 305–34. https://doi.org/10.1146/annurev.immunol.21.120601.141110.

Seo, Hyungseok et al. 2021. “BATF and IRF4 Cooperate to Counter Exhaustion in Tumor-Infiltrating CAR T Cells.” *Nature Immunology* 22(8): 983–95. https://doi.org/10.1038/s41590-021-00964-8.

Serafini, M et al. 2004. “Characterization of CD20-Transduced T Lymphocytes as an Alternative Suicide Gene Therapy Approach for the Treatment of Graft-Versus-Host Disease.” *Human Gene Therapy* 15(1): 63–76. https://doi.org/10.1089/10430340460732463.

Shankaran, Vijay et al. 2001. “IFNγ and Lymphocytes Prevent Primary Tumour Development and Shape Tumour Immunogenicity.” *Nature* 410(6832): 1107–11. https://doi.org/10.1038/35074122.

Shinkai, Yoichi et al. 1992. “RAG-2-Deficient Mice Lack Mature Lymphocytes Owing to Inability to Initiate V(D)J Rearrangement.” *Cell* 68(5): 855–67. https://doi.org/10.1016/0092-8674(92)90029-C.

Silva Morales, Milagros, and Daniel Mueller. 2018. “Anergy into T Regulatory Cells: An Integration of Metabolic Cues and Epigenetic Changes at the Foxp3 Conserved Non-Coding Sequence 2.” *F1000Research* 7: F1000 Faculty Rev-1938. https://pubmed.ncbi.nlm.nih.gov/30613389.

Song, De-Gang et al. 2012. “CD27 Costimulation Augments the Survival and Antitumor Activity of Redirected Human T Cells in Vivo.” *Blood* 119(3): 696–706. https://doi.org/10.1182/blood-2011-03-344275.

Spits, Hergen et al. 2013. “Innate Lymphoid Cells-a Proposal for Uniform Nomenclature.” *Nature Reviews Immunology* 13(2): 145–49.

Spitzer, Matthew H et al. 2017. “Systemic Immunity Is Required for Effective Cancer Immunotherapy.” *Cell* 168(3): 487-502.e15. https://doi.org/10.1016/j.cell.2016.12.022.

Stadtmauer, Edward et al. 2020. “CRISPR-Engineered T Cells in Patients with Refractory Cancer.” *Science* 367(6481): eaba7365. https://doi.org/10.1126/science.aba7365.

Starr, Timothy K, Stephen C Jameson, and Kristin A Hogquist. 2003. “Positive and Negative Selection of T Cells.” *Annual Review of Immunology* 21(1): 139–76. https://doi.org/10.1146/annurev.immunol.21.120601.141107.

Di Stasi, Antonio et al. 2011. “Inducible Apoptosis as a Safety Switch for Adoptive Cell Therapy.” *The New England journal of medicine* 365(18): 1673–83. https://pubmed.ncbi.nlm.nih.gov/22047558.

Steggerda, Susanne M. et al. 2017. “Inhibition of Arginase by CB-1158 Blocks Myeloid Cell-Mediated Immune Suppression in the Tumor Microenvironment.” *Journal for ImmunoTherapy of Cancer* 5(1): 1–18.

van Stipdonk, Marianne J B, Edward E Lemmens, and Stephen P Schoenberger. 2001. “Naïve CTLs Require a Single Brief Period of Antigenic Stimulation for Clonal Expansion and

Differentiation." *Nature Immunology* 2(5): 423–29. https://doi.org/10.1038/87730.

Strauss, Dirk C., and J. Meirion Thomas. 2010. "Transmission of Donor Melanoma by Organ Transplantation." *The Lancet Oncology* 11(8): 790–96. http://dx.doi.org/10.1016/S1470-2045(10)70024-3.

Sujjitjoon, Jatuporn et al. 2021. "GD2-Specific Chimeric Antigen Receptor-Modified T Cells Targeting Retinoblastoma – Assessing Tumor and T Cell Interaction." *Translational Oncology* 14(2): 100971. https://www.sciencedirect.com/science/article/pii/S1936523320304630.

Summers, Charlotte et al. 2010. "Neutrophil Kinetics in Health and Disease." *Trends in Immunology* 31(8): 318–24. http://dx.doi.org/10.1016/j.it.2010.05.006.

Tanyi, Janos L et al. 2015. "Abstract CT105: Safety and Feasibility of Chimeric Antigen Receptor Modified T Cells Directed against Mesothelin (CART-Meso) in Patients with Mesothelin Expressing Cancers." *Cancer Research* 75(15 Supplement): CT105 LP-CT105. http://cancerres.aacrjournals.org/content/75/15_Supplement/CT105.abstract.

Tauffenberger, Arnaud, Hubert Fiumelli, Salam Almustafa, and Pierre J Magistretti. 2019. "Lactate and Pyruvate Promote Oxidative Stress Resistance through Hormetic ROS Signaling." *Cell Death & Disease* 10(9): 653. https://doi.org/10.1038/s41419-019-1877-6.

Tay, Rong En, Emma K Richardson, and Han Chong Toh. 2021. "Revisiting the Role of CD4+ T Cells in Cancer Immunotherapy—New Insights into Old Paradigms." *Cancer Gene Therapy* 28(1): 5–17. https://doi.org/10.1038/s41417-020-0183-x.

Thiery, Jerome et al. 2011. "Perforin Pores in the Endosomal Membrane Trigger the Release of Endocytosed Granzyme B into the Cytosol of Target Cells." *Nature Immunology* 12(8): 770–77.

Thomas, Lewis. 1959. "Discussion of Cellular and Humoral Aspects of Hypersensitive Stress."

Thomas, Simon et al. 2016. "An Optimized GD2-Targeting Retroviral Cassette for More Potent and Safer Cellular Therapy of Neuroblastoma and Other Cancers." *PLOS ONE* 11(3): e0152196. https://doi.org/10.1371/journal.pone.0152196.

Tokarew, Nicholas et al. 2019. "Teaching an Old Dog New Tricks: Next-Generation CAR T Cells." *British Journal of Cancer* 120(1): 26–37. https://doi.org/10.1038/s41416-018-0325-1.

Tumino, Nicola et al. 2021. "Polymorphonuclear Myeloid-Derived Suppressor Cells Impair the Anti-Tumor Efficacy of GD2.CAR T-Cells in Patients with Neuroblastoma." *Journal of Hematology & Oncology* 14(1): 191. https://doi.org/10.1186/s13045-021-01193-0.

Urruticoechea, A et al. 2010. "Recent Advances in Cancer." *Current Pharmaceutical Design* 16(7): 3–10.

Veglia, F, E Sanseviero, and Dmitry I Gabrilovich. 2021. "Myeloid-Derived Suppressor Cells in

the Era of Increasing Myeloid Cell Diversity. PG - 485-498 LID - 10.1038/S41577-020-00490-y [Doi].” (1474-1741 (Electronic)).

Veglia, Filippo, Emilio Sanseviero, and Dmitry I Gabrilovich. 2021. “Myeloid-Derived Suppressor Cells in the Era of Increasing Myeloid Cell Diversity.” *Nature Reviews Immunology* 21(8): 485–98. https://doi.org/10.1038/s41577-020-00490-y.

Van de Velde, Lee-Ann et al. 2017. “T Cells Encountering Myeloid Cells Programmed for Amino Acid-Dependent Immunosuppression Use Rictor/MTORC2 Protein for Proliferative Checkpoint Decisions *.” *Journal of Biological Chemistry* 292(1): 15–30. https://doi.org/10.1074/jbc.M116.766238.

Vella, A T et al. 1998. “Cytokine-Induced Survival of Activated T Cells in Vitro and in Vivo.” *Proceedings of the National Academy of Sciences of the United States of America* 95(7): 3810–15. https://pubmed.ncbi.nlm.nih.gov/9520449.

Venanzi, Emily S, Christophe Benoist, and Diane Mathis. 2004. “Good Riddance: Thymocyte Clonal Deletion Prevents Autoimmunity.” *Current Opinion in Immunology* 16(2): 197–202. http://www.sciencedirect.com/science/article/pii/S0952791504000111.

Verhagen, Johan et al. 2009. “Enhanced Selection of FoxP3+ T-Regulatory Cells Protects CTLA-4-Deficient Mice from CNS Autoimmune Disease.” *Proceedings of the National Academy of Sciences* 106(9): 3306–11.

Villegas, Francisco R et al. 2002. “Prognostic Significance of Tumor Infiltrating Natural Killer Cells Subset CD57 in Patients with Squamous Cell Lung Cancer.” *Lung Cancer* 35(1): 23–28. http://www.sciencedirect.com/science/article/pii/S0169500201002926.

Vitanza, Nicholas A et al. 2021. “Locoregional Infusion of HER2-Specific CAR T Cells in Children and Young Adults with Recurrent or Refractory CNS Tumors: An Interim Analysis.” *Nature Medicine* 27(9): 1544–52. https://doi.org/10.1038/s41591-021-01404-8.

Walker, Alec J et al. 2017. “Tumor Antigen and Receptor Densities Regulate Efficacy of a Chimeric Antigen Receptor Targeting Anaplastic Lymphoma Kinase.” *Molecular Therapy* 25(9): 2189–2201. https://doi.org/10.1016/j.ymthe.2017.06.008.

Wang, Ruoning et al. 2011. “The Transcription Factor Myc Controls Metabolic Reprogramming upon T Lymphocyte Activation.” *Immunity* 35(6): 871–82.

Watanabe, Keisuke, Shunichiro Kuramitsu, Avery D Posey, and Carl H June. 2018. “Expanding the Therapeutic Window for CAR T Cell Therapy in Solid Tumors: The Knowns and Unknowns of CAR T Cell Biology .” *Frontiers in Immunology* 9. https://www.frontiersin.org/article/10.3389/fimmu.2018.02486.

Waterhouse, Paul et al. 1995. “Lymphoproliferative Disorders with Early Lethality in Mice Deficient in <Em>Ctla-4</Em>” *Science* 270(5238): 985 LP – 988. http://science.sciencemag.org/content/270/5238/985.abstract.

Welters, Marij J et al. 2016. “Vaccination during Myeloid Cell Depletion by Cancer

Chemotherapy Fosters Robust T Cell Responses." *Science translational medicine* 8(334): 334ra52-334ra52.

Wilk, Aaron J., and Catherine A. Blish. 2018. "Diversification of Human NK Cells: Lessons from Deep Profiling." *Journal of Leukocyte Biology* 103(4): 629–41.

van der Windt, Gerritje J W et al. 2012. "Mitochondrial Respiratory Capacity Is a Critical Regulator of CD8+ T Cell Memory Development." *Immunity* 36(1): 68–78.

World Health Organization. 2020. "WHO Outlines Steps to Save 7 Million Lives from Cancer." (February): 7–8. https://www.who.int/news-room/detail/04-02-2020-who-outlines-steps-to-save-7-million-lives-from-cancer.

Wu, Guoyao, and Sidney M Morris. 1998. "Arginine Metabolism: Nitric Oxide and Beyond." *Biochemical Journal* 336(1): 1–17. https://doi.org/10.1042/bj3360001.

Wu, Hao et al. 2021. "Lactate Dehydrogenases Amplify Reactive Oxygen Species in Cancer Cells in Response to Oxidative Stimuli." *Signal Transduction and Targeted Therapy* 6(1): 242. https://doi.org/10.1038/s41392-021-00595-3.

Xu, Xin et al. 2019. "NKT Cells Coexpressing a GD2-Specific Chimeric Antigen Receptor and IL15 Show Enhanced In Vivo Persistence and Antitumor Activity against Neuroblastoma." *Clinical Cancer Research* 25(23): 7126–38. https://doi.org/10.1158/1078-0432.CCR-19-0421.

Yoda, Hiroyuki et al. 2019. "Direct Targeting of MYCN Gene Amplification by Site-Specific DNA Alkylation in Neuroblastoma." *Cancer Research* 79(4): 830–40. https://doi.org/10.1158/0008-5472.CAN-18-1198.

Yoneshiro, Takeshi et al. 2019. "BCAA Catabolism in Brown Fat Controls Energy Homeostasis through SLC25A44." *Nature* 572(7771): 614–19.

Zea, Arnold H. et al. 2004. "L-Arginine Modulates CD3ζ Expression and T Cell Function in Activated Human T Lymphocytes." *Cellular Immunology* 232(1–2): 21–31.

Zhan, Hong et al. 2013. "Production and First-in-Man Use of T Cells Engineered to Express a HSVTK-CD34 Sort-Suicide Gene." *PLOS ONE* 8(10): e77106. https://doi.org/10.1371/journal.pone.0077106.

Zhang, Di et al. 2019. "Metabolic Regulation of Gene Expression by Histone Lactylation." *Nature* 574(7779): 575–80. https://doi.org/10.1038/s41586-019-1678-1.

Zhao, Ende et al. 2013. "Chapter 10 - Th17 Cells in Cancer." In eds. George C Prendergast and Elizabeth M B T - Cancer Immunotherapy (Second Edition) Jaffee. San Diego: Academic Press, 129–47. https://www.sciencedirect.com/science/article/pii/B9780123942968000105.

8. APPENDIX

8.1 Fultang, Panetti et al., 2019 Full Paper

EBioMedicine 47 (2019) 235–246

Contents lists available at ScienceDirect

EBioMedicine

journal homepage: www.ebiomedicine.com

EBioMedicine
Published by THE LANCET

Research paper

MDSC targeting with Gemtuzumab ozogamicin restores T cell immunity and immunotherapy against cancers

Livingstone Fultang [a,1], Silvia Panetti [a,1], Margaret Ng [b], Paul Collins [a], Suzanne Graef [a], Nagy Rizkalla [a], Sarah Booth [a], Richard Lenton [a], Boris Noyvert [c], Claire Shannon-Lowe [a], Gary Middleton [a], Francis Mussai [a,*,2], Carmela De Santo [a,2]

[a] Institute of Immunology and Immunotherapy, University of Birmingham, Birmingham, UK
[b] Department of Anatomic Pathology, The Chinese University of Hong Kong, Hong Kong
[c] CRUK Birmingham Centre and Centre for Computational Biology, Institute of Cancer and Genomic Sciences, University of Birmingham, Birmingham, UK

ARTICLE INFO

Article history:
Received 4 June 2019
Received in revised form 8 August 2019
Accepted 12 August 2019
Available online 25 August 2019

Keywords:
MDSC
Gemtuzumab
CD33
Cancer
CAR-T

ABSTRACT

Background: Targeting of MDSCs is a major clinical challenge in the era of immunotherapy. Antibodies which de plete MDSCs in murine models can reactivate T cell responses. In humans such approaches have not developed due to difficulties in identifying targets amenable to clinical translation.

Methods: RNA sequencing of M MDSCs and G MDSCs from cancer patients was undertaken. Flow cytometry and immunohistochemistry of blood and tumours determined MDSC CD33 expression. MDSCs were treated with Gemtuzumab ozogamicin and internalisation kinetics, and cell death mechanisms determined by flow cytome try, confocal microscopy and electron microscopy. Effects on T cell proliferation and CAR T cell anti tumour cy totoxicity were identified in the presence of Gemtuzumab ozogamicin.

Findings: RNA sequencing of human M MDSCs and G MDSCs identified transcriptomic differences, but that CD33 is a common surface marker. Flow cytometry indicated CD33 expression is higher on M MDSCs, and CD33+ MDSCs are found in the blood and tumours regardless of cancer subtype. Treatment of human MDSCs leads to Gemtuzumab ozogamicin internalisation, increased p ATM, and cell death; restoring T cell proliferation. Anti GD2 /mesothelin /EGFRvIII CAR T cell activity is enhanced in combination with the anti MDSC effects of Gemtuzumab ozogamicin.

Interpretation: The study identifies that M MDSCs and G MDSCs are transcriptomically different but CD33 is a therapeutic target on peripheral and infiltrating MDSCs across cancer subtypes. The immunotoxin Gemtuzumab ozogamicin can deplete MDSCs providing a translational approach to reactivate T cell and CAR T cell responses against multiple cancers. In the rare conditions of HLH/MAS gemtuzumab ozogamicin provides a novel anti myeloid strategy.

Fund: This work was supported by Cancer Research UK, CCLG, Treating Children with Cancer, and the alumni and donors to the University of Birmingham.

1. Introduction

Cancer cells exist within an immune microenvironment, containing populations of cells which can coordinate and target the cancer or in contrast be subverted to promote cancer growth and survival [1]. Approaches to boost autologous T cell activity or engineer T cell immu notherapies have seen some dramatic clinical responses [2]. However in solid cancer and non B cell haematological malignancy trials clinical re sponses are disappointing, with poor Chimeric Antigen Receptor T cell (CAR T) expansion and persistence short lived [3 5]. The failure is mainly due to an immunosuppressive microenvironment mainly cre ated by Myeloid Derived Suppressor Cells (MDSCs) in the tumours and blood of patients [6,7]. MDSCs may suppress T cell activity through diverse mechanisms including expression of immune checkpoint sur face molecules, release of nitric oxide or reactive oxide species, produc tion of immunomodulatory cytokines, or the consumption of amino acids [6 9]. Myeloid cells also play critical roles in driving other dis eases. Haemophagocytic Lymphohistiocytosis (HLH) and Macrophage Activation Syndrome (MAS) are a spectrum of rare conditions which may be familial or secondary to cancer, infection, or autoimmunity.

* Corresponding author at: Institute of Immunology and Immunotherapy, University of Birmingham, Birmingham B15 2TT, United Kingdom.
E-mail address: [redacted] (F. Mussai).
[1] These authors contributed equally as first authors.
[2] These authors contributed equally as senior authors.

https://doi.org/10.1016/j.ebiom.2019.08.025

Research in Context

Evidence before this study

Depletion of Myeloid Derived Suppressor Cells (MDSCs), with un conjugated antibodies, in murine cancer models suggests that T cell responses can be reactivated against cancer. In humans, small molecule inhibitors which modulate MDSC intracellular sup pressive mechanisms, have been trialled but have not shown the capacity to deplete MDSCs and restore T cell responses consis tently across cancer groups.

Added value of this study

We identified that although human M MDSCs and G MDSCs are transcriptomically distinct, CD33 expression provides a surface target for both circulating and intra tumoural MDSCs across can cer subtypes. Targeting of MDSCs with the anti CD33 immunotoxin Gemtuzumab ozogamicin leads to immunotoxin internalisation, increased p ATM, and MDSC cell death. The result is restoration of T cell proliferation and enhanced CAR T cell prolif eration and cytotoxicity against solid cancer targets.

Implications of all the available evidence

Our study suggests that Gemtuzumab ozogamicin provides the clinically relevant approach to deplete MDSCs in cancer patients, or pathological myeloid cells in HLH/MAS, and could overcome im munosuppressive microenvironments to reactivate T cell immuno therapy. These findings will be translated into a Phase II clinical trial (GOTHAM).

They result in cytopenias, T cell activation, Natural Killer cell dysfunc tion and severe, life threatening systemic inflammation marked by fever, high ferritin and hypertriglcyeridemia [10,11]. Expansions of my eloid cells which secrete pro inflammatory factors such as IL 6, Il 18, and Il 1β is central to the underlying pathology, yet to date no therapies have directly targeted these cells contributing to a high mortality [12].

In murine models monocytic MDSCs can be readily defined by their expression of surface antigens such as Ly6C or CCR2 [13]. Administra tion of targeted antibodies that specifically deplete murine MDSCs, re sults in reactivation of anti cancer T cell responses and tumour resolution proof of principle that antibody targeting of these cells can have a dramatic and helpful effect on immunity [14]. Although markers for human MDSCs have been identified, such as CD10 or LOX1, expression is subtype specific and clinical agents against these molecules are not well developed [15,16]. Furthermore clinical ap proaches to remove human MDSCs have been limited by complexities of MDSC characterisation, poor correlation between murine models and patients, and their ability to suppress T cells through multiple mechanisms [17]. One of the most clinically successful methods for se lective cell depletion is the use of immunotoxins antibody toxin con jugates which induce cell specific death [18]. Here we investigate potential clinically relevant targets for depleting MDSCs to reactivate T cell immunity.

2. Methods

2.1. Patient samples

Heparinized blood samples were obtained from adult patients with cancers of the lung ($n = 21$), pancreas ($n = 7$), colon ($n = 36$), brain (n = 7), head and neck ($n = 8$), prostate ($n = 10$), breast ($n = 12$), melanoma ($n = 5$) and paediatric patients with Wilms' (n = 5), neuro blastoma ($n = 31$), Ewing's ($n = 2$), non Hodgkin's lymphoma (n = 2), rhabdomyosarcoma (n = 2) at diagnosis, prior to treatment. Blood from healthy donors ($n = 41$) was obtained at the University of Birmingham, UK. Healthy leukocyte cones were provided by the NHSBT Blood Bank (Birmingham, UK).

2.2. Study approvals

In accordance with the Declaration of Helsinki, patient samples were obtained after written, informed consent prior to inclusion in the study. Adult patient samples were collected through the University of Birmingham's Human Biomaterials Resource Centre (HBRC, Birming ham, UK). HBRC is licensed by the Human Tissue Authority to collect process and store project independent human samples for biomedical research. Samples collected by HBRC are released under Research Tissue Bank ethical approval by the North West Research Ethics Committee, Haydock Park (Ref 15/NW/0079). Samples from Birmingham Children's Hospital were collected following Regional Ethics Committee (REC Number 10/H0501/39) approval.

2.3. Flow cytometric analysis of whole blood

All samples were processed within 12 h from collection. Whole blood was lysed prior to staining using the RBC Lysis solution (Qiagen, Germany) according to manufacturer's specification. Immune popula tions were identified by staining with fluorophore conjugated anti CD11b, anti CD33, anti CD3, anti HLA DR, anti CD45, anti CD68, anti CD206, anti CD163, (BioLegend), anti CD14, anti CD15 (eBioscience) antibodies on ice for 30 min. Fluorescence data was acquired using BD Accuri C6 (BD Biosciences), Cyan and/or CytoFLEX (Beckman Coulter) cytometers. Normalised population statistics including the median fluorescence intensities (MFI) were determined using FlowJo (BD Bio sciences, formerly developed by FlowJo LLC).

Where indicated cell death was assessed by propidium iodide stain ing of cells after 72 h incubation with Gemtuzumab ozogamicin (Gift from Pfizer).

2.4. Myeloid cell and lymphocyte isolation

Where indicated myeloid cells were isolated from peripheral blood using a Lymphoprep gradient (STEMCELL Technologies) and enriched from the white cell layer by positive magnetic assisted cell sorting (MACS) using anti human CD14 Microbeads (Miltenyi Biotech) and MACS LS separation columns (Miltenyi Biotech). T lymphocytes were obtained by negative selection after removal of myeloid cells. Cell purities of each distinct population of >98% was confirmed after isola tion by flow cytometry using fluorophore conjugated anti CD14 or anti CD3 antibodies.

2.5. RNA sequencing

MDSCs were isolated from the peripheral blood of prostate, lung, head and neck, breast, and melanoma cancer patients at diagnosis ($n = 3$ per cancer) according to consensus guidelines using flow cytom etry immunophenotyping and T cell proliferation assays as above [13]. RNA was derived from the MACS bead sorted CD14+ M MDSCs and CD15+ G MDSCs from cancer patients at diagnosis. Purity was checked by flow cytometry. Samples were prepared with the Illumina TruSeq RNA Sample Preparation Kit v2. They were sequenced on the Illumina HiSeq2000 platform using TruSeq v3 chemistry, over 76 cycles. Sequencing reads were aligned to GRCh37 human genome using STAR RNA Seq aligner software [19]. Reads mapping to transcripts were counted by the same software. Normalisation of read counts and differ ential expression analysis comparing M MDSCs and G MDSCs was performed using DESeq2 R Bioconductor package [20].

2.6. Immunohistochemistry and scoring

A tissue micro arrays (TMA) of 200 human tumours ($n = 40$ cases each of non small cell lung carcinoma, prostate adenocarcinoma, breast invasive ductal carcinoma, colon adenocarcinoma, and pancreas duct adenocarcinoma) and normal control tissues (US Biomax) were deparaffinised and rehydrated following quality control to confirm di agnosis and antigen preservation. Tumours were stained on a Ventana Discovery Ultra automated system, according to manufacturer's proto col. Heat induced antigen retrieval was performed with cell condition ing 1 buffer (CC1), pH 8.5 (Ventana). Protein blocking was applied with Background Sniper (Biocare Medical, Concord, CA). Staining with anti human CD33 (Abcam) was performed at 37 °C, followed by the ad dition of secondary antibodies (Discovery anti Rabbit HQ) using the Novolink Polymer Detection System (RE7280 K, Leica). Primary anti body incubation were carried out overnight at 4 °C and tissue sections were counterstained with haematoxylin and mounted in DPX (VWR). To assess nonspecific staining, samples were similarly treated but the primary antibodies omitted and replaced with isotype specific IgG (Vec tor Labs Peterborough UK).

Paraffin embedded tissue sections of bone marrow trephines from 8 cancer associated HLH patients at diagnosis were deparaffinised and rehydrated. Antigen retrieval was performed in 50 mM Tris/2 mM EDTA pH 9.0 using a Philips Whirlpool Sixth Sense microwave on a steaming program. Staining with anti human CD33 (Abcam) was per formed using the Novolink Polymer Detection System (RE7280 K, Leica). Primary antibody incubation was performed overnight in a cold room. Sections were counterstained with Gill Nr 3 haematoxylin (Sigma Aldrich) and mounted in Aquatex (Merck).

Antigen expression in immunohistochemistry sections were assigned independently by experienced pathologists. Briefly, to evalu ate the immunostaining intensity in the tumour and bone marrow stroma each slide was examined on an Olympus BX51 microscope. Representative 400× magnification fields of at least 100 tumour cells were selected and photographed with an Olympus DP70 camera and ac companying image software. Fields were assigned an antigen staining intensity score of 0 = negative, + = weak, ++ = moderate, +++ = strong.

2.7. Gemtuzumab ozogamicin

MDSCs were seeded in complete medium at a density of 1×10^6 cells/well of a 12 well plate. Unless otherwise stated, Gemtuzumab Ozogamicin (GO, Pfizer) was added at a concentration of 1 μg/ml and in cubated for 48 h at 37 °C and 5% CO2. Analysis of cell death was moni tored via propidium iodide (PI) (Sigma) uptake quantified on the CyTOFLEX flow cytometer. The cytotoxicity of unconjugated gemtuzumab antibody (Absolute Antibody) (2 μg/ml) and gemtuzumab ozogamicin (2 μg/ml) was similarly compared. For drug internalisation assays, GO was covalently labelled to AlexaFluor 647 fluorophore, with the Alexa Fluor Protein Labeling Kit (Life Technologies, Carlsbad, USA) as per the manufacturer's instructions. 1 μg/ml of labelled GO was added to cells and incubated on ice for 30 min to allow binding to the CD33 receptor, then at 37 °C at different time points for internalisation. Membrane bound non internalised drug was stripped using stripping buffer (0.2 M Glycine HCl, pH 2.2) and the cells analysed by flow cytometry. The MFIs of AlexaFluor 647 was determined using FlowJo (BD Biosciences, formerly developed by FlowJo LLC).

2.8. T lymphocyte proliferation assay

2×10 [5]/well of T cells were cultured in 96 well flat bottom plates coated with anti CD3 (OKT3) antibody (3 μg/mL) and anti CD28 anti body (2 μg/mL) (both eBioscience), in 200 μL R10% supplemented with 0.1% β mercaptoethanol (Thermo Fisher Scientific). Cells were for 4 days incubated at 37 °C, 5% CO_2 and their proliferation determined by ^{3}H thymidine (Perkin Elmer Life Sciences) incorporation assay using a TopCount NXT Scintillation Counter (Perkin Elmer). The suppressive ability of GO treated or untreated MDSCs was determined by direct co culture with T cells. The data is expressed as a percentage of T cell proliferation driven by antibody stimulation in the presence of MDSCs relative to T cell proliferation in their absence (100%).

2.9. ELISA

The concentrations of cytokines within the patient's plasmas at diag nosis, were quantified using a competitive enzyme linked immunoas say according to the manufacturers' instructions. The following molecules were tested: G CSF, TGFβ, VEGF (all R&D Systems), IL 10, IL 4, IL 13, IL 6, IL 15, GM CSF (all BioLegend).

2.10. Transmission electron microscopy

GO treated, patient derived MDSCs were pelleted at a density of 1.5 $\times 10^6$ cells/tube, fixed in 2.5% glutaraldehyde and stained with 1% os mium tetroxide. The samples were dehydrated using ethanol and fixed in a mixture of propylene oxide and resin at 60 °C for 16 h. Sections of 80 nm thick resin and sample were then taken and embedded onto copper slot grids for visualization under transmission electron micros copy (TEM).

2.11. Cell lines

Ewing sarcoma cell line (SKNMC), neuroblastoma cell lines (SKNAS, KELLY, IMR 32 and LAN 1) and mesothelin positive lung cancer cell line (H1299M) were routinely cultured in RPMI 1640 medium. Colorectal cell lines (Caco 2, SW480), caecal adenocarcinoma cell line (SNUC5), the pancreatic carcinoma cell line of ductal cell origin (PANC1) were cultured in DMEM (Sigma). All cell line media was supplemented with 10% *v*/v fetal bovine serum (FBS, Sigma), 100 U/mL penicillin and strep tomycin (Gibco), 1 mmol/l sodium pyruvate (Gibco), and 2 mmol/l L glutamine (Gibco). Cell lines were originally obtained from ATCC and validated for authenticity by DNA short tandem repeats in line with American National Standards Institute ASN 0002 2011 (Northgene). Culture supernatants were harvested 72 h later from culture flask main tained in an incubator at 5% CO_2 in air and at 37 °C. To generate tumour polarised MDSCs, healthy $CD14^+$ cells from leukocyte cones were cul tured for 48 h in tumour conditioned supernatant as previously described [7].

2.12. Immunofluorescence

MDSCs were seeded unto sterile No.1 (13 mm diameter) glass coverslip inserts (VWR) at 1×10^4 per well of a 24 well plate and main tained overnight at routine culture or experimental conditions. Cells were stained with anti CD33 PE, washed in ice cold PBS, fixed in 2% Paraformaldehyde for 20 min at RTP followed by permeabilisation in 0.1% Triton X for 10 min. After permeabilisation coverslips were blocked in a blocking buffer consisting of 5% heat inactivated goat serum (HiNGS) in PBS for 1 h at RTP. Coverslips were then incubated for 1 h with an eFluor 660 conjugated anti human Phospho ATM (Ser1981) an tibody (Clone 10H11.E12 3G5, eBiosciences) diluted 1:100 in 5% HiNGS/ PBS. The coverslips were washed air dried, then mounted in SlowFade gold antifade mountant with DAPI (ThermoFisher Scientific). Cells were examined by fluorescence microscopy using a Zeiss LSM 780 fluo rescence confocal microscope and images acquired using ZEN software suite (Carl Zeiss Microscopy).

2.13. CAR T cell functional assays

T cells were engineered to express chimeric antigen receptors (CAR) for Mesothelin, GD2 and EFGRvIII based on established protocols

[21,22]. T cells from leukocyte cones were transduced with anti Mesothelin, anti EGFRvIII and anti GD2 CAR containing retroviruses 48 h post stimulation with anti CD3/CD28. Successfully transduced T cells were FACS sorted exploiting the truncated CD34 tag added to the construct and purity was checked by flow cytometry.

Tumour cell expression of target antigens was confirmed by flow cytometry using antibodies against mesothelin (Santa Cruz) and GD2 (Biolegend). For EGFRvIII, glioma cells were first dissociated from fresh human tumours within 24 h of surgery. RT PCR was used to detect EGFRvIII expression. RNA was extracted using an RNeasy Mini kit (Qiagen). cDNA was prepared using SuperScriptTM III Reverse Transcriptase (Invitrogen) following the manufacturer's instructions. The PCRproducts were analysed by gel electrophoresis on a 2% agarose gel and were visualised by staining with ethidium bromide. The primer sequences are as follows: Primer 1 (Forward: 5′ ATGCGACCCTCCGGGACG 3′ Reverse: 5′ ATTCCGTTACACACTTTGCGGC 3′) and Primer 2 (Forward: 5′ GAGCTCTTCGGGGAGCAG 3′ Reverse: 5′ GTGATCTGTCACCACATAATTACCTTTTCT 3′) [23,24].

For the chromium assays, CAR T cells were incubated with antigen positive tumour cells and antigen negative controls, at 100:1, 33:1, 11:1, and 3:1 ratios in a 4 h ^{51}Cr release assay [22]. CAR T cells were subsequently co cultured with CFSE labelled target bearing cells (i.e. anti Mesothelin with H1299M, anti EGFRvIII with tumour cells isolated from glioma brain tumours, anti GD2 with LAN 1), in presence of GO treated or untreated MDSCs. Viability and number of tumour and CAR T cells were investigated by flow cytometry using PI staining.

2.14. Statistical analysis

Parametric student *t* tests were used to determine the statistical significance of the difference in paired observations between groups (GraphPad Prism, USA). All *p* values are two tailed and p values <.05 were considered to represent statistically significant events.

3. Results

To identify a MDSC surface target amenable for immunotoxin targeting CD14+ monocytic (M MDSC) and CD15+ granulocytic (G MDSC) MDSCs were isolated by immunophenotype and suppressive ability, according to consensus guidelines, from patients with different cancers (Fig. 1A and B) [13]. Generation of a RNA sequencing library, to identify potential drug targets, revealed significant differences in the transcriptomic profiles of M MDSCs and G MDSCs (Fig. 1C and D). Analysis of the top 300 differentially expressed genes identified 3 potential targets for existing immunotoxins CD74 [25], CD86 [26], and CD33 [27]. Of these, CD33 is the only one which clinically advanced in human trials. CD33 is a transmembrane Sialic Acid Binding immunoglobulin like lectin (SIGLEC) composed of a type 1 membrane protein with two immunoglobulin domains that binds sialic acid and intracellular immunoreceptor tyrosine based inhibitory motifs (ITIMs) [28]. Knockout of the murine CD33 ortholog has no phenotype or role in defining murine MDSC populations [29]. Human CD33 on Acute Myeloid Leukaemia blasts has been successfully targeted by Gemtuzumab ozogamicin (GO), an anti CD33 humanized antibody conjugated to calicheamicin in Phase III clinical trials [27]. We hypothesised that human MDSC CD33 could similarly be targeted, as a strategy across cancer subtypes.

Examination of 200 patient samples revealed significant infiltrations of CD33+ myeloid cells in the tumour stroma compared to healthy tissues (Fig. 2A,B and Supp 1A,B). More rarely abnormal expansion and activation of myeloid cells can lead to a severe and life threatening systemic inflammation Haemophagocytic Lympho Histiocytosis (HLH) or a Macrophage Activation Syndrome (MAS). In these rare patients we also identified a high frequency of CD33+ cells in bone marrow staining (Fig. 2C, Supp Fig. 2). The majority of cancer or HLH samples had high intensity of CD33 positivity (Fig. 3A and B). In the blood, CD33 intensity was greater on the M MDSCs compared G MDSCs (Fig. 3C) and this population is expanded compared to healthy controls (Fig. 3D). Culture of sorted CD33+ MDSCs confirmed their ability to suppress T cell proliferation (Fig. 3E), consistent with a reduction in peripheral T cells observed in patients at diagnosis (Supp Fig. 3A). Notably CD33+ cells sorted from the blood of healthy donors were not immunosuppressive. Thus CD33 is expressed on the MDSCs pathologically expanded in the blood and tumour tissues of adults and children with cancer and which create an immunosuppressive microenvironment.

Incubation of CD33+ MDSCs from cancer patients with ALEXA647 labelled GO confirmed binding predominantly to the M MDSC population (Supp Fig. 3B), and rapid immunotoxin internalisation (Fig. 4A and Supp Fig. 3C). Although the unconjugated gemtuzumab antibody had minimal effect on survival (Supp Fig. 3D), Gemtuzumab ozogamicin induced a dose dependent decrease in viability (Fig. 4B, C, Sup Fig. 3D and 4A) of M MDSCs from patients' PBMCs or tumour polarised CD33+ myeloid cells (Fig. 4D), with no effect on CD33 cells. Suppressive tumour polarised CD33+ cells (Supp Fig. 4C) down regulated HLA DR and upregulated CD68 consistent with a M1 like phenotype (Supp Fig. 4D). GO treatment leads to increased pATM (Fig. 4E, Supp Fig. 5A) consistent with calicheamicin induced DNA damage [30]. Electron microscopy revealed a loss of cell membrane integrity, nuclear condensation, and blebbing marking apoptotic cell death (Fig. 4F and Supp Fig. 5B).

Treatment of circulating or tumour polarised MDSCs, with GO, restores T cell proliferation (Fig. 5A). The finding has potential clinical importance for CAR T therapies against solid tumours, where CAR T cell numbers in the blood and tumours fall rapidly post infusion, despite the presence of target antigens. We hypothesised that circulating immunosuppressive cytokines from tumours could limit CAR T expansion and anti tumour activity. However with the exception of TGF β [31], we found no consistent significant increases in IL 10, IL 4, Il 13, Il 6, GM CSF, G CSF, or VEGF in the blood that could account for the failure across cancer patients (Supp Fig. 6A F). Instead systemic and intra tumoural MDSCs may play a more prevalent pan tumour inhibitory role [32]. CAR T cells against 3 of the most common antigen targets were generated (Supp Fig. 6G) Mesothelin, GD2 and EGFRvIII (Supp Fig. 7A, B,C). Antigen specificity of CAR T cell killing against corresponding tumour cell targets was first confirmed (Supp Fig. 7D,E,F). Mimicking patients' findings, MDSCs suppressed CAR T cell proliferation, irrespective of the scFv, but this was overcome by GO treatment(Fig. 5B,C). MDSCs also impaired CAR T cell cytotoxicity. However GO killing of MDSCs improved the effectiveness of each CAR T construct, leading to a further significant reduction in viable mesothelioma and, neuroblastoma cells (Fig. 5D,E). Thus GO can kill MDSCs, overcome the immunosuppressive microenvironment, and provide a therapeutic boost to CAR T cell activity (Fig. 6).

4. Discussion

The resurgence in T cell immunotherapy approaches for adult and paediatric cancers has highlighted the need for clinically relevant strategies against the underlying immunosuppressive microenvironment. One of the major mechanisms of tumour immune escape, is through the expansion of immunosuppressive MDSCs [33]. It is well established that these cells may be significantly increased in the blood and tumours of adults and children with solid malignancies regardless of tumour type, and are associated with higher stage, metastatic disease, and a worse prognosis. These cells have been polarised by the tumour microenvironment to switch off autologous anti cancer T cells responses and can impair both the manufacturing and efficacy of CAR T cells [21,22,32].

One of the principle challenges in targeting human MDSCs remains their heterogeneous nature, with differences in immunophenotype and intracellular mechanisms of suppression both within the same patient (blood vs tumoural) and across different types of cancer diagnoses.

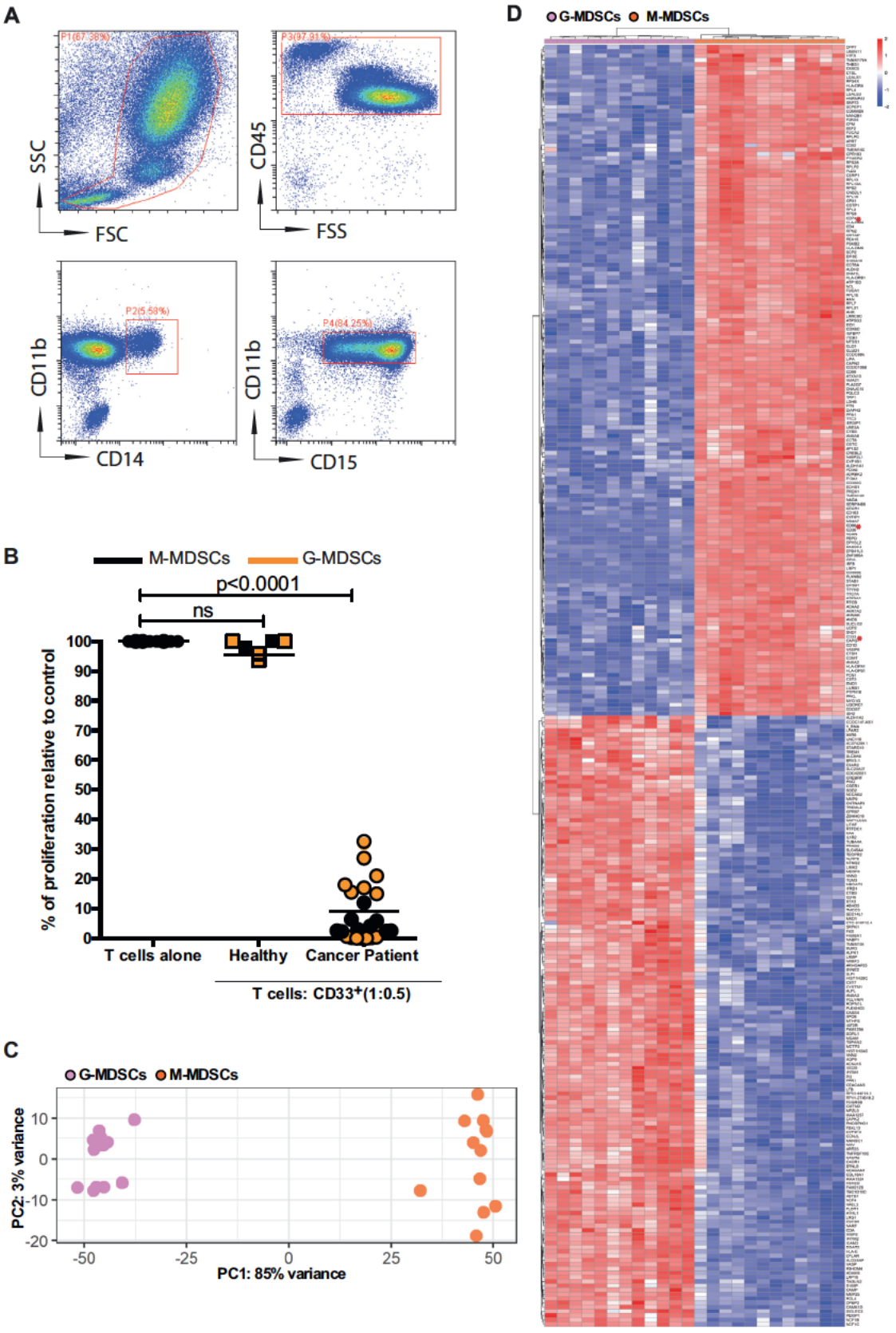

Fig. 1. G-MDSCs and M-MDSCs from cancer patients have distinct transcriptomic profiles. A) Flow cytometry gating strategy, illustrating CD11b + CD14+ or CD11b + CD15+ myeloid cell populations in the blood of patients with cancer. Representative of $n = 200$ patient samples B) Sorted CD14+ and CD15+ myeloid cells from the blood of patients, but not healthy donors, suppress T cell proliferation consistent with M-MDSC and G-MDSC phenotype respectively. Co-culture ratio of 1:0.5 or T cells alone is shown. These cells were used for RNA-sequencing library generation. C) Principle Component Analysis for CD14+ M-MDSCs and CD15+ G-MDSC D) Heatmap of differential expression analysis comparing M-MDSC and G-MDSC samples from cancer patients. Top 300 genes shown.

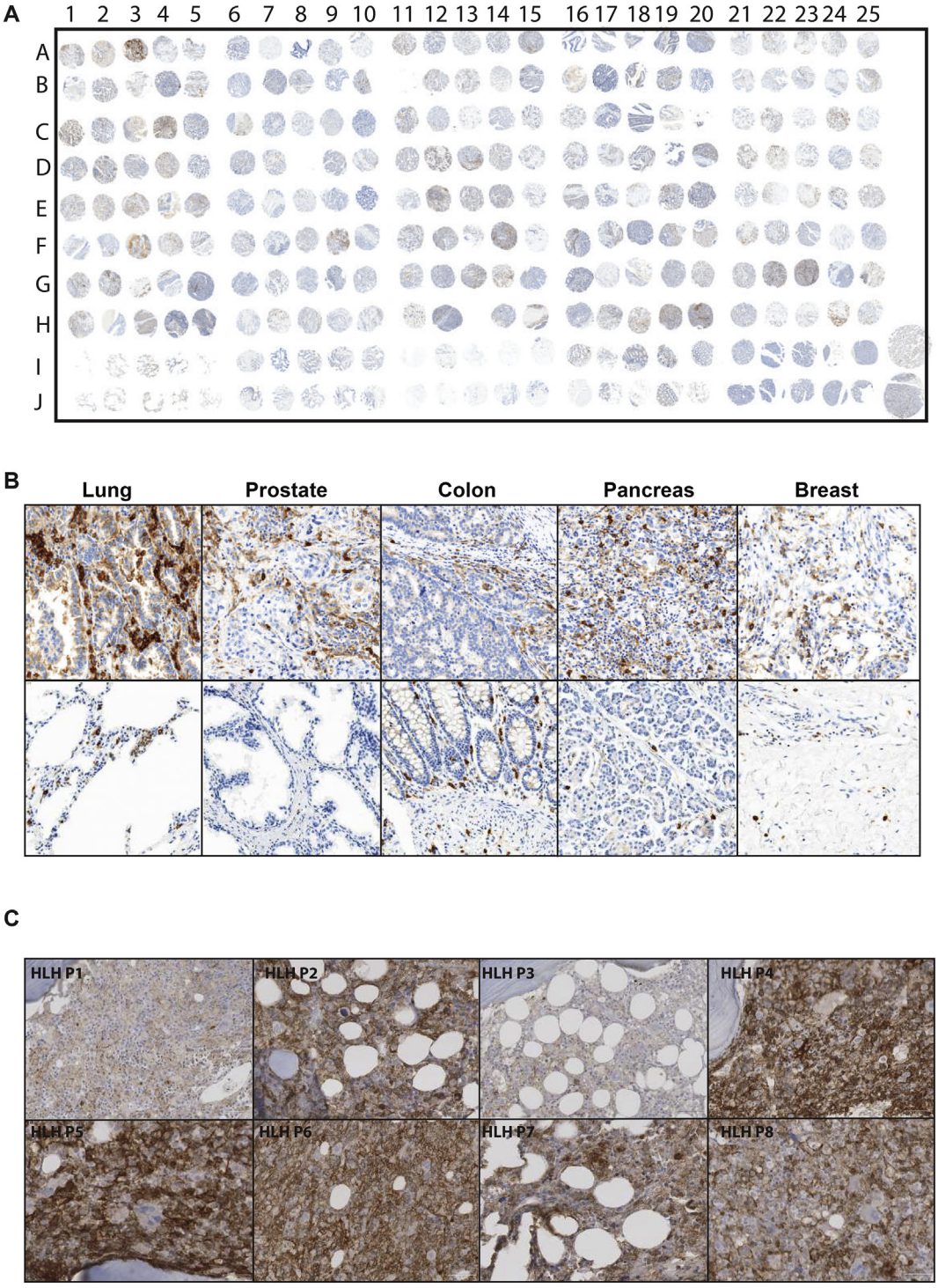

Fig. 2. CD33+ MDSC infiltration in the tumours and bone marrow of cancer and HLH patients. A) Immunohistochemical analysis of tissue microarray (n = 200 cancer patients) B) Photomicrographs of representative CD33+ immunohistochemistry staining within lung, prostate, colon, pancreas, and breast tumours within the TMA (upper panels) and normal healthy control tissues (lower panels) C) Representative immunohistochemical staining of sections from bone marrows of HLH patients ($n = 8$) showing infiltration of CD33+ MDSCs.

Murine MDSCs can be readily characterised by immunophenotype, which has allowed for a detailed study of suppressive pathways and in deed transcriptomic changes [34,35]. However human MDSCs require a multi step approach with relatively crude techniques including density centrifugation. To help identify new targets for clinical translation we generated a RNA sequencing library from both M MDSCs and G MDSCs, to our knowledge the first such attempt at this strategy. It re veals clear separation of the MDSC at the transcriptomic level, confirming that these populations are indeed distinct. Although we focused on screening the library for potential clinical targets to deplete MDSCs, we suggest such data will also allow for an improved under standing of the underlying biology of M MDSCs and G MDSCs and could identify other strategies to isolate or modulate these cells.

Here we have identified how CD33 marks the MDSCs which are found in the blood and tissues of patients across cancers. Binding of si alic acid ligands to CD33 can induce a number of physiological function resulting in inhibition of cellular proliferation and activation, apoptosis, or modulation of cytokine release [36]. However Siglecs, such as CD22,

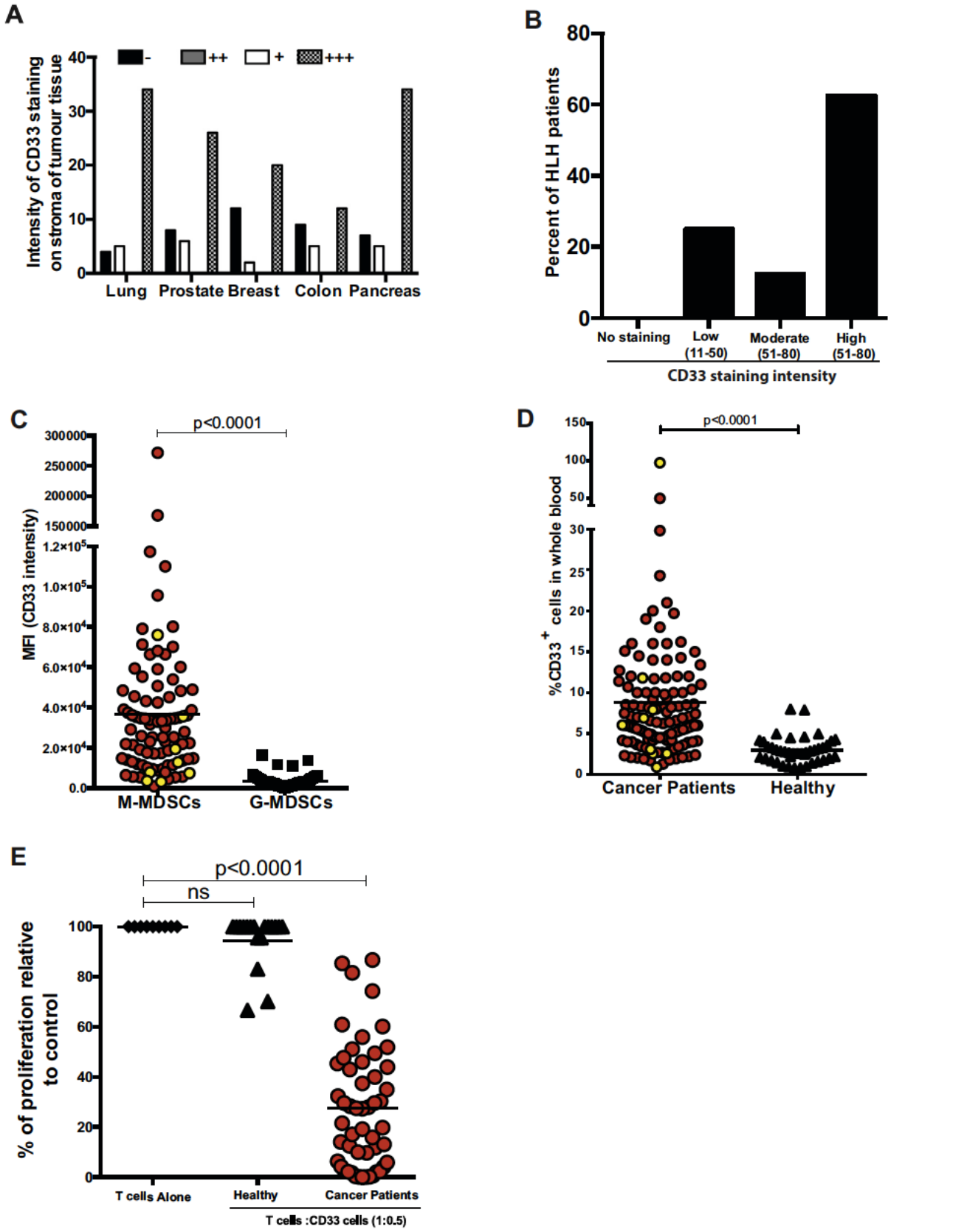

Fig. 3. CD33 expression characterises the MDSC population in the tumours and blood of cancer patients. A) Intensity of CD33+ staining on MDSCs in the stroma of tumour subtypes (B) and bone marrow of HLH patients (C) Median Fluorescence Intensity of CD33 staining on M-MDSCs and G-MDSCs in the blood of cancer (RED) or HLH (YELLOW) patients ($n = 81$). D) Percentage of CD14 + CD33+ M-MDSCs in the blood of cancer patients (RED n = 81) and patients with secondary HLH (YELLOW,$n = 7$) E) T cell proliferation is suppressed following culture with CD33+ MDSCs from the blood of patients at diagnosis.

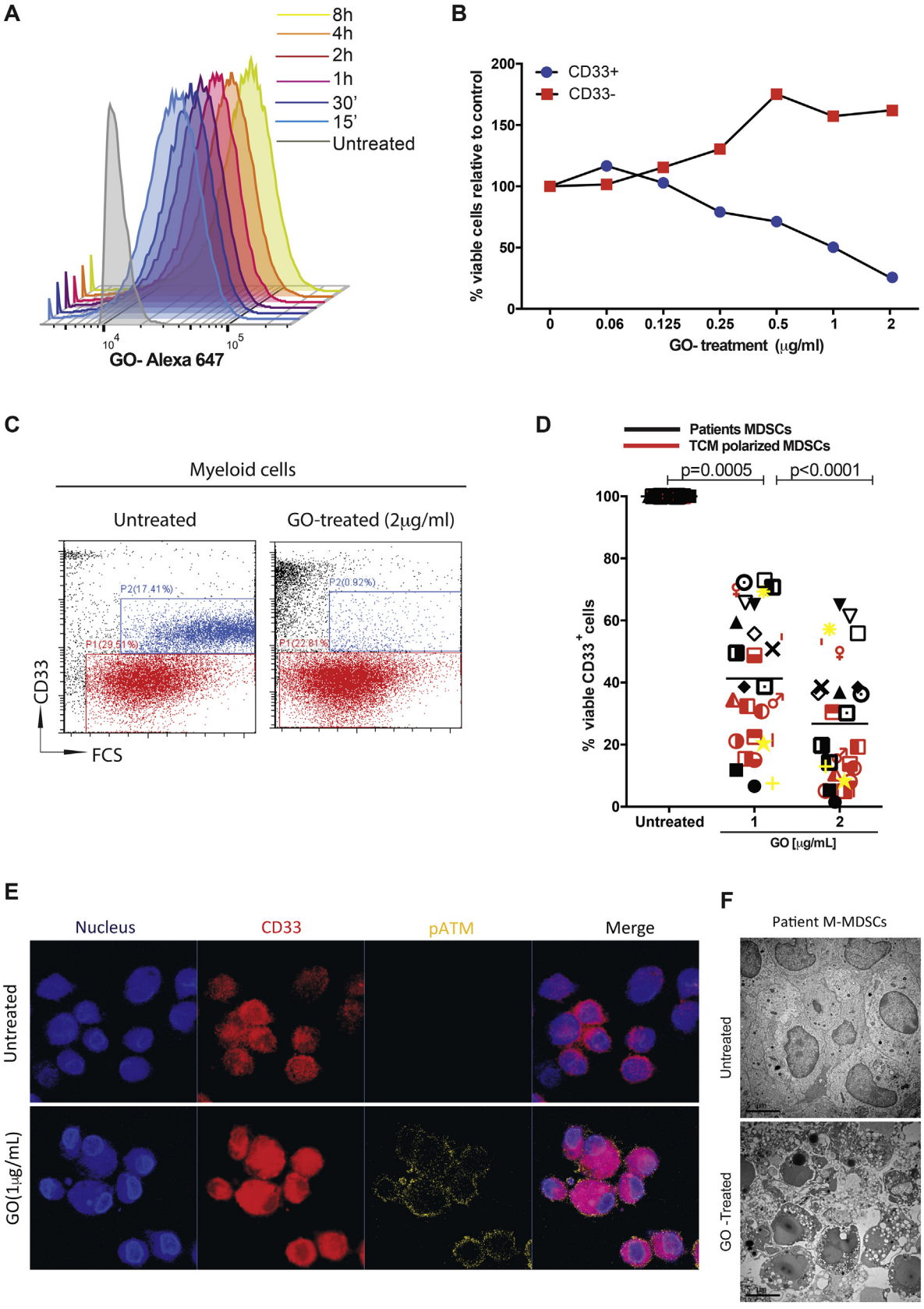

Fig. 4. Gemtuzumab ozogamicin is cytotoxic to MDSCs. A) ALEXA-647-Gemtuzumab ozogamicin is rapidly internalised into MDSCs over time. Flow cytometric representation of 3 independent experiments. Gemtuzumab ozogamicin specifically depletes CD33+ MDSCs from the whole blood of patients ex vivo (BLUE), with no effect on the CD33- populations of cells (RED). Representative dose response curve of cell viability (B) and flow cytometry gating (C) shown D) Gemtuzumab ozogamicin (1 or 2 μg/ml) significantly reduces the viability of CD33+ patient-derived or tumour-polarised MDSCs from different cancer subtypes, as assessed by flow cytometry E) Confocal microscopy of GO-treated (1 μg/ml) CD33+ MDSCs from the blood of patients showing increased p-ATM F) Transmission electron microscopy shows loss of cell membrane integrity, nuclear condensation, and blebbing consistent with apoptotic cell death after 1 μg/ml GO treatment.

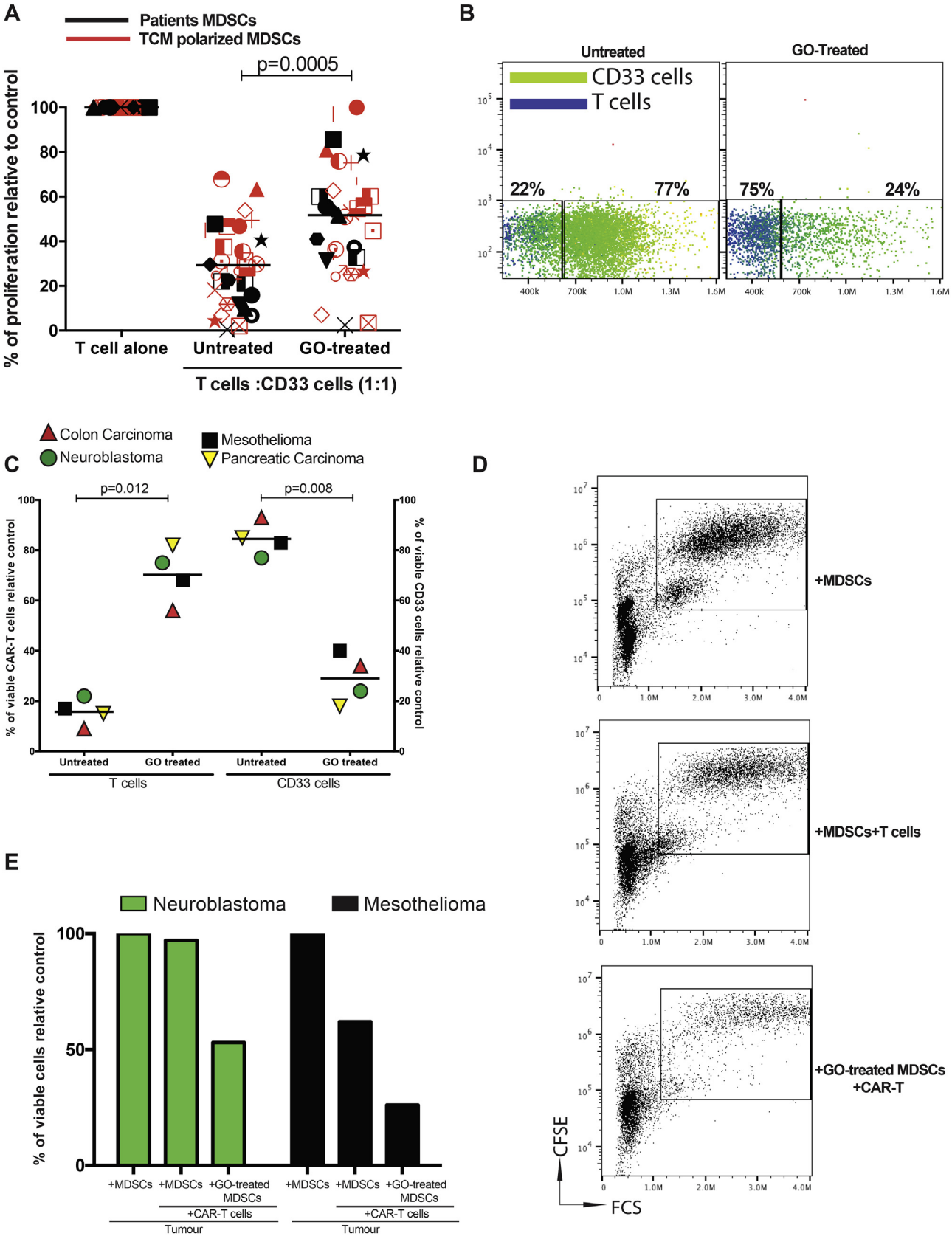

Fig. 5. Gemtuzumab ozogamicin restores T cell and CAR-T cell proliferation and cytotoxicity. A) Treatment of patient-derived or tumour-polarised MDSCs from different cancer subtypes with Gemtuzumab ozogamicin restores T cell proliferation in co-culture as assessed by ^{3}H-thymidine incorporation B) Representative flow cytometry gating showing the enhanced proliferation of CAR-T cells (BLUE) following the depletion of MDSCs by Gemtuzumab ozogamicin in tumour co-cultures C) Gemtuzumab ozogamicin depletion of MDSCs enhances CAR-T cell proliferation, as assessed by flow cytometry. Anti-mesothelin CART cells, anti-GD2 CART cells, and anti-EGFRvIII CART cells D)Representative flow cytometry gating on CFSE-labelled H1299M tumour cells in the presence of anti-mesothelin CAR-T cells and CD33 + MDSCs. E) Gemtuzumab ozogamicin depletion of MDSCs enhances CAR-T cell killing of target tumour cells, as assessed by flow cytometry. Representative of 4 independent experiments.

CD33, Siglec 8, also provide an attractive target for antibody based therapeutic due to their cell specific surface expression and rapid internalisation kinetics [37 39]. CD33 may be targeted through unconjugated antibodies, however these antibodies are not usually cytotoxic and do not lead to sustained depletions of the target cells minimising any therapeutic benefit [40,41]. Instead immunotoxins, such as Gemtuzumab ozogamicin, can induce a cell specific cytotoxicity alone, without reliance on Antibody Dependent Cellular Cytotoxicity. We show that the end result is a depletion, rather than a modulation, of the MDSCs, hence removing the immunosuppression regardless of the mechanism. Although CD33 may also be expressed on normal monocytes and macrophages in healthy individuals, critically it is the MDSCs which represent the bulk of myeloid cells in the cancer patients who would receive Gemtuzumab ozogamicin. Furthermore we show that GO does not bind the CD33 populations of cells, thus immunity provided by granulocytes or T cells remains unopposed.

Myeloid cells also play critical roles in driving the rare but often fatal conditions of Haemophagocytic Lymphohistiocytosis and Macrophage Activation Syndrome [10,11]. Recently the diagnosis of HLH/MAS has become notable due to the use of immunotherapy approaches in cancer patients treated with Chimeric Antigen Receptor T cells or antibodies [42,43]. Although it is recognised that myeloid cells secrete IL 1β or IL 6, modulate T and NK cells, or directly consume erythrocytes are central to the underlying pathology, no therapies have directly manipulated these cells [12]. Instead therapies have centred on multi drug chemotherapies, T cell depletion, or inhibition of Il 1β or IL 6 [44]. As a rare and non malignant disease few treatments have been developed which rationally target the underlying biological mechanisms, contributing to the poor prognosis for these patients (Supp Fig. 8).

Gemtuzumab ozogamicin has already completed Phase III adult trials and is subject to ongoing paediatric trials in children, with a manageable toxicity profile to date [45]. We suggest our findings have major clinical implications for the use of Gemtuzumab ozogamicin as an

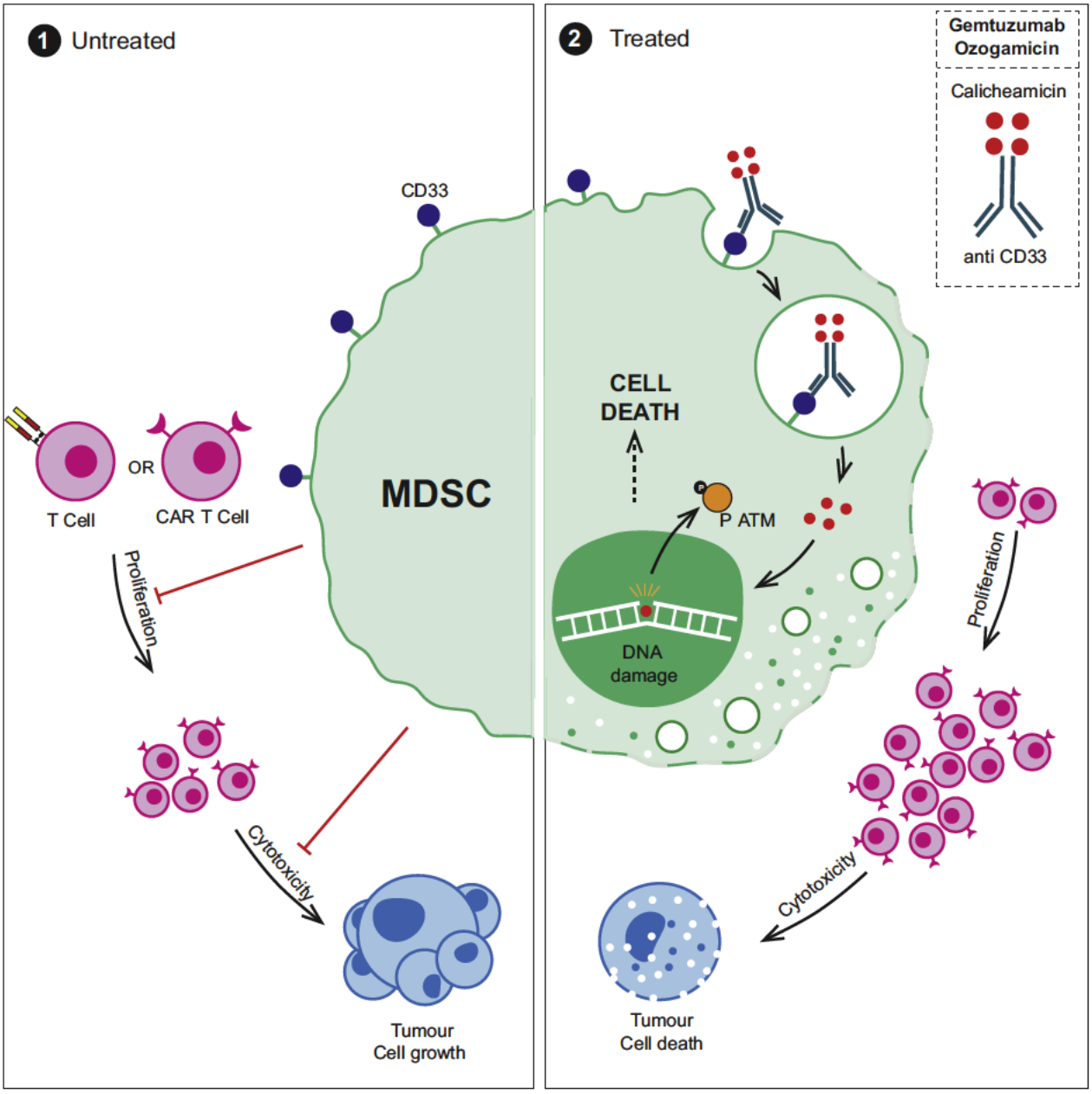

Fig. 6. Schematic illustrating the capacity of MDSCs to suppress T cell and CAR-T cell proliferation and cytotoxicity. Treatment with Gemtuzumab Ozogamicin restores T cell and CAR-T cell proliferation, leading to enhanced tumour cell death.

adjunct to chemotherapies and immunotherapies in adult and paediatric solid cancers. It is possible that patients with the highest frequencies of M MDSCs, such as those with advanced or relapsed disease, may gain the most useful clinical effect from GO therapy by turning immunologically 'cold' tumours, into immunologically hot' ones. Indeed in the context of CAR T cells, co treatment of Gemtuzumab ozogamicin could enhance CAR T cell persistence and anti tumour activity which has limited trial outcomes in solid tumours to date. To this end we will rapidly translate our preclinical findings to investigate the activity of Gemtuzumab Ozogamicin in HAemophagcytic lymphohistiocytosis (HLH) or Macrophage activation syndrome or relapsed/refractory solid tumours in an upcoming Phase II clinical trial (GOTHAM).

Supplementary data to this article can be found online at https://doi.org/10.1016/j.ebiom.2019.08.025.

Author contributions

F.M. and C.D.S. designed the study, supervised research, analysed data, secured funding and wrote the manuscript. F.M. additionally secured ethical approval and was chief investigator of the study. L.F. designed and performed research, S.P. performed research, S.B. performed research, R.L. performed research, P.C. performed research, M.N. performed patient samples, immunohistochemistry analysis and scoring, C·S L, S.G., N.R. and G.M. provided patient samples. B.N. performed RNA sequencing data analysis.

Declaration of Competing Interest

The authors declare no conflicts of interest.

Acknowledgements

The authors thank the patients and parents who contributed samples to the study. Thank you to Victoria Stavrou and Nazia Thakur for assistance with experimental methods. We also thank Paul Stanley and Theresa Morris for technical assistance with electron microscopy. Thank you to Janet Morse, Jane Cooper, Cay Shakespeare, and Sarah Jane Staveley for consenting of patients and collection of samples for this study.

This work was supported by Cancer Research UK, Children's Cancer and Leukaemia Group Little Princess Trust, Treating Children with Cancer, and the alumni and donors to the University of Birmingham. B.N. is funded through the Cancer Research UK Birmingham Centre award.

References

[1] Borst J, Ahrends T, Babala N, Melief CJM, Kastenmuller W. CD4(+) T cell help in cancer immunology and immunotherapy. Nat Rev Immunol 2018;18(10):635–47.
[2] Park JH, Riviere I, Gonen M, et al. Long-term follow-up of CD19 CAR therapy in acute lymphoblastic leukemia. N Engl J Med 2018;378(5):449–59.
[3] Louis CU, Savoldo B, Dotti G, et al. Antitumor activity and long-term fate of chimeric antigen receptor-positive T cells in patients with neuroblastoma. Blood 2011;118(23):6050–6.
[4] DM OR, MP N, A D, et al. A single dose of peripherally infused EGFRvIII-directed CAR T cells mediates antigen loss and induces adaptive resistance in patients with recurrent glioblastoma. Sci Transl Med 2017;9(399).
[5] Beatty GL, Haas AR, Maus MV, et al. Mesothelin-specific chimeric antigen receptor mRNA-engineered T cells induce anti-tumor activity in solid malignancies. Cancer Immunol Res 2014;2(2):112–20.
[6] Khanna S, Graef S, Mussai F, et al. Tumour-derived GM-CSF promotes granulocyte immunosuppression in mesothelioma patients. Clin Cancer Res 2018;24(12):2859–72.
[7] Fultang L, Gamble LD, Gneo L, et al. Macrophage-derived IL1beta and TNFalpha regulate arginine metabolism in neuroblastoma. Cancer Res 2019;79(3):611–24.
[8] De Santo C, Arscott R, Booth S, et al. Invariant NKT cells modulate the suppressive activity of IL-10-secreting neutrophils differentiated with serum amyloid A. Nat Immunol 2010;11(11):1039–46.
[9] de Santo C, Serafini P, Marigo I, et al. Nitroaspirin corrects immune dysfunction in tumor-bearing hosts and promotes tumor eradication by cancer vaccination. Proc Natl Acad Sci U S A 2005;2005(102):4185–90.
[10] Bracaglia C, Prencipe G, De Benedetti F. Macrophage activation syndrome: different mechanisms leading to a one clinical syndrome. Pediatr Rheumatol Online J 2017;15(1):5.
[11] Daver N, McClain K, Allen CE, et al. A consensus review on malignancy-associated hemophagocytic lymphohistiocytosis in adults. Cancer 2017;123(17):3229–40.
[12] Schulert GS, Grom AA. Pathogenesis of macrophage activation syndrome and potential for cytokine- directed therapies. Annu Rev Med 2015;66:145–59.
[13] Bronte V, Brandau S, Chen SH, et al. Recommendations for myeloid-derived suppressor cell nomenclature and characterization standards. Nat Commun 2016;7:12150.
[14] Qin H, Lerman B, Sakamaki I, et al. Generation of a new therapeutic peptide that depletes myeloid-derived suppressor cells in tumor-bearing mice. Nat Med 2014;20(6):676–81.
[15] Marini O, Costa S, Bevilacqua D, et al. Mature CD10(+) and immature CD10( ) neutrophils present in G-CSF-treated donors display opposite effects on T cells. Blood 2017;129(10):1343–56.
[16] Condamine T, Dominguez GA, Youn JI, et al. Lectin-type oxidized LDL receptor-1 distinguishes population of human polymorphonuclear myeloid-derived suppressor cells in cancer patients. Sci Immunol 2016;1(2).
[17] Tobin RP, Davis D, Jordan KR, McCarter MD. The clinical evidence for targeting human myeloid-derived suppressor cells in cancer patients. J Leukoc Biol 2017;102(2):381–91.
[18] Kreitman RJ, Dearden C, Zinzani PL, et al. Moxetumomab pasudotox in relapsed/refractory hairy cell leukemia. Leukemia 2018;32(8):1768–77.
[19] Dobin A, Davis CA, Schlesinger F, et al. STAR: ultrafast universal RNA-seq aligner. Bioinformatics 2013;29(1):15–21.
[20] Love MI, Huber W, Anders S. Moderated estimation of fold change and dispersion for RNA-seq data with DESeq2. Genome Biol 2014;15(12):550.
[21] Mussai F, Wheat R, Sarrou E, et al. Targeting the arginine metabolic brake enhances immunotherapy for leukaemia. Int J Cancer 2018 Nov 28. https://doi.org/10.1002/ijc.32028 [Epub ahead of print].
[22] Mussai F, Egan S, Hunter S, et al. Neuroblastoma arginase activity creates an immunosuppressive microenvironment that impairs autologous and engineered immunity. Cancer Res 2015;75(15):3043–53.
[23] Sok JC, Coppelli FM, Thomas SM, et al. Mutant epidermal growth factor receptor (EGFRvIII) contributes to head and neck cancer growth and resistance to EGFR targeting. Clin Cancer Res 2006;12(17):5064–73.
[24] Yoshimoto K, Dang J, Zhu S, et al. Development of a real-time RT-PCR assay for detecting EGFRvIII in glioblastoma samples. Clin Cancer Res 2008;14(2):488–93.
[25] Chang CH, Sapra P, Vanama SS, Hansen HJ, Horak ID, Goldenberg DM. Effective therapy of human lymphoma xenografts with a novel recombinant ribonuclease/anti-CD74 humanized IgG4 antibody immunotoxin. Blood 2005;106(13):4308–14.
[26] Otten HG, de Gast GC, Vooijs WC, et al. Preclinical evaluation of anti-CD86 immunotoxin in rhesus monkeys: analysis of systemic toxicity, pharmacokinetics, and effect on primary T-cell responses. Cancer Immunol Immunother 2003;52(9):569–75.
[27] Lamba JK, Chauhan L, Shin M, et al. CD33 splicing polymorphism determines gemtuzumab ozogamicin response in de novo acute myeloid leukemia: report from randomized phase III Children's oncology group trial AAML0531. J Clin Oncol 2017;35(23):2674–82.
[28] Crocker PR, Paulson JC, Varki A. Siglecs and their roles in the immune system. Nat Rev Immunol 2007;7(4):255–66.
[29] Brinkman-Van der Linden ECM, Angata T, Reynolds SA, Powell LD, Hedrick SM, Varki A. CD33/Siglec-3 binding specificity, expression pattern, and consequences of gene deletion in mice. Mol Cell Biol 2003;23(12):4199–206.
[30] Amico D, Barbui AM, Erba E, Rambaldi A, Introna M, Golay J. Differential response of human acute myeloid leukemia cells to gemtuzumab ozogamicin in vitro: role of Chk1 and Chk2 phosphorylation and caspase 3. Blood 2003;101(11):4589–97.
[31] Chang ZL, Lorenzini MH, Chen X, Tran U, Bangayan NJ, Chen YY. Rewiring T-cell responses to soluble factors with chimeric antigen receptors. Nat Chem Biol 2018;14(3):317–24.
[32] Stroncek DF, Lee DW, Ren J, et al. Elutriated lymphocytes for manufacturing chimeric antigen receptor T cells. J Transl Med 2017;15(1):59.
[33] Gabrilovich DI, Ostrand-Rosenberg S, Bronte V. Coordinated regulation of myeloid cells by tumours. Nat Rev Immunol 2012;12(4):253–68.
[34] Ouzounova M, Lee E, Piranlioglu R, et al. Monocytic and granulocytic myeloid derived suppressor cells differentially regulate spatiotemporal tumour plasticity during metastatic cascade. Nat Commun 2017;8:14979.
[35] Fridlender ZG, Sun J, Mishalian I, et al. Transcriptomic analysis comparing tumor-associated neutrophils with granulocytic myeloid-derived suppressor cells and normal neutrophils. PLoS One 2012;7(2):e31524.
[36] McMillan SJ, Crocker PR. CD33-related sialic-acid-binding immunoglobulin-like lectins in health and disease. Carbohydr Res 2008;343(12):2050–6.
[37] Mussai F, Campana D, Bhojwani D, et al. Cytotoxicity of the anti-CD22 immunotoxin HA22 (CAT-8015) against paediatric acute lymphoblastic leukaemia. Br J Haematol 2010;150(3):352–8.
[38] Sievers EL, Appelbaum FR, Spielberger RT, et al. Selective ablation of acute myeloid leukemia using antibody-targeted chemotherapy: a phase I study of an anti-CD33 calicheamicin immunoconjugate. Blood 1999;93(11):3678–84.
[39] O'Sullivan JA, Carroll DJ, Cao Y, Salicru AN, Bochner BS. Leveraging Siglec-8 endocytic mechanisms to kill human eosinophils and malignant mast cells. J Allergy Clin Immunol 2018;141(5):1774–85 [e7].
[40] Kossman SE, Scheinberg DA, Jurcic JG, Jimenez J, Caron PC. A phase I trial of humanized monoclonal antibody HuM195 (anti-CD33) with low-dose interleukin 2 in acute myelogenous leukemia. Clin Cancer Res 1999;5(10):2748–55.

[41] Sutherland MK, Yu C, Lewis TS, et al. Anti-leukemic activity of lintuzumab (SGN-33) in preclinical models of acute myeloid leukemia. MAbs 2009;1(5):481–90.
[42] Neelapu SS, Tummala S, Kebriaei P, et al. Chimeric antigen receptor T-cell therapy - assessment and management of toxicities. Nat Rev Clin Oncol 2018;15(1):47–62.
[43] Teachey DT, Rheingold SR, Maude SL, et al. Cytokine release syndrome after blinatumomab treatment related to abnormal macrophage activation and ameliorated with cytokine-directed therapy. Blood 2013;121(26):5154–7.
[44] Marsh RA, Jordan MB, Talano JA, et al. Salvage therapy for refractory hemophagocytic lymphohistiocytosis: A review of the published experience. Pediatr Blood Cancer 2017;64(4).
[45] Duncan C, St Martin A, Perez W, et al. 435- Veno-occlusive disease characteristics in pediatric patients with acute myeloid leukaemia receiving gemtuzumab ozogamicin before allogeneic stem cell transplant. BBBMT 2018;24(3):S302.

8.2 GD2 ARG1 CAR Sequence

MP71 vector backbone

Truncated human CD34

F2A peptide linker

CD8a signal peptide

GD2 14g2A ScFv

CH2 CH3 spacer region

CD8 hinge/transmembrane

41BB intracellular signalling domain (human)

CD3zeta intracellular signalling domain

P2A peptide linker

ARG1 enzyme

(CAR+Enzyme+TAATAATAA = 4302bp)

ctcgagagctttggcgtaatcatggtcatagctgtttcctgtgtgaaattgttatccgctcacaattccacacaacatacgagccggaagcataaagtgtaaagcct
ggggtgcctaatgagtgagctaactcacattaattgcgttgcgctcactgcccgctttccagtcgggaaacctgtcgtgccagctgcattaatgaatcggccaacgc
gcggggagaggcggtttgcgtattgggcgctcttccgcttcctcgctcactgactcgctgcgctcggtcgttcggctgcggcgagcggtatcagctcactcaaaggc
ggtaatacggttatccacagaatcaggggataacgcaggaaagaacatgtgagcaaaaggccagcaaaaggccaggaaccgtaaaaaggccgcgttgctggc
gtttttccataggctccgccccccctgacgagcatcacaaaaatcgacgctcaagtcagaggtggcgaaacccgacaggactataaagataccaggcgtttccccc
tggaagctccctcgtgcgctctcctgttccgaccctgccgcttaccggatacctgtccgcctttctcccttcgggaagcgtggcgctttctcaatgctcacgctgtagg
tatctcagttcggtgtaggtcgttcgctccaagctgggctgtgtgcacgaaccccccgttcagcccgaccgctgcgccttatccggtaactatcgtcttgagtccaac
ccggtaagacacgacttatcgccactggcagcagccactggtaacaggattagcagagcgaggtatgtaggcggtgctacagagttcttgaagtggtggcctaac
tacggctacactagaaggacagtatttggtatctgcgctctgctgaagccagttaccttcggaaaaagagttggtagctcttgatccggcaaacaaaccaccgctg
gtagcggtggtttttttgtttgcaagcagcagattacgcgcagaaaaaaaggatctcaagaagatcctttgatcttttctacggggtctgacgctcagtggaacgaa
aactcacgttaagggattttggtcatgagattatcaaaaaggatcttcacctagatccttttaaattaaaaatgaagttttaaatcaatctaaagtatatatgagtaa
acttggtctgacagttaccaatgcttaatcagtgaggcacctatctcagcgatctgtctatttcgttcatccatagttgcctgactccccgtcgtgtagataactacga
tacgggagggcttaccatctggccccagtgctgcaatgataccgcgagacccacgctcaccggctccagatttatcagcaataaaccagccagccggaagggcc
gagcgcagaagtggtcctgcaactttatccgcctccatccagtctattaattgttgccgggaagctagagtaagtagttcgccagttaatagtttgcgcaacgttgtt
gccattgctgctggcatcgtggtgtcacgctcgtcgtttggtatggcttcattcagctccggttcccaacgatcaaggcgagttacatgatcccccatgttgtgcaaa
aaagcggttagctccttcggtcctccgatcgttgtcagaagtaagttggccgcagtgttatcactcatggttatggcagcactgcataattctcttactgtcatgccat
ccgtaagatgcttttctgtgactggtgagtactcaaccaagtcattctgagaatagtgtatgcggcgaccgagttgctcttgcccggcgtcaatacgggataataacc
gcgccacatagcagaactttaaaagtgctcatcattggaaaacgttcttcggggcgaaaactctcaaggatcttaccgctgttgagatccagttcgatgtaaccca
ctcgtgcacccaactgatcttcagcatcttttactttcaccagcgtttctgggtgagcaaaaacaggaaggcaaaatgccgcaaaaaagggaataagggcgacac
ggaaatgttgaatactcatactcttccttttttcaatattattgaagcatttatcagggttattgtctcatgagcggatacatatttgaatgtatttagaaaaataaacaa
atagggttccgcgcacatttccccgaaaagtgccacctgacgtctaagaaaccattattatcatgacattaacctataaaaataggcgtatcacgaggccctttc

gtcttcaagctgcctcgcgcgtttcggtgatgacggtgaaaacctctgacacatgcagctcccggagacggtcacagcttgtctgtaagcggatgccgggagcag
acaagcccgtcagggcgcgtcagcgggtgttggcgggtgtcggggcgcagccatgacccagtcacgtagcgatagttactatgcggcatcagagcagattgtact
gagagtgcaccatatgcggtgtgaaataccgcacagatgcgtaaggagaaaataccgcatcaggcgccattcgccattcaggctgcgcaactgttgggaagggc
gatcggtgcgggcctcttcgctattacgccagctggcgaaaggggatgtgctgcaaggcgattaagttgggtaacgccagggttttcccagtcacgacgttgtaa
aacgacggccagtgaattagtactctagcttaagtaacgccattttgcaaggcatggaaaatacataactgagaatagagaagttcagatcaaggttaggaaca
gagagacagcagaatatgggccaaacaggatatctgtggtaagcagttcctgccccggctcagggccaagaacagttggaacagcagaatatgggccaaacag
gatatctgtggtaagcagttcctgccccggctcagggccaagaacagatggtccccagatgcggtcccgccctcagcagtttctagagaaccatcagatgtttcca
gggtgccccaaggacctgaaatgaccctgtgccttatttgaactaaccaatcagttcgcttctcgcttctgttcgcgcgcttctgctccccgagctcaataaaagagc
ccacaacccctcactcggcgcgccagtcctccgatagactgcgtcgcccgggtacccgtattcccaataaagcctcttgctgtttgcatccgaatcgtggactcgct
gatccttgggagggtctcctcagattgattgactgcccacctcgggggtctttcatttggaggttccaccgagatttggagacccctgcccagggaccaccgacccc
cccgccgggaggtaagctggccagcggtcgtttcgtgtctgtctctgtctttgtgcgtgtttgtgccggcatctaatgtttgcgcctgcgtctgtactagttggctaact
agatctgtatctggcggtcccgcggaagaactgacgagttcgtattcccggccgcagcccctgggagacgtcccagcggcctcgggggcccgttttgtggcccatt
ctgtatcagttaacctacccgagtcggacttttggagctccgccactgtccgaggggtacgtggctttgttgggggacgagagacagagacacttcccgcccccg
tctgaatttttgctttcggttttacgccgaaaccgcgccgcgcgtcttgtctgctgcagcatcgttctgtgttgtctctgtctgactgtgtttctgtatttgtctgaaaatt
agctcgacaaagttaagtaatagtccctctctccaagctcacttacaggcggccgaattcgccgccgccatgcctcgcggctggacagccctgtgcctgctgtctct
gctgccatccggcttcatgagcctggataataacggcacagccaccccagagctgcctacacagggcaccttcagcaatgtgtccacaaacgtgagctatcagga
gaccacaacccccttctaccctgggatccacaagcctgcaccccgtgtctcagcacggcaacgaagccaccaccaacatcaccgagaccacagtgaagtttacctc
cacctctgtgattacctctgtgtacggaaatacaaactccagcgtgcagtctcagacatctgtgatctccacagtgtttacaacacctgccaatgtgtccaccccag
agacaaccctgaagcccagcctgtctcctggaaatgtgtccgatctgtctaccacctccaccagcctggccacctctcccaccaagccctatacctcctcttctccc
atcctgagcgatatcaaagccgagatcaaatgcagcgggattcgggaagtgaaactgacacagggcatctgcctggaacagaataagacatccagctgcgccg
agtttaagaaagatagaggagagggactggccagggtgctgtgtggcgaagagcaggccgacgccgatgccggcgcccaggtgtgttccctgctgctggcccag
tctgaggtgcgccccccagtgcctgctgctggtgctggccaatcggacagaaattagcagcaagctgcagctgatgaaaaaacaccagagcgatctgaaaaagct
gggcatcctggactttaccgagcaggacgtggcctctcaccagagctacagccagaaaacactgatcgccctggtgaccagcggagccctgctggccgtgctgg
gcatcaccggatatttcctgatgaataggcgcagctggagccccaccggcgaacggctggagctggagcctgtcgaccgagtgaagcagaccctgaactttgatc
tgctgaagctggccggcgacgtggagtccaaccccgggccagggaatATGGCCTTACCAGTGACCGCCTTGCTCCTGCCGCTGGCCTTGCTG
CTCCACGCCGCCAGGCCGGATATTCTGCTCACACAGACCCCACTCTCCCTGCCCGTGTCACTCGGGGATCAGGCTAGCATTT
CTTGCCGCTCATCTCAGTCTCTGGTCCACCGGAATGGGAACACATACCTCCATTGGTACCTCCAGAAACCTGGACAGAGCCC
TAAACTGCTCATCCACAAAGTCTCAAATCGGTTCTCCGGCGTGCCCGATCGCTTTAGCGGATCCGGATCTGGGACCGACTTC
ACACTGAAAATCTCACGAGTGGAGGCTGAGGATCTCGGCGTCTACTTCTGTAGTCAGAGTACCCACGTCCCACCCCTCACCT
TTGGCGCTGGAACAAAACTGGAGCTGAAACGAGCCGATGCTGCTCCTACCGTGTCCATCTTTCCTGGCTCCGGGGGAGGCG
GGAGCGGAGGCGAAGTGAAACTCCAGCAGTCTGGCCCTTCTCTCGTGGAACCTGGCGCTTCTGTGATGATCTCCTGTAAGG
CCTCTGGATCTTCCTTTACCGGCTACAACATGAACTGGGTCCGGCAGAACATTGGCAAATCCCTGGAATGGATTGGCGCCAT
CGATCCTTACTACGGCGGCACATCATACAATCAGAAATTCAAGGGGCGAGCAACACTCACTGTCGACAAATCTTCATCCACC
GCCTACATGCACCTGAAATCTCTCACATCCGAGGATAGTGCTGTCTACTACTGTGTCTCTGGCATGGAATACTGGGGACAGG
GAACTTCTGTCACCGTGTCTAGTGCCAAAACCACACCTCCCTCCGTGTACGGACGAGTCACTGTCTCATCTGCTGAACCAAA
ATCCTGTGACAAAACACACACATGCCCACCTTGTCCTGCCCCTGAACTGCTCGGCGGACCTTCCGTCTTTCTGTTTCCCCCCA

AACCCAAGGATACACTCATGATTTCTAGGACCCCCGAAGTCACTTGTGTCGTGGTCGATGTGTCTCACGAGGATCCTGAAGT
GAAATTCAACTGGTACGTGGACGGAGTCGAGGTCCACAATGCCAAAACAAAACCCCGGGAGGAACAGTACAATAGCACCT
ACCGAGTCGTGTCCGTGCTCACCGTCCTCCATCAGGATTGGCTGAACGGCAAAGAGTACAAGTGTAAAGTGAGTAACAAGG
CTCTCCCCGCTCCTATTGAAAAAACCATCTCAAAAGCAAAAGGCCAGCCTAGGGAGCCTCAGGTCTACACACTGCCACCCTC
ACGGGACGAACTCACCAAAAATCAGGTGTCCCTCACTTGCCTGGTGAAAGGCTTCTACCCTTCCGATATCGCTGTGGAATGG
GAGTCAAATGGGCAGCCCGAAAACAACTACAAAACAACCCCCCCTGTGCTCGATTCCGATGGCTCTTTTTTCCTGTACTCCA
AACTCACCGTGGACAAATCACGCTGGCAGCAGGGGAATGTCTTTTCTTGCTCCGTGATGCACGAGGCCCTCCACAATCATTA
CACCCAGAAATCCCTCTCACTCTCACCCGGCAAAAAGGACCCTAAAACCACGACGCCAGCACCGCGACCACCAACACCGGC
GCCAACCATCGCATCGCAGCCCCTGTCCCTGCGCCCAGAGGCGTGCCGACCAGCGGCGGGGGGGCGCAGTGCACACGAGG
GGGCTGGACTTCGCCTGTGATATCTACATCTGGGCGCCCTTGGCCGGGACTTGTGGGGTCCTTCTCCTGTCACTGGTTATCA
CCCTTTACTGCAAACGGGGCAGAAAGAAACTCCTGTATATATTCAAACAACCATTTATGAGACCAGTACAAACTACTCAAGA
GGAAGATGGCTGTAGCTGCCGATTTCCAGAAGAAGAAGAAGGAGGATGTGAACTGAGAGTGAAGTTCAGCAGGAGCGCA
GACGCCCCCGCGTACAAGCAGGGCCAGAACCAGCTCTATAACGAGCTCAATCTAGGACGAAGAGAGGAGTACGATGTTTT
GGACAAGAGACGTGGCCGGGACCCTGAGATGGGGGGAAAGCCGAGAAGGAAGAACCCTCAGGAAGGCCTGTACAATGA
ACTGCAGAAAGATAAGATGGCGGAGGCCTACAGTGAGATTGGGATGAAAGGCGAGCGCCGGAGGGGCAAGGGGCACGA
TGGCCTTTACCAGGGTCTCAGTACAGCCACCAAGGACACCTACGACGCCCTTCACATGCAGGCCCTGCCCCCTCGCGGCAG
CGGCGCCACCAACTTCAGCCTGCTGAAGCAGGCCGGCGACGTGGAGGAAAACCCTGGCCCCATGAGCGCCAAGTCCAGAA
CCATAGGGATTATTGGAGCTCCTTTCTCAAAGGGACAGCCACGAGGAGGGGTGGAAGAAGGCCCTACAGTATTGAGAAAG
GCTGGTCTGCTTGAGAAACTTAAAGAACAAGAGTGTGATGTGAAGGATTATGGGGACCTGCCCTTTGCTGACATCCCTAAT
GACAGTCCCTTTCAAATTGTGAAGAATCCAAGGTCTGTGGGAAAAGCAAGCGAGCAGCTGGCTGGCAAGGTGGCAGAAGT
CAAGAAGAACGGAAGAATCAGCCTGGTGCTGGGCGGAGACCACAGTTTGGCAATTGGAAGCATCTCTGGCCATGCCAGGG
TCCACCCTGATCTTGGAGTCATCTGGGTGGATGCTCACACTGATATCAACACTCCACTGACAACCACAAGTGGAAACTTGCA
TGGACAACCTGTATCTTTCCTCCTGAAGGAACTAAAAGGAAAGATTCCCGATGTGCCAGGATTCTCCTGGGTGACTCCCTGT
ATATCTGCCAAGGATATTGTGTATATTGGCTTGAGA
GACGTGGACCCTGGGGAACACTACATTTTGAAAACTCTAGGCATTAAATACTTTTCAATGACTGAAGTGGACAGACTAGGA
ATTGGCAAGGTGATGGAAGAAACACTCAGCTATCTACTAGGAAGAAAGAAAAGGCCAATTCATCTAAGTTTTGATGTTGAC
GGACTGGACCCATCTTTCACACCAGCTACTGGCACACCAGTCGTGGGAGGTCTGACATACAGAGAAGGTCTCTACATCACA
GAAGAAATCTACAAAACAGGGCTACTCTCAGGATTAGATATAATGGAAGTGAACCCATCCCTGGGGAAGACACCAGAAGA
AGTAACTCGAACAGTGAACACAGCAGTTGCAATAACCTTGGCTTGTTTCGGACTTGCTCGGGAGGGTAATCACAAGCCTATT
GACTACCTTAACCCACCTAAGTAATAATAAaagcttaacacgagccatagatagaataaaagattttatttagtctccagaaaaaggggggaatgaa
agaccccacctgtaggtttggcaagctagcttaagtaacgccattttgcaaggcatggaaaatacataactgagaatagagaagttcagatcaaggttaggaaca
gagagacagcagaatatgggccaaacaggatatctgtggtaagcagttcctgccccggctcagggccaagaacagttggaacagcagaatatgggccaaacag
gatatctgtggtaagcagttcctgccccggctcagggccaagaacagatggtccccagatgcggtcccgccctcagcagtttctagagaaccatcagatgtttcca
gggtgccccaaggacctgaaatgaccctgtgccttatttgaactaaccaatcagttcgcttctcgcttctgttcgcgcgcttctgctccccgagctcaataaaagagc
ccacaacccctcactcggcgcgccagtcctccgatagactgcgtcgcccgggtacccgtgttctcaataaacccctcttgcagttgcatccgactcgtggtctcgctg
ttccttgggagggtctcctctgagtgattgactgcccacctcgggggtctttcatt

8.3 GD2 ARG2 CAR Sequence

MP71 vector backbone

Truncated human CD34

F2A peptide linker

CD8a signal peptide

GD2 14g2A ScFv

CH2 CH3 spacer region

CD8 hinge/transmembrane

41BB intracellular signalling domain (human)

CD3zeta intracellular signalling domain

P2A peptide linker

ARG2 enzyme

(CAR+Enzymes = 4407bp)

ctcgagagctttggcgtaatcatggtcatagctgtttcctgtgtgaaattgttatccgctcacaattccacacaacatacgagccggaagcataaagtgtaaagcct
ggggtgcctaatgagtgagctaactcacattaattgcgttgcgctcactgcccgctttccagtcgggaaacctgtcgtgccagctgcattaatgaatcggccaacgc
gcggggagaggcggtttgcgtattgggcgctcttccgcttcctcgctcactgactcgctgcgctcggtcgttcggctgcggcgagcggtatcagctcactcaaaggc
ggtaatacggttatccacagaatcaggggataacgcaggaaagaacatgtgagcaaaaggccagcaaaaggccaggaaccgtaaaaaggccgcgttgctggc
gtttttccataggctccgccccccctgacgagcatcacaaaaatcgacgctcaagtcagaggtggcgaaacccgacaggactataaagataccaggcgtttccccc
tggaagctccctcgtgcgctctcctgttccgaccctgccgcttaccggatacctgtccgcctttctcccttcgggaagcgtggcgctttctcaatgctcacgctgtagg
tatctcagttcggtgtaggtcgttcgctccaagctgggctgtgtgcacgaaccccccgttcagcccgaccgctgcgccttatccggtaactatcgtcttgagtccaac
ccggtaagacacgacttatcgccactggcagcagccactggtaacaggattagcagagcgaggtatgtaggcggtgctacagagttcttgaagtggtggcctaac
tacggctacactagaaggacagtatttggtatctgcgctctgctgaagccagttaccttcggaaaaagagttggtagctcttgatccggcaaacaaaccaccgctg
gtagcggtggttttttgtttgcaagcagcagattacgcgcagaaaaaaaggatctcaagaagatcctttgatcttttctacggggtctgacgctcagtggaacgaa
aactcacgttaagggattttggtcatgagattatcaaaaaggatcttcacctagatccttttaaattaaaaatgaagttttaaatcaatctaaagtatatatgagtaa
acttggtctgacagttaccaatgcttaatcagtgaggcacctatctcagcgatctgtctatttcgttcatccatagttgcctgactccccgtcgtgtagataactacga
tacgggagggcttaccatctggccccagtgctgcaatgataccgcgagacccacgctcaccggctccagatttatcagcaataaaccagccagccggaagggcc
gagcgcagaagtggtcctgcaactttatccgcctccatccagtctattaattgttgccgggaagctagagtaagtagttcgccagttaatagtttgcgcaacgttgtt
gccattgctgctggcatcgtggtgtcacgctcgtcgtttggtatggcttcattcagctccggttcccaacgatcaaggcgagttacatgatcccccatgttgtgcaaa
aaagcggttagctccttcggtcctccgatcgttgtcagaagtaagttggccgcagtgttatcactcatggttatggcagcactgcataattctcttactgtcatgccat
ccgtaagatgcttttctgtgactggtgagtactcaaccaagtcattctgagaatagtgtatgcggcgaccgagttgctcttgcccggcgtcaatacgggataataacc
gcgccacatagcagaactttaaaagtgctcatcattggaaaacgttcttcggggcgaaaactctcaaggatcttaccgctgttgagatccagttcgatgtaaccca
ctcgtgcacccaactgatcttcagcatcttttactttcaccagcgtttctgggtgagcaaaaacaggaaggcaaaatgccgcaaaaaagggaataagggcgacac
ggaaatgttgaatactcatactcttccttttcaatattattgaagcatttatcagggttattgtctcatgagcggatacatatttgaatgtatttagaaaaataaacaa

atagggttccgcgcacatttccccgaaaagtgccacctgacgtctaagaaaccattattatcatgacattaacctataaaaataggcgtatcacgaggccctttc
gtcttcaagctgcctcgcgcgtttcggtgatgacggtgaaaacctctgacacatgcagctcccggagacggtcacagcttgtctgtaagcggatgccgggagcag
acaagcccgtcagggcgcgtcagcgggtgttggcgggtgtcggggcgcagccatgacccagtcacgtagcgatagttactatgcggcatcagagcagattgtact
gagagtgcaccatatgcggtgtgaaataccgcacagatgcgtaaggagaaaataccgcatcaggcgccattcgccattcaggctgcgcaactgttgggaagggc
gatcggtgcgggcctcttcgctattacgccagctggcgaaaggggatgtgctgcaaggcgattaagttgggtaacgccagggttttcccagtcacgacgttgtaa
aacgacggccagtgaattagtactctagcttaagtaacgccattttgcaaggcatggaaaatacataactgagaatagagaagttcagatcaaggttaggaaca
gagagacagcagaatatgggccaaacaggatatctgtggtaagcagttcctgccccggctcagggccaagaacagttggaacagcagaatatgggccaaacag
gatatctgtggtaagcagttcctgccccggctcagggccaagaacagatggtccccagatgcggtcccgccctcagcagtttctagagaaccatcagatgtttcca
gggtgccccaaggacctgaaatgaccctgtgccttatttgaactaaccaatcagttcgcttctcgcttctgttcgcgcgcttctgctccccgagctcaataaaagagc
ccacaacccctcactcggcgcgccagtcctccgatagactgcgtcgcccgggtacccgtattcccaataaagcctcttgctgtttgcatccgaatcgtggactcgct
gatccttgggagggtctcctcagattgattgactgcccacctcgggggtctttcatttggaggttccaccgagatttggagacccctgcccagggaccaccgacccc
cccgccgggaggtaagctggccagcggtcgtttcgtgtctgtctctgtctttgtgcgtgtttgtgccggcatctaatgtttgcgcctgcgtctgtactagttggctaact
agatctgtatctggcggtcccgcggaagaactgacgagttcgtattcccggccgcagcccctgggagacgtcccagcggcctcgggggcccgttttgtggcccatt
ctgtatcagttaacctacccgagtcggacttttggagctccgccactgtccgaggggtacgtggctttgttgggggacgagagacagagacacttcccgcccccg
tctgaatttttgctttcggttttacgccgaaaccgcgccgcgcgtcttgtctgctgcagcatcgttctgtgttgtctctgtctgactgtgtttctgtatttgtctgaaaatt
agctcgacaaagttaagtaatagtccctctctccaagctcacttacaggcggccgaattcgccgccgccatgcctcgcggctggacagccctgtgcctgctgtctct
gctgccatccggcttcatgagcctggataataacggcacagccaccccagagctgcctacacagggcaccttcagcaatgtgtccacaaacgtgagctatcagga
gaccacaacccccttctaccctgggatccacaagcctgcaccccgtgtctcagcacggcaacgaagccaccaccaacatcaccgagaccacagtgaagtttacctc
cacctctgtgattacctctgtgtacggaaatacaaactccagcgtgcagtctcagacatctgtgatctccacagtgtttacaacacctgccaatgtgtccaccccag
agacaaccctgaagcccagcctgtctcctggaaatgtgtccgatctgtctaccacctccaccagcctggccacctctcccaccaagccctatacctcctcttctccc
atcctgagcgatatcaaagccgagatcaaatgcagcgggattcgggaagtgaaactgacacagggcatctgcctggaacagaataagacatccagctgcgccg
agtttaagaaagatagaggagagggactggccagggtgctgtgtggcgaagagcaggccgacgccgatgccggcgcccaggtgtgttccctgctgctggcccag
tctgaggtgcgcccccagtgcctgctgctggtgctggccaatcggacagaaattagcagcaagctgcagctgatgaaaaaacaccagagcgatctgaaaaagct
gggcatcctggactttaccgagcaggacgtggcctctcaccagagctacagccagaaaacactgatcgccctggtgaccagcggagccctgctggccgtgctgg
gcatcaccggatatttcctgatgaataggcgcagctggagccccaccggcgaacggctggagctggagcctgtcgaccgagtgaagcagaccctgaactttgatc
tgctgaagctggccggcgacgtggagtccaaccccgggccagggaatATGGCCTTACCAGTGACCGCCTTGCTCCTGCCGCTGGCCTTGCTG
CTCCACGCCGCCAGGCCGGATATTCTGCTCACACAGACCCCACTCTCCCTGCCCGTGTCACTCGGGGATCAGGCTAGCATTT
CTTGCCGCTCATCTCAGTCTCTGGTCCACCGGAATGGGAACACATACCTCCATTGGTACCTCCAGAAACCTGGACAGAGCCC
TAAACTGCTCATCCACAAAGTCTCAAATCGGTTCTCCGGCGTGCCCGATCGCTTTAGCGGATCCGGATCTGGGACCGACTTC
ACACTGAAAATCTCACGAGTGGAGGCTGAGGATCTCGGCGTCTACTTCTGTAGTCAGAGTACCCACGTCCCACCCCTCACCT
TTGGCGCTGGAACAAAACTGGAGCTGAAACGAGCCGATGCTGCTCCTACCGTGTCCATCTTTCCTGGCTCCGGGGGAGGCG
GGAGCGGAGGCGAAGTGAAACTCCAGCAGTCTGGCCCTTCTCTCGTGGAACCTGGCGCTTCTGTGATGATCTCCTGTAAGG
CCTCTGGATCTTCCTTTACCGGCTACAACATGAACTGGGTCCGGCAGAACATTGGCAAATCCCTGGAATGGATTGGCGCCAT
CGATCCTTACTACGGCGGCACATCATACAATCAGAAATTCAAGGGGCGAGCAACACTCACTGTCGACAAATCTTCATCCACC
GCCTACATGCACCTGAAATCTCTCACATCCGAGGATAGTGCTGTCTACTACTGTGTCTCTGGCATGGAATACTGGGGACAGG
GAACTTCTGTCACCGTGTCTAGTGCCAAAACCACACCTCCCTCCGTGTACGGACGAGTCACTGTCTCATCTGCTGAACCAAA

ATCCTGTGACAAAACACACACATGCCCACCTTGTCCTGCCCCTGAACTGCTCGGCGGACCTTCCGTCTTTCTGTTTCCCCCCA
AACCCAAGGATACACTCATGATTTCTAGGACCCCCGAAGTCACTTGTGTCGTGGTCGATGTGTCTCACGAGGATCCTGAAGT
GAAATTCAACTGGTACGTGGACGGAGTCGAGGTCCACAATGCCAAAACAAAACCCCGGGAGGAACAGTACAATAGCACCT
ACCGAGTCGTGTCCGTGCTCACCGTCCTCCATCAGGATTGGCTGAACGGCAAAGAGTACAAGTGTAAAGTGAGTAACAAGG
CTCTCCCCGCTCCTATTGAAAAAACCATCTCAAAAGCAAAAGGCCAGCCTAGGGAGCCTCAGGTCTACACACTGCCACCCTC
ACGGGACGAACTCACCAAAAATCAGGTGTCCCTCACTTGCCTGGTGAAAGGCTTCTACCCTTCCGATATCGCTGTGGAATGG
GAGTCAAATGGGCAGCCCGAAAACAACTACAAAACAACCCCCCCTGTGCTCGATTCCGATGGCTCTTTTTTCCTGTACTCCA
AACTCACCGTGGACAAATCACGCTGGCAGCAGGGGAATGTCTTTTCTTGCTCCGTGATGCACGAGGCCCTCCACAATCATTA
CACCCAGAAATCCCTCTCACTCTCACCCGGCAAAAAGGACCCTAAAACCACGACGCCAGCACCGCGACCACCAACACCGGC
GCCAACCATCGCATCGCAGCCCCTGTCCCTGCGCCCAGAGGCGTGCCGACCAGCGGCGGGGGGCGCAGTGCACACGAGG
GGGCTGGACTTCGCCTGTGATATCTACATCTGGGCGCCCTTGGCCGGGACTTGTGGGGTCCTTCTCCTGTCACTGGTTATCA
CCCTTTACTGCAAACGGGGCAGAAAGAAACTCCTGTATATATTCAAACAACCATTTATGAGACCAGTACAAACTACTCAAGA
GGAAGATGGCTGTAGCTGCCGATTTCCAGAAGAAGAAGAAGGAGGATGTGAACTGAGAGTGAAGTTCAGCAGGAGCGCA
GACGCCCCCGCGTACAAGCAGGGCCAGAACCAGCTCTATAACGAGCTCAATCTAGGACGAAGAGAGGAGTACGATGTTTT
GGACAAGAGACGTGGCCGGGACCCTGAGATGGGGGGAAAGCCGAGAAGGAAGAACCCTCAGGAAGGCCTGTACAATGA
ACTGCAGAAAGATAAGATGGCGGAGGCCTACAGTGAGATTGGGATGAAAGGCGAGCGCCGGAGGGGCAAGGGGCACGA
TGGCCTTTACCAGGGTCTCAGTACAGCCACCAAGGACACCTACGACGCCCTTCACATGCAGGCCCTGCCCCCTCGCGGCAG
CGGCGCCACCAACTTCAGCCTGCTGAAGCAGGCCGGCGACGTGGAGGAAAACCCTGGCCCCATGTCTTTAAGAGGCTCTTT
ATCTCGTCTGCTGCAGACTCGTGTGCACAGCATTTTAAAAAAGAGCGTGCACAGCGTGGCCGTCATTGGAGCCCCCTTCAG
CCAAGGCCAGAAGAGAAAGGGCGTCGAACACGGACCCGCCGCCATCAGAGAAGCTGGTTTAATGAAGAGACTGAGCTCTT
TAGGCTGCCATTTAAAAGACTTCGGAGATTTGTCTTTTACCCCCGTCCCCAAGGACGATTTATACAATAATTTAATCGTGAAC
CCCAGATCCGTGGGACTGGCTAACCAAGAACTGGCCGAGGTCGTGAGCAGAGCCGTGTCCGACGGCTACTCTTGTGTGAC
TTTAGGCGGCGATCACTCTTTAGCCATTGGCACAATCTCCGGACACGCTAGGCACTGCCCCGATTTATGCGTGGTGTGGGT
GGACGCTCACGCCGACATCAATACCCCTCTGACCACCAGCAGCGGCAATTTACACGGACAGCCCGTCAGCTTTTTACTGAG
GGAGCTGCAAGATAAGGTGCCTCAGCTGCCCGGCTTCAGCTGGATCAAGCCTTGTATCAGCAGCGCTTCCATCGTGTACAT
TGGTTTAAGAGACGTGGACCCTCCCGAACACTTCATCCTCAAGAACTACGACATTCAGTACTTCAGCATGAGGGATATCGAT
CGTCTCGGAATCCAGAAGGTGATGGAAAGGACCTTCGATTTACTCATCGGAAAGAGGCAGAGGCCTATCCATTTATCCTTC
GACATCGACGCCTTCGATCCTACACTGGCCCCCGCTACTGGTACACCCGTTGTGGGCGGTTTAACCTATAGGGAGGGCATG
TACATCGCCGAAGAGATCCACAACACCGGTTTACTGAGCGCTCTGGATTTAGTGGAGGTGAATCCTCAGCTGGCCACCTCC
GAGGAGGAGGCCAAAACCACCGCCAATCTGGCCGTGGACGTGATCGCCAGCTCCTTCGGCCAGACCAGAGAGGGCGGCC
ACATTGTGTACGACCAGCTGCCCACACCCAGCTCCCCCGATGAGTCCGAAAACCAAGCTCGTGTCAGAATCTGATAATAACC
CAAGCTTaacacgagccatagatagaataaaagattttatttagtctccagaaaaaggggggaatgaaagaccccacctgtaggtttggcaagctagcttaag
taacgccattttgcaaggcatggaaaatacataactgagaatagagaagttcagatcaaggttaggaacagagagacagcagaatatgggccaaacaggatat
ctgtggtaagcagttcctgccccggctcagggccaagaacagttggaacagcagaatatgggccaaacaggatatctgtggtaagcagttcctgccccggctcag
ggccaagaacagatggtccccagatgcggtcccgccctcagcagtttctagagaaccatcagatgtttccagggtgccccaaggacctgaaatgaccctgtgcct
tatttgaactaaccaatcagttcgcttctcgcttctgttcgcgcgcttctgctccccgagctcaataaaagagcccacaacccctcactcggcgcgccagtcctccga

tagactgcgtcgcccgggtacccgtgttctcaataaaccctcttgcagttgcatccgactcgtggtctcgctgttccttgggagggtctcctctgagtgattgactgcc
cacctcgggggtctttcatt

8.4 Supplementary

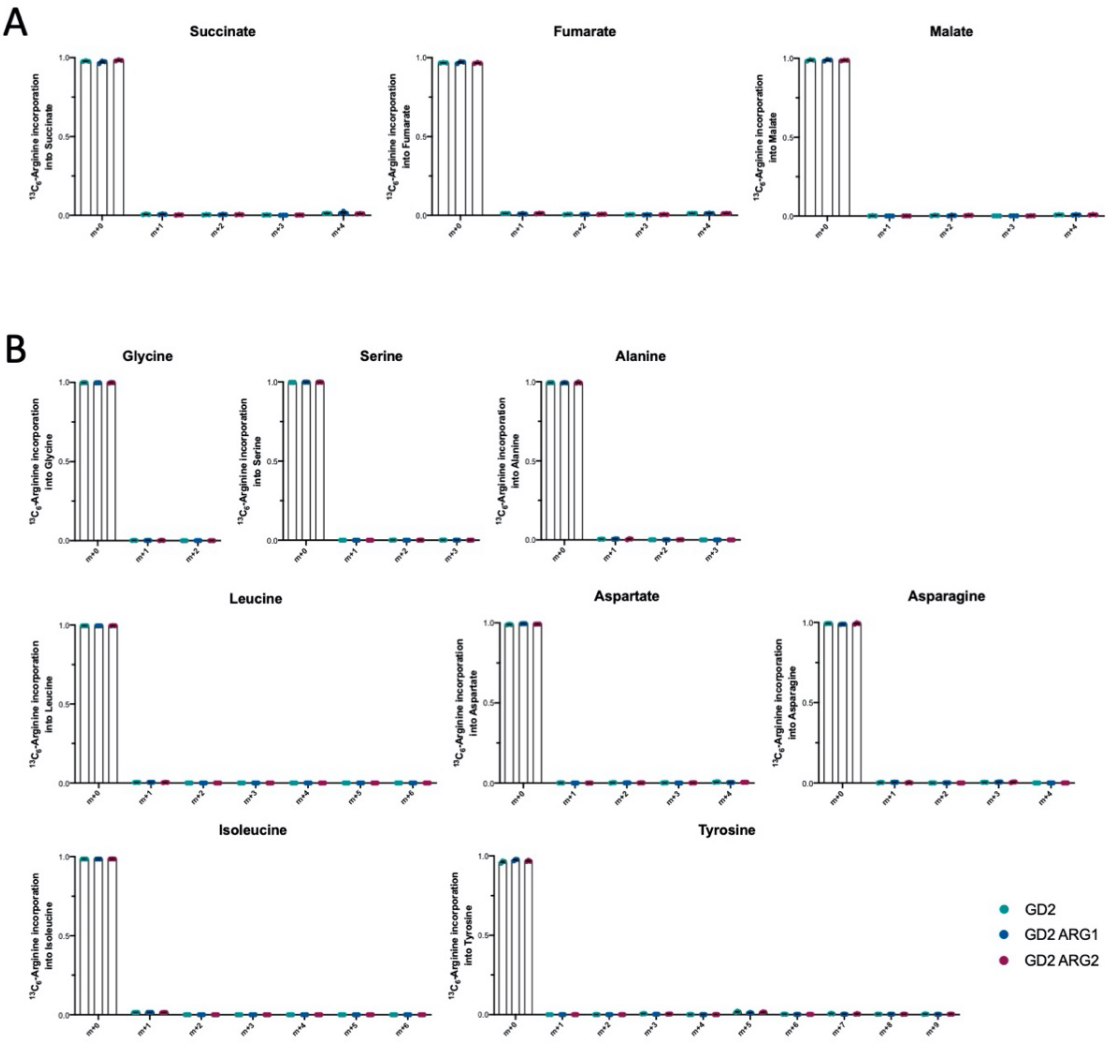

Supplementary 1: L-arginine tracing within intracellular metabolites of CAR-Jurkat cells.

Upon preconditioning in L-arg low microenvironment (48h), CAR-Jurkat cells were incubated with uniformly labelled $^{13}C_6$ L-Arginine for 24h; polar metabolites were extracted and read on a GC-MS. Incorporation of L-arginine was not detected in certain TCA cycle intermediates (A), i.e. succinate, fumarate and malate, and among certain amino acids (B), i.e. glycine, serine, alanine, leucine, isoleucine, aspartate, asparagine and tyrosine. Results are normalised by total metabolite abundance and "m+x" denotes ^{13}C isotopomer distribution.